UNIVERSITY OF

LIVERPOOL

Identification and Robust Control of Automotive Dynamometers

Thesis submitted in accordance with the requirements of the

University *of* Liverpool for the

Degree of Doctor in Philosophy

by

Christian Matthews

June 2007

Acknowledgments

This thesis is dedicated to the memory of my grandfather Geoff Slocombe who gave so much wisdom to everyone who knew him.

Special thanks must go to Tom Shenton who has provided me with support and inspiration in equal measure throughout the course of my research at the University of Liverpool. This time has been made easier and more enjoyable by my colleagues Steph Carroll, Georgios Triantos, Chris Ward, Nick Rivara and especially Paul Dickinson who has been a great friend throughout my time at University.

The experimental work carried out in this thesis would not have been possible without the input of Derek Neary who provided endless practical advice and support. A mention must also go to Dave Harris and everyone else in the Core Services workshop who were always ready with help and advice when it was needed.

My sincere thanks go to all my friends and family who have been there for me when it counted, especially my parents Craig and Mary who have provided an endless supply of patience, love and support.

Finally my greatest appreciation goes to my fianceé Beth who has suffered the dark moods, long hours and at times unhealthy obsession and in return has given me nothing but happiness.

Christian Matthews, 21st June 2007

Statement of originality

This thesis is submitted for the degree of Doctor in Philosophy in the Faculty of Engineering at the University of Liverpool. The research project reported herein was carried out, unless otherwise stated, by the author in the Department of Engineering at the University of Liverpool between August 2003 and August 2006.

No part of this thesis has been submitted in support of an application for a degree or qualification of this or any other University or educational establishment. However, some parts of this thesis have been published, or submitted for publication, in the following papers and internal reports:

- C.Matthews, P.Dickinson and A.T. Shenton, Identification and Robust Control of a Transient Chassis Dynamometer, Submitted to Control Engineering Practice, April 2007.
- C.Matthews, P.Dickinson and A.T. Shenton, Chassis Dynamometer Torque Control System Design by Direct Inverse Compensation, 6th Biennial UKACC International Control Conference, Glasgow, September 2006.
- C.Matthews, P.Dickinson and A.T. Shenton, SIMO MV Controller Performance*, Internal Report - MES/ATS/RHS/052/2006, The University of Liverpool, May 2006.

C.Matthews

June 21st 2007

*Company Confidential

Abstract

In the automotive industry, a drive to reduce costs and to accelerate product development cycles has increased the importance of laboratory based testing and validation. In order to further extend the applicability of this laboratory based development, the test-bed must represent as fully as possible the conditions which are experienced by a vehicle in service on the road.

In the field of powertrain development, a key test-bed tool is the Dynamometer. The dynamometer has evolved from a simple passive absorption brake, used to measure power and torque, through to the modern active dynamometer system based on AC and DC motor technology which can provide dynamic simulation of road load conditions. These active dynamometer systems, both directly coupled engine dynamometers and rolling road chassis dynamometers have become an important tool in the evaluation of vehicle emissions and performance as well as the calibration of electronic control strategies.

This thesis presents a methodology for the systematic development of closed loop dynamometer torque controllers. The methodology is aimed at achieving improved performance in both static and transient testing, and its effectiveness is examined and confirmed through its application on two different dynamometer systems. The methodology is based upon the use of linear black-box system identification, modern filtering techniques and robust control design methods which when used together are highly complimentary and so form a coherent development path. The main focus of the work presented is in the practical application of linear system identification, filtering and robust control techniques to solve a set of practical problems which are faced when designing high performance dynamometer controllers. The novel application of established linear system identification and control methods is shown to provide a practical and effective way of designing controllers which should be applicable to many different types and configurations of dynamometer.

Contents

Nomenclature

ABV Air Bleed Valve

ADC Analogue to Digital Conversion

ARMAX Auto Regressive Moving Average eXogeneous Model Structure

ARX Auto Regressive eXogeneous Model Structure

ASAM Association for Standardisation in Automation and Testing

BJ Box Jenkins Polynomial Model Structure

CAN Controller Area Network

CPU Central Processing Unit

DAC Digital to Analogue Conversion

DIC Direct Inverse Compensator

DIO Digital Input/Output

EDC Engine Dynamometer Controller

EMS Engine Management System

FPGA Field Programmable Gate Array

LAN Local Area Network

LIN Local Interconnect Network

LTI Linear Time-Invariant

MISO Multiple Input Single Output

MLPRBS Maximum Length Pseudo Random Binary Input

MOST Media Oriented Systems Transport

MUT Machine Under Test

PAU Power Absorption Unit

PAU Power Absorption Unit

PC Personal Computer

PCM Powertrain Control Module

PID Proportional, Integral, Derivative controller structure

PPR Pulses Per Revolution

PRBS Pseudo Random Binary Input

PWM Pulse Width Modulation

RCP Rapid Control Prototyping

SISO Single Input Single Output

TTL Transistor-Transistor Logic

ZTC Zero Torque Control

List of Figures

Part I

Introduction

Chapter 1

Dynamometers

1.1 The Dynamometer in Automotive Applications

A Dynamometer is a device for measuring the forces exerted by a machine. Duke Gaspard de Prony (1755-1895) is credited with the invention of the first friction brake dynamometer device in 1821. The device which he proposed Fig.1.1 utilised a wooden clamp which is placed around the shaft of a rotating machine. Braking load is adjusted by tightening the clamp to increase the frictional force exerted on the shaft. The clamp is connected to a 'torque arm' of known length which was weighted at its free end until it was balanced, providing a steady-state measurement of the shaft torque, and if the rotational speed was known, power could be calculated. This type of measurement gave rise to the concept of 'Brake Horsepower'.

The fundamental mode of operation of the so called 'De Prony' brake forms the basis of most dynamometer systems which have followed, all utilise some form of brake which absorbs the power generated by a machine under test (MUT). For this reason the term 'Power Absorption Unit' or PAU has been widely adopted to describe the braking unit in a dynamometer system. The method of braking utilized in modern PAU's is diverse, but the principle mode of operation has remained constant. A significant development in dynamometer technology has been the advent of active PAU's which are capable of adding energy to the system, as well as acting as a brake. This has led to the possibility of using Dynamometers for active load simulation and not merely passive power absorption.

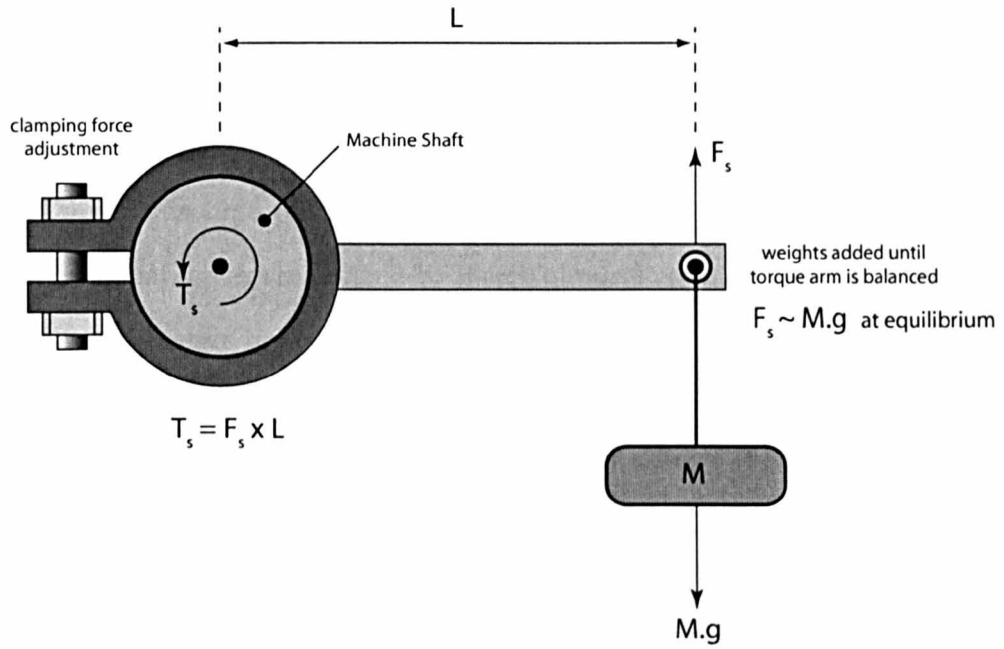

Figure 1.1: The de Prony brake

In one of the earliest popular industrial references to the term Dynamometer, railway cars were utilised as special carriages, containing braking equipment for the measurement of tractive forces, to be pulled by a test locomotive. Charles Babbage* has been credited as the creator of the first example of such a machine, which was used to assess the relative merits of competing railway gauges in co-operation with Brunel around 1838-39 [Wil02, Sch02]. Around the same time, Froude presented work on a hydraulic dynamometer which was used for testing the power of propellor screws, used in the new generation of Iron clad warships. However, the most common and best known application for dynamometers is in the field of automotive engineering, testing and development.

The adoption of reciprocating internal combustion engines for powering automobiles led to an immediate development race in search for increased power and efficiency. Increasingly detailed and sensitive engine development required testing equipment to match. In time the emerging technologies, first hydraulics and then electricity, allowed more flexible and higher capacity testing to be performed. The use of weights for load balancing was soon replaced by spring balances and eventually electrical loadcells which could be used to record measurements and

*Babbage, often acknowledged as a father of computing, was incidentally inspired in his work on computing by Prony who is perhaps more famous for his tables of Logarithms, developed using teams of human computers to process complex calculations.

ultimately provide feedback for closed loop load control. Initially, load was adjusted manually by tightening or loosening tensioning devices, making it slow and impractical to adjust the load during testing. The introduction of hydraulic dynamometers provided a more flexible testing arrangement since this type of brake tends more reliable and far less subject to wear than those where frictional forces are applied by direct physical contact. From a control perspective hydrostatic dynamometers improved matters since load could be modified by adjusting valves or sluice plates, but did not revolutionise the field. The electrical dynamometer, and more particularly the Eddy Current Dynamometer, opened the way for Dynamometer control systems to be implemented which were capable of rapid, automatic control of breaking load. In time, improved and affordable solid-state drive technology for AC and DC dynamometers brought the possibility of highly automated load control along with active four quadrant operation capable of adding as well as dissipating energy.

The following section provides discussion on some of the common dynamometer PAU's and seeks to develop a picture of the way in which dynamometers, and their load control systems, have developed.

1.2 Engine Dynamometers

The engine-dynamometer system (Fig.1.2) typically consists of a test engine which is directly coupled to a dynamometer via a transmission shaft. The torque is measured either by an in-line flange type torque transducer or by a total reaction torque measurement arrangement. The rotational speed is typically measured using a shaft encoder or tachometer.

There are two torque actuators, one each for the engine and the dynamometer. In the case of the dynamometer, this will depending upon the type of dynamometer which is used (e.g. valve position in hydraulic dynamometers, or excitation current in electrical dynamometers 1.4). In the case of the engine, air, fuelling, spark angle or usually a combination of all three provide torque actuation. Where an existing engine management strategy exists, the drivers throttle pedal is used to provide a realistic way of reflecting the drivers input during operation in the vehicle.

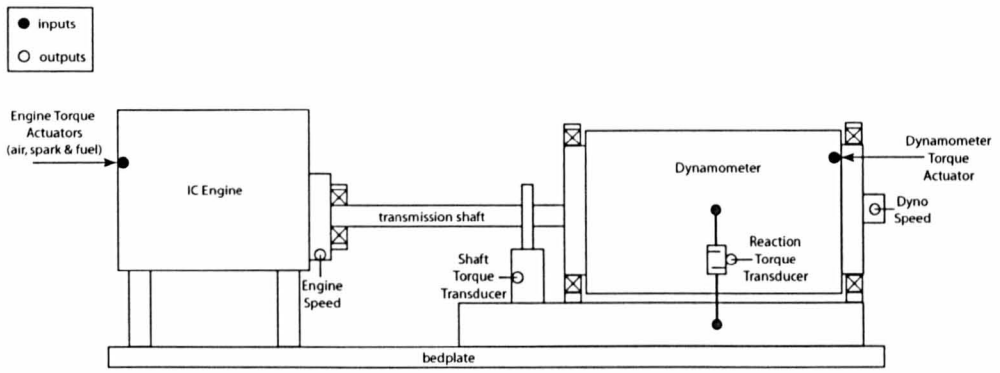

Figure 1.2: Overview of an Engine-Dynamometer

1.3 Chassis Dynamometer

An alternative to the directly coupled engine dynamometer is the chassis dynamometer (sometimes also called a vehicle dynamometer or rolling road). In this type of machine, the dynamometer brake or motor is connected to rollers which are in contact with the tyres of a test vehicle. The vehicle drives on the the rolls which are mechanically connected to a dynamometer.

There are two common roller (roll) configurations used in chassis dynamometers, namely single roll and twin roll.

1.3.1 Twin Roll Chassis Dynamometer

Twin roll dynamometers have a pair of smaller diameter (typically 220mm or 8.65 inches) rolls which the vehicle tyres sit between (Fig.1.4 & 1.3). This type of system has been widely adopted for the purpose of diagnostic testing, especially in after-sales repair or UK MOT type emissions testing applications. The smaller roller size means that the infrastructure and space required to install this type of dynamometer is less than for the larger diameter single roll machines. Twin roll chassis dynamometers are not usually used for development testing because they are less capable in terms of simulating realistic on-road conditions. This is due to two main factors. Firstly the tyre contact with the rollers does not realistically reproduce the contact seen between a tyre and the road surface, resulting in larger than normal levels of rolling resistance. Secondly the smaller diameter rollers, combined with a compact, relatively low capacity brake, are normally incapable of providing a base inertia sufficient to permit full vehicle inertia simulation.

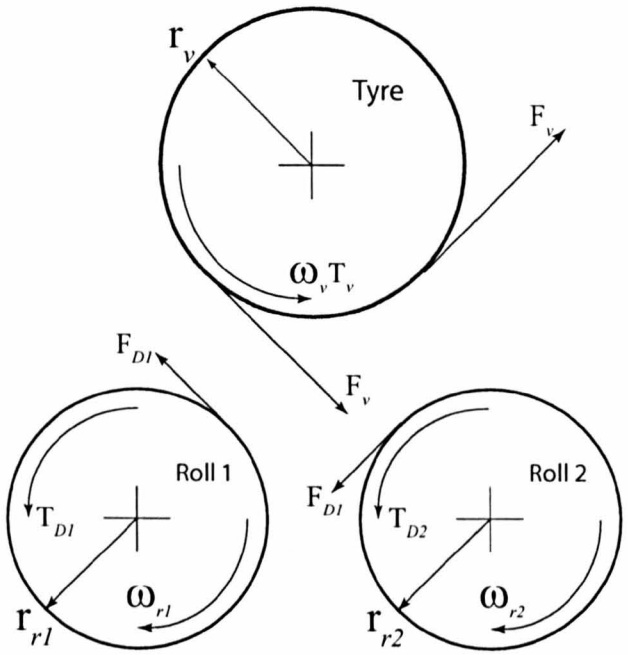

Figure 1.3: Free Body Diagram of a Twin Roll Chassis Dynamometer

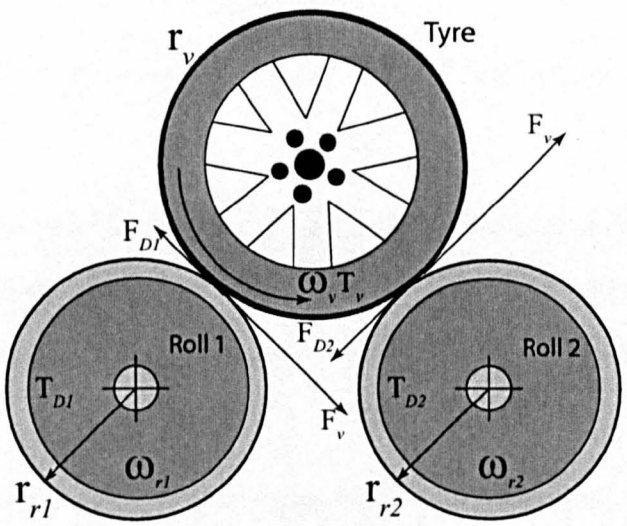

Figure 1.4: Twin Roll Chassis Dynamometer

1.3.2 Single Roll Chassis Dynamometer

Single roll chassis dynamometers (Fig.1.6 & Fig.1.5) have been adopted as the standard for vehicle development as well as legislative emissions testing and certification. The rolls typically have a diameter of 1.2 metres (48 inches). The vehicle torque (T_v) is transmitted to the roller through a force (F_v) acting at the tyres, leading to the roller rotating with an angular velocity (ω_r). If the dynamometer is operating as a brake then the load torque (T_d) acts in opposition to the vehicle torque through a force (F_D) at the roll.

The rolls are normally mounted with the dynamometer motor in the middle of the arrangement with the rolls mounted either side hence the common term 'motor in the middle'. Other single roll dynamometers are arranged with the dynamometer motor mounted at the end of the arrangement. The large diameter rollers mean that infrastructure and space requirements are significant and the cost of this type of dynamometer tends to be somewhat higher than twin roll machines. On the other hand increased packaging space available means that larger dynamometer brakes are practical and the absorption capacity of this type of machine can be significantly higher than for twin roll dynamometers. The combination of larger diameter, high inertia rolls with a (usually) active PAU means that inertia simulation is possible in these systems.

1.3.3 Modes of Dynamometer Control

There are four basic control strategies which may be adopted when using a dynamometer [PM99]. These are control of:

- **Position** - In this mode, the position of either the engine or dynamometer torque actuator is controlled open-loop. The term position is used loosely since the actuation of for example an electro-mechanical dynamometer may actually be something else such as the excitation current.

- **Speed** - the speed of the engine-dynamometer is controlled using closed loop control, with the dynamometer torque and engine torque actuators as input variables.

- **Torque** - the shaft torque of the engine-dynamometer is controlled normally using a closed loop control system. External loads are simulated by applying torque using a signal to the

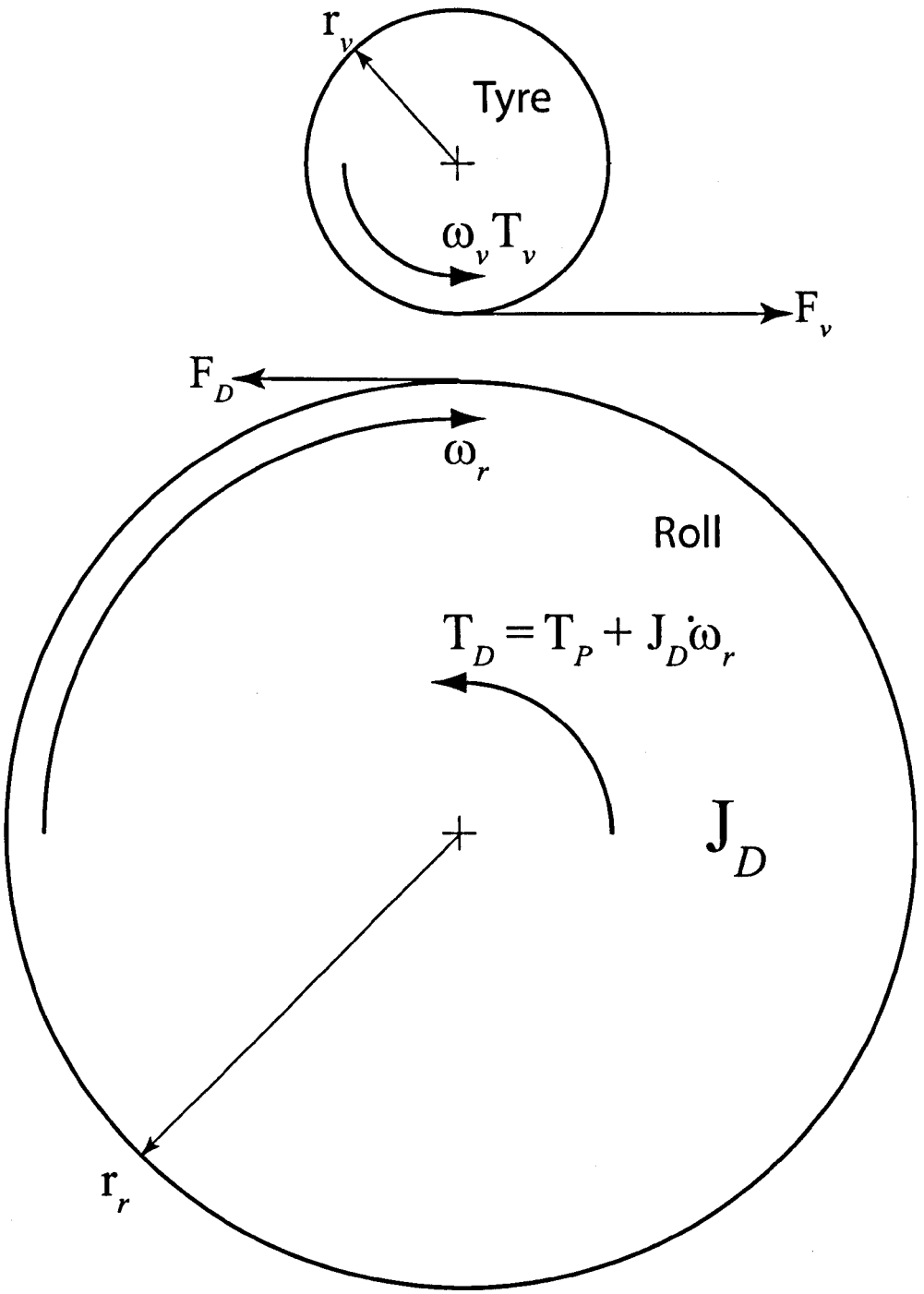

Figure 1.5: Free Body Diagram for a Single Roll Chassis Dynamometer

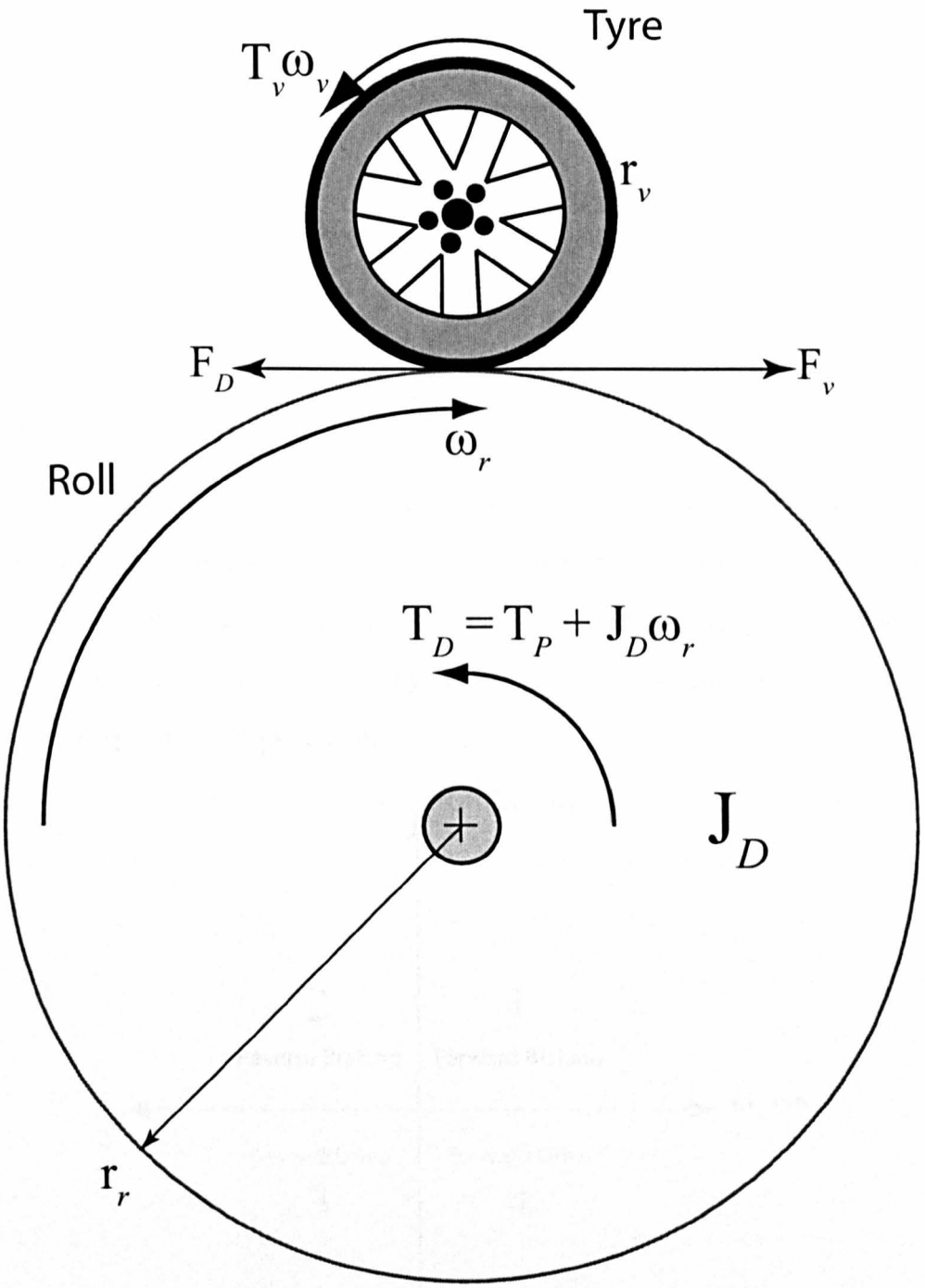

Figure 1.6: Single Roll Chassis Dynamometer

dynamometer torque actuation channel, while a computer based 'driver model' controls the engine's torque actuator which is typically the throttle pedal.

- **Power** - torque and speed of the engine-dynamometer are controlled simultaneously in order to track an engine power profile. This mode is typically used for emissions testing cycles which are prescribed in terms of concurrent torque and speed trajectories.

1.4 Types of Dynamometer

1.4.1 Passive Dynamometers

Passive dynamometers dissipate energy by providing a braking load on the output of the MUT. They are sometimes described as two-quadrant machines, since they operate in only two (1 & 2) of the four possible quadrants of the operating envelope described in Figure.1.7. In a two-quadrant machine, the torque applied is always positive and will act in opposition to the motion of the MUT. Because they are only capable of extracting energy from the system, they are sometimes also referred to as passive dynamometers. This section provides an overview of the most common passive dynamometers.

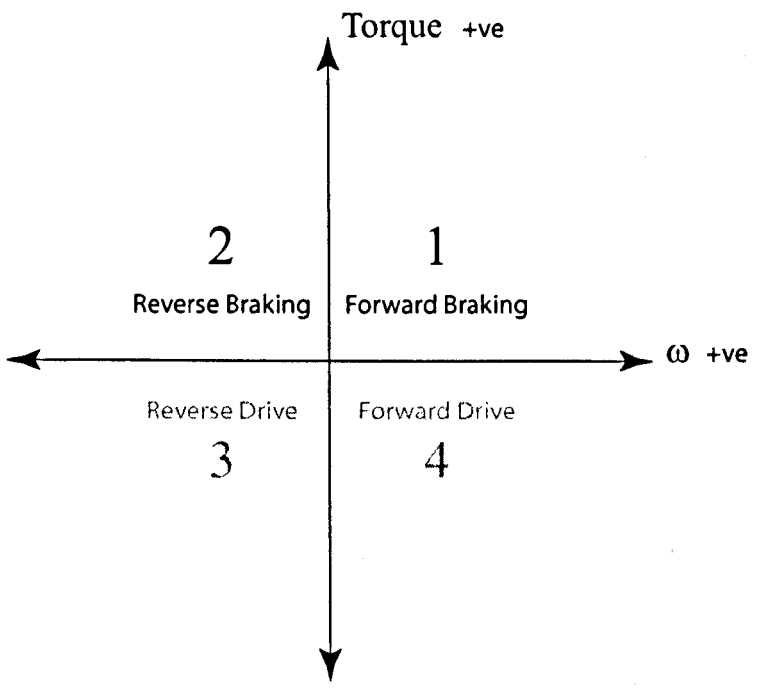

Figure 1.7: Passive Dynamometer machines operate in only two quadrants

Contact Friction Brake

The earliest form of the dynamometer, exemplified by the Prony brake, is the friction brake (Fig.1.8) and is physically and conceptually the simplest form of dynamometer. Load is applied by simply introducing friction, while the reaction torque is measured using a lever arm, and a loadcell or a simple spring based balance. In early examples, the frictional forces were introduced using a simple plain clamping arrangement (as in the Prony brake), or sometimes a rope which is wrapped around a drum connected to the output shaft of the machine being tested. In order to maintain favourable operating conditions, these machines are usually water cooled since the energy dissipated by the brake is mainly transferred as heat.

Some modern forms of the friction brake make use of a metal disk with hydraulically actuated callipers which apply the frictional force through pads made of special materials. These machines are very similar to the disk brakes commonly used in vehicle braking systems. They have the advantage that they can apply braking loads even at zero speed. This makes them particularly useful in low speed testing.

Hydraulic Dynamometer

Hydraulic dynamometers develop braking torque through the viscous forces in a fluid (usually water or oil) which are set up between a rotor, connected to the driven shaft and stators built into the casing (Fig.1.9). Vortices are developed, the energy of which is dissipated as heat in the working fluid. There are two main variants of the hydraulic dynamometer, depending upon whether the amount of fluid in the casing is maintained constant, or is varied. The type of system used has an important bearing upon the way in which load control is achieved as well as upon the speed and resolution of control which can be expected:

- **Constant Fill**: The resistance in a constant fill hydrokinetic dynamometer is varied by inserting or withdrawing plates between the rotors and stators. This modifies the amount of shear force generated, controlling the formation of vortices and thus the load which is applied. This method provides relatively low resolution of control over the applied load, and is slow. The constant fill hydraulic dynamometer is therefore poorly suited to an

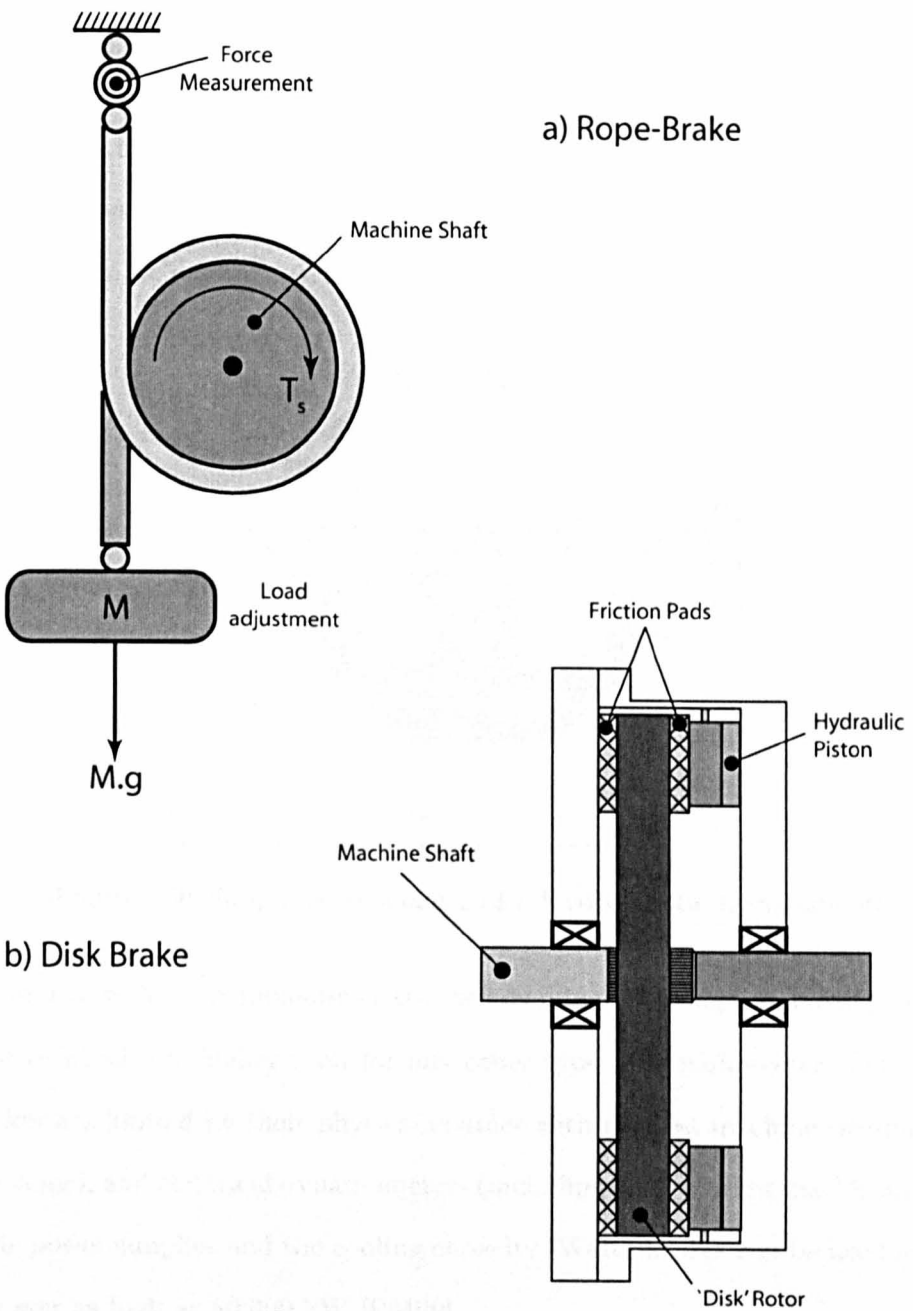

Figure 1.8: Friction Brake Dynamometers - a) Rope brake. b) Disk brake.

automated load control system, and is certainly unsuitable for transient testing.

- **Variable Fill**: The variable fill dynamometer operates in the same fashion as the constant fill machine except that instead of inserting 'sluice' plates to control the generation of vortices, the load is controlled by varying the amount of fluid in the system. The variable filling of the system can be achieved by using fast acting servo controlled valves and is therefore much more suitable for automated testing than the constant fill dynamometer. The resolution with which the load can be varied is greater since the amount of fluid in the casing can be continuously varied.

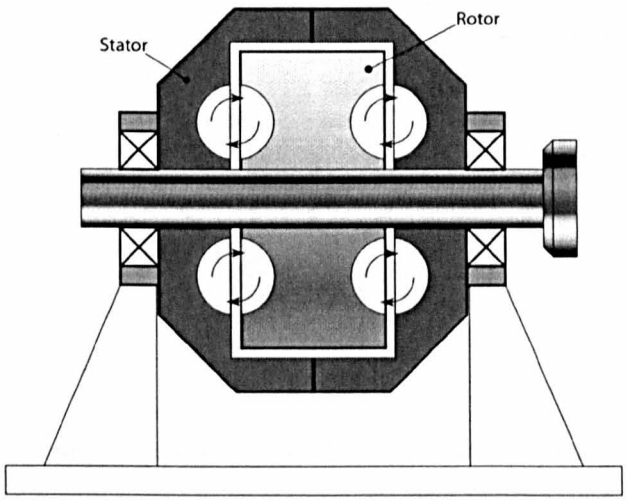

Figure 1.9: Simplified schematic of a Hydrokinetic Dynamometer

In general, hydraulic dynamometers have the advantage of being capable of providing braking load capacities which are higher than for any other type of dynamometer. On the other hand friction brakes are limited by their physical contact with the test machine (leading to wear and cooling problems), and electrical dynamometers (including eddy current machines) are limited by the available power supplies and the cooling capacity. Water brakes can be used for applications requiring power as high as 80'000 kW [PM99].

Eddy Current Dynamometer

The eddy current dynamometer (Fig.1.10) is an electrical machine which consists of a steel rotor disk which rotates between a pair of so called loss plates. A magnetic field is generated by a

pair of excitation coils and as the rotor passes through the magnetic field, eddy currents are induced, dissipating power as heat which is removed by a water cooling system integrated within the loss plates. The load applied by the dynamometer is controlled by modifying the current which is supplied to the excitation coils. This mode of control allows the torque applied by the eddy current dynamometer to be modified very rapidly compared with friction or hydraulic dynamometers.

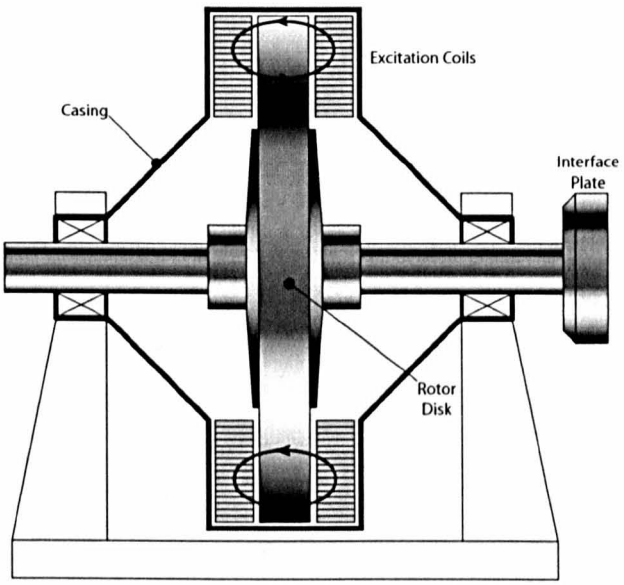

Figure 1.10: Simplified schematic of an Eddy-Current Dynamometer

1.4.2 Active Dynamometers

Active dynamometers are capable of both extracting and supplying energy and are sometimes described as four-quadrant machines, since they may operate in all of the four possible quadrants illustrated in Figure.1.11.

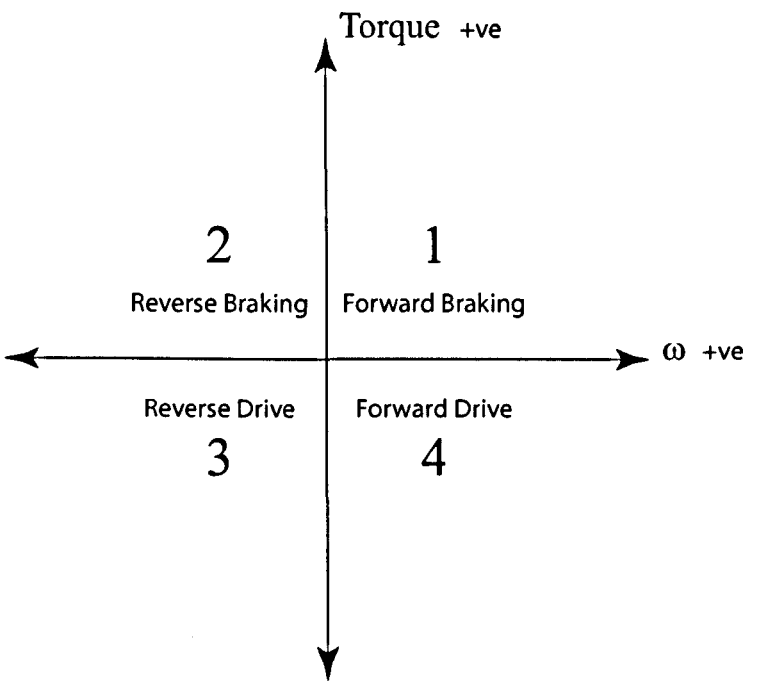

Figure 1.11: Active Dynamometer machines operate in all four quadrants

Hydrostatic Dynamometer

Active hydrostatic dynamometers use a pump to supply high pressure fluid to a hydraulic motor which is controlled using a servo valve. This arrangement allows the dynamometer to supply load in both directions since it can both add and remove energy from the system.

The hydrostatic dynamometer may have an inertia of as little as one tenth of its electrical counterparts, and can be an attractive option from a cost perspective when more than one motor is required since many hydrostatic motors can be operated from a single large hydraulic power source [DW89, BBM97]. The bandwidth of the hydrostatic dynamometer is determined by the frequency response of the servo control valve. In the past this has been proven to limit the speed of control response which is possible, but with improving hardware, high levels of performance can now be achieved [BM99].

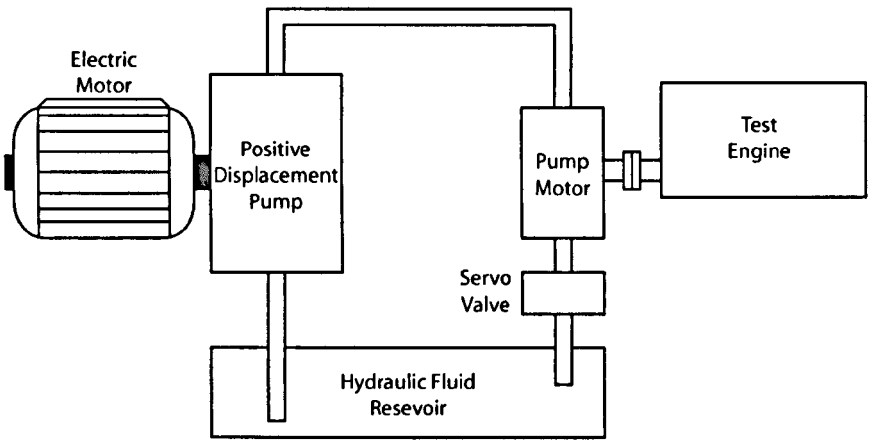

Figure 1.12: Schematic of a Hydrostatic Engine Dynamometer (adapted from [BBM97])

DC Electrical Dynamometer

A DC dynamometer uses a variable speed DC motor as the basis for the power absorption unit. The DC motor consists of a rotating armature winding and a stationary field winding. The interaction of the two resulting magnetic fields generates a tangential motor force which creates a torque in the motor shaft. The variable armature power supply is delivered by the commutator, while the field is often subjected to a constant excitation. In this case the motor torque is directly proportional to the armature current, and motor speed is proportional to armature voltage, providing a simple method of control. A full bridge rectifier is usually employed to provide a Direct Current supply at sufficiently high capacity for large, high-torque, motors.

Direct current dynamometers suffer from a relatively low power to inertia ratio, and the physical complexity which is associated with commutation, but are popular choice for use in dynamometer systems due to their high torque capability and because of the relatively cheap electronic drive systems which are available.

AC Electrical Dynamometer

The AC dynamometer uses a motor supplied by an alternating current supply, and is also capable of operating in four quadrants. AC motors are less expensive than DC machines but because they are required to operate at varying speeds, a variable frequency drive is required, increasing the cost significantly. The control of such machines is a challenging and historically expensive task which has been a barrier to their adoption. The use of AC dynamometer systems

has increased dramatically in recent years as the cost of the rather complex variable frequency drive systems, and intermediate power electronics has become lower. The AC dynamometer is now typically capable of performance comparable with the DC dynamometer and some of the advantages of the AC dynamometer can be considerable. Reduced inertia can be a particular benefit in transient engine dynamometer applications, and the absence of the requirement for commutation systems is highly attractive.

1.5 Dynamometer Testing Modes

The type of dynamometer which is selected, along with the mode of control which is employed, will depend upon the testing objective and the required duty cycle. The duty-cycle of a dynamometer can vary from a few hours per day in the case of a machine used for detailed experimental engine research through to almost continuous running in the case of dynamometers used for durability testing. In steady-state testing applications (see section 1.5.1), the range of operating frequencies will be relatively narrow as the dynamometer will only be required to track static or slowly moving set points. Events of interest will occur over a time scale of several seconds and the frequency range of interest may only be up to around 10Hz. In dynamic or transient testing, (see section 1.5.2) a wider bandwidth machine will be required for tracking transient load trajectories. In these applications, the events of interest may occur over time scales lasting significantly less that one second and so the frequency range of interest may exceed 1kHz.

The following sections examine the different modes of usage of dynamometer systems, and contrasts the requirements which are associated with different testing objectives.

1.5.1 Static Testing

The static mode of testing involves the measurement of engine performance and operating parameters at steady-state set points. This method of testing is the classical mode, but is still widely used.

Performance Curves

The performance of an engine or vehicle is often described in terms of the torque-speed and power-speed curves which are produced through static dynamometer testing. In this mode, the engine is operated at a fixed throttle position and the dynamometer is operated in speed control mode to track a setpoint. At each set-point, Load torque (T) and speed (ω)[†] are logged. This procedure is repeated over the full range of operating speeds and the data from each set-point is plotted to give a torque-speed curve. Since power (P) is given by the relationship $P = T \times \omega$, the power-speed curve can also be plotted using the same information. This technique can be extended by taking other informative measurements at each set-point, such as fuel consumption or inlet manifold pressure, to obtain characteristic curves which provide information about the performance of the engine. If the testing is extended by introducing a third variable, such as throttle position, then a three dimensional mapping can be performed.

Mapping

Static testing is not limited to characterising the speed dependent power or torque characteristics of an engine. An example of a modern application of static testing is in characterising an engine and controller parameters for the regulation of air-fuel ratio (AFR) which is a function of multiple input variables (air, spark and fuel) as well as engine speed and load. AFR should be controlled to maintain a Stoichiometric mixture[‡]. This is important not only because it represents efficient use of fuel, but also because the performance of Three-Way Catalytic converters (TWC) is highly sensitive to AFR (Fig.1.13) and must operate in a narrow window of $\pm 0.1\%$ [GO04] around the operating point $\lambda = 1$. Static mapping is used to characterise the response of the engine over its operating speed or load range, and performs the crucial role of providing 3D lookup tables which are implemented in the feed-forward path of the engine's fuelling control strategy. Figure.1.14 shows an example of a fuelling map developed for this purpose. The static testing procedure defining each set-point is usually automated, with each set-point predefined in a test program which is read by the dynamometer controller and the driver simulator, or engine controller. Note

[†]The terms speed and angular velocity are used interchangeably throughout this thesis

[‡]For gasoline fuels, the Stoichiometric AFR is typically 14.7:1 and is given the normalised value $\lambda = 1$

that a large number of set-points are required to characterise such a typical complex response surface.

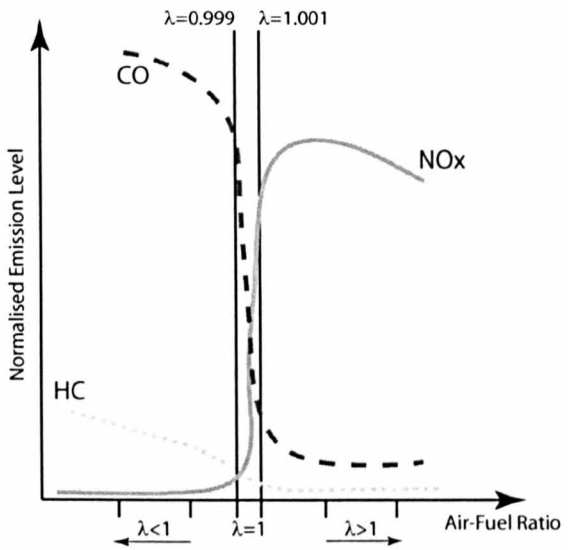

Figure 1.13: Efficiency of a 3-Way Catalytic Converter

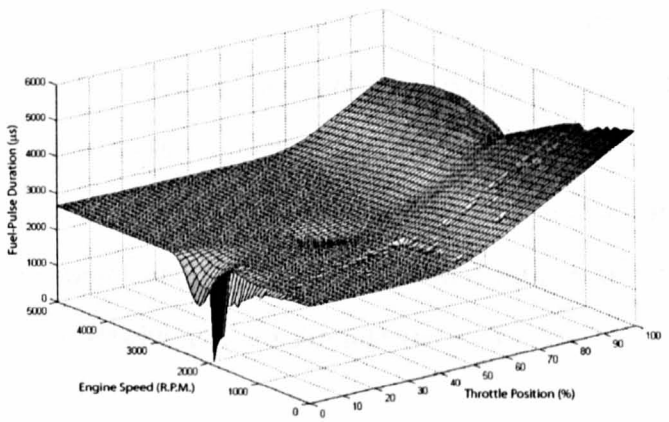

Figure 1.14: Example of a fuel map

Static testing provides results which reflect the steady-state response of the engine to a particular combination of conditions. This has only limited scope in practice since in most conditions the engine's operating conditions will be in a state of change, in terms of loading, driver input (which has a direct effect upon the induced air) and engine speed (especially in urban driving where many gear changes may be expected). If the aim of testing is extended to include an examination of the engine in the context of the vehicle in a broader sense, then a transient testing solution is required.

1.5.2 Transient Testing

Transient dynamometer testing differs from static testing because instead of controlling to stationary set-points, the dynamometer controller is required to track constantly changing references. This fundamentally changes the requirements of the control strategy from providing steady-state accuracy to providing fast acting tracking performance. Transient testing is required in order to examine the dynamic behaviour of a test engine or vehicle and does not merely facilitate faster or more efficient steady-state characterisation. Table.1.1 shows the time scales which are associated with some typical transient vehicle events.

Transient Emissions Testing

Most emissions testing cycles (e.g. ECE (Fig.1.15) and US EPA (Fig.1.16 & 1.17)) are specified in terms of standardised trajectories of speed against time or speed and load against time. In this case, it is important that the testing cycle can be tracked quickly and with precision. Clearly, a dynamometer which has the capability for high bandwidth torque actuation is important, and the control system must be designed to provide high speed tracking performance. Part of the judgement which must be made regarding the bandwidth of the controller which is required will be the transient time-scale which is important in a specific testing application. Guidelines regarding four important time scales associated with testing for different aspects of the powertrain are given in [PM99] and are summarised in Table.1.1.

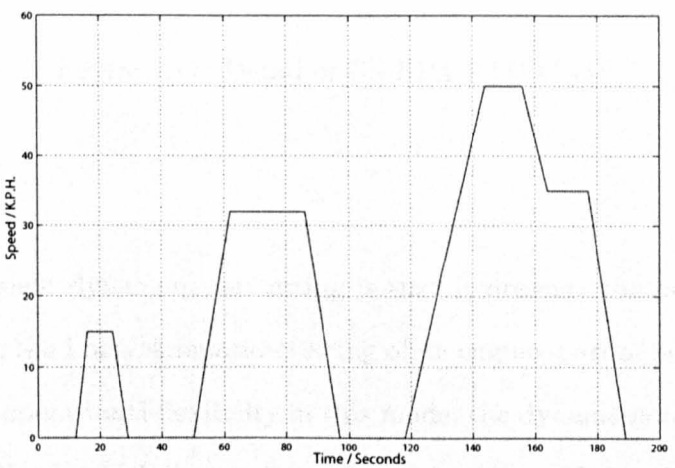

Figure 1.15: ECE Transient Testing Cycle

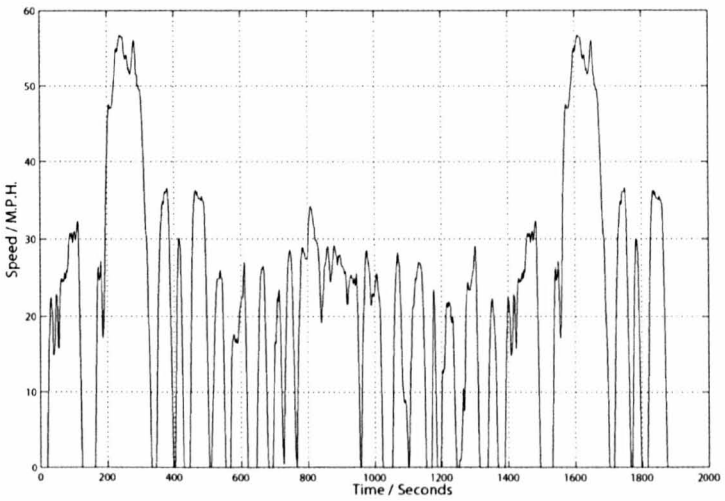

Figure 1.16: US EPA FTP Cycle

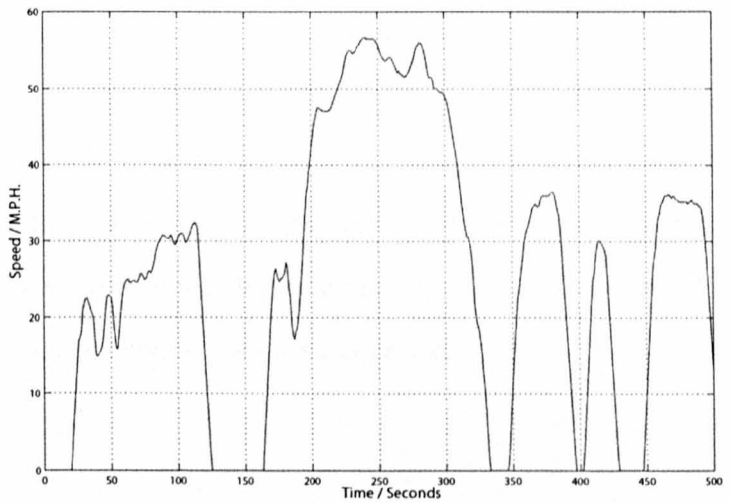

Figure 1.17: Detail of US EPA FTP Cycle

Dynamic Simulation

An advantage of transient dynamometer testing is that it presents the potential for providing real-time 'Hardware in the Loop' simulation testing of an engine, partial powertrain assembly or complete vehicle. For operational flexibility in this mode, the dynamometer must be capable of supplying the range of loads which the components under test would experience during operation on the road. An active dynamometer is therefore a highly desirable component of a true transient

Time Scale	Applications
0 - 0.2 s	Driveline Torsional Vibration
0.5 - 2 s	Gear Shift
1 - 10 s	Driver initiated transients (e.g. Throttle Tip-In)
1 - 10 mins	Engine warm-up. (Essentially Quasi-Static)

Table 1.1: Transient Time-Scales. Taken from [PM99].

dynamometer system since for dynamic simulation it must be capable of providing load in both positive and negative directions.

The dynamometer in this type of application should no longer be thought of as merely a brake, but as a simulated load which replaces the absent vehicle components along with the inertial, aero-dynamic and frictional forces which must be overcome on the road. The dynamometer control system must track a simulation algorithm which calculates the appropriate amount of torque load which should be applied to replicate a particular mode of operation. The simulation algorithm which is applied will depend upon which aspect of the vehicle behaviour is of interest.

The model will typically provide simulation of four basic sources of loading, namely inertia, aerodynamic drag, rolling resistance and gravitational forces associated with climbing a gradient (Fig.1.18). These forces are usually described as the road-load forces. (See Appendix A for a more detailed derivation of typical road-load equations).

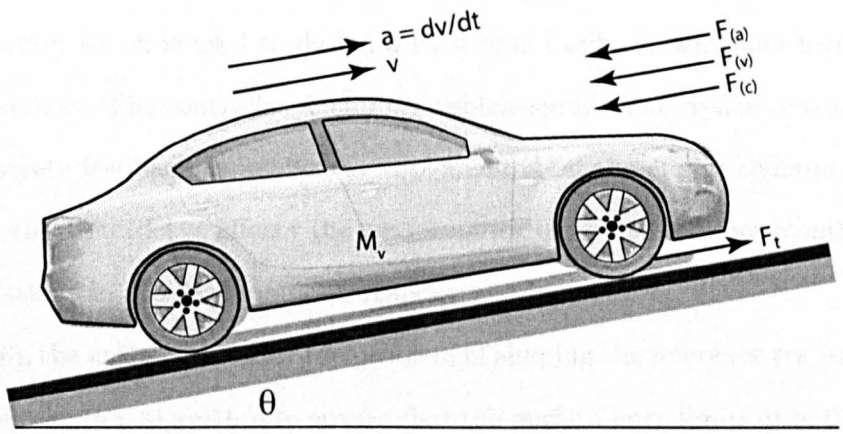

Figure 1.18: Simple Road-Load Model

In addition to road-load forces, it may be important to simulate other dynamic loading associated with components of the vehicle which are not present in the test bed. For example, in engine dynamometer testing, the transmission and driveline are usually not part of the test-bed, but it may be desirable to simulate the presence of these components for validation or calibration of engine control systems, or in emissions testing. In this case, the dynamic loading must also be provided by the dynamometer and so is added to the tracking signal delivered to the dynamometer controller. Several authors have presented work which develops control strategies incorporating dynamic simulation models.

An engine dynamometer controller with an integrated vehicle simulation model is presented in [PI95] for the purpose of Emissions testing at vehicle start-up. The authors present three methods of controlling the dynamometer using physically motivated models to generate tracking references and, in the case of a linear multivariable speed-velocity controller, to linearise the non-linear clutch and engine behaviour.

Similarly, [Voi91] presents an interesting study which incorporates system modelling, system identification and feedback control to provide vehicle load simulation on an engine dynamometer testbed. The vehicle model is used to calculate a load set-point based upon driver input and angular velocity of the test engine. A simplified vehicle model of a 1.6L VW Golf with a Diesel engine is used. The model includes the four basic road-load forces along with the torsional driveline stiffness and friction. The model also includes provision for simulating the load required during gear shifts. A transfer function model of the dynamometer is developed using system parameter estimation which is used to design a PI torque feedback controller using a frequency domain design method. The controller, including vehicle simulation, dynamometer inertia compensator and discrete feedback controller, is implemented on the engine dynamometer system. It is found that the time delay affects the performance of the closed-loop control, leading to undamped oscillations in the dynamometer response.

In [GdRK+06], the authors consider the problem of shaping the reference trajectory produced by the dynamic simulation algorithm to ensure that the performance limits of both the hardware under test, and the test-bed itself are not exceeded. This is a good idea for two reasons. Firstly it is clear that any dynamometer will have limits to its performance, and if the test trajectories

which are proposed exceed the possible performance of the dynamometer (in terms of slew rate of torque or speed for example) then the test-bed will fail to track the reference accurately and the results of the test cycle will not be representative. This fact may not be apparent to the dynamometer operator and so misleading results may be propagated. The second reason to bound the dynamometer control reference is that it is possible that a particular test trajectory could lead to damage of either the hardware under test, or the test-bed itself. The authors present the shaping process in three stages. First is the definition of a pre-filter which is applied to the torque and speed measurments and whose purpose is to provide smoothed signals which can be numerically integrated. The smoothed signals are used in an inverse model to calculate the input which will be required to achieve the desired trajectory. These predictions are compared with the performance limits to establish feasibility. Finally the performance limits are enforced by the application of a Kalman filter which responds to the potential breech of performance limit by modifying the trajectory by modifying the shaft-torque state, engine speed state or both.

This principle model based mode of operation has been extended in different ways using novel combinations of hardware as well as more specialised simulation models. For example, [JZJ+05] presents a method for testing the operation of a vehicle's traction control system using a wheel-hub Dynamometer. The simulation model provides a load reference which imitates tyre slip due to a split coefficient of friction between two driven tyres. This can be designed to represent the vehicle losing traction and so will provoke the traction control system to operate. The operation of the vehicle traction control system can therefore be simulated in the laboratory, and the calibration of the traction control system can be studied in a repeatable environment.

When testing is carried out using a chassis dynamometer, the control system is usually only required to provide simulation of the road-load since all of the dynamic components of the powertrain are present during testing. In this case, inertia simulation is the most significant control challenge.

Inertia Simulation

Inertia simulation is a challenging aspect of dynamic simulation in transient dynamometer testing. If the inertia of the rotating mass of a dynamometer system deviates from that of the test

vehicle which is being simulated, then the transient behaviour of the system will not be realistic and so the inertia must be simulated. This may be done physically, by tuning the mass of the system, or electronically where the inertia load becomes part of the simulated dynamic loading which is applied by an active PAU.

There are two common ways of providing physical inertia simulation. The first approach is to design a dynamometer with exactly the required physical inertia to match the vehicle or powertrain components under test. In this case, the PAU is responsible only for applying road-load forces and any dynamic loads which are required for driveline simulation. The problem faced when considering this type of system is its lack of flexibility for the system to be used to examine other vehicles or components.

Dynamometer systems which have variable physical inertia have been used, particularly in chassis dynamometers. In this case, flywheels are usually mechanically switched into and out of the system using gearbox and clutch systems. This configuration has the advantage of providing scope for inertia tuning (although only in discrete intervals), but suffers from added complexity and cost. Also, the dynamics of the system, its gearboxes, shafts and clutches, becomes inherent to the gathered results and may interfere with dynamic simulation tests, especially when the torsional behaviour of the driveline is of interest.

Electrical dynamometers, and advances in the speed and performance of torque control which may be achieved using them, have opened the way for a third inertia simulation approach. Here the dynamometer has a fixed inertia (usually lower than that of the typical test vehicle) and a PAU which is capable of high speed torque control. The dynamometer simulates the inertia of the vehicle by applying a torque which is proportional to the angular acceleration of the system. This type of system has the benefit of operational flexibility and is the most commonly applied solution in modern dynamometer systems. However, for highly transient testing, the performance of the PAU torque control must be very high due to the large magnitude and very rapid rates of change which may be seen in the load trajectory.

In the case of Chassis dynamometer testing the challenge of inertia simulation is particularly difficult. The inertia of the vehicle on the road is directly replaced by the inertia of the rolls, plus inertia simulation applied by the PAU. During transient tests, simulated inertia loading will

be the dominant load applied by the PAU, especially at low road speeds, and will typically have a rate of change which is orders of magnitude faster than that due to other road-load forces.

In addition to presenting significant challenges in relation to the speed of tracking performance which is demanded of inertia simulation other practical problems exist. The Inertia simulation algorithm requires a real time measurement of angular acceleration which cannot be taken directly. The angular velocity measurement provided by the main shaft encoder or tachometer can be numerically differentiated online, but this approach is sensitive to signal noise as well as minor speed fluctuations caused by external disturbances. The result of this is that the calculated acceleration may often be unusable in its raw state. For this reason, carefully considered signal processing must be applied to smooth the speed signal prior to numerical differentiation.

1.6 Closed-Loop Dynamometer Control

The literature reported in Section 1.5 provides insight into the process of selecting an appropriate mode of testing and creating control references for the dynamometer regulator, but does not address the important process of establishing a system for tracking the set-point or reference. It is well known that feedforward control methods present advantages in terms of speed and efficiency, but they are also limited by their high sensitivity to both internal and external perturbations. For this reason, closed-loop feedback control is almost universally applied to the dynamometer control problem.

For successful dynamometer control, the load simulation model must be complemented by a feedback-loop which exhibits two important properties:

1. **Performance** - the time response of the closed loop control must be sufficiently fast to track rapidly changing references.

2. **Robustness** - the performance and stability of the control loop must be robust to the non-linear characteristics of the dynamometer which often lead to significant plant uncertainty.

The application of feedback control to the dynamometer torque problem has been described by a number of authors. Early examples of this can be found in [MF37] and [MF50]. Later

studies [BT83] used experimentally derived information from step-response tests along with the Zeigler-Nichols design method to define fixed parameters for PID controllers.

It was found in the course of these studies that system nonlinearity would force the operator to re-tune the parameters of the controller when moving between set-points during a testing program. The implementation of this can be simplified from an operational perspective by scheduling controller gains using a look-up table but not without associated problems. These include system perturbations caused by the transition from one set of controller parameters to the next. These problems can themselves be lessened by using so called 'bumpless transfer' strategies which often involve resetting the output of the integrating elements of the controller. The problems associated with scheduled control tend to be be worse when the testing application is transient, since the operating point of the dynamometer may be continuously changing.

Adaptive and Self-Tuning Control

In order to overcome the shortcoming of scheduled, fixed-parameter controllers when applied to the nonlinear dynamometer system, adaptive or self-tuning control has been explored [TRFV90]. In adaptive control a recursive estimation algorithm is used to update an online plant model (often of a simplified nature) which is in turn used in an appropriate algorithm which calculates and modifies the controller parameters accordingly [TVRF92]

In a series of publications [KBJ+91a],[KBJ+91b],[KBJ+], an eddy-current dynamometer system is controlled using self-tuning control. An adaptive pole-placement technique is used along with on-line system parameter estimation using a recursive Kalman Filter. The method is applied in real-time to an engine-dynamometer and shows that significant improvements can be achieved compared to a fixed PID controller which is retuned manually.

Improvements to this method are presented in [Kin92]. A three dimensional map of the dynamometer speed and torque dependency is derived using steady-state spot point measurements taken from the open loop engine dynamometer system. The map is then used to provide *a priori* information about the likely parameters of the plant model to the estimation stage of the self tuning control algorithm.

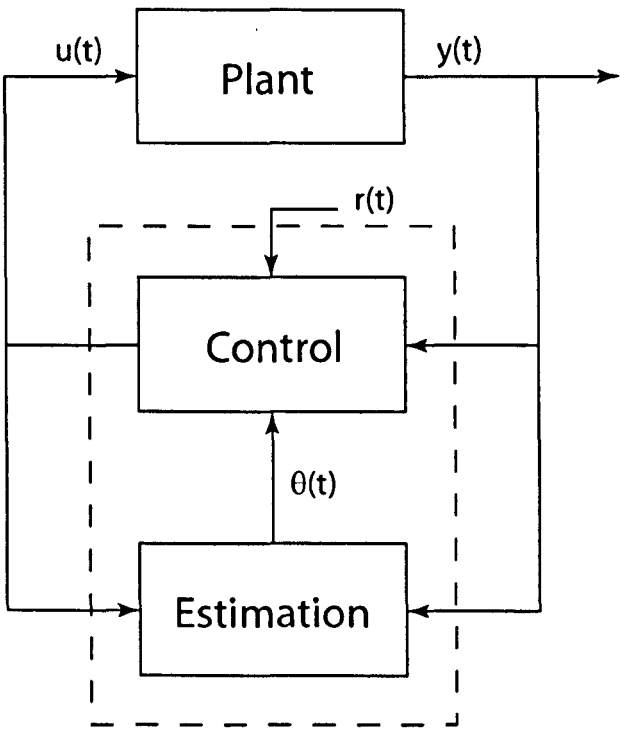

Figure 1.19: Generalised Self-Tuning Control Scheme

Multivariable Speed-Torque Control

In some circumstances, such as emissions testing cycles, the dynamometer control problem becomes a multivariable problem. In these cases it is typical for speed and torque to be simultaneously controlled. The control channels are usually the torque actuator of the dynamometer, and throttle position of the test engine.

In [SNP96] the authors propose a method which decomposes the speed and torque control channels of the engine-dynamometer system into fast (torque) and slow (speed) subsystems which can be characterised by large and small eigenvalues respectively. A two stage design procedure is used to assign eigenvalues for the two subsystems from which two separate feedback controllers are designed and applied to a theoretical model of the engine dynamometer system.

In [BFT97], the testing objective is to track pre-specified engine speed and torque trajectories such as those seen in the US EPA FTP Cycle. The engine-dynamometer consists of an eddy current dynamometer which is coupled to a large (8.3L) turbocharged diesel engine. The problem is treated as a robust multivariable control problem with the dynamometer excitation and engine fuelling as input control channels. The authors develop a simplified frequency domain model

using system parameter identification which is applied to an existing model structure. The non-linear dynamics of the coupled engine-dynamometer are handled by modelling the plant as an uncertain LTI system. A sequential controller design method is applied, with the 2 dimensional multivariable control design problem solved by performing a pair of single loop control designs using a QFT loop shaping technique. The candidate controller is implemented in the dynamometer control hardware and tested using step response tests and an example transient emissions testing cycle. The results of the step response tests show that fast speed control can be achieved using this method, although the torque response is less impressive. In the case of the example transient test cycle, reasonable speed control is achieved although it is affected by a steady-state offset when tracking ramp references.

The same multivariable dynamometer control problem is considered in [NSHT00], where the authors present a control method for engine speed and torque for an engine-dynamometer system using a decoupling control strategy. In contrast, [Yan98] argues that decoupling the control loops may be undesirable in some situations and applies Model Reference Adaptive Control (MRAC) to the speed-torque control of a Turbocharged Diesel Engine Dynamometer system. The control method is applied to a simulation model showing encouraging results, although no experimental validation is offered.

1.6.1 Chassis Dynamometer Control

The body of work which has been published in relation to Chassis dynamometer control is limited. The focus of many publications in this field has been that of generalized control strategies which acknowledge the role of feed-forward and feedback control along with generalised road-load simulation. A pair of SAE papers [DG81, TOO80] discuss the development of a total road load algorithm for feed forward control. The authors acknowledge the requirement for a feedback element for regulation of steady state error and tracking performance. These studies give limited analysis of the requirements of the feedback system or analysis of the procedure for a successful controller design, but do establish the basic requirements of a chassis dynamometer which is to be used in transient testing applications.

A significant number of references to chassis dynamometer control can be found through a

patent search, for example [FD79, Bel95, Car01, SM02]. Among these examples, [Car01] stands out by advocating the usage of a model based control system with a PID controller for the feedback element, although no methodology for the design of this controller, or discussion of robustness or performance is included.

In addition, standards have been defined in relation to chassis dynamometer performance required for standardized emissions tests where inertia simulation is necessary [Age91, DBM96, AB+00].

The dominance of patents published on the subject compared to academic journals and conference papers and other detailed technical articles highlights one of the possible reasons why there is little published information related to this subject, namely commercial sensitivity. The organizations which are actively engaged in chassis dynamometer development may not sense any strategic advantage in sharing their methods or findings with the public domain. This is understandable given the competitive nature of the automotive industry and the sensitivity which dynamometer manufacturers have about the relative performance of their own product in comparison with their competitors.

1.7 Standardisation in Testing and Automation

Recently there has been a concerted effort made within the automotive industry to define standardised conventions, methods and procedures for testing and automation systems. This emerging standardisation is consistent with the trend for developing a standardised set of protocols such as those for communications (e.g. CAN(Controller Area Network), LIN(Local Interconnect Network) and MOST(Media Oriented Systems Transport)) which have a universal meaning and application within the industry. The Association for Standardisation in Automation and Testing (ASAM) continues to define standards which are applicable to Dynamometer systems [Tsc05]. The ASAM standards define means for creating common understanding across a full range of technical functions within the field of testing and automation. In its simplest form, this provides universal descriptions to define control signals, status flags and feedback variables. The extension of this is the development of standard Application Programmers Interfaces (API)

to allow systems integration between hardware and software to be more fully achieved within a modular testing arrangement built from components developed by different companies. At this time, ASAM compliance should be seen as an important feature of a commercial dynamometer system.

1.8 Example Dynamometer Control Problems

The requirement for high performance dynamometer control has been highlighted by considering the nature of modern automotive development challenges, many of which have increased emphasis on transient events. The following section describes two dynamometer control problems which will form the basis of the work presented in this thesis.

The first example relates to Chassis Dynamometer control. High performance robust transient tracking control is required for road-load simulation. The second relates to a specific engine dynamometer control problem where a steady-state set point is tracked in the face of significant disturbances and noise.

1.8.1 Chassis Dynamometer Control: High Speed Torque Tracking

Driveability defines the perceived quality of a vehicle with respect to performance and comfort and is usually reserved for description of functions related to the Powertrain. Customers are increasingly discerning about vehicle quality, and much work has been done to establish metrics for the characterization of those aspects of a vehicle which affect driveability [LS98, DH99].

Many driveability challenges relate to transient performance of the driveline, a key example is the Shuffle mode. Shuffle is characterized by a longitudinal oscillation, usually around 5-15Hz, which is linked to the first torsional mode of the driveline when excited by torque transients delivered by the engine [CMP96]. Shuffle has arguably become a greater problem in modern vehicles where the driveline has been optimised for efficiency, leading to a system with reduced viscous friction which would otherwise act as a damper on the shuffle mode. The study of shuffle phenomena is ongoing, and is still considered a challenging issue for calibration engineers who must tune the driveability strategy while continuously constrained by emissions regulations and performance criteria.

Transient chassis dynamometer testing in the study of this problem offers the advantage of the controllable laboratory environment, with the scope for repeatable testing which may otherwise not be possible. Access to heavy equipment such as emissions testing systems may be impractical and repeatible testing may be difficult on a test track, or public road[WJ72, D$^+$00, DM00, Tho02]. It is clear therefore that high performance transient dynamometer torque

control must be available for the accurate replication of road-load conditions in the laboratory. Inertia simulation [DG81, DBM96, TMR02] is of specific importance in this application since the transient rates of change in acceleration may be locally very significant and as such, the controller must be fast enough to ensure that the inertial loading is 'in-phase' with the transient event. Some authors [PM01] have cast doubt upon the fundamental suitability of the chassis dynamometer for this mode of testing. However, as the level of performance of the dynamometer control system increases, the results which may be achieved may be expected to converge with those observed 'on the road'. The way in which this may be achieved is by providing the fastest possible level of performance through the reduction of response time.

Problem Outline

The Liverpool Chassis Dynamometer studied in this thesis is being continuously developed as a tool for transient testing applications. Within the dynamometer control hardware there is significant flexibility in terms of implementation, and customization through the use of a rapid control prototyping system. For these reasons, it is considered an excellent platform for investigating the potential of modern modelling and control techniques applied to the Dynamometer control problem.

The US EPA provide guidelines for the torque response of chassis dynamometers where inertia simulation is required. These metrics have therefore been adopted as benchmarks for the evaluation of the performance of candidate controllers considered in this thesis.

In addition to the challenges of modelling and control, signal processing issues are important because of the superimposed dynamics of the torque sensor arrangement.

1.8.2 Engine Dynamometer Control: Zero Shaft Torque Control

The zero shaft torque control (ZTC) problem involves simulating an engine at idle on an engine-dynamometer system. The objective is to control the shaft torque to zero and as such simulate the condition where the engine is decoupled from the driveline. This is equivalent to operating the engine in a de-clutched condition, when in reality the engine is mechanically coupled to a dynamometer with a significant excess of physical inertia. The idling condition forms part

of many transient testing cycles and so the dynamometer must be capable of simulating this specific condition while maintaining the capability to operate at all other load and speed conditions required. Idle speed testing has commonly been carried out using special low inertia dynamometers which provide optimised conditions for testing at this operating point, but which are incapable of operating over the broader range of torque and speed which is required by modern emissions testing cycles. The zero shaft torque control problem is characterised by the following considerations:

- **Inertia compensation** - the additional inertia of the dynamometer drive shaft, the torque transducer, couplings and the inertia of the dynamometer itself must be compensated for by providing a corrective torque which is proportional to the angular acceleration of the system.
- **Shaft Dynamics** - In addition to inertial effects, compensation for the shaft dynamics of the dynamometer must be made. Structural oscillations in the shaft will cause periodic fluctuations which are excited by the crank pulsing of the engine torque output.
- **Controller Interaction** - Interaction between the test engine's idle speed control system and the dynamometer torque control loop which may be antagonistic must be minimised.
- **Stochastic Combustion Effects** - The stochastic behaviour of the engine at low speeds may introduce chaotic torque fluctuations to the system and may require attenuation.

Problem Outline

When operating in zero shaft-torque conditions, torque fluctuations about the set point reference are significant, with a maximum amplitude of around 15 Nm. The objective of the work carried out here was to study how the magnitude of the shaft torque fluctuation could be reduced through the application of improved feedback control strategies.

The requirement was to achieve performance which was better than that of the existing engine dynamometer controller (EDC) and therefore to provide evidence of the potential improvements which could be achieved through a systematic modelling and control methodology.

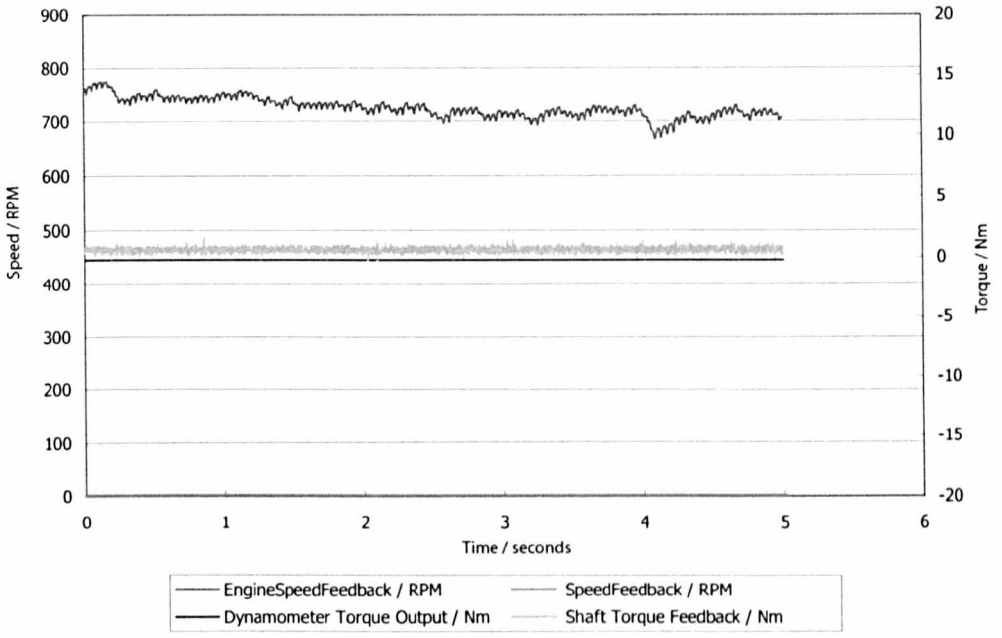

Figure 1.20: Target ZTC performance

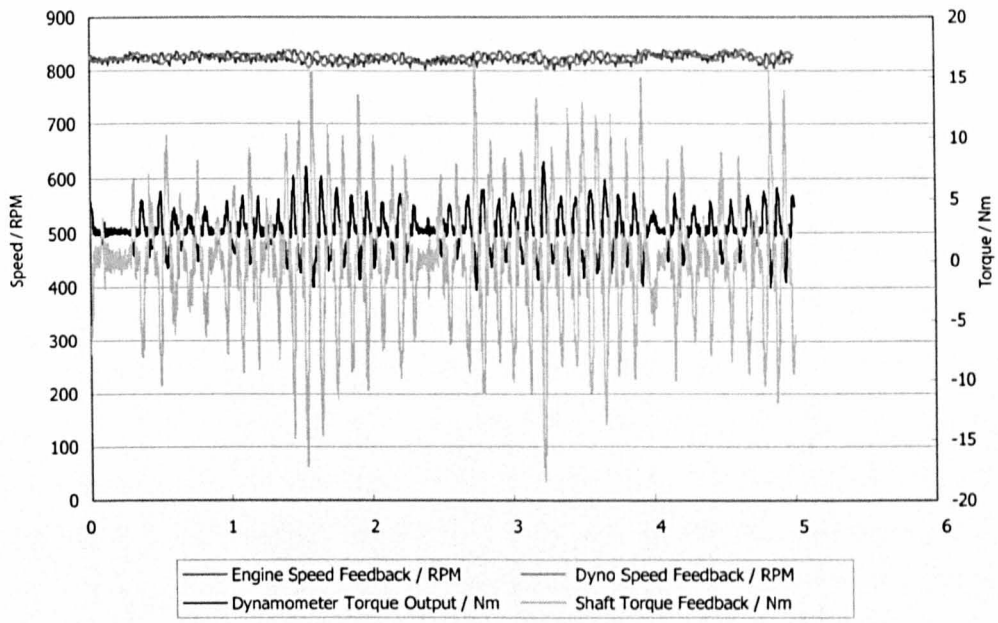

Figure 1.21: Existing ZTC control strategy

The zero shaft torque control work discussed in this project was performed in conjunction with SRH systems who provided background information and a design brief, relating to desired performance improvements. All of the system identification experiments and controller implementation and testing was performed by the partner organization's engineers using testing facilities located in Kyoto, Japan.

Chapter 2

Overview & Contributions

2.1 Overview of Thesis

The structure of the remaining parts of the thesis is as follows:

- Part I - Introduction

  The remainder of Part I of this thesis comprises of three sections which are designed to deliver relevent background to the techniques which were used in the dynamometer control methodology which is applied in Part II and Part III.

  - Chapter 3 - System Identification

    Provides a review of the topic of linear black-box system identification. This includes an overview of the individual steps involved in the linear identification process along with detail regarding appropriate model structures.

  - Chapter 4 - Control

    Delivers a background review regarding the standard feedback control problem. The popular $\mathcal{H}_\infty$ control paradigm is discussed with reference to two different approaches to its application, namely $\mathcal{H}_\infty$ Parameter Space and the $\mathcal{H}_\infty$ Algebraic Riccati Equation method.

  - Chapter 5 - Filtering Introduces selected topics in the field of filtering. An overview of both causal and non-causal frequency domain filtering is provided. The Kalman

filter is introduced in two different forms.

- Chapter 6 - Experimental Set-up Delivers an overview of the hardware arrangements which were used in each of the two dynamometer control problems which are presented in this thesis.

- Part II - Chassis Dynamometer

This section describes the development of a transient torque controller for the Liverpool chassis dynamometer.

- Chapter 7 - Chassis Dynamometer System Identification

  Describes the characterisation, linearisation and system identification work which was carried out in order to establish an appropriate frequency domain model of the chassis dynamometer.

- Chapter 8 - Chassis Dynamometer Torque Control

  Describes the design of two different robust feedback controllers which were designed for the Liverpool chassis dynamometer. The first controller is a third order controller designed using the $\mathcal{H}_\infty$ Parameter Space design method. Early results achieved using this method are presented to illustrate the improvements which were achieved through the implementation of Direct Inverse Compensation to linearise the system. The final controllers are presented using a novel augmented feedback structure which incorporates a Kalman filter for attenuation of oscillatory sensor noise. The controller is implemented and tested on the Liverpool chassis dynamometer.

  The second design which is presented is a full order controller designed using the $\mathcal{H}_\infty$ Algebraic Riccati Equation method. The full order design is compared with the low order of the $\mathcal{H}_\infty$ Parameter Space controller to investigate the potential performance improvements which can be achieved with an increased order solution.

- Part III - Engine Dynamometer

  This section describes the development of a zero shaft-torque controller for an active DC engine dynamometer.

  - Chapter 9 - Engine Dynamometer System Identification

    Describes the characterisation and system identification work which was carried out in order to establish an appropriate frequency domain model of the engine dynamometer.

  - Chapter 10 - Engine Dynamometer Zero Shaft-Torque Control

    Describes the design of three different sets of robust feedback controllers which were designed for implementation and testing on the SRH Kyoto Engine dynamometer. The first set of controllers are $\mathcal{H}_\infty$ Parameter Space controllers with a comparable structure to the PI/PID structure used in the existing engine dynamometer controller. The second set of controllers are $\mathcal{H}_2$ optimised controllers which are designed to explore the benefits of minimum variance control on the zero-shaft torque control problem. Finally a novel SIMO feedback structure with $\mathcal{H}_\infty/\mathcal{H}_2$ controllers is proposed and a set of designs are performed to generate candidate controllers for testing and evaluation. Each set of controllers is implemented and tested on the engine dynamometer and results are presented.

- Part IV - Conclusions

  Conclusions regarding the key findings and contributions of the work presented in this thesis are summarised.

2.2 Contribution of Thesis

This thesis presents a systematic methodology for the design and implementation of control strategies applied to automotive dynamometer systems. The underlying methodology has general applicability and should be suitable for the design of feedback controllers for most dynamometer types. In order to show the effectiveness of the method, it is successfully tested using two real dynamometer control problems. It is shown through the treatment of these prob-

lems that the application of modern signal processing, system identification, modelling, control and implementation methods provide a useful systematic framework for the development of dynamometer control systems.

2.2.1 Chassis Dynamometer Torque Control

The work presented in this thesis which relates to the development of a chassis dynamometer torque controller represents the first of two a novel studies into how a systematic model based approach may be applied to significantly improve the achievable performance of the torque control loop. The proposed methodology uses linear black-box system identification to develop suitable plant models for controller design. Two different variants of the modern $\mathcal{H}_\infty$ control paradigm are applied to the design of robust feedback controllers for torque tracking. In both cases the results are shown to exceed the US EPA legislative acceptance requirements for dynamometer torque control response by some margin. The following summary highlights the key contributions which the presented work has made to the field:

- An example of how black box linear system identification can be used to develop validated models of a DC dynamometer.
- An example of how simple inverse compensation scheme may be effective in significantly reducing the degree of uncertainty in a set of identified LTI system models for a dynamometer system.
- Confirmation that the structural dynamics of the torque measurement arrangement typically used in Gimble mounted dynamometer systems may superimpose significant oscillatory components onto the feedback from the system.
- The application of non-causal filtering for the removal of the coloured sensor noise disturbances from data in the pre-processing stage of the system identification process.
- The application of model based Kalman filtering as a solution for attenuating the coloured sensor noise which is associated with the torque measurement system. In addition, it is shown how this model based filter may be implemented as part of an augmented closed loop structure without affecting the stability of the system.

2.2.2 Engine Dynamometer Shaft Torque Control

The second experimental study presented in this thesis shows how the methodology has general applicability through its application to a distinctly different dynamometer control problem. The zero shaft torque control problem was studied in collaboration with a partner organisation, SRH Systems. The partner organisation performed the experimental work using hardware based in Kyoto, while the modelling and design activities were all performed remotely in Liverpool. The presented methodology follows the same sequence of system identification and controller design as in the chassis dynamometer work, but is tailored to the specific control problems which the engine dynamometer presents. Linear black-box identification is successfully applied in order to model the plant and is found to be an effective and efficient way of characterising the important dynamics of the system. Three different sets of trial controllers are designed using $\mathcal{H}_\infty$ and $\mathcal{H}_2$ methods. The controllers were implemented and tested on the SRH engine dynamometer based in Japan. The results illustrate how the application of a systematic modelling and design procedure can improve the performance achieved using both low order and modern full order controller solutions. The following summary highlights the key contributions which the presented work has made to the field:

- An example of how, through collaboration with engineers in a remote location, a successful modelling and control control methodology can be applied without direct access to the test hardware.

- An example of how a methodical design process, such as that offered by the Parameter Space technique, can be used to better design three term controllers such as the PID which is applied in the existing engine dynamometer controller.

- The proposal of a novel SIMO feedback control structure for the zero shaft torque control problem. This approach combines two different control loops which affect a single control actuation channel. Both $\mathcal{H}_2$ optimised MV control and $\mathcal{H}_\infty$ optimised tracking control are applied using the Algebraic Riccati Equation design method. The results achieved using this control structure are shown to exceed those obtainable through single loop SISO designs.

Chapter 3

System Identification

3.1 Introduction

In this section, suitable system identification methods for generating frequency domain models of the Chassis Dynamometer and Engine Dynamometer are presented. The system identification process was carried out using the Matlab System Identification Toolbox. The methodology used follows the flowchart(Figure. 3.1) which is similar to that described by Stoica and Söderström [SS89] and separately by Ljung [Lju99] outlining the generalised system identification process. The diagram illustrates the basic steps associated with system identification and illustrates the iterative nature of the process, as well as the role which *a priori* knowledge of the system can have in informing decisions made at various stages in the process. The following subsections provide outline discussion of each of the stages of system identification process as described in Figure. 3.1. Following on from this, the system identification methodology is applied directly to the Chassis Dynamometer and Engine Dynamometer systems, and black-box models are generated, and validated.

3.2 Black-Box System Identification

The Black-Box modelling approach assumes no prior physical understanding of a system and both the model structure and parameters are determined by using system identification methods. This approach is wholly reliant upon the use of input-output data collected from the real system,

and the resulting model parameters are not directly related to phenomenological characteristics of the system. The advantage of this type of modelling approach is that it can be used to establish system models where there is either a partial or complete lack of physical insight into the system. The usefulness of black-box modelling is not limited to situations where physical insight is limited or absent. It may also be a fast way of establishing a model or set of models for controller design.

3.3 Design of Experiment

For the system identification modelling approach to be successful, the experimental tests which are performed must be carefully designed. *A priori* knowledge of the system is clearly an advantage when designing the experiment but is not always available. In situations where the properties of the system are poorly understood, the design of the experiment becomes part of the iterative system identification process. For example, the selection of perturbation signals and data acquisition factors, such as sampling frequency, are often associated with presumed knowledge of the system bandwidth which may not initially be known. In this case an initial set of identified system models, even when sub optimal in performance, may provide useful information regarding changes which should be made in the design of the experiment to improve the model which is achieved on the next iteration.

3.3.1 Perturbation Signals

The input signal for system identification is an extremely important factor in the quality of the model which can be achieved. As such, it must be carefully selected. There are three key considerations which must be made when selecting an input signal. These are discussed below:

1. **Frequency Content**

   For the dynamics of the system to be correctly identified, the power distribution of the input data must be sufficiently rich across the frequency range of interest that it will excite the system across its bandwidth, and therefore provide a characteristic response. The use of step type input signals has been commonly adopted for this reason, as they are naturally

rich in frequency content(as seen in the reconstruction of a square wave function through infinite superposition of sinusoidal components). The input is often described in terms of a sampled, filtered white noise source because this type of signal is known to contain a very wide range of frequency contents. Signals such as the Pseudo Random Binary Signal (PRBS) and the multi level Random-Walk Input have been commonly adopted for this reason.

2. **Amplitude**

   In many linear system identification applications, the amplitude of the input signal is limited to a small range, and in the case of a (PRBS), to only two distinct levels. This provides sufficient information for the information of linear systems since the response of a system is directly proportional to the input. In reality however, few real systems are linear and so a linear model is often only valid for a small input range.

   If a set of linear models are to be identified, which will define the nonlinear system as a linearised system over a range of operating conditions then the amplitude may be varied in order to capture the uncertainty in the system response, due to nonlinearity.

   If the system is linearised using some other method, such as inverse compensation, then the linearised system may be identified using the same types of input. In this case it is still common to identify the system at a range of operating points, since this will still provide information about the model uncertainty required to represent residual nonlinearity due to imperfect linearisation.

   An alternative approach to the PRBS type of input is a multiple level input such as the so called random-walk input. This type of input may be particularly suited to systems where a non-zero input mean may lead to a saturated response (e.g. integrating systems) or cause the system to leave its safe or desirable operating envelope (e.g. exceeding maximum roller speed).

3. **Sampling Rate**

   The selection of an appropriate sampling rate is important since it defines the resolution at which response information will be collected. A typical guideline [Lju05] for this is that the

sampling rate should be around 10 times the approximate bandwidth of the system, or put another way, there should be between 4 and 6 samples along the rise time of the system. This means that the rate of change of the input signal must be designed to match the sampling rate. It may sometimes be desirable to oversample (use a higher than necessary sampling rate) in order to allow the user to decide later what degree of down sampling is appropriate to achieve a successful model. An excessively fast sampling rate may lead to high order models due to over parametrisation which occurs when the sampling frequency is inappropriately high compared to the bandwidth of the system. In this case a lower order model which is equally effective can be identified using data which has been downsampled. For binary input signals where the input exists at only two discrete levels, the frequency with which the state can change will be an integer multiple of the sampling frequency. This must be carefully selected to ensure that following a change in the state of the input signal, it is maintained for long enough for the characteristic response of the system to be seen. Likewise, the maximum duration (in terms of samples) for which the input may stay at one level should be limited. This is known as a Maximum Length PRBS or MLPRBS.

3.4 Data Preprocessing

Raw data which has been collected for system identification may not be immediately suitable for use with an identification algorithm and will often require processing to make it suitable. The following section discusses some of the typical issues which may require preprocessing and the common strategies which are applied to treating the data.

3.4.1 Removal of Offsets and Trends

Offsets in system identification data are steady state, or slowly varying, bias which affect the input/output data. The presence of offsets or trends can have a negative effect upon the quality of the estimate achieved in linear system identification and so should be removed.

Where there is a constant offset or bias, caused for example by the physical units of a measurement such as absolute pressure or temperature then a practical and straightforward method of processing is to simply subtract the mean of the data from each sample, re-basing the

data at zero. For slowly varying trends, such as low frequency disturbances, then the solution may be to explicitly fit the disturbance with a linear function and to normalise about the varying mean values. For low frequency disturbances, low-pass or band-stop filtering may be another practical solution to the problem (see 3.4.3).

3.4.2 Removal of Outlier Points

Outlier points are anomalous pieces of data which are caused by measurement errors or localised anomalous events (for example misfires in an IC engine) in the system being identified. They can have a severely detrimental effect upon the model estimate and so sections of data containing outliers should either be avoided, or if it is not possible to find a suitable set of 'clean' data then the outliers can be dealt with as 'missing' data points. Solutions for dealing with this scenario are expanded upon in greater detail by Ljung[Lju99].

3.4.3 Prefiltering

Unwanted frequency components of the identification data, such as those associated with known external noise sources or disturbances, can be attenuated or eliminated from the data using filtering. According to Ljung [Lju99], filtering both the input and output data through the same filter does not affect the input output relationship, provided that the system is linear. The type of filter which is used depends upon the specific application, and the type of disturbance which is present in the data. For sampled data systems, an anti-aliasing filter should be applied, with a cutoff frequency at half of the sampling frequency (or Nyquist frequency). This eliminates ambiguous or 'folded' frequencies caused by aliasing of high frequency components at lower frequencies. If the data contains noise or disturbances at well defined frequencies then band-stop filter may be applied to achieve targeted attenuation of specific frequency bands. Similarly, if it is desirable to identify dynamics in a particular frequency range then a band-pass filter can be applied. This attenuates frequencies either side of the pass band and can be used to eliminate both low frequency disturbances and high frequency noise simultaneously. The topic of filtering is revistited in some more detail in Section 5.

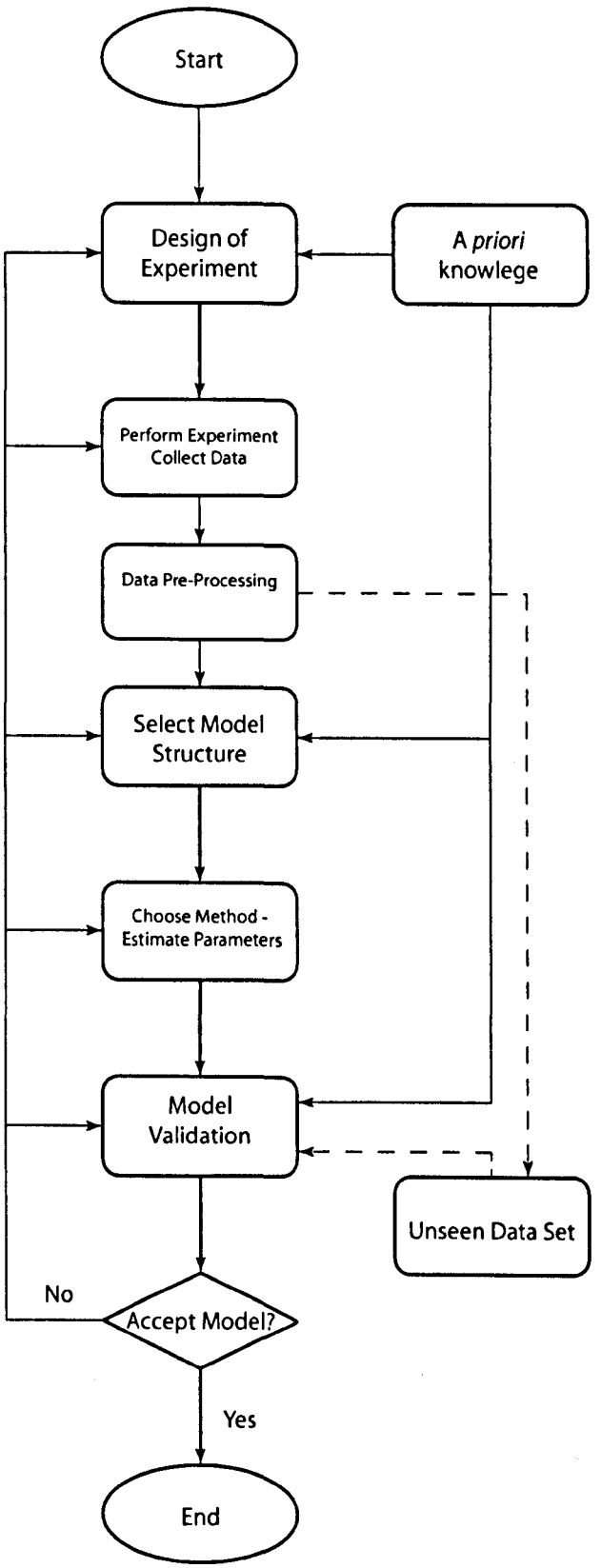

Figure 3.1: Generalised System Identification process

3.5 Linear Polynomial System Structure

The most popular linear model structures which are used in dynamic system identification are polynomial structures describing discrete systems. It is most convenient to work in terms of discrete systems, since data is sampled at discrete intervals, but discrete systems can be easily converted into continuous models (in terms of the Laplace operator s) afterwards. The Matlab System Identification Toolbox [Lju05] provides means for performing system identification using any of the three most common polynomial structures, Box-Jenkins (BJ), ARMAX and ARX.

A generalised polynomial model, representing a MISO system can be expressed as

$$A(q^{-1})y(t) = \sum_{i=1}^{nu} \left(\frac{B_i(q^{-1})}{F_i(q^{-1})} u_i(t - nki) \right) + \frac{C(q^{-1})}{D(q^{-1})} e(t) \tag{3.1}$$

3.5.1 Box-Jenkins Model

The Box-Jenkins (or BJ) model is a special case of the generalised polynomial model type. In the BJ model, $A(q^{-1})$ is set to unity. Equation.3.2 shows a SISO formulation of the BJ model structure.

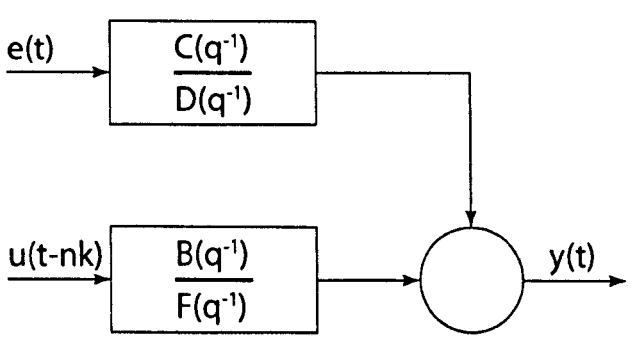

Figure 3.2: Box-Jenkins Model Structure

$$y(t) = \frac{B(q^{-1})}{F(q^{-1})} u(t - nk) + \frac{C(q^{-1})}{D(q^{-1})} e(t) \tag{3.2}$$

Where,

$$B(q^{-1}) = b_1 q^{-1} + ... + b_{n_b} q^{-n_b+1} \tag{3.3}$$

$$C(q^{-1}) = 1 + c_1 q^{-1} + ... + c_{n_c} q^{-n_c} \tag{3.4}$$

$$D(q^{-1}) = 1 + d_1 q^{-1} + ... + d_{n_d} q^{-n_d} \tag{3.5}$$

$$F(q^{-1}) = 1 + f_1 q^{-1} + ... + f_{n_f} q^{-n_f} \tag{3.6}$$

Where i, j, k and l are polynomial parameters $i = 1, ..., n_b$ $j = 1, ..., n_c$ $k = 1, ..., n_d$ $l = 1, ..., n_f$. The order of each polynomial defined by n_b, n_c, n_d and n_f. The delay order of the system is defined by n_k in terms of the number of samples in the time delay.

3.5.2 ARMAX Model

In the ARMAX model, the denominators $F(q^{-1})$ and $D(q^{-1})$ in the generalised polynomial, and BJ models, are set to unity, leaving the single common denominator $A(q^{-1})$. The ARMAX model is therefore a further more specialised case of the generalised polynomial model structure.

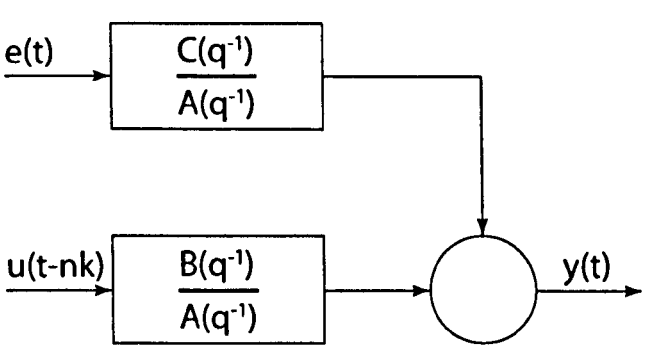

Figure 3.3: ARMAX Model Structure

$$A(q^{-1})y(t) = B(q^{-1})u(t - nk) + C(q^{-1})e(t) \tag{3.7}$$

$$y(t) = \frac{B(q^{-1})}{A(q^{-1})}u(t - n_k) + \frac{C(q^{-1})}{A(q^{-1})}e(t) \tag{3.8}$$

The polynomials are defined by;

$$A(q^{-1}) = 1 + a_1 q^{-1} + ... + a_{n_a} q^{-n_a} \tag{3.9}$$

$$B(q^{-1}) = b_1 q^{-1} + ... + b_{n_b} q^{-n_b+1} \tag{3.10}$$

$$C(q^{-1}) = 1 + c_1 q^{-1} + ... + c_{n_c} q^{-n_c} \tag{3.11}$$

Where i, j and k are the polynomial parameters $i = 1, ..., a_n$ $j = 1, ..., b_n$ with the order of each polynomial defined by n_a, n_b and n_c.

3.5.3 ARX Model

The ARX model is a highly simplified special case of the generalised polynomial linear model. The colouring filter for the disturbance channel is simplified by setting $C(q^{-1})$ to unity.

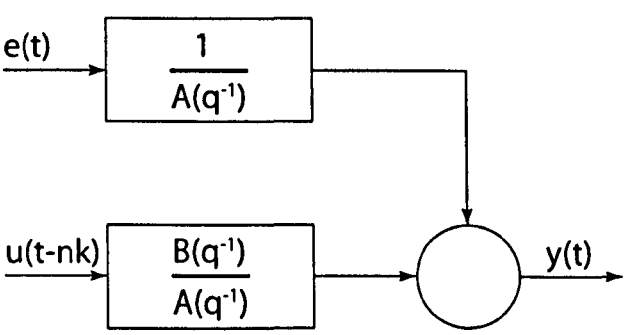

Figure 3.4: ARX Model Structure

$$A(q^{-1})y(t) = B(q^{-1})u(t - n_k) + e(t) \tag{3.12}$$

$$y(t) = \frac{B(q^{-1})}{A(q^{-1})}u(t - n_k) + \frac{1}{A(q^{-1})}e(t) \tag{3.13}$$

Again, i and j are polynomial parameters $i = 1, ..., n_a$ $j = 1, ..., n_b$, with the order of each polynomial defined by n_a and n_b.

In each of the model structures described above, the usage of model order parameters, n_a,

n_b, n_c, n_d, n_f and n_k are consistent with the conventions of the Matlab System Identification Toolbox.

3.6 Order Selection and Model Validation

Having established which type of linear system structure is suited to a specific system identification problem, the matter of determining system order, and therefore the appropriate number of parameters, becomes the next matter of interest. Put simply, this process determines the complexity of the system, and ensures that the system dynamics are properly represented. The order selection process is an example of the truly iterative nature of the system identification process, since the correct model order can often only be decided by actually comparing the results given by a range of model orders, and selecting the final model order by analysis of the results. *A priori* information about the system can be useful when determining a starting point for the range of model orders to be considered. Furthermore, the boundaries between model order selection and model validation are blurred since many of the processes involved are identical.

The distinction which can be drawn between order selection and model validation is that the latter process will typically form the final iteration of the process. Once the model order has been selected, the validation process will be used to provide final confirmation of the effectiveness of the model structure and order selected. In both structure selection and model validation, tests should be performed against unseen input-output data, collected from the system during tests at the same operating point. Unseen data has not been used in the parameter estimation process, thus ensuring that the identified model has general applicability to the system.

Typically, model order selection and validation is performed using a combination of criteria which help to assess how good a finite parameter linear model approximates the real system. Part of this process is inevitably a matter of common sense and experience, but some quantitative analysis can be performed in order to help make an objective choice. The quantitative analyses which are used in order selection can be set in terms of three criteria, discussed in the following subsections.

Quality of Fit

Quality of fit is used to describe how well the model recreates the dynamics of the system, in terms of closeness of fit. Initially, this can be best judged by visual comparison between an overlaid plot of a model output compared with the actual system output for the same sequence of inputs. Later, a measure of fit such as the *coefficient of determination* may be used to describe the difference in quality of fit achieved by different candidate structures. The coefficient of Determination or the R^2 value is defined by

$$R^2 \equiv 1 - \frac{\sigma_e^2}{\sigma_y^2} \tag{3.14}$$

Where σ_e is the variance of the residuals and σ_y is the variance of the output data. The value of R^2 occurs in the interval 0 to 1. By examining Definition.3.14 it is apparent that as $\sigma_e^2 \rightarrow 0$ then $R^2 \rightarrow 1$, which would indicate a perfect model fit. It is worth noting that the maximum value of R^2 which can be achieved is dependent upon the specific modelling problem. This fact means that there is no universal value of R^2 which is considered to be acceptable and so the measure of fit is relative and an acceptance criteria must be judged on a case by case basis.

Statistical Analysis of Residuals

An analysis of the modelling error (or residuals ϵ) can prove very informative [SS89, Lju99]. For a system affected by Gaussian (white) noise or disturbances, the ideal residual would be zero-mean and Gaussian. The residuals should also be independent of all past and future inputs if the system model has adequately described the system dynamics and the system being identified is open loop. In reality most systems will display noise or disturbances which are not perfectly Gaussian, and the model will not perfectly describe the actual system, so these tests must be performed within some confidence interval to allow for the imperfect statistical assumptions which are applied. In the following work, a pair of different statistical tests are used to examine these criteria:

The 'whiteness' of $\epsilon(t)$ is checked by examining the autocorrelation (r_ϵ) of the residuals. The

autocorrelation test examines the cross correlation between the residual and itself at different lags (τ). In other words this test examines the data for periodic or harmonic contents. For white residuals, $r_\epsilon(\tau)$ should be close to zero for all $\tau > 0$.

- if the model residuals ($\epsilon(t)$) are white then:

  $r_\epsilon(\tau) = 0$ for $\tau > 0$

The independence of $\epsilon(t)$ with respect to past and future inputs is examined by performing a cross-correlation test. This has two functions. Firstly, to determine how well the model describes the identified system by checking for residual model dynamics. Secondly, by observing cross-correlation with past inputs, a check for feedback in the identified system can be made.

- if the model is a poor description of the system then:

  $r_{\epsilon u}(\tau) \neq 0$ for $\tau \geq 0$

- if the model is a good description of the system then:

  $r_{\epsilon u}(\tau) = 0$ for $\tau \geq 0$

- if the identified system contains feedback, then it can be expected that:

  $r_{\epsilon u}(\tau) = 0$ for $\tau < 0$

Model Efficiency

An appropriate way of judging the efficiency of a model structure is to apply the so called '*parsimony principle*' [SS89]. In short this is a common sense rule which states that for a range of two or more candidate model structures, each of which gives a similarly good description of the system, the model with the least complexity (smallest number of parameters) should be selected.

3.7 Model Uncertainty

The identified system model, like all mathematical approximations, is uncertain. The fixed LTI (Linear Time-Invariant) model which results from the linear system identification process is

only a linear estimate of the system behaviour for the identified system, under certain operating conditions. Most real systems are nonlinear and depending upon the severity of the nonlinearity and the range of operating points modelled, the use of a linear system representation may limit the accuracy which can be achieved from the model. The LTI model is assumed to be 'time-invariant' which means that its parameters are fixed in time and therefore the system is assumed to behave the same at all times. In reality, many systems will behave differently over time. The causes of this can vary enormously, from local environmental factors such as temperature, humidity or pressure, through to longer-term factors such as wear. Finally, despite the efforts which are made during the design of the experiment, to ensure that as broad a spectrum of dynamics as is possible are perturbed and captured, high frequency dynamics are often difficult to describe in a compact model and will be an additional source of uncertainty.

The subject of plant uncertainty raises important considerations when designing for Robustness in control. What follows in this section is a brief description of the ways in which uncertainty can be quantified. The question of how the quantitative uncertainty can be usefully employed in controller design to provide a level of robust stability is discussed more fully in section 4.4.1.

3.7.1 Structured Uncertainty

One example of structured uncertainty is commonly illustrated [DFT91] by consideration of a simple system such as the second order transfer function 3.15. It may be that the value of the parameter a is known only in so far as that it lies in the range between $[a_{min}, a_{max}]$. The set of possible plants is therefore defined by the set $\mathcal{G}$.

$$\frac{1}{s^2 + as + 1} \tag{3.15}$$

$$\mathcal{G} = \left\{ \frac{1}{s^2 + as + 1} : a_{min} < a < a_{max} \right\} \tag{3.16}$$

3.7.2 Unstructured Uncertainty

Unstructured uncertainty differs from the structured form because it is defined in terms of generalised perturbations in the plant. Unstructured uncertainty can often be more useful than structured uncertainty since it allows general perturbations arising from unmodelled dynamics, especially at high frequencies, to be included in the analysis.

Multiplicative Uncertainty

A commonly used form of unstructured uncertainty is so called Multiplicative uncertainty. This form of uncertainty assumes that the system is affected by a multiplicative frequency dependent perturbation of nominal plant. Figure.3.5 illustrates the way in which the nominal plant is perturbed by a factor Δ_m according to the equation,

$$G(s) = (1 + \Delta_m(s))\, G_0(s) \tag{3.17}$$

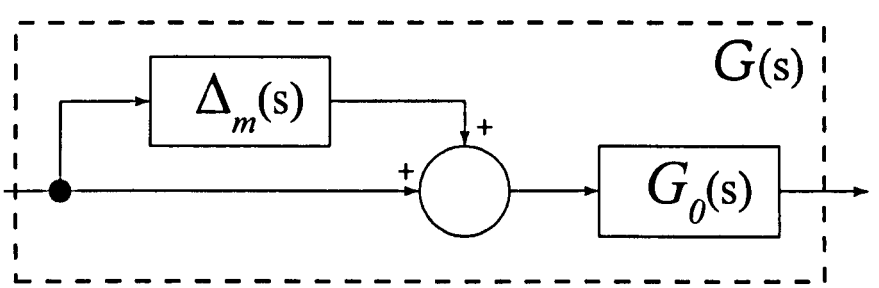

Figure 3.5: Nominal Plant G_0 affected by Multiplicative uncertainty Δ_m

The uncertainty can be derived from identified system models by utilizing a method described by Petridis and Shenton [PS03, Pet00]. In their method, the set of identified models are fitted at each of a discrete range of frequencies by a circular template in the complex plane (Fig. 3.6). The centre point of each circle defines the nominal system, while the radius of the circle defines the uncertainty. From this information, Δ_m can be defined at each frequency as illustrated in Fig.3.6.

It should be noted that this 'disk like' form of uncertainty tends to be inherently conservative. The assumption (illustrated in figure.3.6) that the uncertainty takes a circular form is an approximation which is not always closely representative of reality. Consider the dashed line

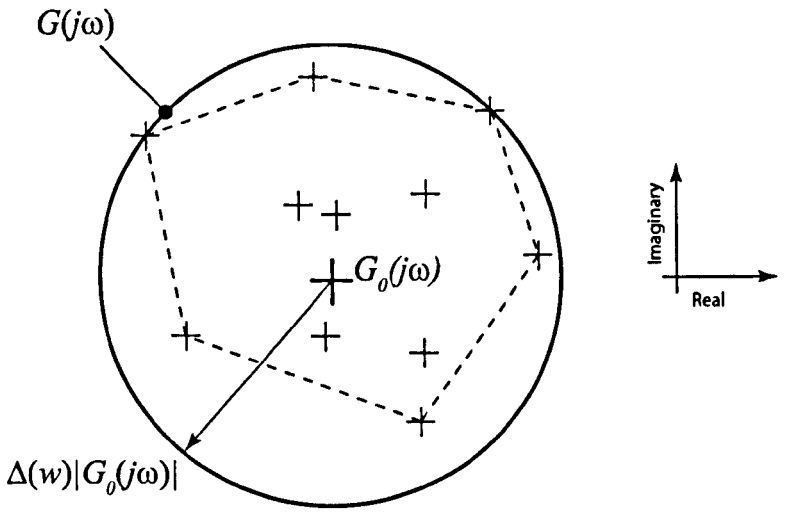

Figure 3.6: Complex template which defines the uncertainty in the plant G at a single frequency ω. Taken from [Pet00].

in figure.3.6. This shows the boundary of a hypothetical template which describes the uncertainty of the plant at the same frequency points as the circular template, but with somewhat less conservatism. The less conservative template may better describe the system uncertainty, but it is also considerably more complex to define and use mathematically, and for this reason, many believe that the reduction in conservatism is not worth the additional effort required to compute the boundary and make it useful in control applications. For this reason, the circular uncertainty template has been widely adopted despite its possible conservatism.

3.8 Nonlinear Inverse Compensation

For linear control design methods, a linear system model is required, but real systems are almost always nonlinear. Linear models may be a poor approximation to the real system, especially over a large operating range. Sometimes, the nonlinear system can be described by a set of linear models which can be thought of as a linearisation about discrete operating points. The range of linear models can then be used to define model uncertainty in the face of plant nonlinearity, and used to design a control system with enough robustness to cope with the broad range of possible dynamics. This approach usually results in a significant reduction in overall performance at any

specific operating point, but can provide a useful and practical way of dealing with the presence of system nonlinearity.

Another approach is to linearise the system by placing a nonlinear inverse model of the system in the feedforward or feedback path of the system. The product of the two elements is in theory a linear system with unit system gain and no dynamics. The practical reality is that perfect inverse compensation can rarely be achieved since the nonlinear system is strictly causal, and this cannot be reversed in the inverse model which will also be only an approximation to the real system. The process of determining that a system contains significant non-linearity, and that an inverse compensation scheme is appropriate are part of the system characterisation and design of experiment stages of the methodology. It is also an example of when the iterative nature of the process is particularly important, since it may only be through attempting linear system modelling and failing to achieve satisfactory results, that the investigation into system non-linearity and the associated non-linear modelling which is required, will become part of the process and therefore considerations in the design of experiment stage.

In circumstances where nonlinear behaviour is observed and where it is possible to model the nonlinearity, there are a number of possible ways of generating an inverse compensator. These include:

- Direct system identification of a dynamic nonlinear inverse.
- Direct system identification of a quasi-static nonlinear inverse
- Algebraic inversion of a nonlinear forward model

The introduction of an inverse compensator, even when it is not a perfect inverse of the nonlinear system, can significantly reduce the multiplicative uncertainty which is associated with system nonlinearity. The reduction in model uncertainty is beneficial since the performance of the controller which can be achieved will increase for any guaranteed level of robustness which is required to be maintained.

In the work which follows, the system nonlinearity which is associated with the characteristics of the Chassis Dynamometer was linearised using a static nonlinear inverse. The derivation of this inverse model can be recalled from Section 7.4, where it was found that a 3rd order

polynomial was a good fit to the quasi-static behaviour of the system. The benefits of the nonlinear inverse scheme in this application is demonstrated in [MDS06] and in particular it was shown that the multiplicative uncertainty associated with an LTI model of the chassis dynamometer could be reduced over all frequencies and that the controller performance could consequently be increased significantly without loss of robust stability.

3.9 Conclusions

In this chapter the subject of linear black-box system identification has been reviewed. The following summary highlights some of the key findings:

- The Design of Experiment is the first stage of the system identification process, but is usually revisited throughout the iterative system identification process. The frequency content, amplitude and sampling of the input signal are important aspects of this.
- Pre-processing the identification is done to make it suitable for the parameter estimation process and will typically involve the removal of offsets, trends and outlying points as well as applying appropriate filtering. It may also involve splitting data into an identification set and a validation set.
- The linear polynomial model structure is the most popular choice when performing a linear system identification. The ARX and ARMAX model structures are two common variants of the more general Box-Jenkins structure.
- The Selection of model order is usually an iterative process which involves comparing the attributes of models identified with different orders and selecting the most appropriate based on a combination of performance and efficiency. Coefficient of determination (R^2), residual cross-correlation and residual auto-correlation can be used to establish the performance of the model while the 'parsimony principle' provides a pragmatic way of judging efficiency.
- The model validation process uses the performance and efficiency measures which are used throughout the system identification process to provide final confirmation that an

identified model is acceptable.

- The system identification process can be correctly described as an iterative cycle where many choices are informed by *a priori* information derived from previous attempts at model identification. In this regard, prior experience of identifying a particular class of system will be a significant advantage.

- Model uncertainty, particularly non-parametric multiplicative uncertainty, can be defined by considering the range of frequency response characteristics of a set of identified models.

Chapter 4

Control

4.1 Introduction

For transient dynamometer control problems such as those investigated in this thesis, it has been seen how a high level of control performance is required if time response specifications are to not only be met but improved upon. Furthermore, it has been shown throughout the preceding system identification investigations that the dynamometer systems which are of interest in this thesis are subject to significant uncertainty due to plant perturbations, sensor noise and external disturbances. The presence of these characteristics make the problem a well suited candidate for the application of feedback control.

This chapter provides a brief introduction to the topic of classical feedback control, and gives background which will aid the selection of correct specifications for the dynamometer controller designs. The subject of closed loop sensitivity functions will highlight how properties such as tracking performance and robust stability, which are both crucial requirement for the chassis dynamometer control problem, may be specified in the frequency domain by considering the closed loop sensitivity of the system to low frequency disturbances and to noise. Modern control concepts are subsequently introduced, showing how the classical specifications can be used within a modern framework to provide optimal controllers by optimising the $\mathcal{H}_\infty$ or $\mathcal{H}_2$ norms of the weighted closed loop sensitivities.

4.2 Classical Control

The term classical control applies to linear closed-loop systems theory which was developed between the 1930's and the early 1960's*. Classical control is concerned with methods for synthesising a desired closed-loop response by designing and implementing a controller which modifies the frequency response characteristics of the open-loop system by introducing feedback. The classical methods were developed through successive discoveries in stability and frequency response analysis [Nyq32, Bla34, Bod40, Eva50]. The work of Evans, Black, Nyquist, Nichols and Bode was crucially important in establishing these methods which still underpin the fundamentals of modern linear control methods today.

This section begins by visiting some important concepts in classical control, and introduces a method by which specifications for controllers can be defined using frequency domain sensitivity weighting functions for the closed loop system. The development of such specifications will prove to be an important part of the controller designs which are later developed to solve the dynamometer control problems where design for closed loop performance and stability are important.

4.2.1 The Closed-Loop system

Consider the closed loop system shown in Fig.4.1. The system response (y) should track a reference input (r) as closely as possible. The error (e) needs to be minimised, but the system is effected by disturbance (d) and sensor noise (n). The plant is defined by the transfer function $G(s)$ and the transmission of the disturbance is governed by the transfer function $G_d(s)$.

The input to the plant is defined by (4.1) while the overall plant model is can be defined as in (4.2). Combining (4.1) and (4.2) gives an expression for the closed loop response (4.3) and

*The starting point for classical control is sometimes acknowledged to be Watt's flyball governor which introduced feedback control to industrial steam engines in the milling industry. Improvements to his invention led to the first analysis of the problem of closed loop stability and ultimately the work of Routh and Hurwitz. Later, a telecommunications revolution and the invention of the feedback amplifier provided accelerated development of important practical theories by Black, Bode and Nyquist [Nyq32, Bla34, Bod40]. This momentum was increased with the onset of the second world war between 1939 and 1945, specifically with application to the field of Radar. After the war had finished, some of the previously classified work which had been closely guarded during hostilities was released, and a proliferation of new work was generated. The Root Locus of Evans [Eva50], was one of the earliest formalised design or synthesis methods and is still taught and used today. The dawn of modern control is sometimes pinpointed as being the first ever IFAC (International Federation of Automatic Control) conference hosted in Moscow in 1960.

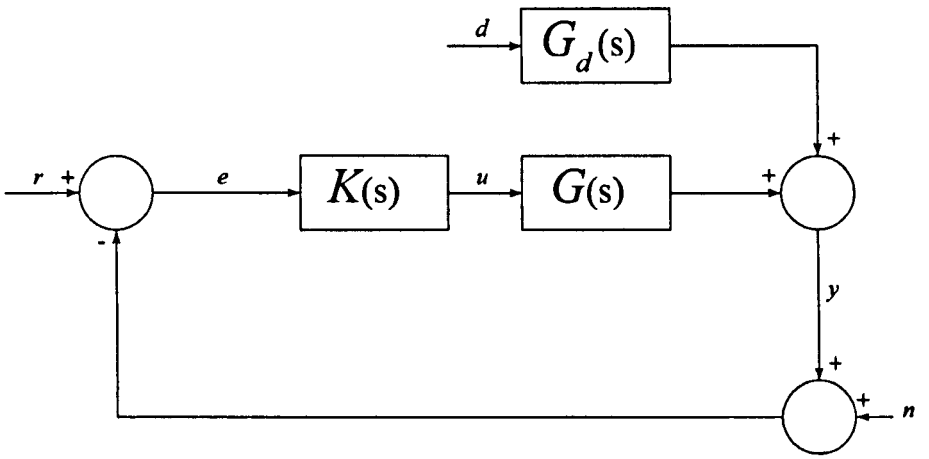

Figure 4.1: Closed loop system with disturbance d and sensor noise n

(4.4).

$$u(t) = (r - y - n)K(s) \tag{4.1}$$

$$y = G(s)u + G_d d \tag{4.2}$$

$$y(1 + G(s)K(s)) = rG(s)K(s) - nG(s)K(s) + G_d d \tag{4.3}$$

$$y = \frac{G(s)K(s)}{1 + G(s)K(s)}r - \frac{G(s)K(s)}{1 + G(s)K(s)}n + \frac{G_d}{1 + G(s)K(s)}d \tag{4.4}$$

4.2.2 Sensitivity Functions

Frequency domain specifications for feedback control can be defined in terms of the closed-loop sensitivity functions which describe how the closed loop system will respond to disturbances and noise which are present in the system. Here we consider the two most common sensitivities, and the ones which will be used in relation to the dynamometer control problems. They are the Primary sensitivity function and the complementary sensitivity function.

Primary Sensitivity

The primary sensitivity function $S(j\omega)$ is given by the equation

$$S(j\omega) \equiv \frac{1}{1 + G(j\omega)K(j\omega)} = \frac{1}{1 + L(j\omega)} \tag{4.5}$$

This function describes how the system output (y) will respond to disturbances (d), which will usually occur at lower frequencies (in terms of the system bandwidth). Reducing the sensitivity of the system to these disturbances, by ensuring that the magnitude $|S(j\omega)|$ is bounded at low frequencies, will result in improved tracking or disturbance rejection performance. The primary sensitivity function is therefore a statement of the way in which the presence of feedback reduces the sensitivity of a system to disturbances. It is apparent that by increasing the gain of $K(s)$ the primary sensitivity is reduced, and performance will nominally be increased. The improvement of tracking is of key importance to the chassis dynamometer control problem where the objective is to closely follow road-load trajectories. Similarly, the rejection of shaft torque disturbances is desirable in the zero shaft torque problem where the magnitude of the shaft torque fluctuation about its set-point is the main objective.

Complementary Sensitivity

The complementary sensitivity function $T(j\omega)$ is given by the equation

$$T(j\omega) \equiv \frac{G(j\omega)K(j\omega)}{1 + G(j\omega)K(j\omega)} = \frac{L(j\omega)}{1 + L(j\omega)} \tag{4.6}$$

This complementary function describes the sensitivity of the system output (y) to sensor noise (n), which is typically present at higher frequencies. It is accordingly desirable to limit the sensitivity of the system to noise by ensuring that the magnitude $|T(j\omega)|$ is bounded at the higher frequencies. Increasing the gain of $K(s)$ will increase the magnitude of the complementary sensitivity function and therefore the closed loop sensitivity to noise. This is a statement of a fundamental problem of feedback control which is that it tends to amplify noise at certain frequencies.

In classical control, the loop function $L(s)$ is shaped using bounds on the sensitivity functions

($S(s)$ and $T(s)$) as a way of defining design specifications. It must be noted that because the objectives of specifications which are defined in terms of S and T compete directly, the controller design process will inevitably involve a degree of compromise throughout.

The fundamental compromise between the primary and complementary sensitivities can be illustrated by defining the relationship in (4.7),

$$S(j\omega) + T(j\omega) = \frac{1}{1 + L(j\omega)} + \frac{L(j\omega)}{1 + L(j\omega)} = 1 \tag{4.7}$$

this shows that at any frequency, if one sensitivity is reduced, then the other must increase accordingly. This phenomena is sometimes referred to as the 'waterbed effect'.

4.2.3 Weighted Sensitivity Functions

The user can places bounds on a closed loop sensitivity by defining a weighting function. The upper bound on the magnitude of the sensitivity function is defined by convention as $1/W_n$, where the user defines the positive, stable, minimum phase function W_n.

Primary Weighted Sensitivity Function

A wighting function W_S may be applied to the primary sensitivity according to the the inequality

$$\left| \frac{1}{1 + G(j\omega)K(j\omega)} \right| \leq \frac{1}{W_S(j\omega)} \tag{4.8}$$

Or

$$|S| \leq \frac{1}{W_S(j\omega)} \tag{4.9}$$

This means that the primary sensitivity of the system should be bounded at all frequencies such that it is less than or equal to the inverse of the weighting function $1/W_S$. The shape of $1/W_S$ should therefore be selected such that it displays low gain at low frequencies in order to ensure reduced sensitivity to low frequency disturbances.

Complementary Weighted Sensitivity Function

In the same way, the weighted complementary sensitivity function can be described by

$$\left| \frac{G(j\omega)K(j\omega)}{1+G(j\omega)K(j\omega)} \right| \leq \frac{1}{W_T(j\omega)} \tag{4.10}$$

Or

$$|T| \leq \frac{1}{W_T(j\omega)} \tag{4.11}$$

This means that the complementary sensitivity of the system should be bounded at all frequencies such that it is less than or equal to the inverse of the weighting function $1/W_T$. The shape of $1/W_T$ should therefore be selected such that it displays low gain at high frequencies in order to ensure reduced sensitivity to noise.

4.3 Concepts in Modern and Robust Control

4.3.1 Uncertainty and Robustness

System uncertainty is a problem which can impact on both the performance and stability of the closel loop system and the dynamometer control explored in this thesis is no exception. The sources of system uncertainty can be varied, but in the case of the dynamometer control problem the key sources are plant nonlinearity and sensor noise. Uncertainty will reduce the achievable performance of the dynamometer controller because the stability margins of the system will also be uncertain and so some conservatism will be required in order to ensure that the closed loop system will always remain stable. This so called Robustness is an important feature of a controller since for safe operation stability must be guaranteed. However, excessive robustness will lead to a design which is too conservative which will usually have performance which is artificially limited. The solution to this problem is to design for robustness in a systematic way in order to limit the conservatism of the controller while maintaining confidence in the stability of the system.

In the preceding section 4.2.3, it was shown that frequency domain specifications can be used to define bounds on a nominal system, with the aim of providing nominal level of performance and stability along with reduced sensitivity to disturbances and noise. What is not addressed by this analysis however is the question of plant uncertainty, or more specifically how a controller can be designed which will provide performance, stability or preferably both despite this uncertainty.

Recalling section 3.7, the topic of model uncertainty was introduced in reference to the quantification of the uncertainty inherent in an identified LTI model of the chassis dynamometer system. It was shown that Multiplicative uncertainty provides flexible way of describing the relative system uncertainty, in a manner which is mathematically efficient, and which can be conveniently derived from identified system models.

The closed loop system, with uncertain plant, is shown in Fig.4.2. The block diagram can be simplified by substituting with the closed loop transfer function $M(j\omega)$ (4.12), giving the two block system shown in Fig.4.3. By application of small gain theory [BB95], robust stability is guaranteed if the inequality in 4.13 is met [DFT91].

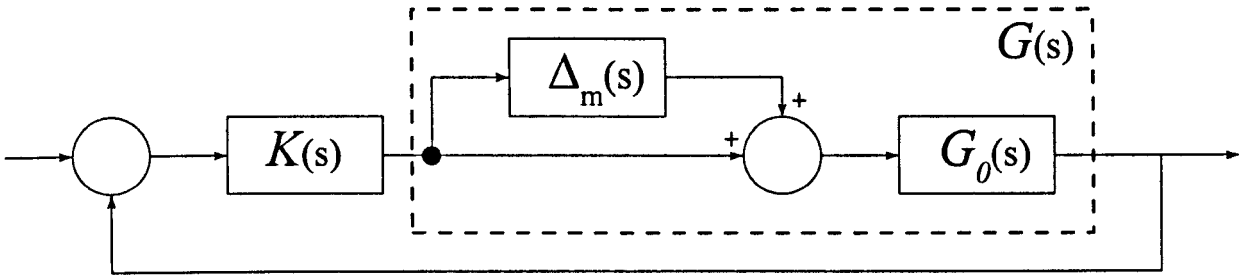

Figure 4.2: Closed-Loop system with uncertain plant

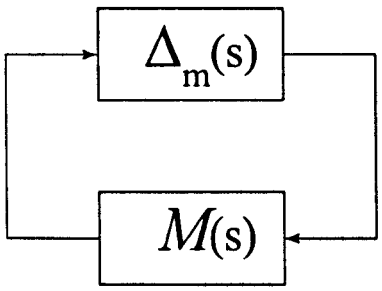

Figure 4.3: Two-Block representation of the uncertain closed-loop system

$$M(j\omega) = \frac{-K(j\omega)G_0(j\omega)}{1 + K(j\omega)G_0(j\omega)} \tag{4.12}$$

$$|\Delta_m(j\omega)||M(j\omega)| < 1 \tag{4.13}$$

Observing that the closed loop transfer function ($M(j\omega)$) is equivalent to the complementary sensitivity function (4.6), we can substitute $M(j\omega)$ with $T(j\omega)$ in 4.13. This shows that for robust stability to be achieved, the complementary sensitivity function must be constrained at all frequencies by the inverse of the multiplicative uncertainty. That is

$$|T(j\omega)| < \frac{1}{\Delta_m(j\omega)} < \Delta_m(j\omega)^{-1} \tag{4.14}$$

Where an uncertainty model of the system does not exist, or where one cannot be easily obtained then the designer can still design robustness into the closed loop system by choosing complementary sensitivity weighting function which reflects the expected nature of the plant uncertainty. For example, in most cases the plant uncertainty will increase with frequency and so a sensible complementary weighting function $1/W_T$ will be shaped with the aim of maintaining

performance at lower frequencies by providing a lower level of robustness but will constrain the system more severely as frequencies increase in order to provide a greater degree of protection against un-modelled plant dynamics and the effects of noise.

4.3.2 Norms

Norms describe the magnitude associated with a mathematical object, be that a vector or function. They are an important and useful concept in control since performance is often described in terms of the size of a particular signal associated with the system [DFT91]. A generalised definition for a Norm, sometimes called the p-Norm is

$$\|x\|_p = \left(\int_{-\infty}^{\infty} |x(t)|^p \, dt \right)^{1/p} \tag{4.15}$$

The subscript notation in the terms $\mathcal{H}_2$ and $\mathcal{H}_\infty$ relate to the order of the norm, that is $p = 2$ and $p = \infty$ respectively.

The ∞-norm

Starting with the ∞-norm, if $p = \infty$ then the norm becomes

$$\|x(n)\|_\infty = \max_n |x_i(n)| \tag{4.16}$$

The term $x(n)$ is a generalised mathematical object, and can be replaced by a transfer function such as a sensitivity function, like $S(j\omega)$, in which case the ∞-norm is

$$\|S(j\omega)\|_\infty = \max_{j\omega} |S(j\omega)| \tag{4.17}$$

The interpretation of $\|S(j\omega)\|_\infty$ is therefore that it represents the maximum frequency response of the system $S(j\omega)$.

The 2-norm

The 2-norm (4.18) is given by

$$\|x(n)\|_2 = \left(\int_{-\infty}^{\infty} |x_i(n)|^2 \, dt\right)^{1/2} \tag{4.18}$$

It is of interest since its form is very similar to that of the expression for signal power

$$E = \int_{-\infty}^{\infty} |x_i(n)|^2 \, dt \tag{4.19}$$

This implies that the 2-norm itself gives some measure of the total energy (E) in a signal such that

$$E = \|x(n)\|_2^2 \tag{4.20}$$

As has been seen, the object associated with the norm may be a transfer function, and so the 2-norm may be re written, in terms of $S(j\omega)$

$$\|S(j\omega)\|_2 = \left(\int_{-\infty}^{\infty} |S(j\omega)|^2 \, d\omega\right)^{1/2} \tag{4.21}$$

This result will be useful when considering $\mathcal{H}_2$ control where the $\mathcal{H}_2$ norm is defined, for a transfer function $S(j\omega)$, by the equation

$$\|S(j\omega)\|_2 = \left(\frac{1}{2\pi}\int_{-\infty}^{\infty} |S(j\omega)|^2 \, d\omega\right)^{1/2} \tag{4.22}$$

The application of norms in control

Norms are important as they provide a measure, relevant to the control problem, which can provide a basis for optimisation. As shall be seen, the $\mathcal{H}_\infty$ and $\mathcal{H}_2$ norms of weighted sensitivity functions provide useful constraints for the synthesis of feedback controllers.

In $\mathcal{H}_\infty$ control, bounds are placed upon the magnitude ($\mathcal{H}_\infty$ norm) of the closed-loop frequency response which allows the sensitivity of the system to disturbances or noise to be limited according to a target weighting. This means that a controller can be designed to provide tracking

performance or noise and disturbance rejection by shaping the sensitivity weighting functions appropriately.

A generalised minimum variance controller is designed to minimise the variance at the output of the closed loop system. In $\mathcal{H}_2$ control, the energy at the controller input or system output can be reduced by minimising the $\mathcal{H}_2$ norm of the corresponding closed-loop sensitivity functions. The $\mathcal{H}_2$ control method can therefore be used to design minimum variance controllers if the method is applied only to reducing the variance at the output of the system.

4.4 $\mathcal{H}_\infty$ Control

The $\mathcal{H}_\infty$ control paradigm has emerged as the leading optimal control tool since its development by Zames [Zam81], Doyle and Glover [DG+89] and Kwakernak [Kwa91], as well as others, in the early nineteen eighties. The $\mathcal{H}_\infty$ method involves two processes, firstly the definition of specifications which are based upon the ∞-norm of the weighted sensitivity function or functions. Second is the controller design and optimisation process whereby the specifications are met as closely as possible by directly shaping the weighted sensitivity transfer functions.

4.4.1 Constraints and Specifications

Nominal Stability

Nominal stability is the most fundamental requirement of any closed loop system, and simply ensures that under nominal conditions, the system will not be unstable.

Nominal Performance

For nominal performance, it is required that the $\mathcal{H}_\infty$ norm should conform to the inequality

$$\|S(j\omega)W_s(j\omega)\|_\infty \leq 1 \tag{4.23}$$

Where $W_s(j\omega)$ is the weighting for the primary sensitivity function $S(j\omega)$.

Robust Stability

Robust Stability, in contrast with nominal stability, ensures that the closed loop system will be stable for any plant within the set of uncertain plants. This ensures that unless the behaviour of the system deviates from the plant for which the controller is designed, it should remain stable. Recalling Section 4.3.1, it was shown that for robust stability to be achieved, the complementary sensitivity function must be bounded at all frequencies by the multiplicative uncertainty Δ_m such that:

$$|T(j\omega)| < \frac{1}{\Delta_m(j\omega)} = \Delta_m(j\omega)^{-1} \tag{4.24}$$

Comparing this with the definition for the weighted complementary sensitivity function (4.10), shows that the multiplicative uncertainty defines the appropriate weighting for Robust stability (i.e $W_T = \Delta_m(\omega)$).

$$\|T(j\omega)\Delta_m(\omega)\|_\infty \leq 1 \tag{4.25}$$

Mixed Sensitivity

In section 4.2.2 it was shown how the performance provided by minimising the primary sensitivity function ($S(s)$) must always be traded off against the conflicting but equally desirable reduction in sensitivity to noise which is achieved through minimising the complementary sensitivity function ($T(s)$). Furthermore, it is also known from section 4.4.1, that the complementary sensitivity function also has an important role to play in the provision of robustness to plant uncertainty. Therefore, the trade-off can be seen in even more striking terms as a compromise between performance and robust stability.

It is clear that in any application a combination of performance and robust stability is very important and so some method for achieving both simultaneously is highly desirable. This compromise can be achieved, albeit with some added conservatism, by using mixed sensitivities.

In this formulation, two weighted sensitivity functions are considered simultaneously by minimising the $\mathcal{H}_\infty$ norm of a single objective function

$$\left\| \sqrt{|W_S S|^2 + |W_T T|^2} \right\|_\infty = \left\| \begin{matrix} W_S S \\ W_T T \end{matrix} \right\|_\infty \leq \gamma \tag{4.26}$$

The variable γ is introduced as a means for defining the level of performance which is achieved by the mixed sensitivity design. The mixed sensitivity formulation provides a useful way of designing for both performance and robust stability simultaneously and is therefore ideal for application in the dynamometer torque control problems presented in this thesis.

4.4.2 $\mathcal{H}_\infty$ Algebraic Method

The first of the Algebraic Riccati Equation methods for designing $\mathcal{H}_\infty$ feedback controllers was proposed by Doyle and Glover in 1989 [DG+89] and is a powerful and popular method which provides an optimal design for a given set of specifications. The controller is designed by solving a Riccati Equation which is in itself a non-trivial exercise, but the ARE method extends this by performing a frequency domain optimisation by so-called gamma (γ) iteration. In the mixed sensitivity formulation of the standard $\mathcal{H}_\infty$ problem, the optimal solution will be one which meets the specifications for the lowest possible value of γ. The optimisation procedure therefore requires a search algorithm to be used (for example Binary Search or a Genetic Algorithm). As γ decreases, the controller which results approaches the $\mathcal{H}_\infty$ optimal controller.

The implementation of the ARE method of $\mathcal{H}_\infty$ controller design is not trivial but has been made accessible by a number of computer packages, such as Matlab, Scilab or GNU Octave [†] which provide the user with means for performing the design procedure given a nominal plant model, and appropriate weighting functions. The main algorithm which is applied is often referred to as the DGKF algorithm after the authors of the paper which originally proposed the method[‡].

The ARE method, so applied has the advantage that where the plant and specifications present the possibility of an optimal solution, it can be found relatively quickly. The weakness

[†]Matlab is a commercial mathematics package which is widely used in both industry and academia. Information is available at www.mathworks.com. Scilab is an open-source mathematics package available free from www.scilab.org, GNU Octave is an open-source mathematics package which is largely compatible with Matlab syntax and available free from www.octave.org

[‡]The acronym stands for Doyle-Glover-Khargonekar-Francis

of this method is that it relies upon the user's experience and judgement in the choices of weighting functions.

In many engineering applications, the desired outcome of a controller design can usually be best defined in terms of a time domain performance, but many controller design methods require the user to provide frequency domain specifications. As has been seen, these specifications have useful physical interpretations but do not translate directly to time response characteristics. Where the user has some flexibility to shape the controller design, this can be overcome by making a judgement about how the specifications are to be best met to achieve both frequency response and time response objectives. In the case of ARE however, the optimisation procedure is automatic and provides an optimal solution in terms of the frequency domain specifications only. This means that the weighting functions are the only controls which the engineer has over the way the controller is designed. The selection of weighting functions can therefore be the most time consuming aspect of performing a successful ARE $\mathcal{H}_\infty$ design.

The order of a controller designed by this method is given by the sum of the order of the weighting functions along with that of the nominal plant model. Weighting functions must be proper rational functions and those with complicated shaping will have more poles, leading to higher order controllers. For this reason, it is common for the weighting functions to be reduced order approximations of the ideal shape [Pet00]. In the case of the complementary sensitivity weighting function, it is prudent to ensure that the approximate weighting function shape fully encloses the multiplicative uncertainty of the plant, ensuring robust stability at the cost of making the design more conservative. Pure time delays in the plant cannot be handled explicitly by the ARE method since it requires a rational transfer function model. This can be overcome by using a Padé approximation at the cost of increased model order.

The result of the combined effect of weighting function order and plant order is that controllers designed by the ARE method tend to be very high. With modern hardware, controller order may not be such a barrier to implementation, but is a consideration which has historically limited the adoption of this type of controller. In such applications as engine management systems or proprietary dynamometer controllers where lookup tables are used to implement PID structures and not high order linear systems.

4.4.3 $\mathcal{H}_\infty$ Parameter Space Method

The following overview of the $\mathcal{H}_\infty$ Parameter Space method [BS97, BS99] describes how parameter planes may be generated with regard to the three most common sensitivity transfer functions, namely:

- Primary Sensitivity

$$S(j\omega) = \frac{1}{1+GK} \tag{4.27}$$

- Complementary Sensitivity

$$T(j\omega) = \frac{KG}{1+GK} \tag{4.28}$$

- Control Effort Sensitivity

$$U(j\omega) = \frac{K}{1+GK} \tag{4.29}$$

Recall that for nominal performance, the $\mathcal{H}_\infty$ norm is constrained by the weighted primary sensitivity function:

$$\left\| \frac{W_1}{1+GK} \right\|_\infty \leq 1$$

This inequality is satisfied if,

$$|1 + \Re(GK) + \Im(GK)|^2 - |W_1|^2 \geq 0 \tag{4.30}$$

The expression can be expanded to give the equation

$$1 - |W_1|^2 + 2(K_r G_r - K_i G_i) + \left(K_r^2 + K_i^2\right)\left(G_r^2 + G_i^2\right) \geq 0 \tag{4.31}$$

Repeating this process for other sensitivities, it can be shown that all take the same general form and that a combined expression, including all three of the key sensitivities, can be written [BS97] in combined form

$$1 - |W_1|^2 + 2(K_r G_r - K_i G_i) + (1 - W_6^2)(K_r^2 + K_i^2)(G_r^2 + G_i^2 - W_4^2) \geq 0 \tag{4.32}$$

For the generation of any parameter plane only one of the weighting functions W_1,W_4 and W_6 can be non-zero at any time.

The plant model G and the weighting (W_1,W_4 or W_6) are known, while K_r and K_i are the unknown variables of interest. The form of the inequality 4.32 for any given sensitivity is that of a conic section (equation 4.33).

$$ax^2 + 2hxy + by^2 + 2gx + 2fy + c \geq 0 \tag{4.33}$$

The boundary of this region is defined by an equality and at any individual frequency, a conic section can be plotted for $x = K_r$ and $y = K_i$ using the parameters shown in Table.4.1.

	a	b	c	f	g	h
W_1	$G_r^2 + G_i^2$	$G_r^2 + G_i^2$	$1 - \|W_1\|^2$	$-G_i$	G_r	0
W_4	$(1 - W_6^2)(G_r^2 + G_i^2)$	$(1 - W_6^2)(G_r^2 + G_i^2)$	1	$-G_i$	G_r	0
W_6	$G_r^2 + G_i^2 - W_4^2$	$G_r^2 + G_i^2 - W_4^2$	1	$-G_i$	G_r	0

Table 4.1: Parameters for conic sections

For example, the conic section relating to W_1 is given at each frequency by,

$$1 - |W_1|^2 + 2(K_r G_r - K_i G_i) + (K_r^2 + K_i^2)(G_r^2 + G_i^2) = 0 \tag{4.34}$$

The sensitivity constraint is therefore plotted in a plane representing the real and imaginary components of the controller (K_r and K_i). The conic section (usually an ellipse) must be mapped into the parameter space so that individual controller parameters can be selected.

The controller structure must be fixed, and in the the transfer function form of the PID is adopted. This structure is convenient since the number of parameter planes generated is manageable in a manual iterative tuning process, and the resulting controller gains can be implemented in hardware where the capacity for higher order control structures is not available.

$$K(j\omega) = K_r + jK_i = \frac{-b_2\omega^2 + jb_1\omega + b_0}{-a_2\omega^2 + ja_1\omega + a_0} \tag{4.35}$$

Only two controller parameters are considered as variables at any one time, with the other parameters being fixed. A starting controller is defined, either arbitrarily or by taking an initial controller which is to be tuned. The initial controller may be an existing set of controller gains which are to be improved, or even a controller which has been designed using another design process such as ARE $\mathcal{H}_\infty$ and which has subsequently been subject to an order reduction process. If the controller is to be designed from scratch, then the gains b_2, b_1 and b_0 can be set to zero.

At each frequency, the solutions to equation 4.34 are mapped into a plane which represents the two controller parameters of interest. For example, the parameter plane representation for variables b_0 and b_1 is given by the equation.

$$X = b_0 + jb_1\omega = (K_r + jK_i)\left(-a_2\omega^2 + ja_1\omega + a_0\right) + b_2\omega^2 \tag{4.36}$$

Where the pair of parameters are given by,

$$b_0 = \Re(X)$$

$$b_1 = \frac{\Im(X)}{\omega}$$

This process is repeated for each sensitivity. The mapped boundaries are superimposed onto one and another to generate a region within which each of the sensitivities are simultaneously met or exceeded. A point, representing a combination of the two controller parameters is selected. The initial controller is updated with the selected parameters. The next parameter plane, representing a different pair of parameters can then be plotted and the process repeated in each plane until a satisfactory design is acheived.

Chapter 5

Filtering

5.1 Introduction

The problem of noise corrupted signals in real engineering systems can be a difficult one to solve. The dynamometer control studies which are presented in this thesis are both examples of applications where unwanted disturbances are superimposed upon important signals and thus the appropriate application of filtering can prove advantageous.

This section introduces the filtering methods which were utilised in this thesis. Both frequency-domain and model based methods were used, and are described accordingly. It was found that the choice of filtering strategy was crucial to achieving satisfactory results for both system identification and control.

5.2 Frequency Domain Filtering

A frequency domain filter is designed to modify the frequency response of a system, usually by either emphasising or attenuating certain frequency ranges. The literature on this topic is extensive but a brief overview of the different basic types of filter is provided in this section.

The four most common types of frequency domain filter are described below. In the examples shown, the filters are of an 'Elliptic' design. This type of filter is known to provide among the highest rates of roll-off against order of all frequency domain filters. The designs were all carried out utilising a simple m-file script in Matlab, and used the Signal Processing Toolbox.

Low Pass filters (e.g. Bode magnitude and phase plot in Fig.5.1) allow low frequencies to pass through while attenuating higher frequencies. The low pass filter is defined in terms of cut-off frequency and stop-band attenuation. Low pass filters are often routinely applied to signals in order to eliminate high frequency noise from RF and EM radiation sources. A low pass filter can also be implemented as an anti-aliasing filter. In this case, the cut-off frequency is defined to provide attenuation beyond the Nyquist frequency ($f_N = f_s/2$).

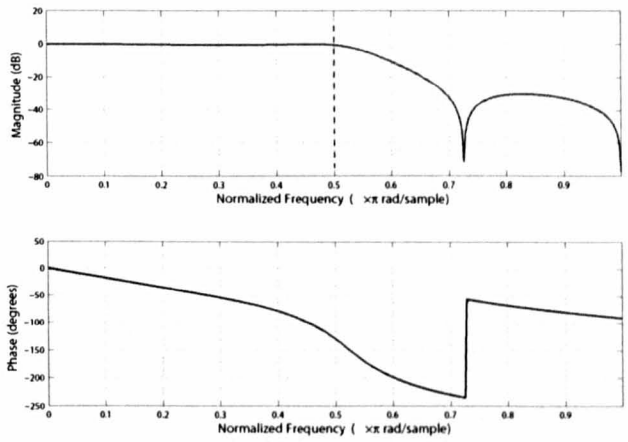

Figure 5.1: Low Pass filter

High Pass filters (e.g.Bode magnitude and phase plot in Fig.5.2) allow higher frequencies to pass through, while low frequencies, including DC dynamics are attenuated. This type of filter is often used to remove DC bias and low frequency interference acting on higher frequency signals such as communications transmissions.

Band Pass filters (e.g. Bode magnitude and phase plot in Fig.5.3) define one or more frequency bands within which dynamics are passed, and outside of which the frequencies are attenuated. This type of filter can be used to highlight important frequencies in a noise affected signal.

Band Stop filters (e.g. Bode magnitude and phase plot in Fig.5.4) define one or more frequency bands within which dynamics are attenuated and ouside which, frequencies are passed.

As the order of a filter is raised, the rate of roll-off of the filter can be increased, defining sharper boundaries between pass bands and stop bands. This typically comes at the cost of

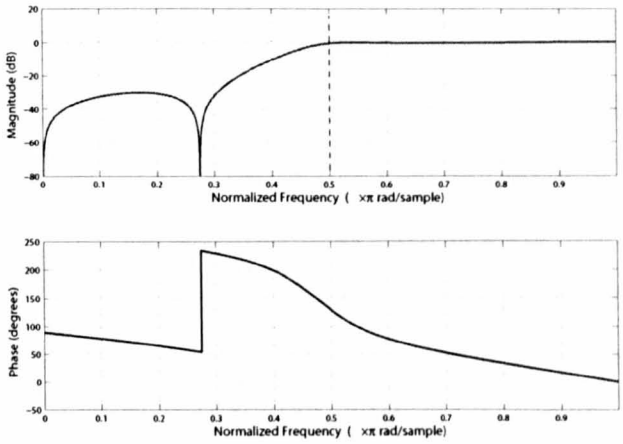

Figure 5.2: High Pass filter

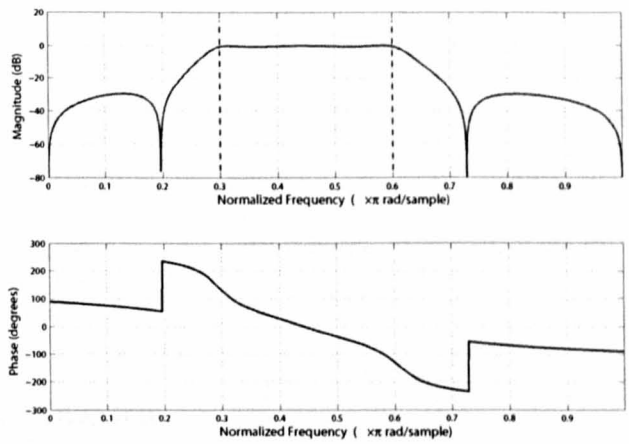

Figure 5.3: Band Pass filter

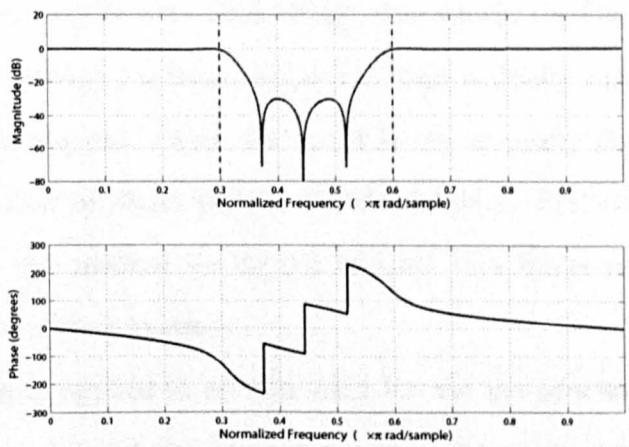

Figure 5.4: Band Stop filter

increased phase shift, and in the case of digital filters, additional time delays. When a filter is implemented on-line, the compromise between attenuation, rate of roll-off and the introduction of phase-shift or time delays must be considered carefully with regard for the impact which filtering may have upon the quality or characteristics of the signal.

In the dynamometer control problems which are presented in this thesis, it was found that the frequencies which needed to be attenuated were at low frequencies relative to the bandwidth of the system. This meant that in order to attenuate the target frequencies without distorting the surrounding low frequency dynamics, a very high rate of rolloff was required. Because of this constraint, it was impossible to design causal frequency domain filters which were sufficient effective in attenuating the required frequencies, without imposing significant additional time delay and phase shift to the filtered response. In light of the objectives of the dynamometer control problems, which is generally to increase transient performance, it was judged that the use of a frequency domain filter in the feedback path of the control system was not appropriate.

In applications where filtering is not required to be performed online, such as the pre-processing stage of the system identification process, non-causal frequency domain filtering may be an attractive solution.

5.2.1 Non-Causal Filtering

For sampled data systems, non causal or zero-phase filtering (Fig.5.5), can be utilised if the data is to be filtered off-line. The principle of non-causal filtering is that the data (y) is passed normally through a frequency domain filter ($F(z)$) after which, the filtered data (y_f) is reversed (y_{fr}) and passed back through the filter, before the data is finally time reversed once again to restore it to the correct sequence order, the result is the acausally filtered output (y_{af}). This process adds no time delay or phase shift to the filtered data. F(z) can be almost any type of digital filter, although this method should not be used with filters which depend strongly on their phase response for correct operation.

Non-causal filtering is applied in section 7.5.2 for the pre-processing stage of the system identification procedure. A band-stop filter was used to attenuate specific problem frequencies which existed in the captured data. In the case of the chassis dynamometer, the structural

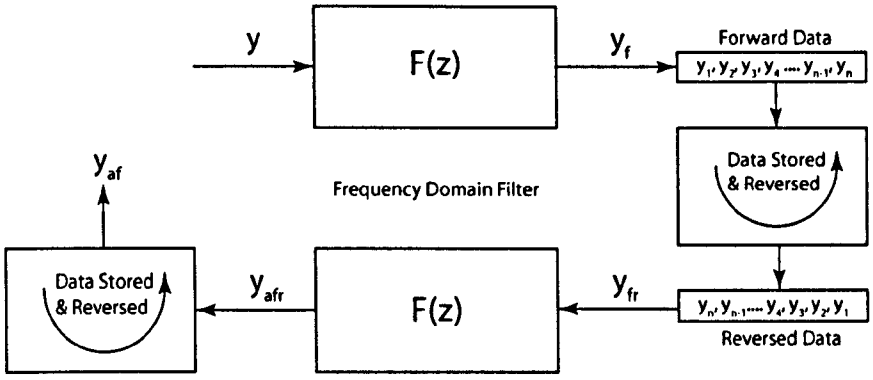

Figure 5.5: Acausal Filtering

dynamics of the torque measurement system was responsible for an oscillatory component at around 20Hz, and was removed from the identification data using a non causal elliptic band stop filter.

The benefits of using non-causal filtering in this type of application include the fact that high order filters, and thus extremely high rates of roll off can be applied without adding phase shift or time delay to the filtered data. This means that the filter may be applied in a very targeted manner over a specific frequency band.

5.3 The Kalman Filter

The Kalman filter is an optimal model based solution to the linear filtering problem. It is a special form of state-estimator which is, in its optimal form, updated on-line to provide a filtered measurement output given an input which is the noise affected measurement sequence. The Kalman Filter method was first presented by Kalman and Bucy in 1960 [KB60], although others in the field performed similar work (most controversially Swerling [Swe58] who attempted to claim priority for the theory [Sor70]), obtaining similar results around the same time. In many respects the Kalman filter has been viewed as an inevitable extension of the work of Gauss [Gau63], Weiner [Wei49] and many others who developed the field of Least-Squares prediction over the intervening 140 years. Despite this, the impact of the Kalman filter is extremely difficult to over-state, and it has an enormous number of important applications in many diverse engineering applications. With this popularity has come a massive body of complementary work, presenting many different formulations and extensions, proposed and adopted for equally many applications. An excellent historical perspective of the work leading up to and including the Kalman filter is presented by Sorenson [Sor70], while both Kalman's early papers on the work provide a rigorous background on the fundamentals of the subject [KB60, KB61].

In this thesis the linear Predictor-Corrector form of the Kalman filter algorithm [Can86], is adopted due to its simplicity and practical effectiveness. The Kalman filter is introduced to filter the torque feedback with the aim of attenuating the oscillatory sensor noise without introducing significant phase-lag or time delays. It is shown that a steady-state Kalman filter can be designed using this algorithm, which does not require on-line updates. This type of Kalman filter takes advantage of the asymptotic convergence of the filter parameters, and is computed off-line, by running the recursive Kalman filter algorithm with acquired input/output data. Another way of calculating the steady-state solution is to solve the covariance equation which takes the form of an algebraic Riccati equation in the linear case[KB61].

5.3.1 State-Space System Representation

Consider the generalised dynamic system defined by the discrete state and output equations in 5.1 and 5.2 respectively. The system has a state transmission matrix A, an input transmis-

sion matrix B and measurement matrix C. The system is affected by process noise $w(t)$ and measurement noise $v(t)$.

$$x(t) = Ax(t-1) + Bu(t-1) + w(t) \tag{5.1}$$

$$y(t) = Cx(t) + Du(t) + v(t) \tag{5.2}$$

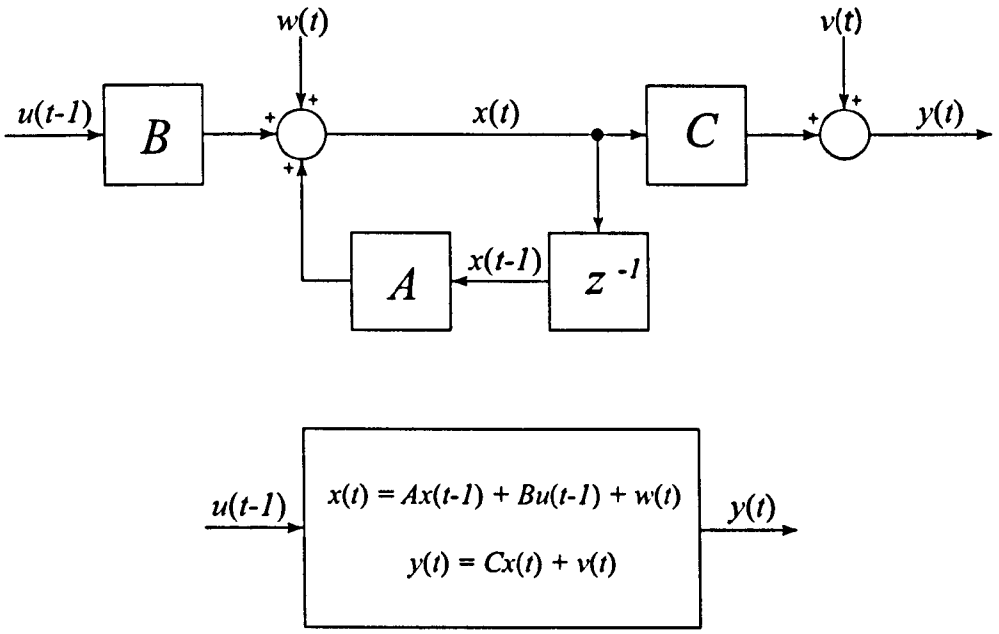

Figure 5.6: Block diagram representation of a State-Space system

5.3.2 Kalman Filter:Predictor-Corrector Form

The Kalman filter Algorithm implemented presented here is the Predictor-Corrector form as presented by Candy [Can86].

In the following algorithm, the estimated state vector is represented by $\hat{x}$, the covariance matrix is $\widetilde{P}$ and the Kalman gain vector is K. Predicted state vectors and covariance matrices are described by the suffix $(t|t-1)$ which notates that the prediction for the current time-step t is calculated using data at the previous time step $t-1$. The updated predictions, using the updated Kalman Gains, are denoted with the suffix $(t|t)$. Updated predictions from a previous time step are denoted by $(t-1|t-1)$. The algorithm is as follows:

Prediction

$\hat{x}(t|t-1) = A(t-1)\hat{x}(t-1|t-1) + B(t-1)u(t-1)$ (State Prediction)

$\widetilde{P}(t|t-1) = A(t-1)\widetilde{P}(t-1|t-1)A'(t-1) + R_w(t-1)$ (Covariance Prediction)

Innovation

$e(t) = y(t) - \hat{y}(t|t-1) = y(t) - C[\hat{x}(t|t-1)]$ (Innovation)

$R_e(t) = C[\hat{x}(t|t-1)]\widetilde{P}(t|t-1)C'[\hat{x}(t|t-1)] + R_v(t)$ (Innovation Covariance)

Gain

$K(t) = \widetilde{P}(t|t-1)C'[\hat{x}(t|t-1)]R_e^{-1}(t)$ (Kalman Gain)

Correction

$\hat{x}(t|t) = \hat{x}(t|t-1) + K(t)e(t)$ (State Correction)

$\widetilde{P}(t|t) = [I - K(t)C[\hat{x}(t|t-1)]]\widetilde{P}(t|t-1)$ (Covariance Correction)

Initial Conditions

$\hat{x}(0|0)$ and $\widetilde{P}(0|0)$

The first stage of the algorithm is prediction. Here the state-space model is used to predict the states. The measurement is then introduced and used to produce the innovation which is the source of change in the predicting system. The estimates of states and covariance are then corrected. Figure 5.7 which is taken from [Can86] illustrates the prediction and correction stages which occur for consecutive time-steps in the generalised case.

Clearly, this algorithm is an on-line process where the Kalman gain and covariance is modified at each step. This leads to the computational burden of implementing the algorithm which in some cases may be impractical or impossible. A potential solution is to use the sub-optimal Kalman filter.

The principle of the sub-optimal filter is that the Kalman gain, and covariance prediction will converge to a constant value as $n \rightarrow \infty$. This can be used to great practical effect when the system is time invariant, as the Kalman filter will display nearly the same level of performance as the optimal version, but with significant reduction in computational burden. The sub-optimal Kalman filter can be expressed by a state-space equation where the state transmission matrix A_k is given by,

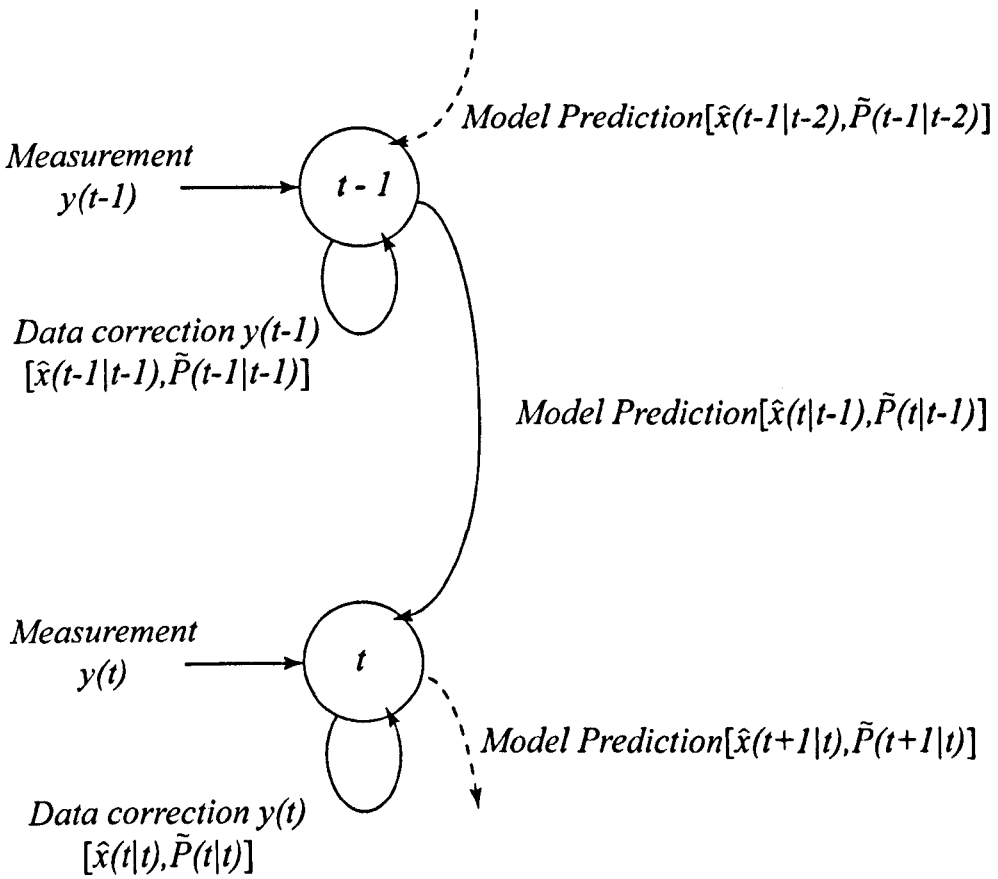

Figure 5.7: Predictor Corrector form of the Kalman Filter (from Candy)

$$A_k = [A - K_\infty C] \tag{5.3}$$

The input transmission matrix B_k is given by,

$$B_k = [B - K_\infty D \;\; K_\infty] \tag{5.4}$$

The measurement matrix C_k is given by,

$$C_k = C \tag{5.5}$$

The state equation is therefore,

$$\hat{x}(t) = A_k \hat{x}(t-1) + B_k u(t-1) \tag{5.6}$$

The filtered output y_f is accordingly given by the output equation,

$$y_f(t) = C_k \hat{x}(t) \tag{5.7}$$

The steady-state Kalman filter can therefore be implemented on-line using look-up tables.

An alternative to this data driven method for determining the steady state Kalman filter is to find the covariance prediction by solving an algebraic Riccati equation. This method uses the predictor form of the Kaman filter, which is discussed in the following section.

5.3.3 Kalman Filter:Predictor Form

In the predictor form of the Kalman filter, only predictions of states and covariances are used, and no update is performed using measurements. This form of the Kalman filter lends itself to use in steady-state Kalman filters since the covariance estimate can be calculated by solving an algebraic Riccati equation. The predictor form of the Kalman Filter algorithm is as follows:

Prediction

$\hat{x}(t+1|t) = A(t)\,\hat{x}(t|t-1) + B(t)\,u(t) + K_p(t)\,e(t)$(State Prediction)

$\widetilde{P}(t+1|t) = A(t)\widetilde{P}(t|t-1)A'(t)+W(t)R_w(t)W'(t)-K_p(t)R_e(t)K_p'(t)$(Covariance Prediction)

Innovation

$e(t) = y(t) - \hat{y}(t|t-1) = y(t) - C(t)\hat{x}(t|t-1)$(Innovation)

$R_e(t) = C(t)\widetilde{P}(t|t-1)C'(t) + R_v(t)$(Innovation Covariance)

Gain

$K(t) = \left[A(t)\widetilde{P}(t|t-1)C'(t) + W(t)R_{wv}(t)\right]R_e^{-1}(t)$(Kalman Gain)

Initial Conditions

$\hat{x}(0|0)$ *and* $\widetilde{P}(0|0)$

The covariance prediction in this form of the Kalman filter algorithm is a discrete Riccati equation, and can be solved to find the steady-state solution, $\widetilde{P}_\infty$. This can be substituted into R_e and K to calculate the steady-state Kalman gains K_∞. Note that as with the predictor-corrector form of the Kalman filter, the steady-state solution is only valid for a time invariant system.

5.4 Conclusions

In this chapter the subject of filtering has been reviewed. The following summary highlights some of the key findings:

1. Frequency domain filters provide a useful tool for shaping the frequency response characteristics of noisy data, but this must be traded against the potential for phase distortion and added time delays.

2. Non-Causal filtering may be applied when filtering is performed off-line. This method provides filtered data with zero-phase shift and no additional time delay. This technique is well suited to the pre-processing of identification data.

3. The Kalman filter is a model based optimal filter which is implemented on-line and evolves its gains through a recursive algorithm.

4. The Kalman filter typically assumes that the noise which is affecting the system is Gaussian, with the magnitude of the noise characterised by covariance matrices. Although this assumption is seldom accurate, the results of the technique when applied to real systems with coloured noise can be of a high performance.

5. A sub-optimal or steady-state variation of the Kalman filter can be trained offline using experimental data and has been shown to provide comparable results to its optimal counterpart, while providing simpler implementation.

Chapter 6

Experimental Setup

6.1 Introduction

This section provides a detailed overview of the experimental setup used in the work presented throughout the thesis. The set-up for the chassis dynamometer and engine dynamometers are described separately. A brief overview of some of the important operating principles of the DC motor and Drive systems are provided in order to give a practical background for the work carried out throughout the rest of the thesis. In addition a description of the instrumentation used on each dynamometer system is given with reference to its application in the respective control problem. Where necessary, commercial confidentiality has been protected by omitting information which is of a potentially sensitive nature.

6.2 The Chassis Dynamometer

The Liverpool chassis dynamometer is typical of the modern 'motor-in-the-middle' type which is prevalent in modern industrial applications. The main components of the dynamometer are a DC dynamometer motor or Power Absorption Unit (PAU) and a pair of large diameter steel rolls. The rolls are mounted at either end of the PAU transmission shaft. The purpose of the rolls is to provide a surface on which the vehicle's driven wheels run, and to provide an equivalent resistive force to that which would be experienced during operation on a road surface. Schematics showing the front and side views of the configuration are shown in Figs. 6.1 and

6.2 respectively. In addition, the dynamometer system, along with the control system which is responsible for operating the electric PAU, and the sensors which are used for feedback and status monitoring, are shown schematically in Fig.6.3.

The tangential force applied to the vehicle wheel F_w produces an equal and opposite reaction force F_d at the dynamometer roller and similarly the torque applied by the vehicle to the vehicle wheel T_w requires a reaction torque $T_p = \frac{r_r}{r_w} T_w$ to be supplied by the motorised power-absorption unit (PAU). The combined physical inertia J_d comprising the inertia of the rollers, J_r and the PAU, J_p is 505 kg.m^2 in the Liverpool dynamometer which equates to a base test vehicle mass of 1357 kg. For vehicles of differing mass, inertia simulation must be employed to provide realistic loading during transient events.

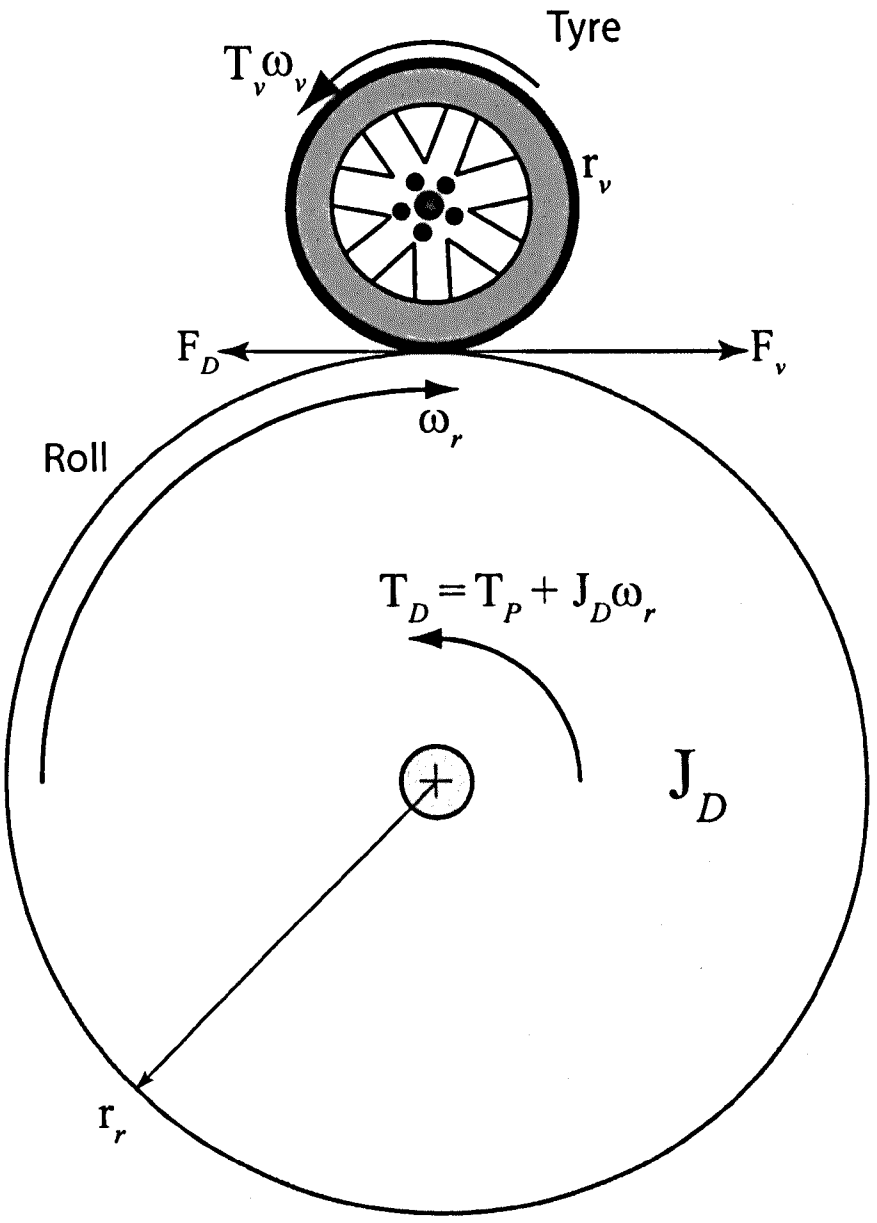

Figure 6.1: Front view schematic of the chassis dynamometer roller and test vehicle tyre

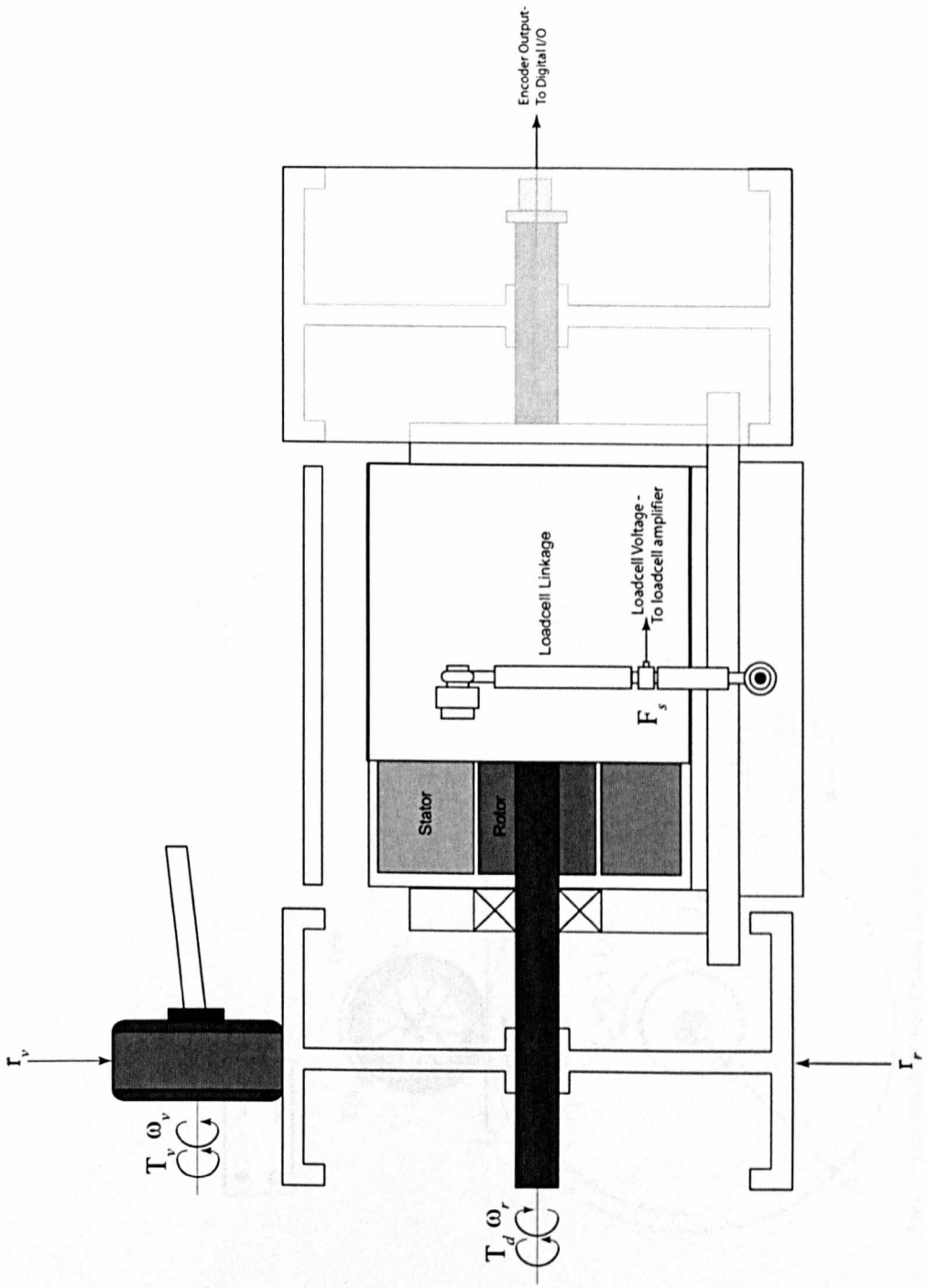

Figure 6.2: Side Schematic of the Chassis Dynamometer

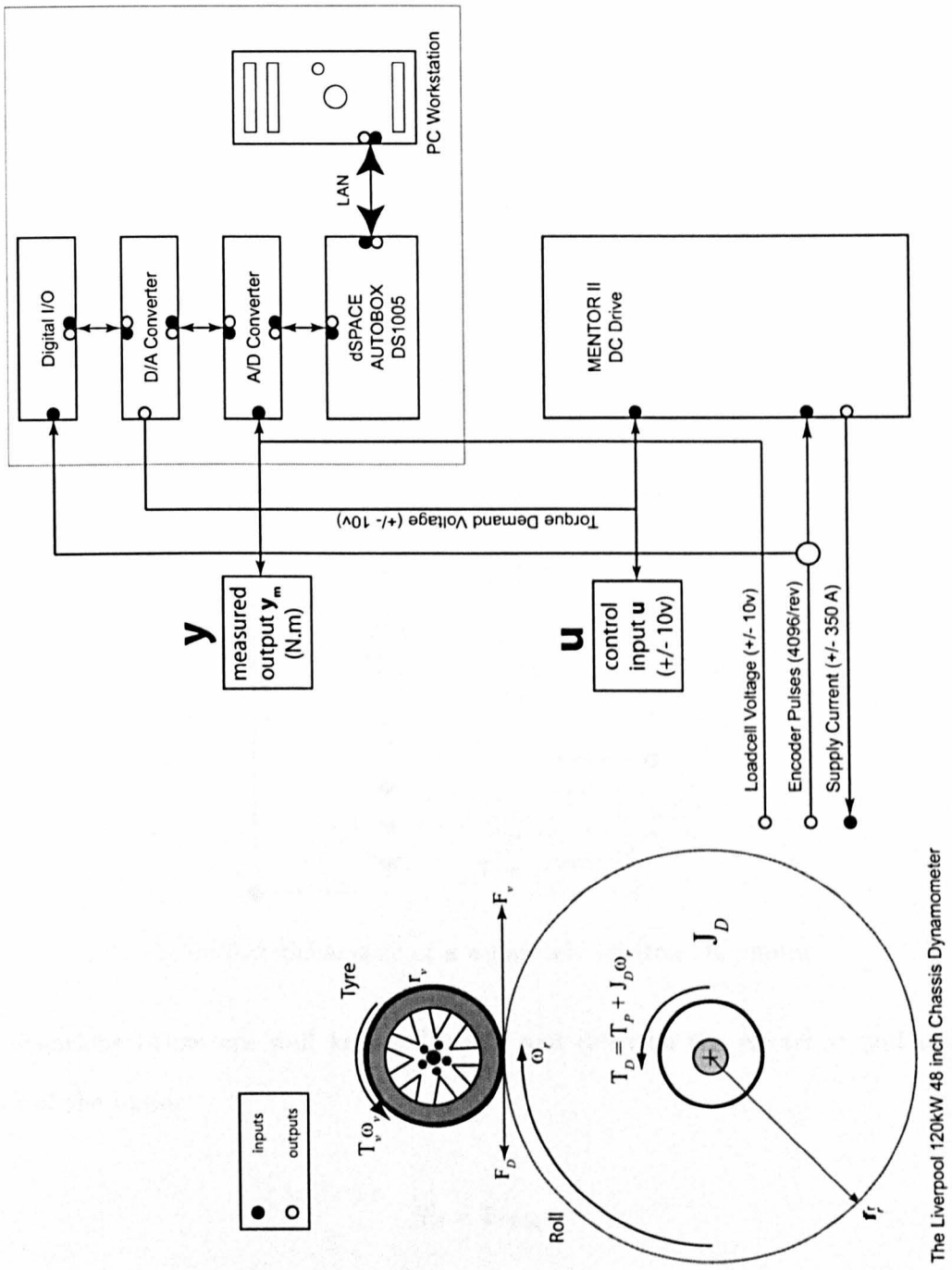

Figure 6.3: Chassis Dynamometer System overview

6.2.1 DC Power Absorption Unit

The dynamometer motor or Power Absorption Unit (PAU) has a maximum absorption capacity of 120kW. The motor is a separately excited unit, with a maximum armature current of 300 Amps and a maximum field current of 5.8 Amps. The physical inertia of the motor is 0.7 $kg.m^2$. Its specifications are described in more detail in Table.6.1.

Parameter	Notation	Value
Full-Load Armature Current:	i_a	280 *Amps*
Armature Voltage:	v_a	380 *Volts*
Field Current (max):	i_f	5.8 *Amps*
Field Voltage:	v_f	300 *Volts*

Table 6.1: DC Motor Specifications

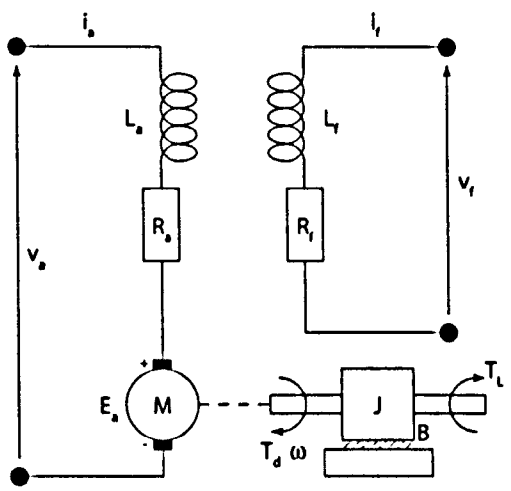

Figure 6.4: Schematic of a separately excited DC motor

The equations below are well known [Leo01] and describe the electrical and mechanical behaviour of the motor.

$$T_d = ki_f i_a \tag{6.1}$$

$$T_d = J_d \frac{d\omega}{dt} + B\omega + T_L \tag{6.2}$$

$$v_a = i_a R_a + L_a \frac{i_a}{dt} + e_a \tag{6.3}$$

$$v_f = i_f R_f + L_f \frac{i_f}{dt} \tag{6.4}$$

6.2.2 The DC Drive

The PAU is powered by a Control Techniques MentorII DC Drive unit. This unit has a maximum rated output of 350 Amps and operates as a Four Quadrant machine with regenerative braking.

The drive converts a 3-phase AC supply into a rectified DC supply which is connected to the armature of the DC motor. The internal electronics form a fully controlled 3-phase SCR (Silicon Controlled Rectifier) bridge rectifier (Fig.6.5). A field current controller is integrated into the drive, providing basic control and speed dependent weakening of the current supplied to the field windings of the motor.

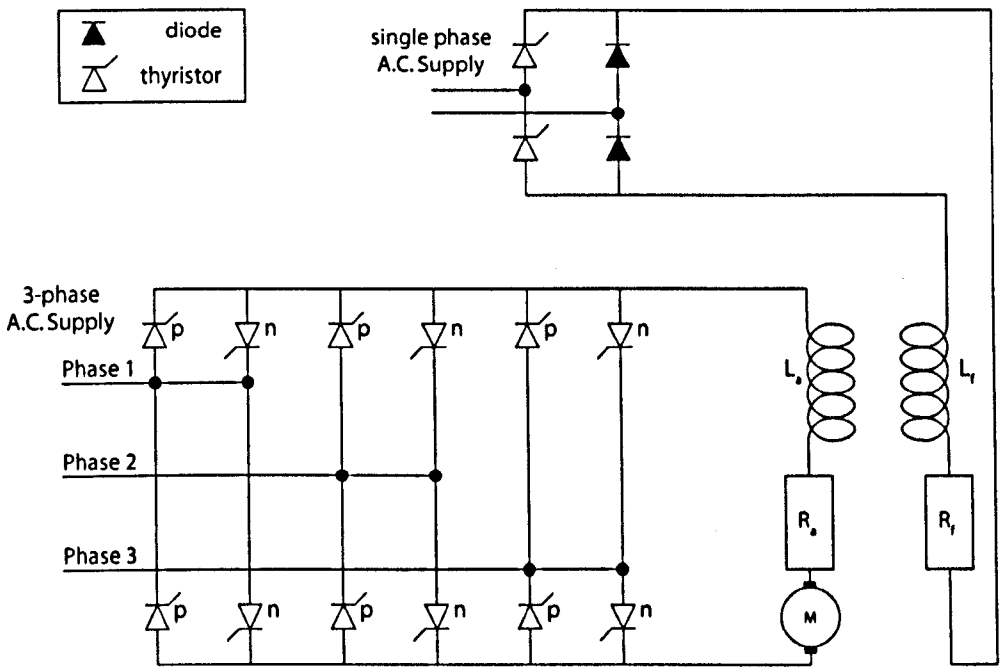

Figure 6.5: 3-Phase Bridge Rectifier

The four-quadrant operation of the drive allows the motor (Fig.6.6) to operate in both forward and reverse directions in either drive or regenerative braking mode. Below the threshold speed (ω_t), in what is commonly known as the Armature control region, motor torque is controlled by varying the armature current, while the field current is held at a fixed level. Above the threshold speed, the motor operates in what is known as the field weakening region. In

this operating condition the armature voltage is maintained at its maximum rated level while the field current is weakened to allow over-speed operation. In this region, the torque delivered reduces as the motor speed increases allowing maximum power to be continuously delivered. The armature control region is usually assumed linear in behaviour whereas the operation in the field weakening region displays a speed dependent nonlinearity.

The drive operates with a cascade controller structure as exemplified by Leonhardt [Leo01]. A fast inner armature current control loop (described in more detail below) provides torque actuation for speed and position control which are implemented as slower external loops in the cascade. In addition to closed loop torque regulation for the outer cascade loops, the fast current loop provides an important safety critical function in the form of protection against instantaneous over-current events. The current loop provides direct control of motor torque by making use of the relationship whereby, in the Armature control region, the torque generated is directly proportional to the armature current. This fact is exploited in speed and position control modes, where steady-state torque control accuracy is of limited importance since it is primarily used as control effort in tracking or disturbance rejection applications, and so does not require absolute accuracy in order to be effective. This relationship between armature current and motor torque is an important and useful one, but cannot be relied upon to provide accurate direct control of torque at the motor shaft (or in the case of the chassis dynamometer, at the roller surface). For this reason, most DC dynamometers make use of an external torque sensor to provide feedback for torque control.

Current control loop

The DC drive unit provides closed loop armature current control, tracking an external reference signal or more typically, the demand from a slower outer speed or position control loop. If the field current is assumed to be constant, as is the case in the armature control region, then the torque output of the PAU (equation.6.1) can be expressed in a simplified form.

$$T_d = k_t i_a \tag{6.5}$$

By rearranging 6.3, and taking Laplace transforms, the relationship between armature volt-

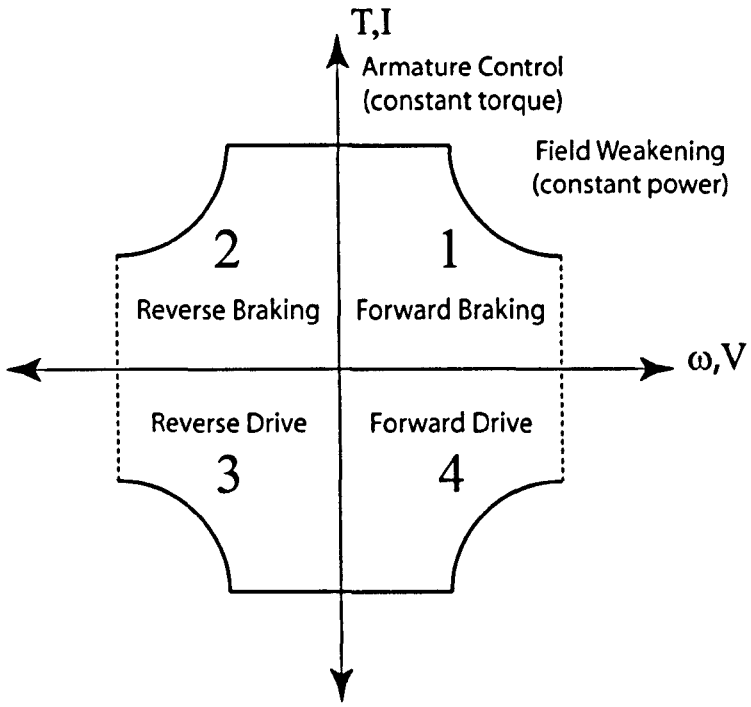

Figure 6.6: Constant power and constant torque

age and current can be expressed in the form.

$$I_a(s) = \frac{V_a(s) - E_b(s)}{R_a + sL_a} \tag{6.6}$$

The back e.m.f. E_b is given by

$$E_b(s) = k_b\Omega(s) \tag{6.7}$$

Where the Laplace transform representation of the rotor speed is,

$$\Omega(s) = \frac{T_d - T_L}{J_d s + B} \tag{6.8}$$

Therefore, by substituting (6.7) and (6.8) into (6.6), and assuming no external loads ($T_L = 0$), a transfer function for the relationship between armature current and armature voltage is given by

$$G_M(s) = \frac{I_a(s)}{V_a(s)} = \frac{sJ_d + B}{(R_a + sL_a)(sJ_d + B) + K_bK_m} \tag{6.9}$$

A block diagram representation of this relationship is shown in Fig.6.7.

It is known that the voltage output from the DC drive is directly proportional to the firing angle of the SCR bridge circuit and that a time delay is present due to the delay between individual thyristors firing. This gives a transfer function between firing angle and armature voltage.

$$G_D(s) = K_f e^{-sT} \tag{6.10}$$

Combining G_D and G_M gives a transfer function G which describes the input-output characteristics between the firing angle and the armature current.

$$G(s) = K_f \frac{sJ_d + B}{(R_a + sL_a)(sJ_d + B) + K_b K_m} e^{-sT} \tag{6.11}$$

$$G(s) = \frac{K_f J_d s + K_f B}{J_d L_a s^2 + (BL_a + R_a J_d)s + (R_a B + K_b K_m)} e^{-sT} \tag{6.12}$$

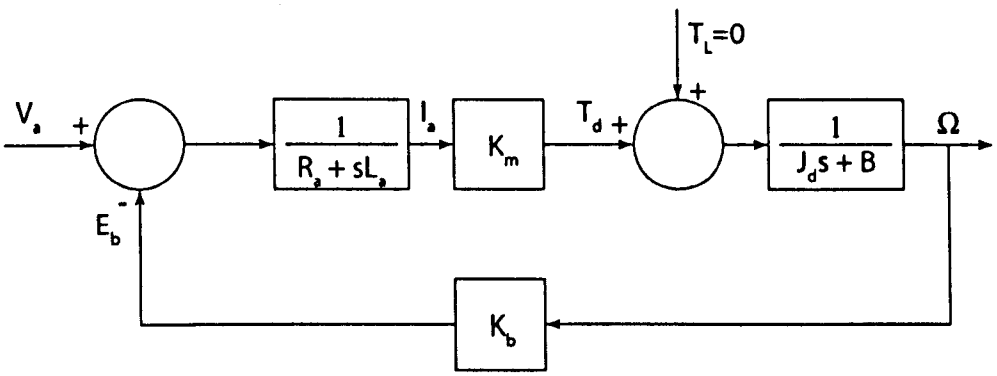

Figure 6.7: Block Diagram representation of the DC Dynamometer

The transfer function models $G_M(s)$ and $G_D(s)$ describe the current control loop (Fig 6.8) of the DC drive. The feedback control is normally a three term PID with parameters tuned online during comissioning to provide the desired level of performance.

It is in this basic current control mode that the DC drive operates in the following work. However, the current control mode ignores the presence of any external loads since they cannot

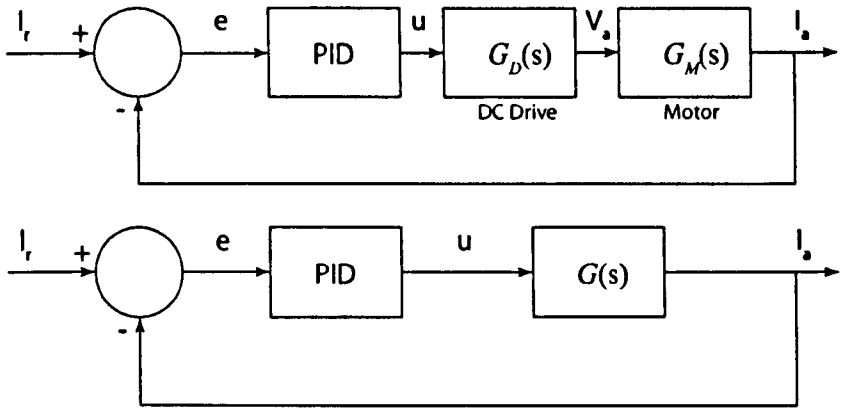

Figure 6.8: Current control loop

be observed. As mentioned previously, this is of little concern when the current control loop is implemented for its usual application as the fast internal loop in a cascade controller for speed or position since it merely provides corrective control effort and as such steady state accuracy in terms of torque is unimportant.

In the approach described here, the DC drive and PAU are considered as a combined black box system and the PAU torque measurement as feedback for the controller, with the current reference signal as control effort. The system is modelled using system identification techniques to establish a transfer function plant model of the current control system. This has the advantage that a robust controller may be designed and implemented which tracks a physical measurement of the torque output from the PAU. This means that disturbances such as external loads and unmodelled friction losses are included in the feedback.

Direct control of the firing angle of the bridge circuit, using measured torque feedback, was considered as a more direct approach which would bypass the internal current loop. However, it was assessed that the risks associated with possible damage which might occur in the event of instability were too great. Also, given the fast fundamental response of the system in torque control mode, the outlined approach provided scope for high performance while enjoying the benefits of the safety limits imposed by the DC drive while operating in current control mode.

6.2.3 Torque Measurement System

The PAU torque is measured by a loadcell linkage connected between a 'torque arm' (which is fastened to the motor casing and terminates at a known distance from the center axis) and the dynamometer base.

Total reaction torque is measured indirectly by measuring the axial reaction force in the loadcell linkage. This linkage consists of an HBM U2B axial loadcell connected between linkage bars. At either end, the linkage bars connect to the dynamometer via male rod ends with high precision spherical bearings which prevents bending moments from being imposed on the loadcell. High precision components were selected in order to minimise the amount of backlash present in the linkage*. The torque generated by the dynamometer motor is calculated from the loadcell measurment according to the equation;

$$T_p = F_s R_l \tag{6.13}$$

In an idealised system the loadcell should measure only the reaction force associated with the torque generated by the PAU. In fact, the loadcell linkage, torque arm and motor casing form a dynamic system which responds to the load applied during a transient motor event. The result of this is that the loadcell measures force components due to these transient dynamics, superimposing extra dynamics on the signal of interest which is solely that applied through the rollers to the test vehicle. Fig.6.9 shows a simplified schematic of the torque measurement arrangement.

The effects of structural dynamics corrupting the measurment in this type of arrangement have been observed in previous authors' work [ST+94, Thr04]. A more detailed investigation into these dynamics is provided in section 7.3.

*During development carried out on the Liverpool Chassis Dynamometer, it was found that the backlash present in the standard linkage was significant. This was clearly visible as a discontinuity in the measured loadcell outputs during torque reversals

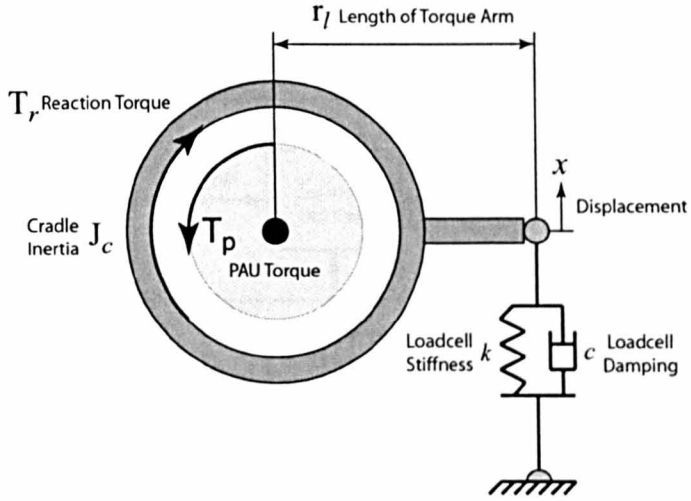

Figure 6.9: Loadcell measurment system model

6.2.4 Rapid Prototyping and Data Acquisition

The Liverpool Chassis dynamometer uses a dSPACE Rapid Control Prototyping (RCP) platform for implementation of control and data acquisition functionality. The architecture of the system is shown in Figure. 6.10.

The target system is based within a dSPACE Autobox hardware system which is an expandable modular unit accepting hardware cards, each of which delivers specific functionality. The core component of the system is the target processor card (dS1005) which houses the system CPU as well as LAN hardware for interfacing with the host PC. The target platform is extended with the addition of boards which offer input and output functionality to match the requirements of the application.

The target is programmed using code which is automatically generated using the Matlab Real-Time Workshop software. The system architecture is developed within the Simulink modelling environment, with input and output channels accessed using the platform specific dSPACE RTI blockset. The Simulink model is 'built' using Real-Time workshop, compiled and uploaded to the dS1005 platform over the LAN BUS.

User interaction with the system is achieved using the dSPACE ControlDesk software. This software provides a graphical user interface for the manipulation, visualisation and capture of parameters and data associated with the real-time model running on the target hardware. A virtual control panel for the Chassis dynamometer was developed by the author using this

software.

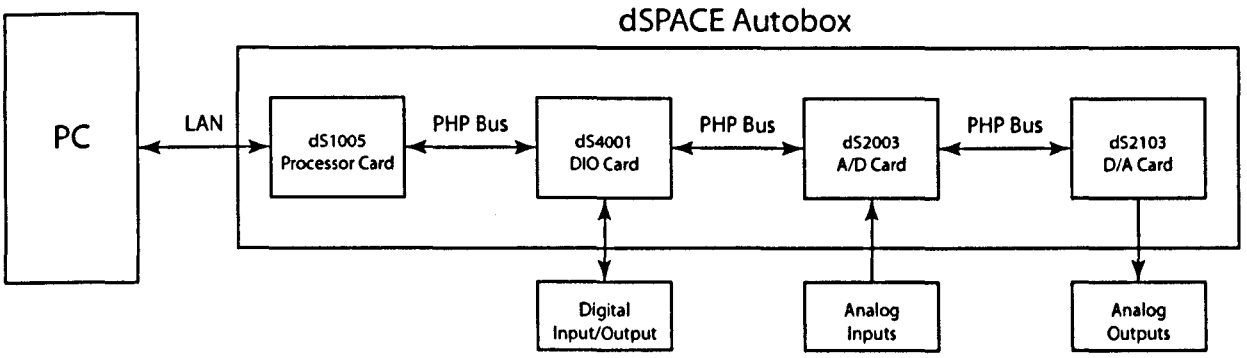

Figure 6.10: Overview of the dSPACE AutoBox System

The following subsections give a brief overview of the modular hardware which was used.

Digital Input/Output

The Digital Input/Output (DIO) interface is a dS4002 Card. This provides 32 DIO channels including Interrupt Request (IRQ) channels and timing functionality for generating PWM and square-wave frequency signals. In this application, the DIO capability is mainly reserved for functions relating to vehicle control.

Analogue Input/Output

Digital to Analogue conversion (DAC) functions are provided by a dSPACE dS2103 board which has a resolution of 16 bits and a bi-polar output range of ± 10 volts. The primary function of the D/A conversion within the dynamometer test cell is to provide the analogue torque demand input to the DC drive and the speed control reference to the Vehicle cooling fan drive. In addition, the DAC hardware provides channels for operating vehicle systems such as the automated clutch pedal actuator.

Analogue to Digital conversion (ADC) is handled by a dSPACE dS2003 board which has a resolution of 16 bits and maximum range of ± 10 volts. The A/D conversion is used to measure the output of the loadcell and tachometer hardware. In addition, PAU armature and field currents are measured in the DC drive and can be monitored.

6.2.5 Instrumentation

Torque Measurment - Axial Loadcell

The load transducer used in the torque measurement arrangement is an HBM U2B Axial strain type loadcell with a maximum capacity of 10 kN. This unit was chosen due to its relative axial stiffness, compared with typical S-Beam strain loadcells [†]. The loadcell provides an output which is amplified using an instrument amplifier. The amplified output signal is transmitted as a 4-20 mA current before ohmic conversion to a voltage for analogue to digital conversion.

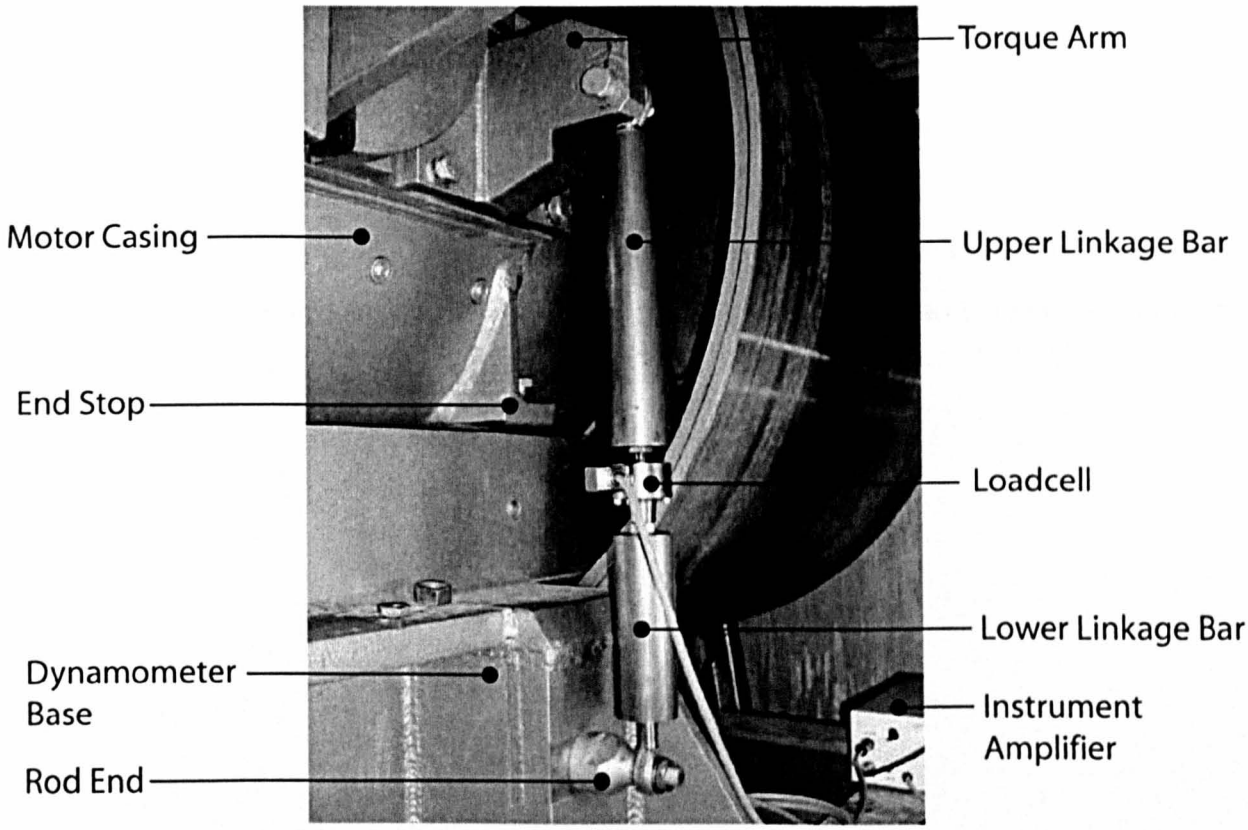

Figure 6.11: Loadcell Linkage

[†]The standard S-beam loadcell which was originally fitted to the dynamometer was replaced in an attempt to reduce the effect of the sensor structural dynamics. It was hoped that an increase in stiffness would in turn increase the natural frequency of the structural mode and therefore allow a clearer distinction between the low frequency dynamics of the dynamometer and the structural dynamics of the torque measurment system. It was found that the actual improvement was small compared with the improvements seen in increasing the quality of the rod-end bearings in the loadcell linkage

Roller Speed Measurement - Angular Encoder

The roller speed is measured by an optical encoder which generates 4096 TTL pulses per revolution. The frequency of rotation is measured from the primary pulses, and converted to an analogue output which is proportional to angular velocity, using frequency to voltage conversion hardware. The angular velocity measurement is subject to a periodic fluctuation which occurs once per revolution and is associated with small imbalances in the rolls. This fluctuation is problematic because it affects the calculated roller acceleration quite severely. For this reason, the roller speed must be pre-filtered before it is used in the road-load simulation algorithm. (See Section.5)

Armature and Field Current Measurement

The current which is supplied to both the Armature and Field of the PAU is monitored using current transducers installed within the MentorII Drive. This allows an uncalibrated measurement to be made of the current supplied to the motor.

6.3 The Engine Dynamometer

The engine testing facility described here is owned and operated by SRH Systems. The following provides an overview of the engine dynamometer along with its control hardware and instrumentation.

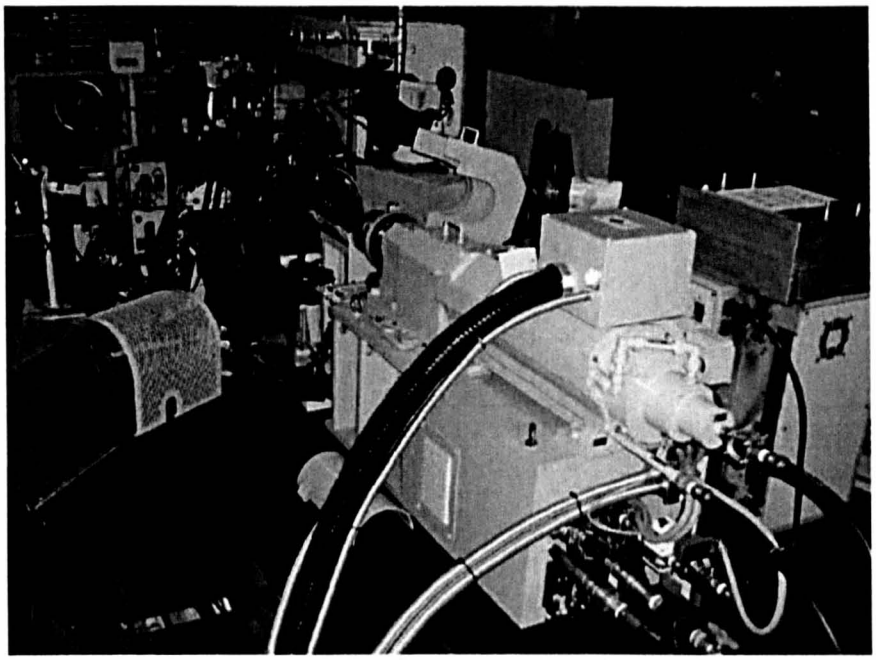

Figure 6.12: The Transient Engine Dynamometer

6.3.1 Permanent Magnet DC Power Absorption Unit

The engine Dynamometer is a TOYO low inertia permanent magnet DC machine. The Dynamometer is controlled with a DC drive unit. An analogue reference input signal to the DC Drive defines the torque required from the dynamometer. Dynamometer speed feedback is provided by an integrated 480 PPR encoder, while torque feedback is provided by an external transducer.

6.3.2 Transmission Shaft, Torque Transducer and Coupling

The test engine is coupled to the Dynamometer via a transmission shaft, torque transducer and flexible coupling. The transmission shaft is a proprietary component, designed to display a torsional resonant frequency of around 10 Hz. The resonant frequency of the shaft is selected

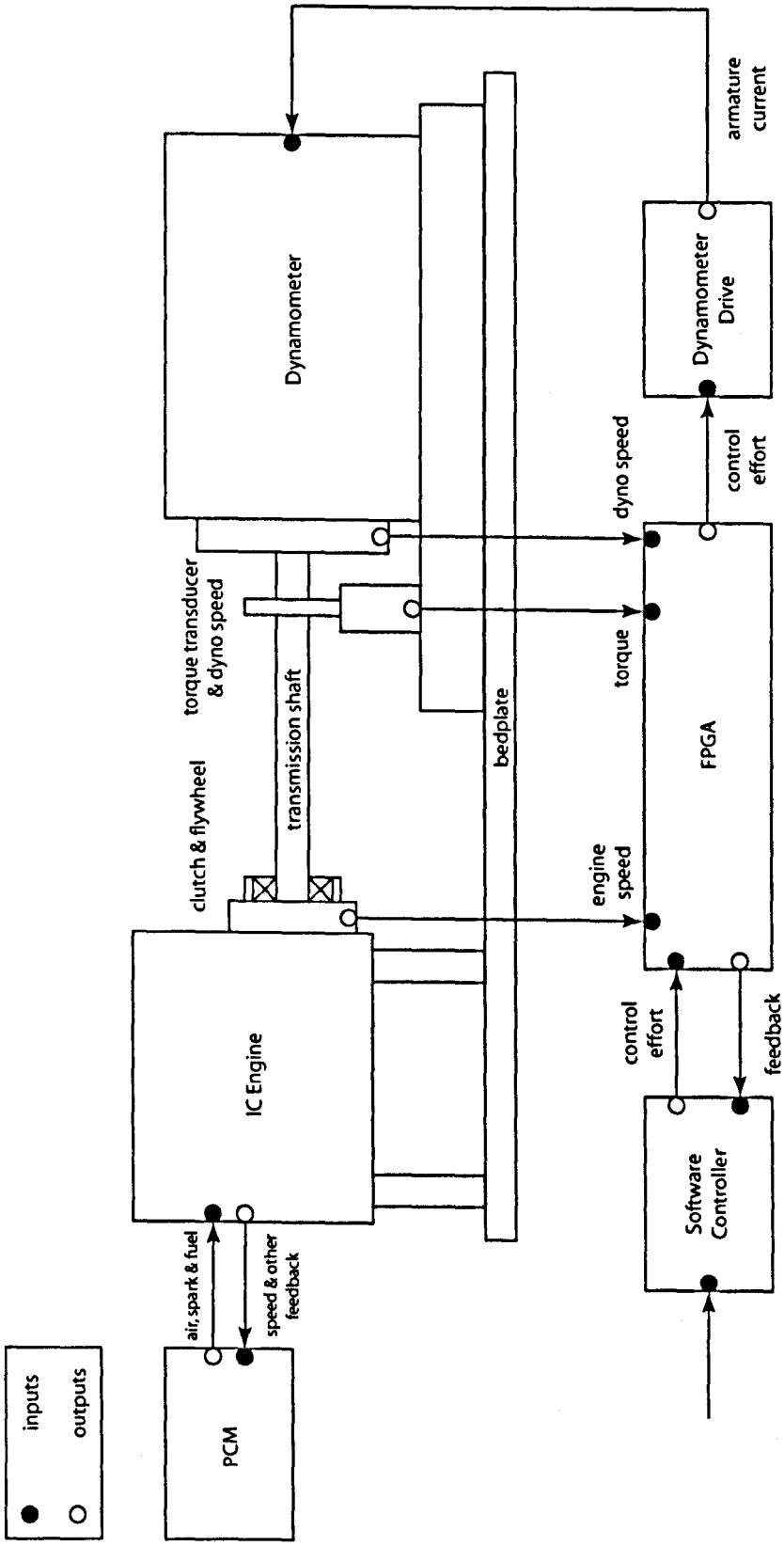

Figure 6.13: Schematic of the Engine Dynamometer System

to ensure that the test engine does not excite the resonant frequency of the shaft within its operating range. Because the resonance occurs at a frequency very much below the operating frequency of the engine, it should only be excited momentarily during cranking and switch off.

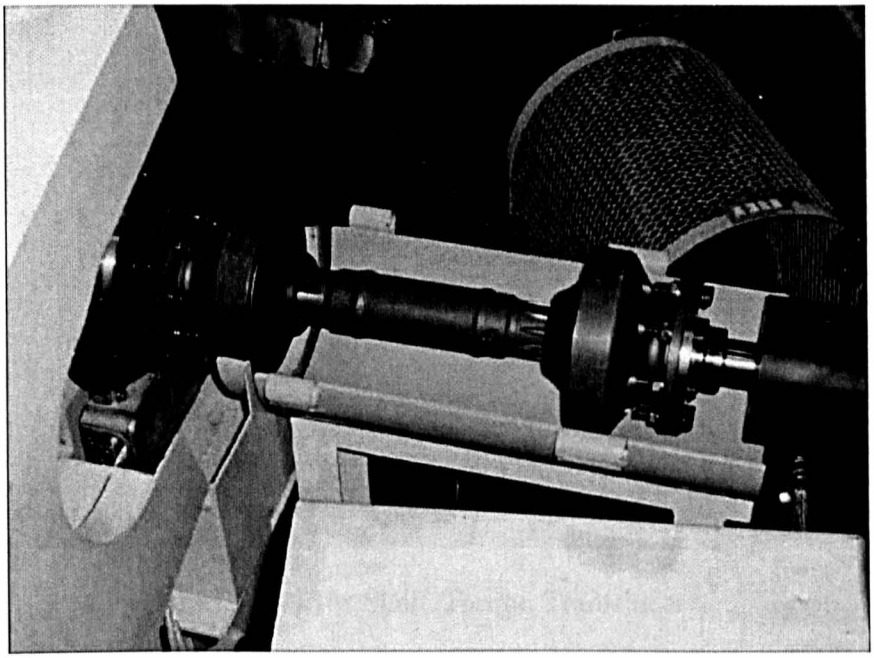

Figure 6.14: Dynamometer Transmission Shaft

The torque transducer is a HBM non contact flange coupled system with high torsional stiffness.

6.3.3 The Test Engine

The test engine is a 2.8 litre 4-cylinder Gasoline engine and has an idle speed of 750 RPM. The engine is coupled to the dynamometer shaft by means of a high stiffness automotive clutch which is maintained in its engaged state throughout testing. The objective of the zero shaft torque testing procedure is to simulate the scenario where the clutch is disengaged and the engine operates at idle. Throttle position is not accessible as an input parameter in the zero shaft torque control condition but an Air Bleed Valve (ABV) is subject to actuation by the Engine Management System (EMS).

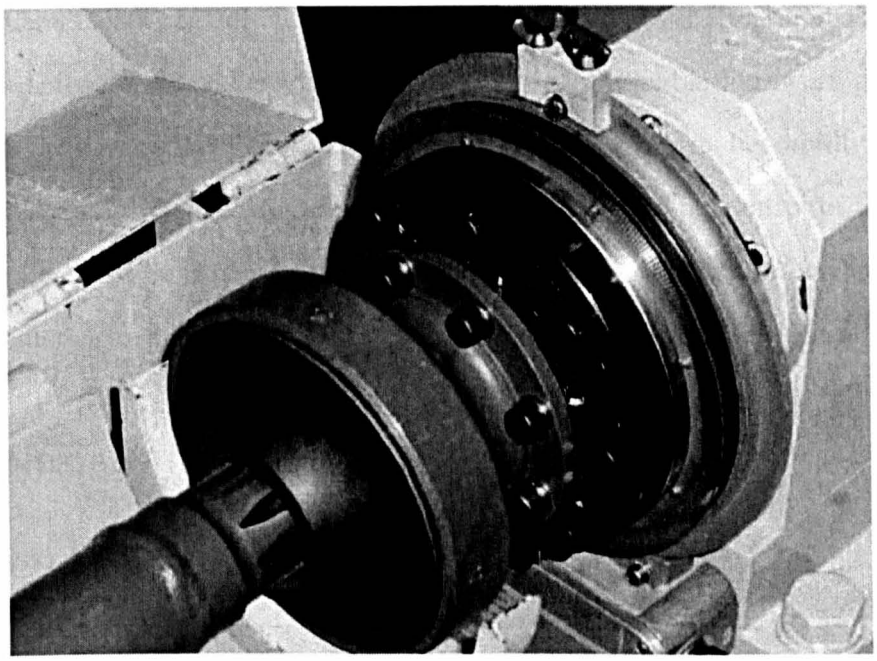

Figure 6.15: Shaft Torque Transducer

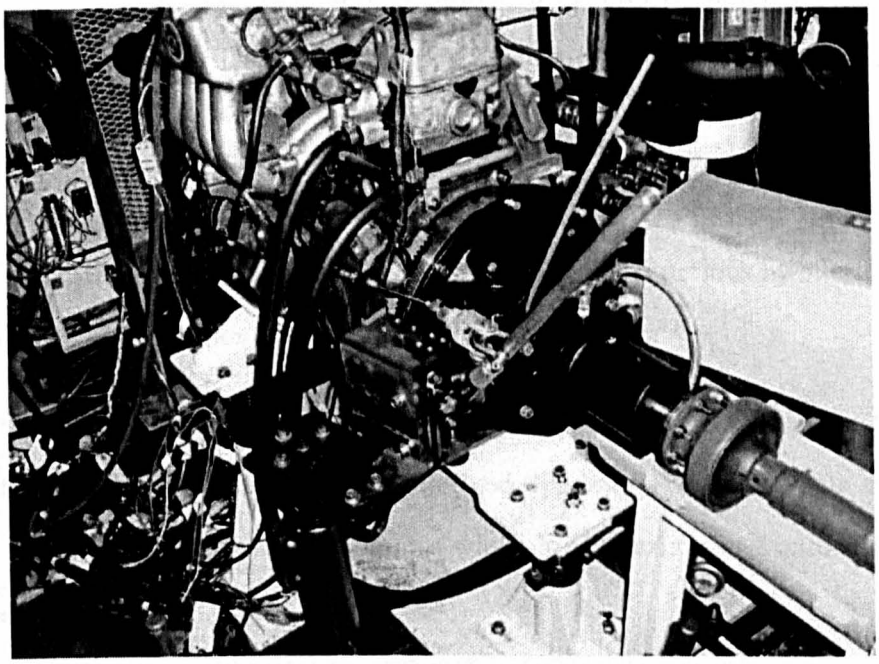

Figure 6.16: Test engine coupled to transmission shaft

6.3.4 PAU Control Hardware and Software

The engine dynamometer control hardware is based around a Field Programmable Gate Array (FPGA) and a software controller. The FPGA is a programmable hardware platform which provides access to a very large number of logical gates which can be rapidly configured to define a complex digital control system with appropriate inputs and outputs. The system is programmed using software drivers and in this case the control architecture, including candidate feedback controllers, can be implemented within the Matlab/Simulink modelling environment.

6.4 Conclusions

6.4.1 Chassis Dynamometer

1. The Chassis Dynamometer PAU (Power Absorption Unit) is a DC machine, with a power output of 120kW. The system is operated below its threshold speed of 450 RPM, to ensure that it operates in the Armature control region.

2. All control, signal processing and data acquisition operations are performed using a dSPACE Autobox RPC system. This hardware is interfaced with a PC via a LAN connection and is programmed using Real-Time workshop via Matlab/Simulink and Control Desk software.

3. The PAU is powered by a 4-quadrant DC Drive. It is operated in current control mode while additional Torque, Speed or Position controllers are implemented as external cascade loops. The current control loop provides important safety functions by offering over-current and acceleration protection to the motor.

4. PAU torque is measured via the total reaction force measured between a torque arm on the cradle mounted motor casing and the fixed dynamometer base. This measurement is subject to significant structural dynamics which are superimposed onto the actual motor response.

6.4.2 Engine Dynamometer

1. The engine dynamometer is being developed to provide a full spectrum simulation of road-load conditions for engine testing. Zero shaft torque control is one special requirement of this capability and is used to simulate the engine in a de-clutched state.

2. The engine dynamometer PAU is a low inertia DC permanent magnet machine. The PAU is powered by a DC drive which is provided with external control signals from the FPGA hardware.

3. Shaft torque control is implemented in an external software controller which is interfaced with the FPGA.

4. Feedback of the transmission shaft torque is provided using a flange-type shear stress torque transducer which has high torsional stiffness.

Part II

Chassis Dynamometer Identification & Control

Chapter 7

Chassis Dynamometer System Identification

The following section describes the characterisation and system identification process which was applied to the Liverpool chassis dynamometer. Firstly, basic input-output tests are used to provide insight into the fundamental behaviour of the system. The characterisation process provides important information about the nonlinear nature of the chassis dynamometer system, and a static nonlinear inverse compensator is accordingly applied to provide a linearised system. A Linear system identification process, after that described in the previous section, is applied, resulting in an LTI system model, along with quantified uncertainty.

7.1 Quasi-Static System Characterization

For the purpose of characterising the DC behaviour of the system, Quasi-static characterization was performed using a slow sine sweep input at a frequency of $0.1 rad/s$. The input-output relationship was considered for both drive input to armature current (Fig.7.1), as well as drive input to PAU torque, measured at the loadcell (Fig.7.2).

The DC relationship between the drive input and the PAU torque is found to be nonlinear. Using least-squares curve fitting method, a good fit is found to be a 3rd order polynomial with no bias term. This means that a linear system model will not predict the steady state response

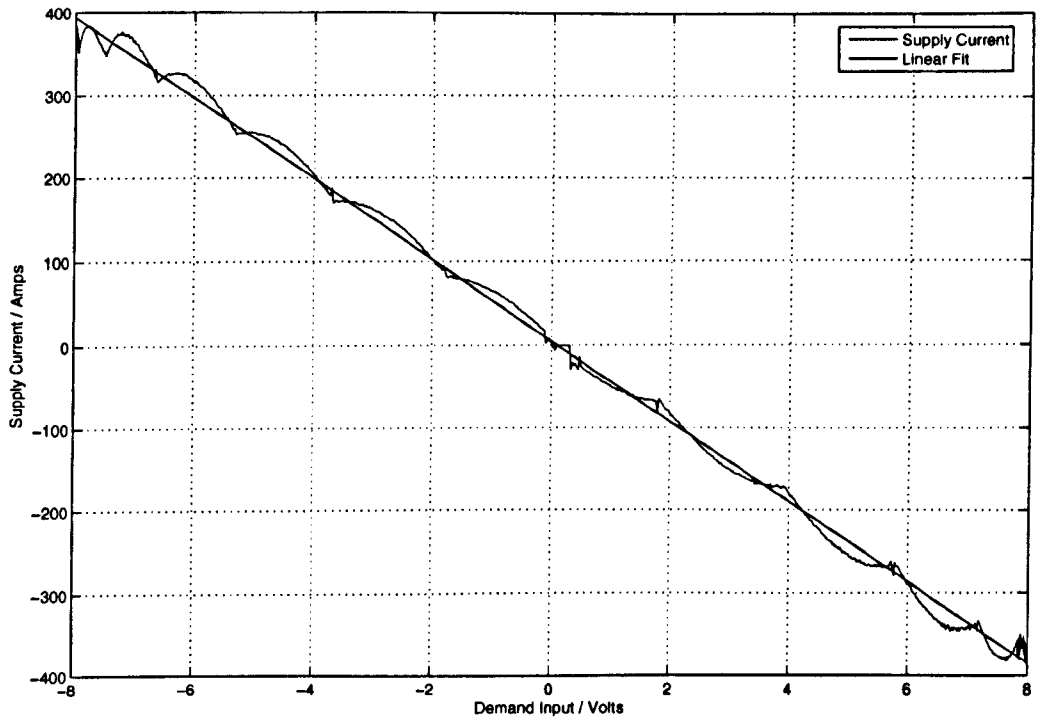

Figure 7.1: Relationship between Drive Input voltage and Armature current in the Armature control region

of the system. As will be discussed, the introduction of a nonlinear inverse model into the system may provide satisfactory linearisation of the system, making a linear model more suitable.

7.2 Open-Loop Step Response

The step response tests were performed on the open loop system to establish a basic understanding of the system's dynamic response, along with an estimate of the system time delay.

A range of step demand voltages were applied to the analogue input of the DC drive, and the system torque response was measured and logged at a rate of 1kHz. Figure.7.3 shows a typical step response. It was observed (Fig.7.4) that a time delay of between 8 and 10 ms was present in the system.

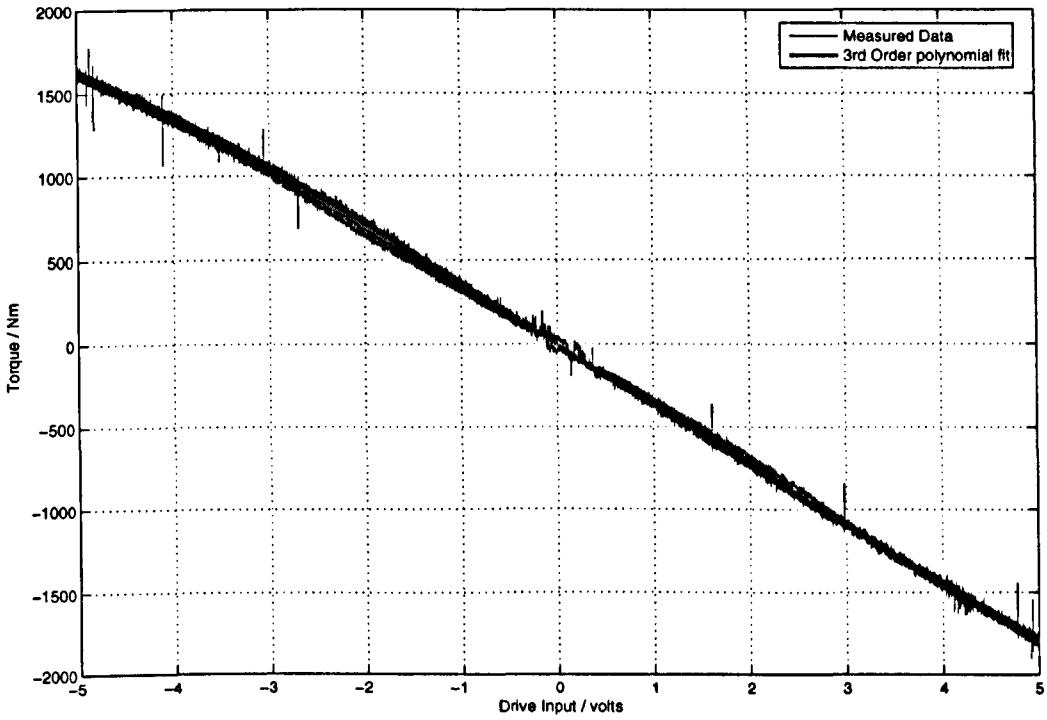

Figure 7.2: Relationship between Drive Input voltage and Measured Torque in the Armature control region

7.3 Structural Dynamics of the Torque Measurement System

It was apparent from the open loop characterization of the chassis dynamometer system, that the torque feedback of the PAU torque is affected by an oscillatory component. Figure.7.5 shows the power spectral density of the torque response to a step input. A clear resonance is visible at 18Hz which characterises the oscillation seen in the measured response. This was somewhat unexpected since the established understanding of the behaviour of the DC motor is that the response to a step change in armature current should be low pass, with no oscillation and that since the electrically generated torque in a DC motor is proportional to the Armature current, its torque response should behave similarly. The step response tests showed that the armature current supplied by the DC drive was not oscillatory and that the oscillation was therefore probably not a result of a poorly damped current control loop. It was therefore thought that the oscillation was a result of the structural dynamics of the torque measurement arrangement. In order to establish the validity of this hypothesis, some experimental investigations were carried

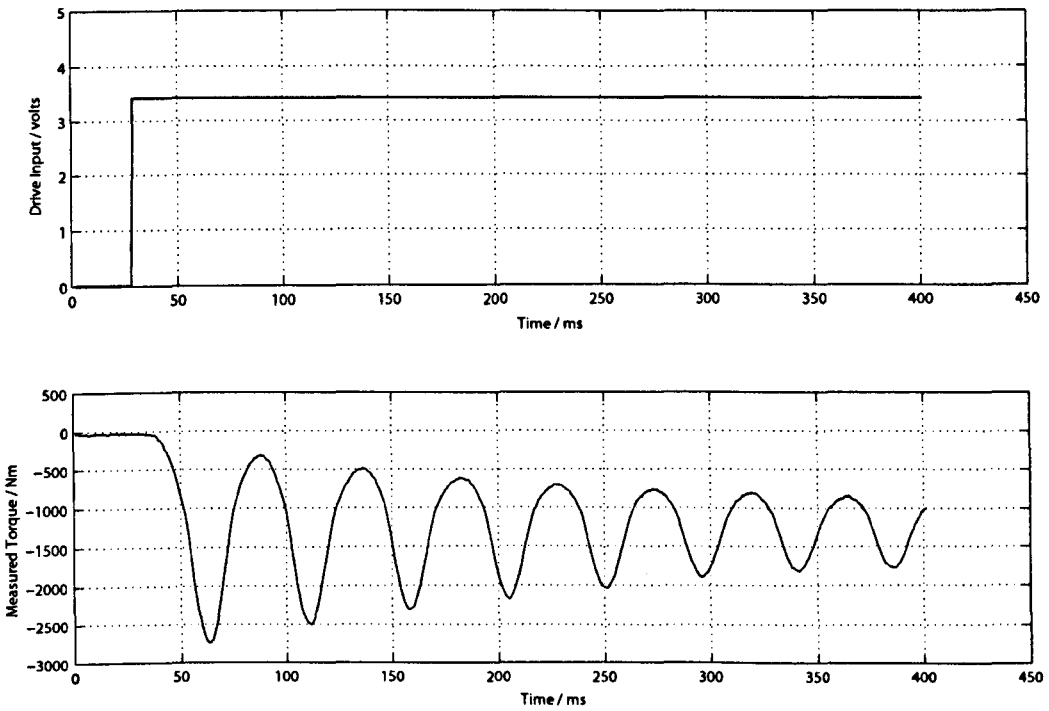

Figure 7.3: Open Loop Step Response

out.

7.3.1 Experimental Investigation

A set of tests were performed to establish whether the oscillatory component of the response could be viewed as sensor noise. An Accelerometer was mounted on the top surface of the loadcell, and the torque measurement arrangement was impulse loaded in 2 locations (Fig.7.6) using a weighted, rubber tipped, hammer. The uncalibrated response of the accelerometer was logged. Figure 7.7 shows a typical time response plot for such a test. The data which was collected was subjected to a spectral analysis, typical results are shown in figures 7.8 and 7.9. It can be seen that there are clear peaks in the frequency response at 18.5Hz and 20Hz respectively, coinciding closely with the oscillatory component of the torque response which was observed.

Previous authors [ST+94] observed dynamics in the same frequency range (circa 20Hz), and proposed an active cancellation method which uses the accelerometer output, subtracted from the load-cell output, to reconstruct the actual torque response. It is proposed that using a stiffer

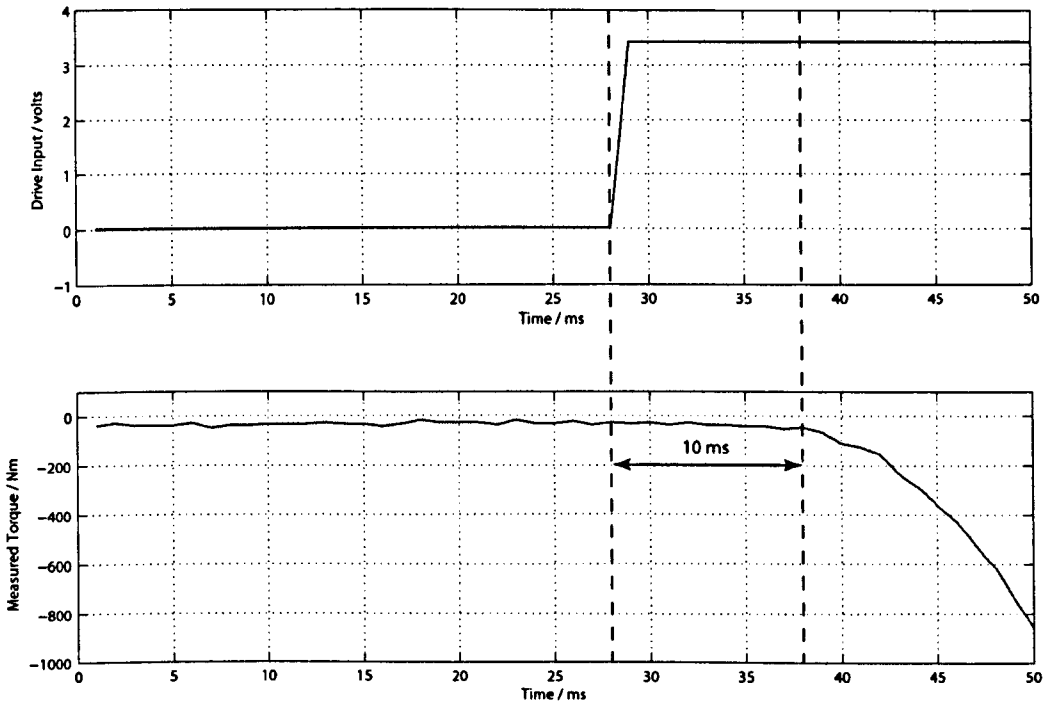

Figure 7.4: Time Delay Estimation

load-cell linkage arrangement would increase the natural frequency to around 30Hz.

Having established the existence of the sensor dynamics, and with previous precedents to suggest that this component should be eliminated in order for high performance control to be possible, candidate filtering approaches were considered. This is discussed in more detail in section 5.

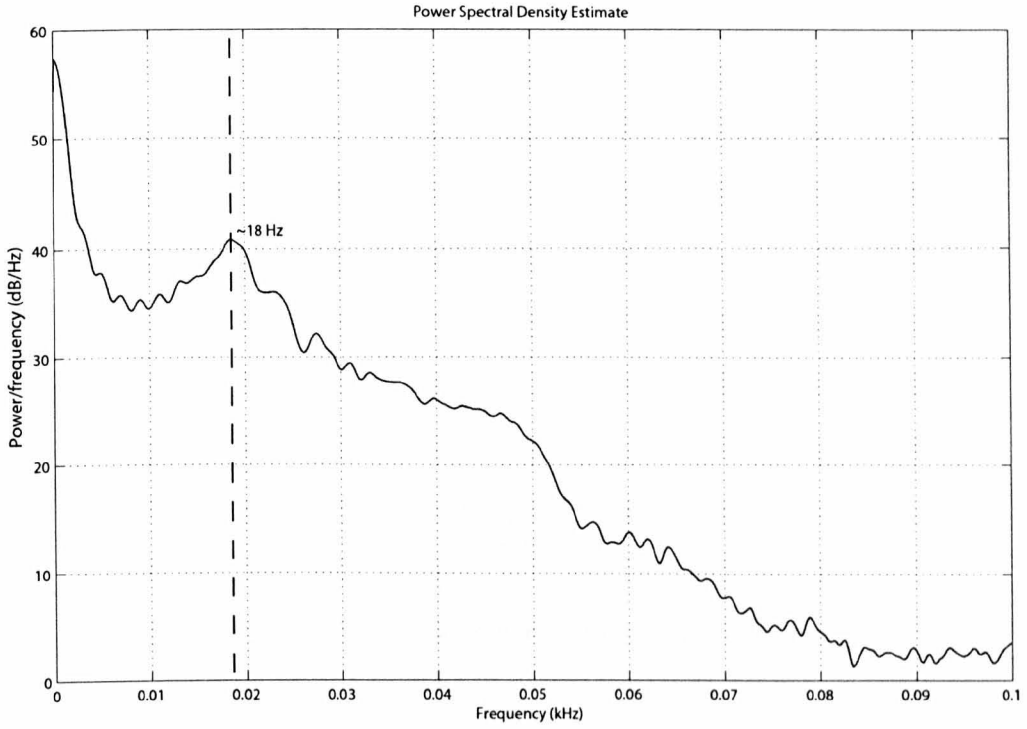

Figure 7.5: Chassis Dynamometer Torque Response

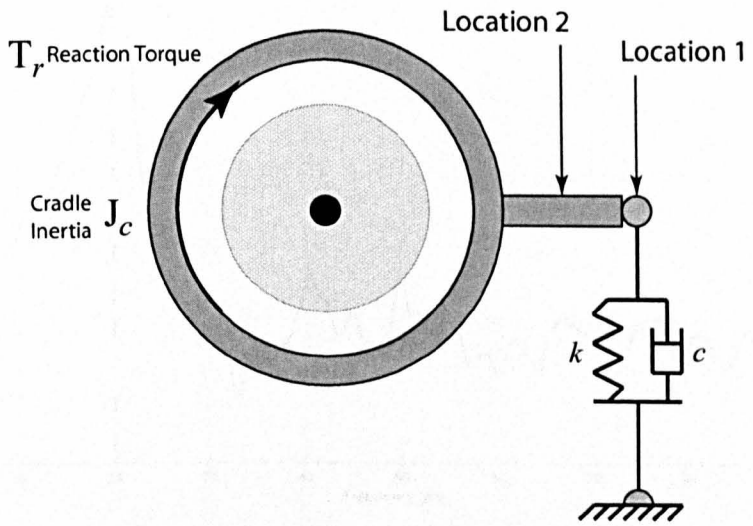

Figure 7.6: Locaton of impulse loading applied to the torque measurement arrangement.

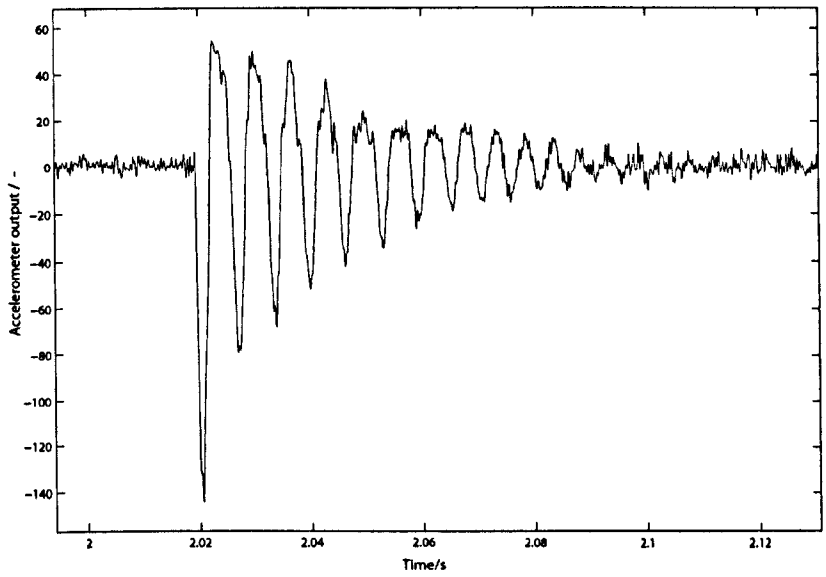

Figure 7.7: Accelerometer response to Impulse load

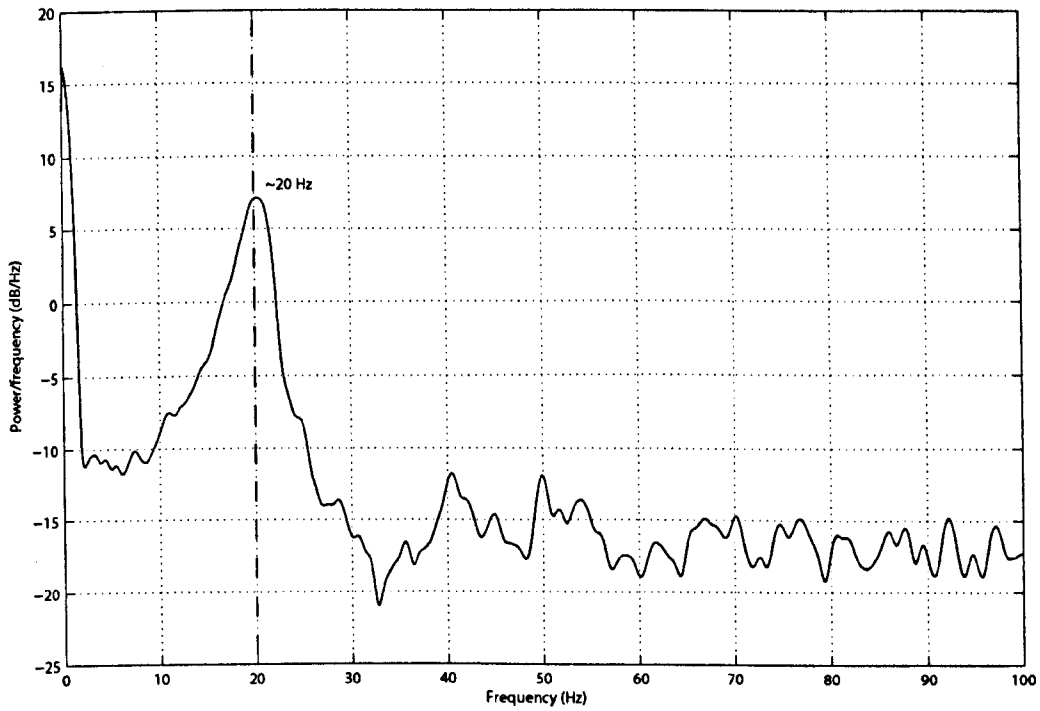

Figure 7.8: PSD of the accelerometer response for hammer test applied at Location 1

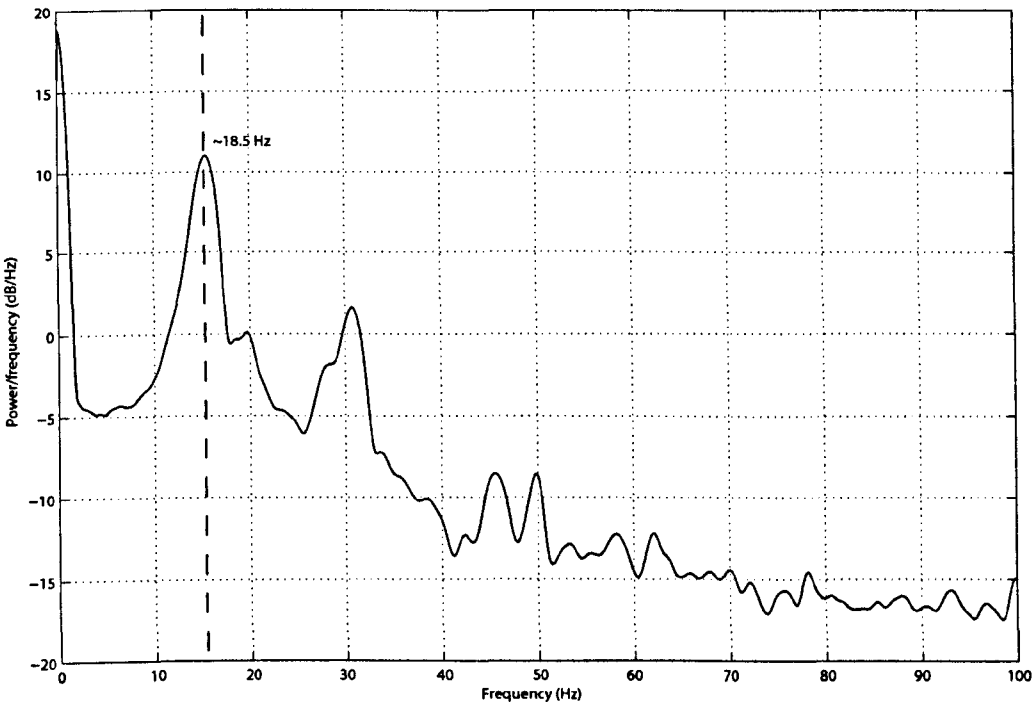

Figure 7.9: PSD of the accelerometer response for hammer test applied at Location 2

7.4 Static Inverse Compensation

It is clear from the quasi-static characterization performed in the previous section, that the DC characteristics between the applied reference input, and the torque generated by the motor, is nonlinear. This section shows how a direct inverse compensator (DIC) may be designed which effectively linearises the system. This process allows linear system identification methods to be used to develop system models for controller design. It has been shown [MDS06] that this method significantly reduces the multiplicative uncertainty associated with linear system models and as such aids in improving the performance and robustness of resulting controllers.

The obvious disadvantage of a static inverse compensation scheme is that frequency dependent nonlinearity (should it exist) is not linearised, but the judgement about whether this is required can only be made through analysis of the results which are achieved through a number of different methods. In the case of the chassis dynamometer, attempts were made to identify a suitable nonlinear dynamic inverse using a NARMAX structure, but it was found that there was little or no advantage in a dynamic inverse model over a static one and so static inverse was selected as it is computationally less demanding to implement, and easier to identify.

Fig 7.10 shows the inverse relationship between the input reference voltage to the DC drive, and the PAU torque output. The curve is fitted with a 3rd order polynomial. The residuals of the polynomial fit are compared with those for a linear fit in Figure.7.11. The residuals indicate that the 3rd order polynomial does not provide a perfect fit, especially

The nonlinear inverse compensator (Λ) is of the form:

$$v(T) = p_1 T^3 + p_2 T^2 + p_3 T \tag{7.1}$$

With the following parameters p_1 to p_3.

Parameter	Value
p_1	$-5.47e^{-11}$
p_2	$-8.878e^{-8}$
p_3	-0.002775

Table 7.1: Inverse Compensator Parameters

By implementing this compensator in the open loop system, and by changing the system

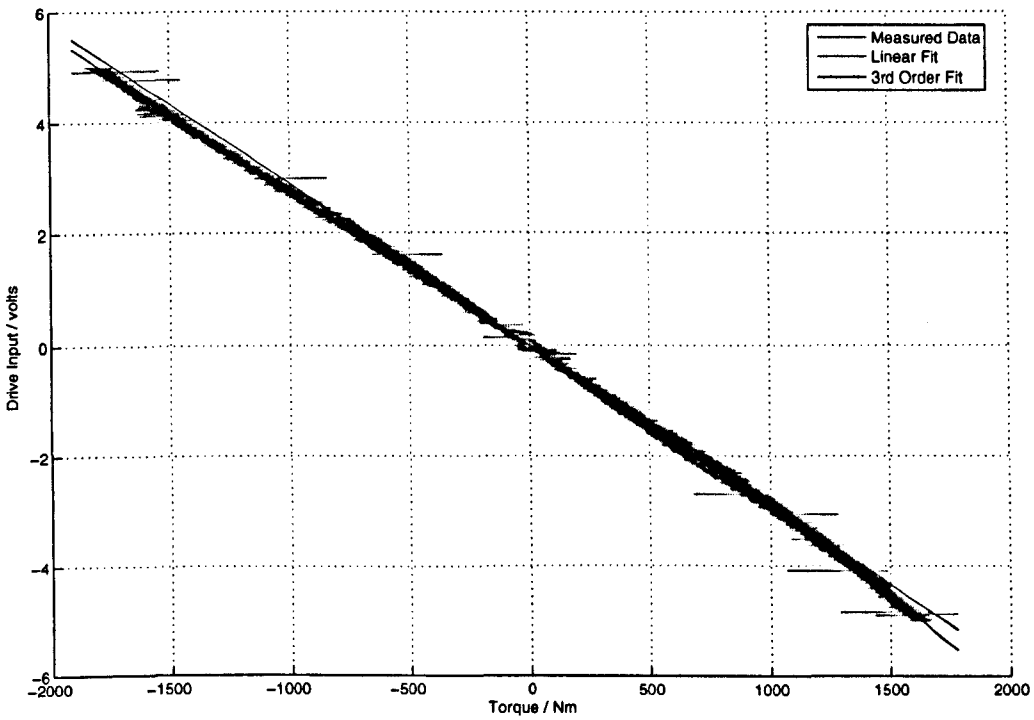

Figure 7.10: Static Nonliner Inverse Model

input to desired torque rather than a reference voltage then the resulting compensated open loop system will be linearised and will have unit DC gain.

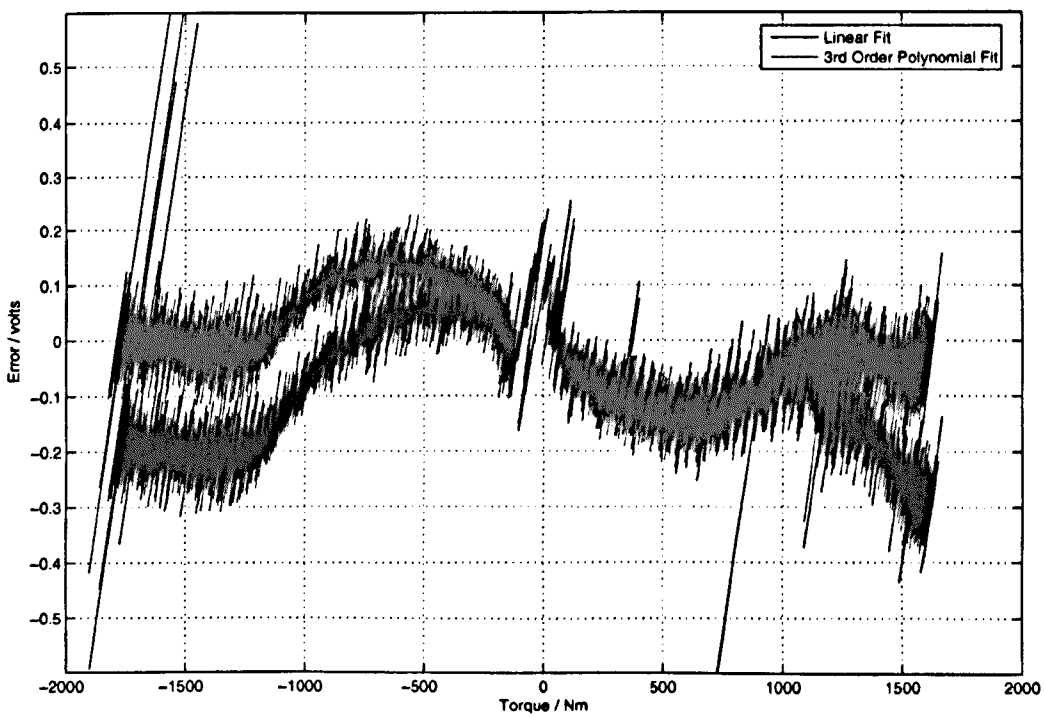

Figure 7.11: Residuals in the inverse fit for linear and nonlinear inverse models

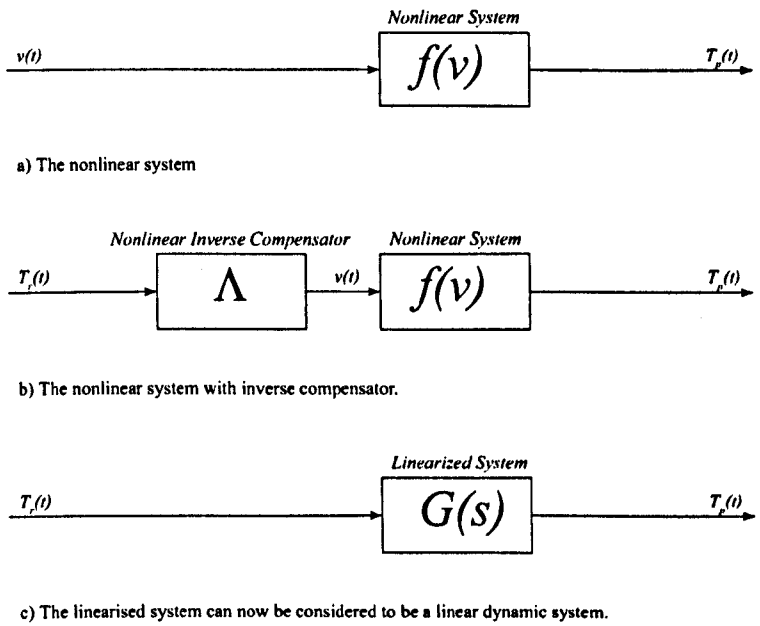

Figure 7.12: Inverse compensation implemented to provide a linearised plant

7.5 Linear System Identification: Chassis Dynamometer

The following section describes the system identification method applied to the development of a black-box model of the Liverpool Chassis Dynamometer. The method outlined applies to the linearised system, where an inverse compensator has been designed and implemented in the real open-loop system.

7.5.1 Input Perturbation and Response Data Acquisition

The input signal is a Random-Walk type perturbation which was designed to have a mean of close to zero. The zero mean input helped to ensure that the torque acting on the unloaded roller did not result in the PAU speed exceeding the threshold speed of 450 RPM, and entering the nonlinear field weakening region. Four sets of input data where used (Table. 7.2), each data set had a different maximum amplitude, the purpose of which was to model the system uncertainty due to residual amplitude dependent nonlinearity in the system.

Data Set	Max Amplitude / N.m
1	750
2	1000
3	1250
4	1500

Table 7.2: Maximum amplitude of input perturbation to the Chassis Dynamometer

The PAU torque response data was sampled at an interval of 1 ms, with no on-line filtering applied.

7.5.2 Data Pre-Processing

The data which was collected through the input-output tests was pre-processed prior to the system identification process. Principally, the data was filtered using a non-causal band-stop filter. The band stop filter was an elliptic type design and the stop-band, selected to coincide with a narrow range of frequencies around that of the resonant frequency observed in the spectral analysis of the torque response. The aim of this pre-filtering process was to attenuate the superimposed structural dynamics which were superimposed upon the PAU response. The system time delay, which was found to be 10ms (or 10 samples) was removed from the identification

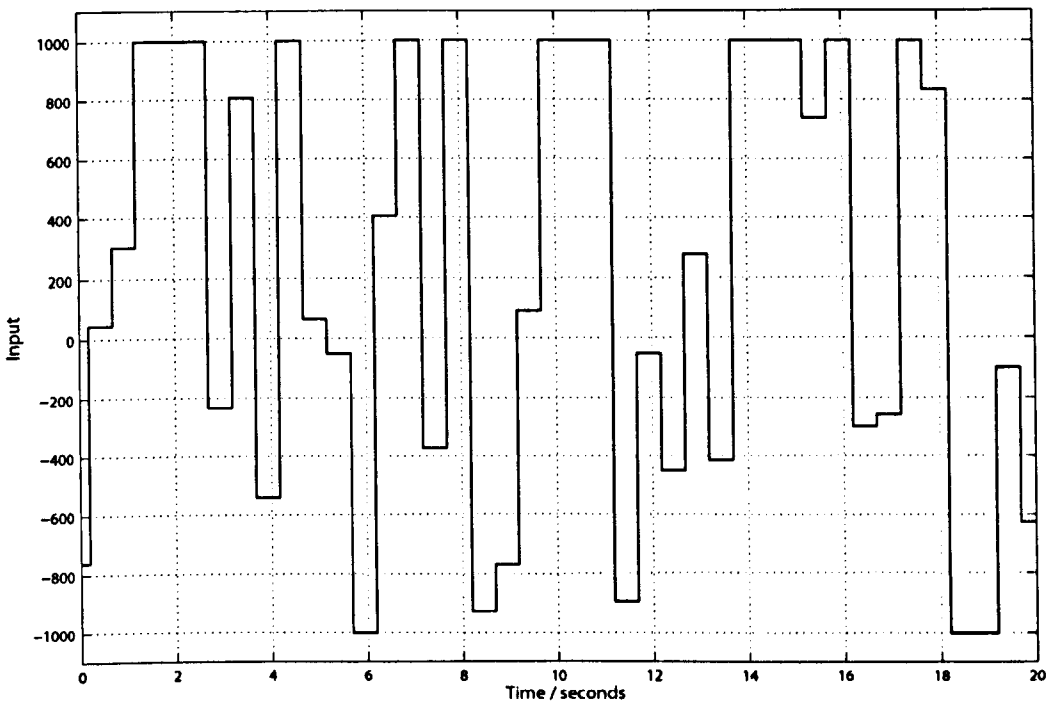

Figure 7.13: Example of Random Walk ID input

data by shifting the input by 10 samples. The pure time delay is reintroduced to the system after the identification process.

7.5.3 Model Structure Selection

The model structure was selected using quality of fit, residual analysis and parsimony of model order as the basis for the choice of coefficients. In addition to objective performance measures, prior knowledge of the system was used in order to further inform the selection.

It was understood that the residual sensor dynamics would add an oscillatory component to the torque response data used in the system identification. Furthermore, it was clear that in order to capture these dynamics, a higher model order would be required. The armature current measurements showed that the approximate torque response of the PAU was fundamentally of a low order, and that it would be appropriate to limit the model order search to below 3rd order. It was therefore decided that the focus should be on finding a model structure which would identify the low order dynamic behavior of the drive and PAU, while ignoring the higher order

sensor dynamics.

When performing the structure selection, it was found that the coloured nature of the unmodelled sensor dynamics produced non-white residuals. This rendered typical cross-correlation and auto-correlation analysis less effective than normal, since the interpretation of the statistical tests was less clear than in the case where white residuals could be expected. The model structure which was eventually selected is shown in 7.2. This structure excludes the 10 sample pure time delay which may be restored after identification to give a discrete transfer function shown in 7.3.

$$G(z) = \frac{\phi_1}{z^2 + \phi_2 z + \phi_3} \tag{7.2}$$

$$G(z) = \frac{\phi_1}{z^2 + \phi_2 z + \phi_3} \times \frac{1}{z^{10}} = \frac{\phi_1}{z^{12} + \phi_2 z^{11} + \phi_3 z^{10}} \tag{7.3}$$

7.5.4 Identified models

Model	ϕ_1	ϕ_2	ϕ_3
$G_1(z)$	0.1008	−0.6765	−0.2241
$G_2(z)$	0.04574	−1.551	0.5964
$G_3(z)$	0.04356	−1.463	0.5066
$G_4(z)$	0.1914	−0.9419	0.1316

Table 7.3: Linear Identified System Models

Figure.7.14 shows the Nyquist plots for the four models which were identified. The Bode magnitude plots for the same models are shown in Figure.7.15. In both plots, the way in which model uncertainty increases with frequency can be observed visually.

The discrete identified system transfer function models can also be expressed as continuous system models, plus a pure time delay.

7.5.5 Model Validation

The four identified models where validated in line with the methods described in section3.6. Unseen data, collected concurrently with the identification data, but not used in the estimation algorithm, was used for the validation process. Firstly quality of fit was considered.

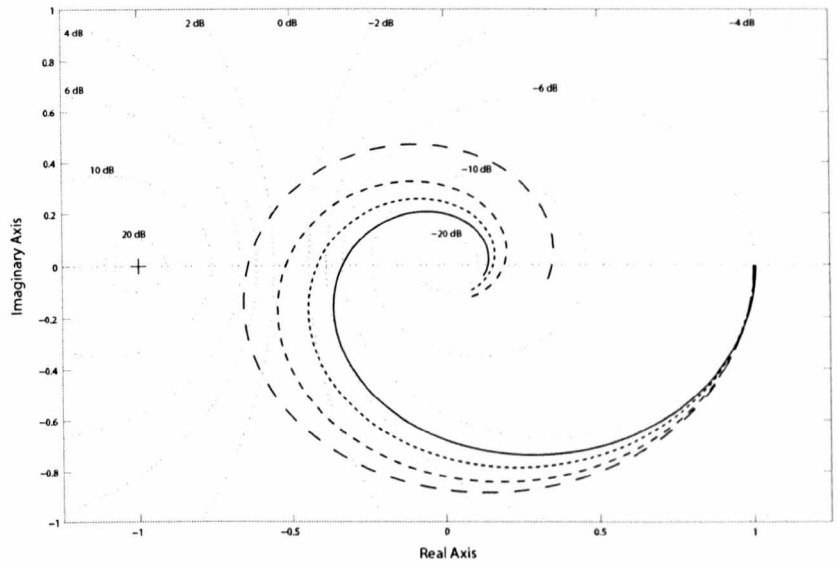

Figure 7.14: Nyquist plot of the identified models

7.5.6 System Simulation Model

The objective of creating a system simulation model is to combine the identified model of the PAU and drive, with a physical model of the torque measurement system to create a simulation model of the system. This has the main objective of further verifying that the oscillatory component of the measured torque can indeed be considered to be sensor noise caused by the dynamics of the measurement arrangement. A simplified physical model of the torque measurement arrangement is shown in figure.7.16. This can be modelled as a simple mass-spring-damper system, where the loadcell output is the force in the spring-damper element. Figure. 7.17 shows a simulink model of the system. The parameters used in the physical model are estimates selected to be realistic for the system and then tuned to match the response of the actual system.

The input to the simulation model is a set of identification data inputs, while the simulation output is compared with the measured system output from an experiment using the same input data. The simulation output compared with the measured output is shown in figure. 7.18.

It is apparent that there is a good level of fit between the simulated and measured outputs, indicating that the simulation model is a fair representation of the dynamometer system, including the sensor dynamics. A spectral analysis of the simulated output, in comparison with the measured output, shows that the same resonant peak is observed at around 18Hz (Figure.7.19).

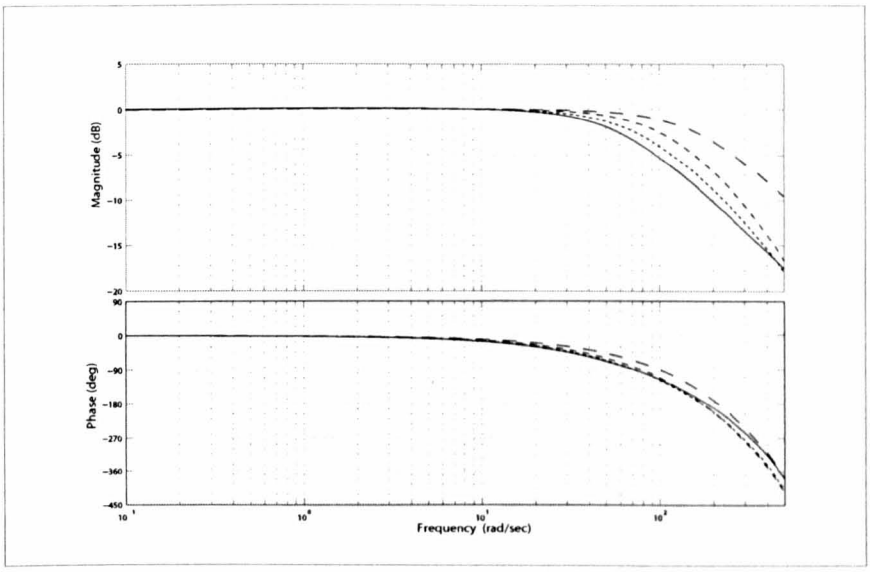

Figure 7.15: Bode Gain and Phase plots of the identified systems

7.5.7 Model Uncertainty

The uncertainty in the identified system models may be analysed in terms of the multiplicative uncertainty in the system over the operating range considered in the identification process. The method for developing a quantitative uncertainty model is adopted from previous work by Petridis and Shenton. [PS02]. In this method, a complex uncertainty template is defined at each frequency. The template is a circle in the complex plane which describes a region encompassing all of the identified models at a particular frequency. Figure. 7.20 shows a Nyquist plot of the four identified system models, along with the circular complex uncertainty templates, plotted over a range of discrete frequencies.

The multiplicative uncertainty is calculated by taking the ratio of the systems magnitude response at each frequency to the magnitude of the uncertainty (radius of the uncertainty template) at the same frequency. A bode magnitude plot of the multiplicative system uncertainty is shown in figure. 7.21.

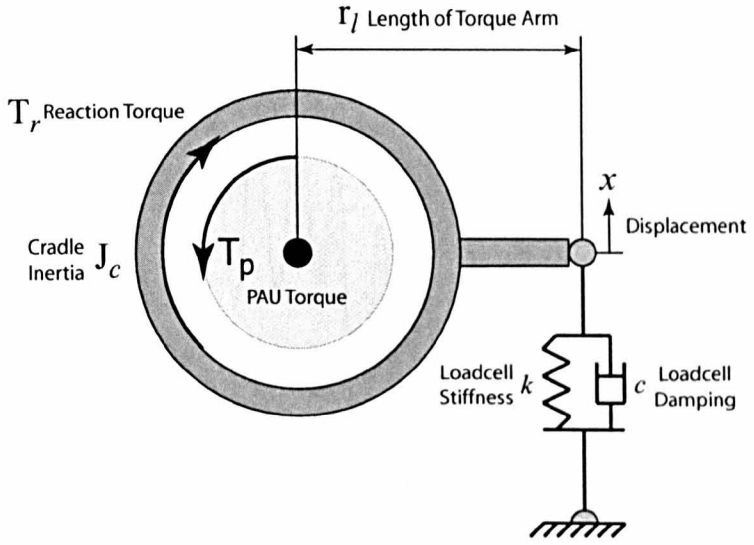

Figure 7.16: Loadcell measurment system physical model

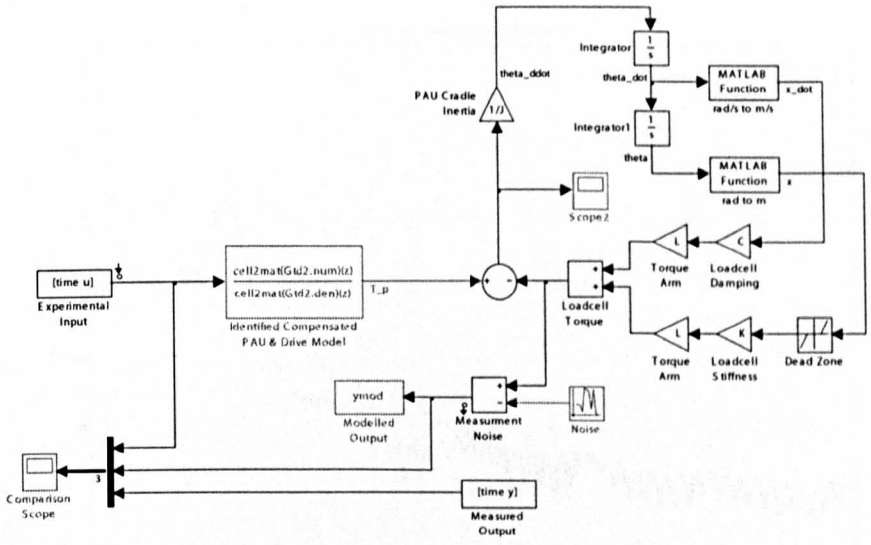

Figure 7.17: Simulink model of the physical torque sensor system

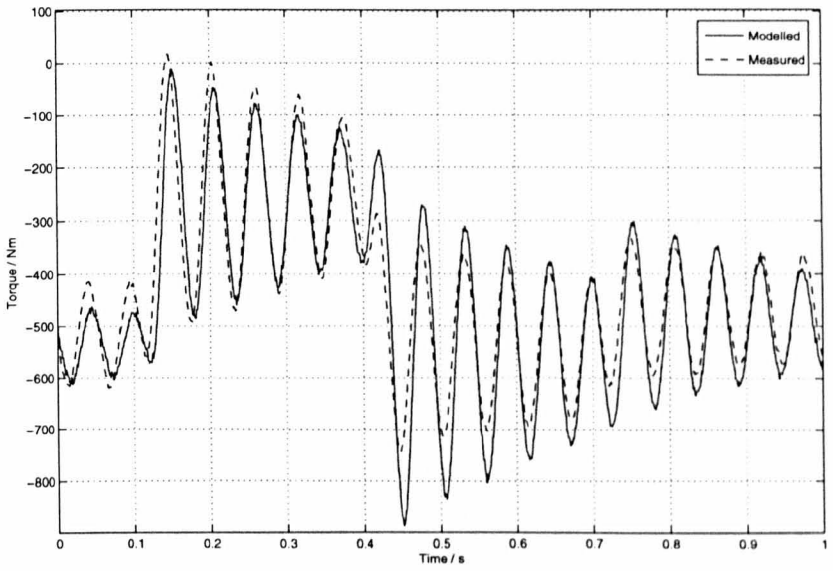

Figure 7.18: Comparison of time response

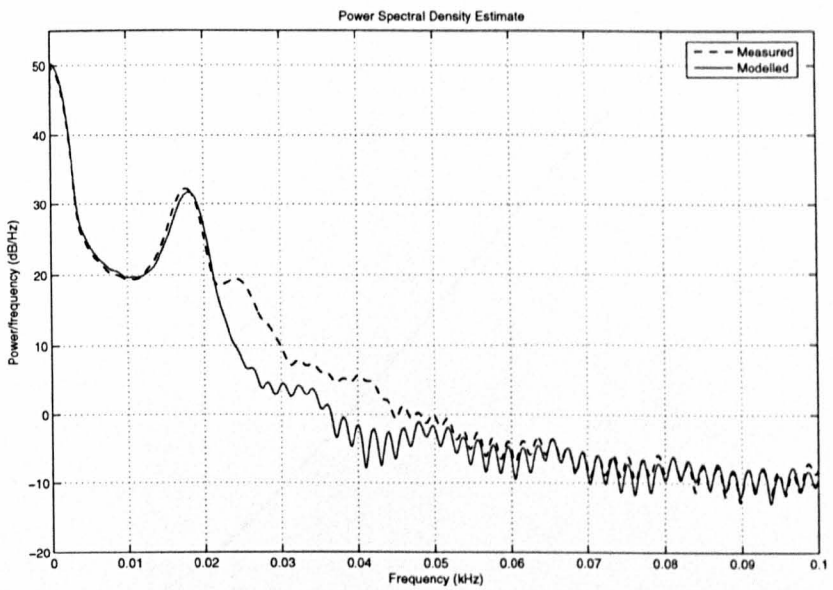

Figure 7.19: Power Spectral Density of Measured system response compared to modelled system response

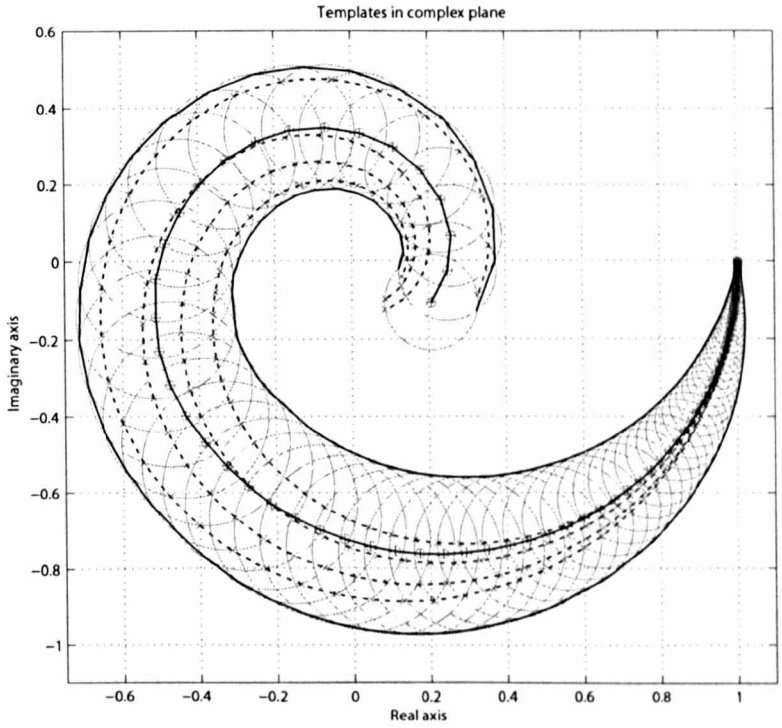

Figure 7.20: Identified system models fitted with complex uncertainty circles

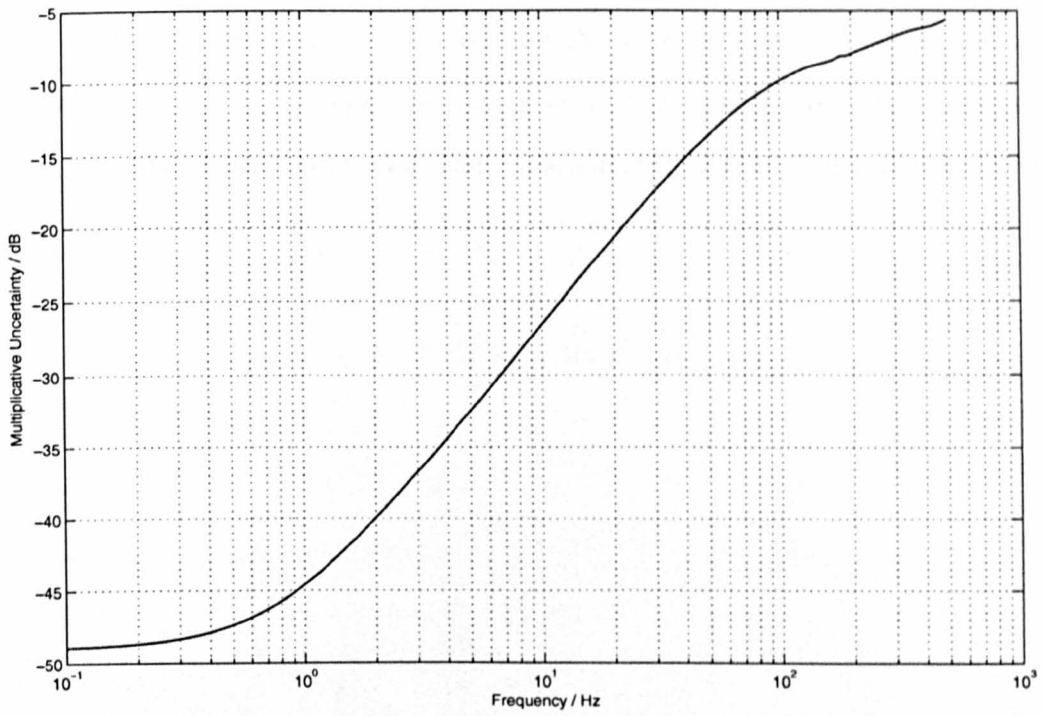

Figure 7.21: Multiplicative uncertainty defined over the frequency range 0Hz to 500Hz

7.6 Conclusions

This section has described the linear system identification process as applied to the chassis dynamometer system. The following summarised the main conclusions arising from this work:

1. The combined Chassis Dynamometer PAU and DC drive unit were found to display non-linear DC behaviour. This was characterised by a third order polynomial relationship.

2. The system was found to have a time delay of 10ms.

3. A direct nonlinear inverse model of the system was found to provide effective linearisation of the system.

4. A resonant frequency was identified in the torque response of the dynamometer at a frequency of around 18 Hz. The source of this mode of vibration was found to be the structural dynamics associated with the torque measurement system.

5. Impulse loading tests on the system, instrumented with an accelerometer, confirmed the existence of a natural mode of vibration in the loadcell arrangement of 18-20Hz.

6. Armature current measurement showed that the approximate torque response of the dynamometer torque was damped second order with a small overshoot, comparisons confirmed that the second order identified dynamometer system model displays comparable behaviour.

Chapter 8

Chassis Dynamometer: Transient Torque Control

This section describes how two different $\mathcal{H}_\infty$ design methods were used to synthesise candidate controllers for a transient torque tracking control problem. The nominal system model, identified in section 7.5, is used as the basis of the main design sections, along with the multiplicative uncertainty model which helps to shape the weighting functions.

For the case of the $\mathcal{H}_\infty$ Parameter Space design method, an outline is given relating to the evolution of the design including interim results which illustrate how the design was improved through three distinct iterations of design. The detailed design is carried out using the latest evolution of the identified system models based on the compensated plant.

In order to explore the potential limits of performance, a modern full order $\mathcal{H}_\infty$ ARE controller is designed using the same plant model and augmented controller structure as for the $\mathcal{H}_\infty$ Parameter Space design.

In both cases, a mixed sensitivity design is carried out. The time response performance of the controllers is verified through simulation before implementation in the Liverpool Chassis dynamometer for evaluation. US EPA standards are used for comparison.

8.1 The iterative design process

The evolution of a satisfactory Chassis Dynamometer torque controller using the Parameter Space control design method was achieved after three key evolutionary phases. The following section describes these stages and offers interim results which illustrate the development path.

8.1.1 Uncompensated Plant, No Filtering

Firstly, system models of the uncompensated plant model were identified, including a multiplicative uncertainty model, and a preliminary attempt to design a suitable closed loop controller was made. This investigation showed that the model uncertainty was large, mainly due to plant nonlinearity and significant sensor noise associated with the torque measurement system. The controller design was assessed through simulation (Fig.8.1) and found to provide unsatisfactory performance compared with the adopted US EPA benchmarks. The response time (to 90% of steady-state) was found to be 215ms and the settling time (to 2% of steady-state) was 1.15s. The peak response amplitude was 133% of the settled response. It was found that performance could not be improved without reducing closed loop stability margins to unacceptably low levels.

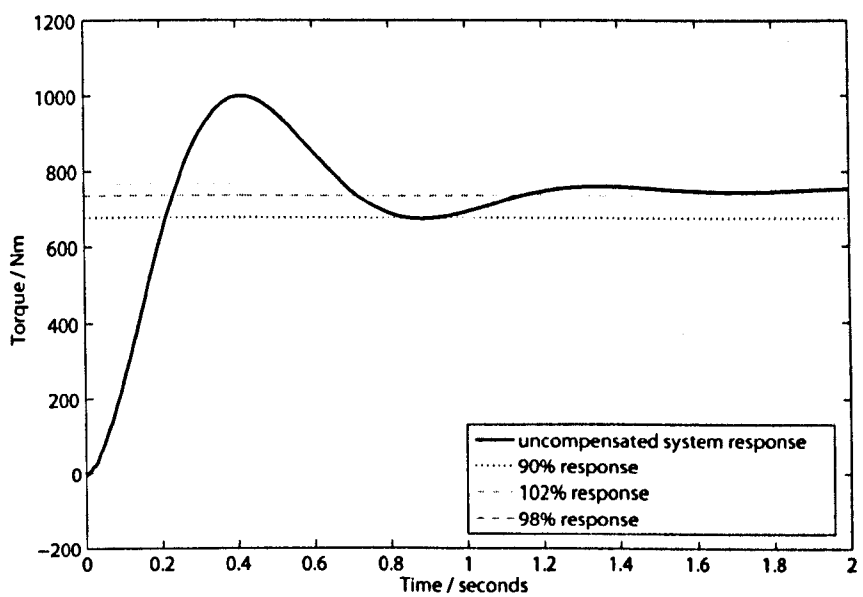

Figure 8.1: Time Response of the closed loop controller designed without compensation or feedback filter

8.1.2 Compensated Plant, No Filtering

Second, a nonlinear inverse compensation scheme was applied to the forward path of the system. The nonlinear inverse was shown to effectively reduce the nonlinearity associated with the plant, and the model uncertainty was reduced accordingly [MDS06]. The controller design was tested in simulation (Fig.8.2) and was found to be a significant improvement over the uncompensated system. The response time (to 90% of steady-state) was found to be 83ms and the settling time (to 2% of steady-state) was 565ms. The peak response amplitude was 137% of the settled response. While the results for the compensated system were greatly improved compared with the uncompensated system, the closed loop time response was found still to be outside of those stipulated by the US EPA benchmarks. It was apparent that the superimposed oscillations caused by sensor noise in the feedback path reduced the performance which could be achieved while maintaining acceptable margins to stability.

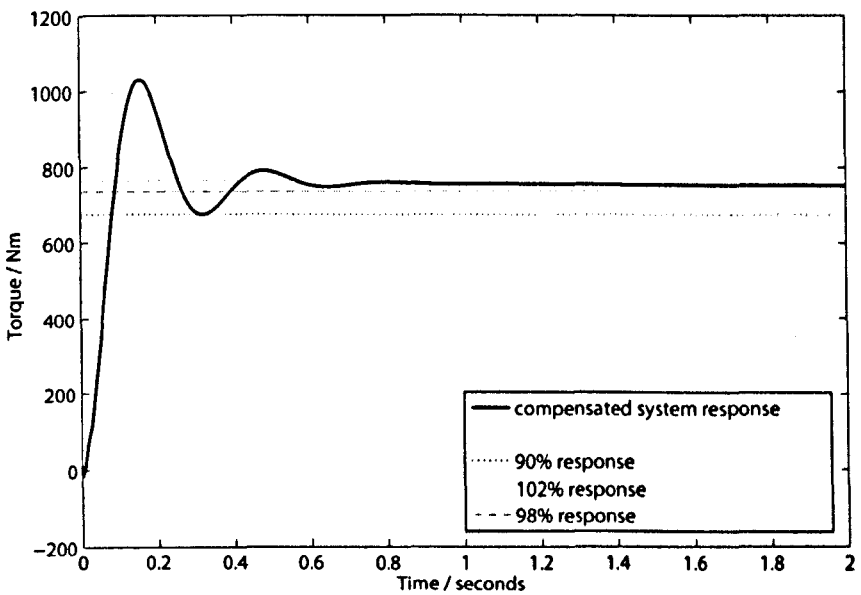

Figure 8.2: Time Response of the closed loop controller designed with inverse compensation but without feedback filter

8.1.3 Compensated Plant, Filtering

Thirdly, it was recognised that the oscillatory sensor noise associated with the structural dynamics of the torque measurement system were a significant barrier to improvement in controller

performance. Experimental investigation had established that the oscillatory components of the torque feedback were associated with a 18Hz mode of vibration which was superimposed upon the loadcell output, but which was not a component of the actual dynamometer torque response.

Different filtering strategies were explored and it was established that causal frequency domain filter solutions would not be suitable due to the phase shift, and time delay which were inherent in their design and implementation. Model based filtering, and specifically the Kalman Filter were explored and subsequently adopted as a means for providing effective attenuation of the unwanted superimposed sensor noise, without adding significant unwanted phase shift or time delay to the feedback path of the closed loop.

In addition to the implementation of online filtering of the feedback signal, the system identification data was subjected to an additional degree of pre-processing through the application of a non-causal bandstop filter for attenuation of the 18Hz structural mode. The use of a non-causal filter, and the fact that the pre-processing was performed offline, meant that very high rates of rolloff and attenuation could be used to remove a very narrow frequency range, while leaving the remaining spectral characteristics of the identification data relatively unaffected. The resulting identification data was used to identify a set of system models based on the linearised, filtered system response, and was found to match the expected dynamic characteristics of the DC PAU more closely than had previously been achieved.

The feedback controller presented in the following section was based on this evolution of the design cycle.

8.2 Controller Structure

This section describes the structure of the control system which was applied to the Chassis Dynamometer system. Firstly a typical feedback system structure is considered and compared with an augmented structure which includes a Kalman filter for the attenuation of the oscillatory sensor noise arising from the torque measurement system.

8.2.1 Standard Feedback Structure

Figure.8.3 shows the standard feedback control structure. The torque tracking reference is r and the error in the feedback (y_m) is e. The control input to the compensated plant G is u. The PAU output (y) is affected by significant sensor noise caused by the oscillatory sensor dynamics which were observed and characterised in section 7.3. Studies using the Liverpool Chassis dynamometer found that the sensor noise has a severe effect upon the achievable controller performance and that it must therefore be attenuated from the feedback signal. The Kalman filter formulation described in section 5 was therefore adopted and successfully implemented. The following section describes the augmented controller structure and comments on some of its properties.

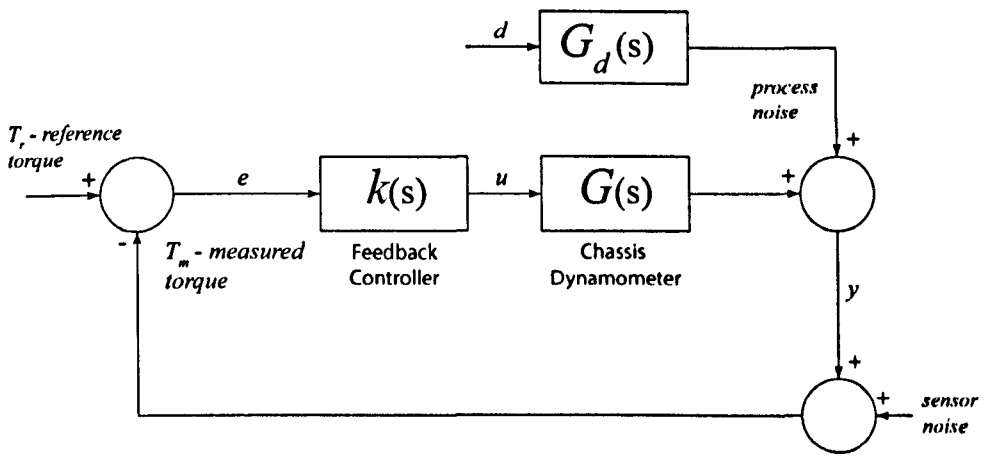

Figure 8.3: Simple Feedback Structure applied to the Chassis Dynamometer

8.2.2 Augmented Feedback Structure

The augmented feedback control structure is shown in Fig.8.4. Transfer functions $F_1(s)$ and $F_2(s)$ are the pair of Single Input Single Output (SISO) transfer functions which describe the Multiple Input Single Output (MISO) Kalman filter system.

A linear analysis of the block diagram (Fig.8.4) shows that the error input to the feedback controller K is given by

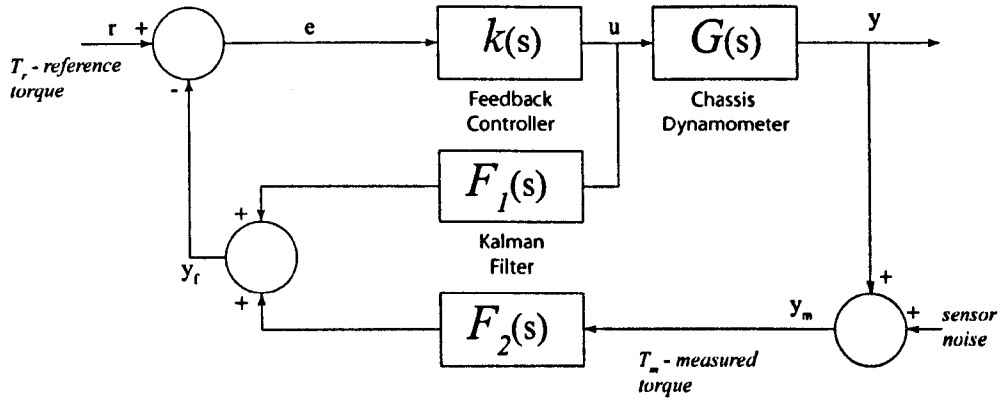

Figure 8.4: Transfer function representation of the feedback system, with Kalman filter

$$e = r - F_1 u - F_2 y_m \tag{8.1}$$

and that the controlled input (u) to the plant ($G(s)$) is given by

$$u = Ke \tag{8.2}$$

Substituting 8.1 into 8.2 gives

$$u = Kr - KF_1 u - KF_2 y_m \tag{8.3}$$

Collecting common factors of u on the left hand side of the equation, and dividing through by F_2 gives

$$u\left(1 + KF_1\right) F_2^{-1} = K\left(F_2^{-1} r - y_m\right) \tag{8.4}$$

If a modified error term e_a is given by $e_a = F_2^{-1} r - y_m$ then

$$u = \left(1 + KF_1\right)^{-1} F_2 K e_a \tag{8.5}$$

This result shows that that the feedback system may be described in a form which includes the effects of the Kalman filter in a single feedback loop with an augmented controller K_a

$$K_a = \frac{u}{e_a} = (1 + KF_1)^{-1} F_2 K \tag{8.6}$$

The revised feedback system is shown in figure 8.5. It is apparent that there is only a single feedback loop for stability analysis and that the reference signal is modified by a pre-filter (F_2^{-1}).

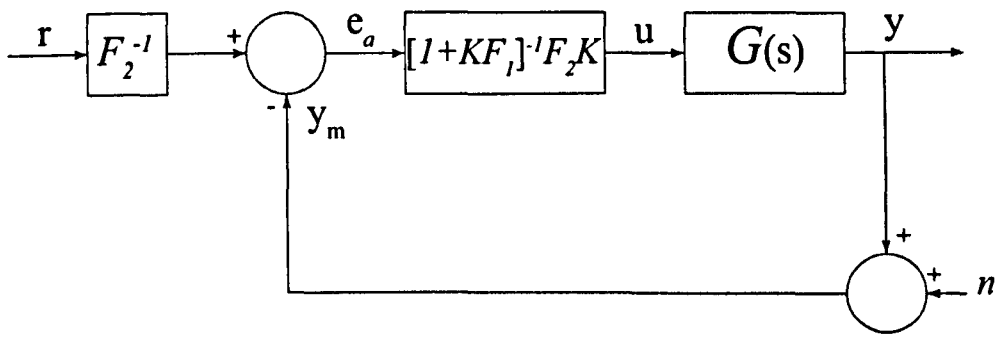

Figure 8.5: Revised feedback structure with augmented controller

Since the pre-filter has no effect upon the closed loop stability of the system, the robustness may be analysed using the loop function,

$$L_k = K_a G = [1 + KF_1]^{-1} K F_2 G \tag{8.7}$$

This feedback structure was adopted and used throughout the following controller design and implementation. It was found to offer a significant reduction in the transmitted sensor noise without introducing significant extra time delay or phase distortion.

8.3 $\mathcal{H}_\infty$ Parameter Space Controller Design

The first $\mathcal{H}_\infty$ design is performed using the Parameter space method. The design process generates a controller with a fixed low order structure comparable with a classical PID regulator. The PID regulator is still the most popular, and commonly used controller in industrial applications and the following method could be easily used to design a PID regulator which could be implemented in existing hardware with tunable parameters.

The nominal plant model used for the controller design is $G_0(s)$. This plant model was identified in Chapter 7 using data which was preprocessed to attenuate the oscillatory sensor

dynamics. The plant model is described by the continuous (s-domain) transfer function with a pure time delay:

$$G_0(s) = \frac{\theta_1 s^2 + \theta_2 s + \theta_3}{s^2 + \theta_4 s + \theta_5} e^{-sT} \tag{8.8}$$

The controller $K(s)$ has a fixed structure:

$$K(s) = K_r + jK_i = \frac{b_2 s^2 + b_1 s + b_0}{a_2 s^2 + a_1 s + a_0} \tag{8.9}$$

8.3.1 Primary Sensitivity Weighting Function

Recall that for nominal performance, it is required that the $\mathcal{H}_\infty$ norm should conform to the inequality,

$$\left\| \frac{W_s(j\omega)}{1 + G(j\omega)K(j\omega)} \right\|_\infty \leq 1 \tag{8.10}$$

where $W_s(j\omega)$ is the weighting for the primary sensitivity function $S(j\omega)$. The selection of an appropriate set of weighting functions is an important part of the design process but can be difficult due to the lack of direct translation between the frequency and time domains. For this reason, the shaping of weights was performed using guidelines as outlined in [SP96], while tuning was performed through an iterative process of trial controller designs combined with simulation of the closed loop system. The selected weight (W_s) was shaped to provide tracking performance, with high gains at low frequencies, while high frequency disturbances were attenuated at higher frequencies by decreasing the gain. The selected primary sensitivity weighting function was

$$W_S = \frac{0.2s + 4}{s} \tag{8.11}$$

A Bode magnitude plot of the inverse of the primary sensitivity weighting function ($1/W_S$) is shown in Figure.8.6. Remembering that the primary sensitivity function S is bounded by the weighting, according to the inequality $||S|| \leq 1/W_S$, this figure illustrates how the weighting function provides reduced sensitivity to low frequency disturbances by reducing the magnitude of the sensitivity function at low frequencies.

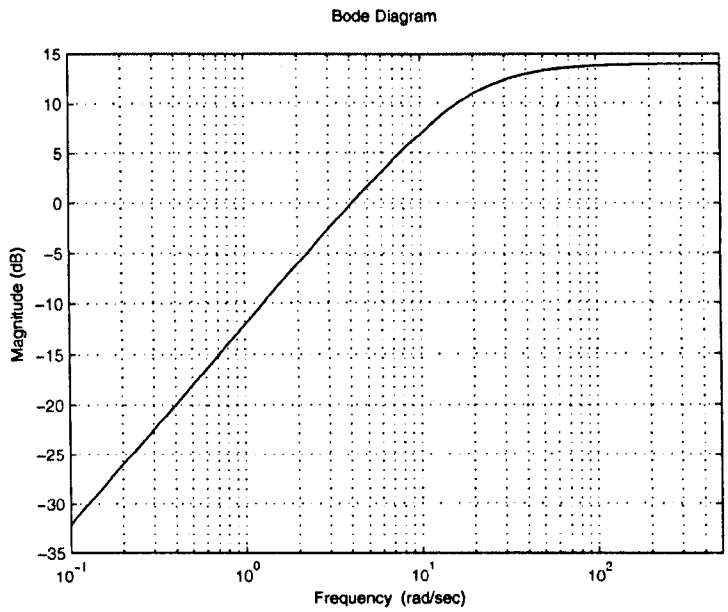

Figure 8.6: Primary Sensitivity Weighting Function ($1/W_S$)

8.3.2 Complementary Sensitivity Weighting Function

In section.4.3.1, it was shown that the complementary sensitivity weighting function bounds the complementary sensitivity according to the inequality

$$|T(j\omega)| < W_s(j\omega)^{-1} \tag{8.12}$$

Furthermore, it was shown how the multiplicative uncertainty associated with the system can be used to define a bound on the system which will provide robust stability, according to the inequality

$$|T(j\omega)| < \Delta_m(j\omega)^{-1} \tag{8.13}$$

In light of this useful relationship, the complementary sensitivity function is selected using the multiplicative uncertainty model as a guideline to provide a constraint which will guarantee robust stability. The complementary sensitivity weighting function is shaped to the multiplicative uncertainty model which was identified as part of the system identification process. W_T is given by the equation,

$$W_T = \frac{0.01s}{0.022s + 2.2} \tag{8.14}$$

Figure.8.7 shows a Bode magnitude plot of the inverse of the complementary sensitivity weighting function $(1/W_T)$, along with the corresponding inverse multiplicative uncertainty model. The weighting function W_T is shaped to the multiplicative uncertainty at higher frequencies, and it can be seen that according to the inequality $||T|| \leq 1/W_T$, the selected weighting function reduces the sensitivity of the system to high frequency disturbances and plant perturbations.

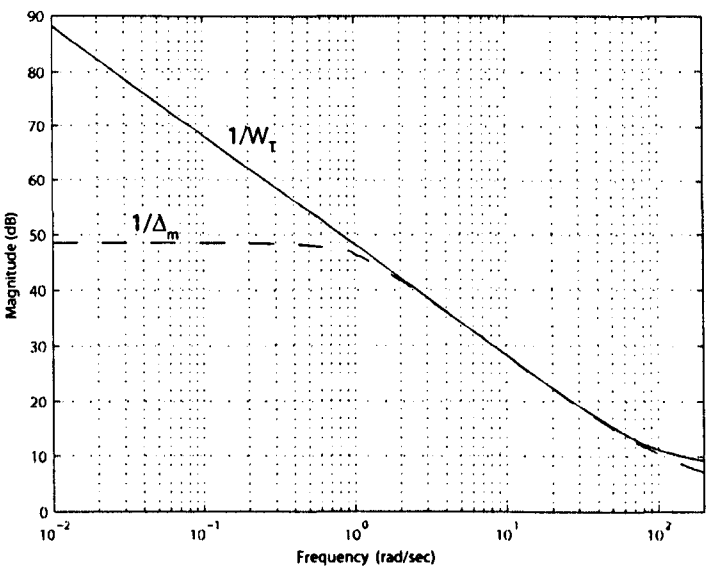

Figure 8.7: The complementary sensitivity function (T) is bounded by the complementary weighting function such that $|T(s)| \leq \frac{1}{W_T(s)}$. For robust stability the weighting function is selected to approximate the multiplicative uncertainty $(\frac{1}{W_T(s)} \approx \Delta_m^{-1})$

8.3.3 Parameter Space Torque Controller Design

Parameter Space Design Procedure

The design procedure using the parameter space method is iterative. Parameters are selected in each of the parameter planes (b_0b_1 and b_1b_2) in turn, using simulated time response and closed loop frequency response to guide the selection process. The process is repeated until it is judged

that an appropriate balance between time response performance frequency domain specifications have been achieved. In the case where the required performance cannot be achieved using the selected specifications, then it may be necessary to revisit the selection of appropriate weighting functions, or even to reconsider the structure of the control problem.

In the case of the design carried out for the chassis dynamometer torque controller, it was found that the addition of a non-zero b_2 parameter led to immediate problems regarding system stability and so the design problem was simplified by being limited to the $b_0 b_1$ parameter plane. Figure 8.8 shows the $b_0 b_1$ parameter plane with both sensitivities plotted. For both Primary and Complementary sensitivities, the conic section which defines the closed loop weighted sensitivity is plotted in terms of variation with controller parameters b_0 and b_1. This is done at each of a range of predefined frequencies which cover the system bandwidth. The area which represents the set of permissible controller parameters is therefore enclosed by the locus generated by the two superimposed sensitivities. The cross in Figure.8.8 indicates a pair of controller parameters selected from within the region inside which the frequency domain specifications are met or exceeded. A sensible choice of parameters may be the centre of this region. However, one of the benefits of the Parameter Space controller design approach is that there is flexibility to select parameter from anywhere within this region, providing means for tuning time response while meeting or exceeding the specifications. The frequency domain specifications are shown in Figures 8.9, along with the actual closed loop sensitivity functions achieved for the parameter pair defined by the cross in Figure.8.8. The uncertainty in the closed loop system response is shown in Figure.8.10.

$$K(s) = \frac{0.272s + 31.63}{0.002s^2 + s} \tag{8.15}$$

8.3.4 Simulated Closed-Loop Time Response

The time response of the closed loop system is simulated using the nominal plant model and the candidate controller. The results of this simulation are shown in Figure 8.11.

The simulation shows that the closed loop time response is predicted to have a response time of 50ms and a settling time of 90ms. The overshoot is well below the maximum of 20%. The

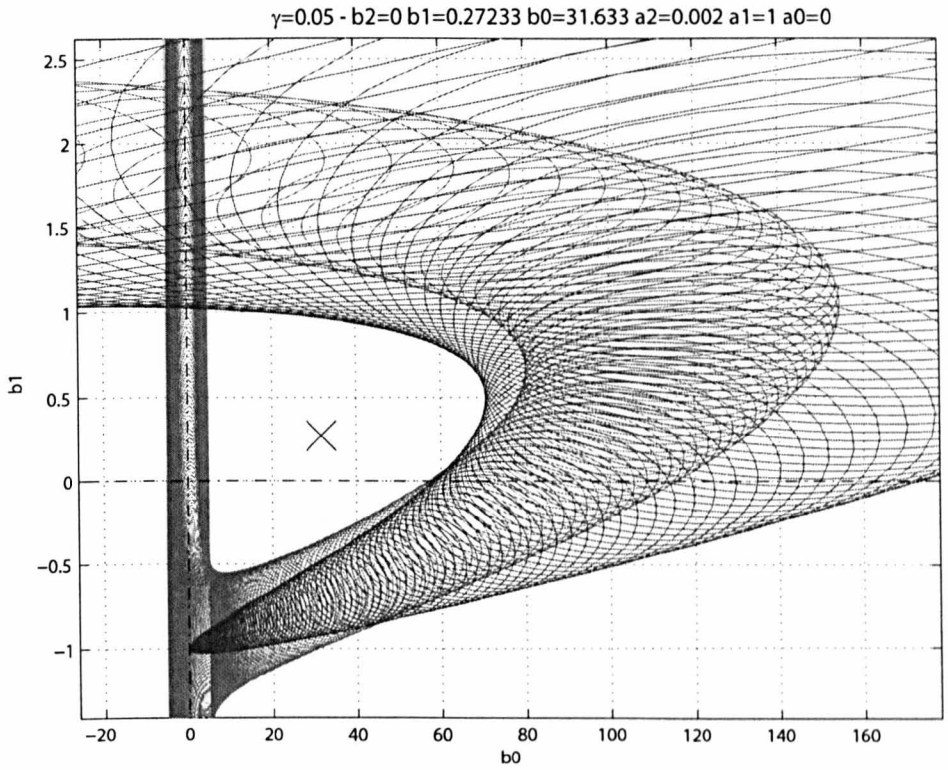

Figure 8.8: The mixed sensitivity parameter plane for $b_0 b_1$. The cross shows the location of the selected controller gains

response is well damped and does not show evidence of oscillation.

The expected robustness of the controller was investigated by checking the gain and phase margins of the loop function for the augmented system,

$$L(s) = G(s)[I + K(s)F_1(s)]^{-1}K(s)F_2(s) \tag{8.16}$$

For the $\mathcal{H}_\infty$ Parameter Space controller, the corresponding gain and phase margins were thus determined to be 33.6 dB and ∞° respectively.

The theoretical response of the controller is therefore shown not only to exceed the US EPA requirements but also to display significant level of expected robustness, therefore making it a good candidate for implementation and experimental validation.

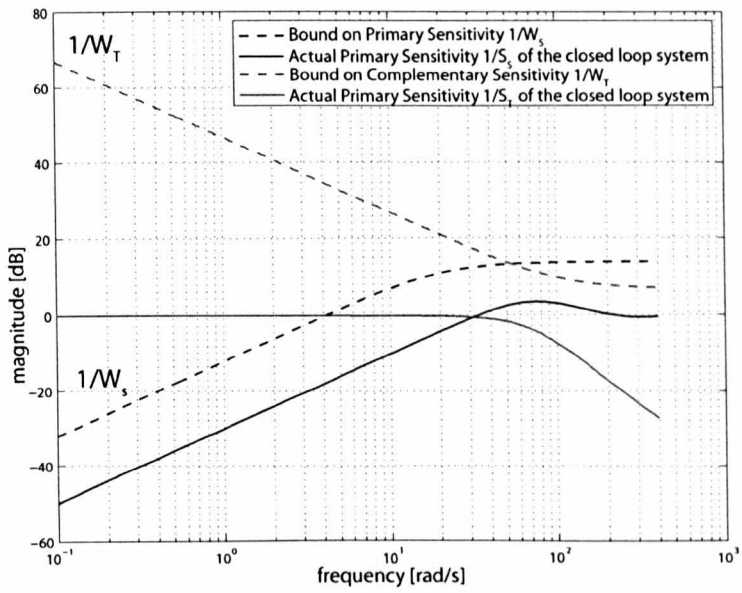

Figure 8.9: Closed-Loop Primary and complementary Sensitivities compared with bounds

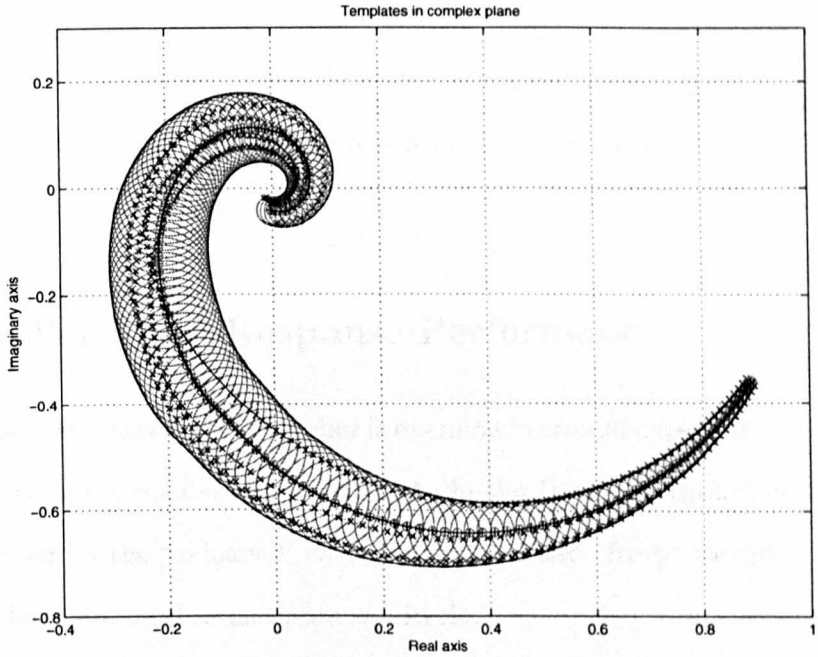

Figure 8.10: Uncertain Closed-Loop Response

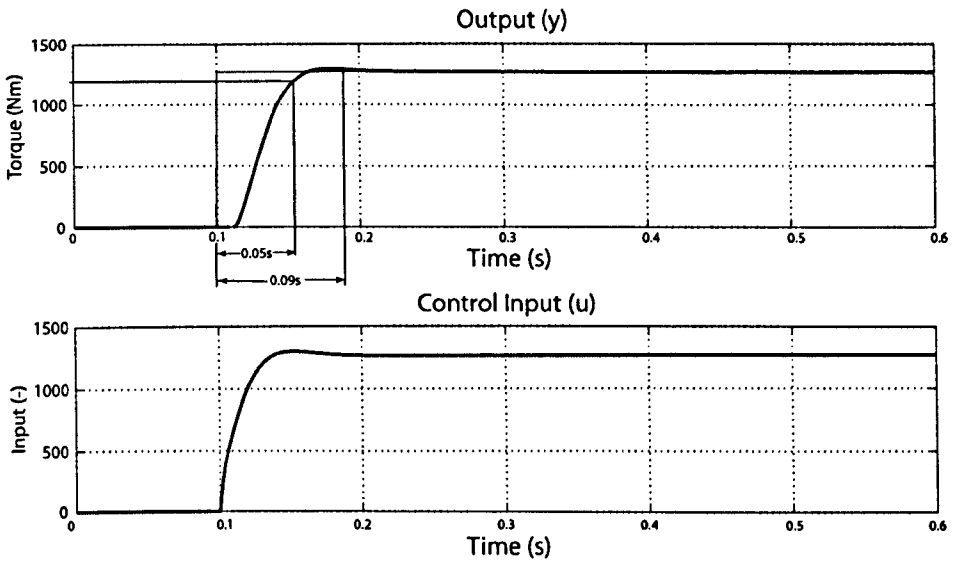

Figure 8.11: Simulated closed-loop system response

8.4 Implementation

The implementation of the candidate controller is illustrated in fig.8.12 which shows how the feedback controller is implemented in the dSPACE real-time hardware target. Control signals to the dynamometer drive, and feedback measurements from the torque measurement system are handled by DAC and ADC hardware. The real-time target is programmed using automatically generated code which is derived from a Simulink block diagram (Figure.8.13). User access to variable parameters such as torque demand is available through the ControlDesk layout which acts as a virtual instrumentation panel.

8.5 Controller Time Response Performance

The performance of the candidate controller is examined through experimental testing performed in-line with the US EPA regulations [Age91]. As in the US EPA regulation, the time response tests are performed on the 'unloaded' chassis dynamometer. Response time, settling time and maximum overshoot are used as acceptance criteria.

The US EPA requirement [Age91, AB+00] for time response tests requires a step change in tractive force of 450 lbf be requested by the control system. In SI units, this is an force of 2001 N which equates to a torque of 1220 Nm for a 1.22 m (48 inch) diameter chassis dynamometer.

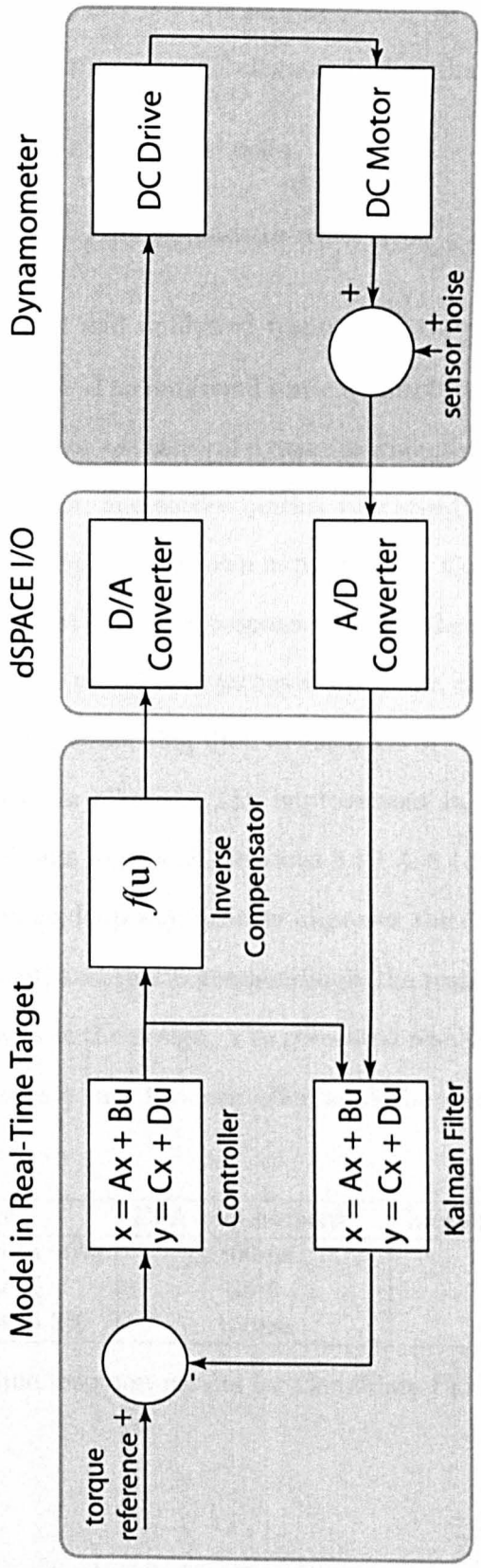

Figure 8.12: Block Diagram representation of the Controller Implementation

The following acceptance criteria are then outlined:

- Time Response - Response time must in all cases be less than 100 milliseconds
- Overshoot - No more than 125% of final value
- Settling Time - Less than 150 milliseconds to reach ±2%

Figure.8.14 shows the filtered and unfiltered response of the closed-loop system to a step change in load demand of 1200Nm. The unfiltered response displays the characteristic oscillation which is caused by the torque sensor's structural dynamics while the filtered closed loop response shows a small amount of overshoot, and settles quickly to a steady state response.

A detailed view of the time response is shown in figure.8.15. Comparing the results with the US EPA acceptance criteria [Age91], the 90% response time for the filtered system is 50ms which is 50ms faster than required. The overshoot reaches a maximum of 5% which is well within the 25% maximum allowed. The system settling time to reach 2% of its steady-state is 100ms which is 50ms faster than the maximum allowed. The improvement in the quality of these results, compared with the previous design iterations (Sections 8.1.1 & 8.1.2) shows that the addition of the Kalman filter in the feedback loop significantly improves the closed loop performance with regard to settling and overshoot, and that correspondingly the response time could be improved without reducing the robustness of the design. The presented results significantly exceed the US EPA requirements and so indicate that the controller would be suitable for transient emissions testing with inertia simulation.

Criterion	EPA-requirement	Measured-response
response time to 90%	100ms	50ms
overshoot-%	25%	5%
settling time to 2%	150ms	100ms

Table 8.1: Benchmark time response results for Candidate Parameter Space Controller

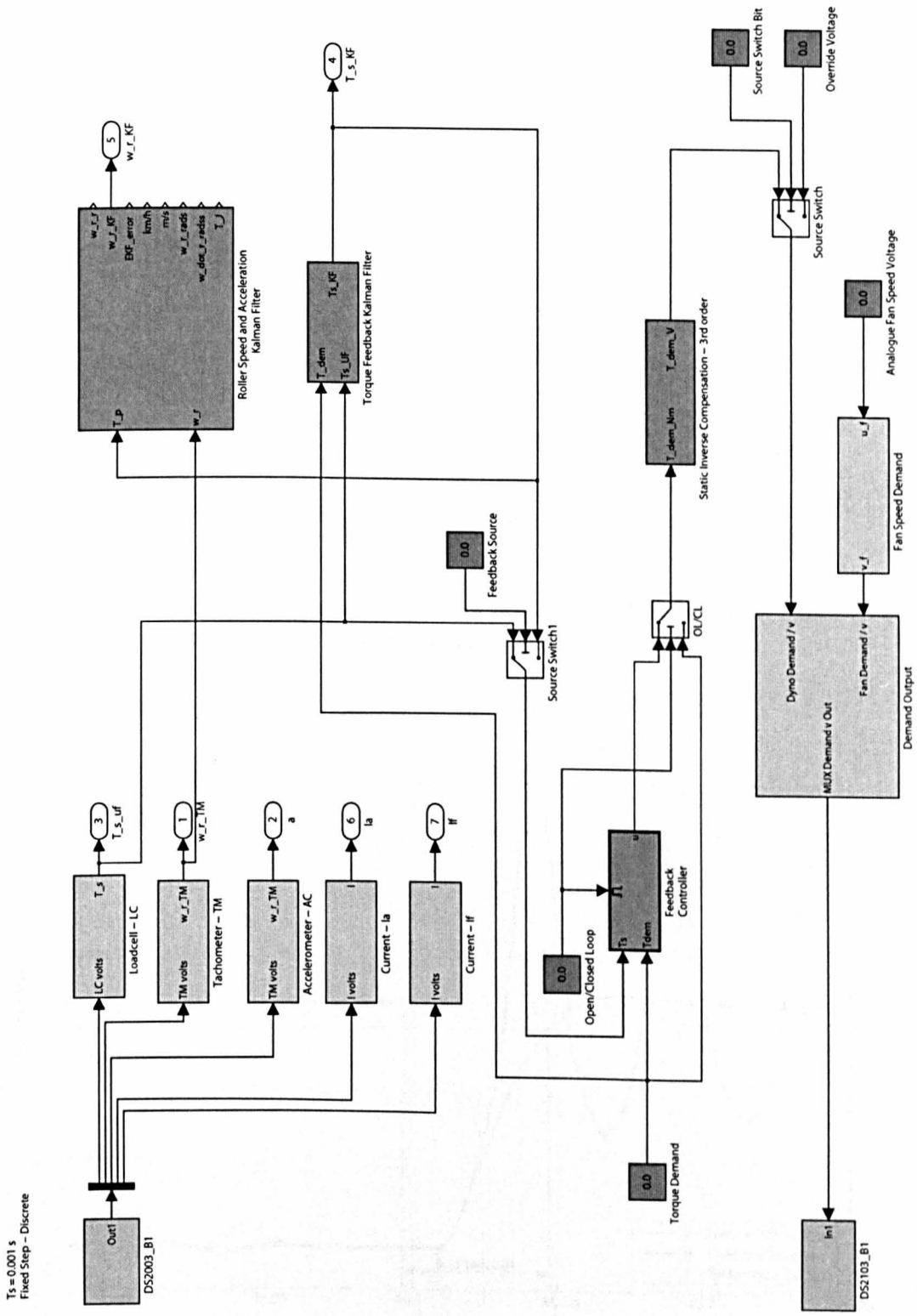

Figure 8.13: Simulink model for Real-Time implementation

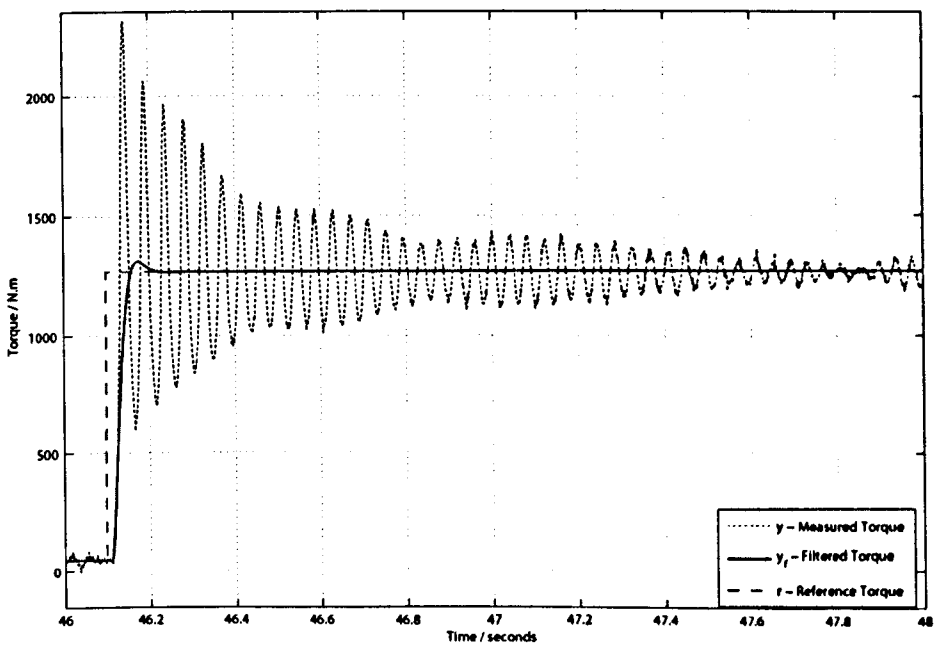

Figure 8.14: Closed-loop time response to a step demand of 1200Nm. Plot shows both filtered and unfiltered responses superimposed over demand

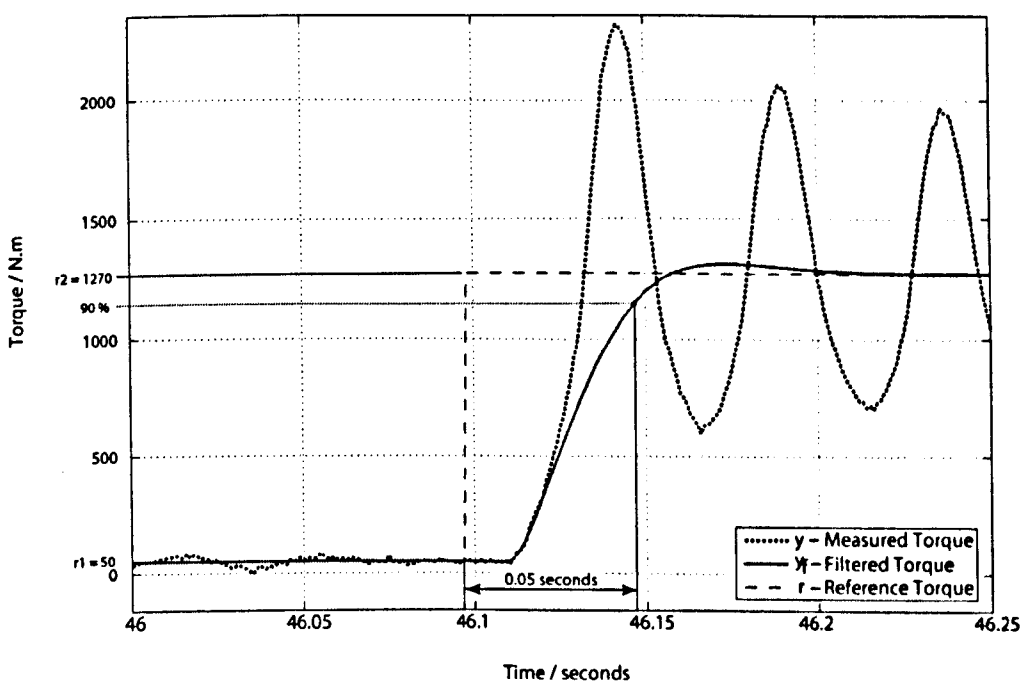

Figure 8.15: detail of step

8.6 Algebraic $\mathcal{H}_\infty$ Controller Design

In this section, a full order Algebraic $\mathcal{H}_\infty$ controller design is performed in order to explore the benefits which an optimised full order controller may present to further improving the performance of the Chassis dynamometer Torque controller. The control design is achieved using the DGKF algorithm [DG+89] as implemented in the Robust Control Toolbox [CS98]. The design is carried out in the continuous domain, using the Tustin bilinear transformation to convert from the identified discrete transfer function model with pure time delay, to a continuous model with rational time delay approximation. The continuous plant model structure is shown in Eqn.8.17.

$$G_0(s) = \frac{\phi_1 s^{10} + \phi_2 s^9 + \phi_3 s^8 + \phi_4 s^7 + \phi_5 s^6 + \phi_6 s^5 + \phi_7 s^4 + \phi_8 s^3 + \phi_9 s^2 + \phi_{10} s + \phi_{11}}{s^{10} + \phi_{12} s^9 + \phi_{13} s^8 + \phi_{14} s^7 + \phi_{15} s^6 + \phi_{16} s^5 + \phi_{17} s^4 + \phi_{18} s^3 + \phi_{19} s^2 + \phi_{20} s + \phi_{21}} \tag{8.17}$$

The increased order of the plant model which is required by the rational approximation of the time delay is one of the reasons why the order of the controller which is achieved through this method will tend to be high. The total order of the controller will be the sum of the order of the nominal plant model, along with the weighting functions which must also be rational functions. The controller design may therefore be deemed to have an excessively high order or to be excessively conservative and there is no direct way of imposing a limit on the order or structure of a controller designed in this way. Order reduction techniques may be subsequently applied to the controller but the result cannot be relied upon to meet the original specifications.

8.6.1 Sensitivity Weighting Functions

Primary Sensitivity Weighting Function

The $\mathcal{H}_\infty$ Algebraic Riccati Equation method of control design offers an optimal solution for a given set of weighting function specifications. The shaping of the weighting function is therefore the main tool which the designer has available for influencing the characteristics of the resulting controller. Some guidelines regarding appropriate shapes for the common weighting functions

are outlined in [SP96] and [CS98]. Tracking is generally obtained in the design by shaping the primary sensitivity weight such that it provides high gains at low frequencies. Another way of thinking about this is to consider the inequality $||S|| \leq 1/W_s$. This indicates that to minimise the sensitivity of the closed loop system to low frequency disturbances, then $1/W_s$ should be low at low frequencies. The weighting functions used in the $\mathcal{H}_\infty$ ARE method here are different to those used in the $\mathcal{H}_\infty$ Parameter Space design presented previously. The reason why different weights were selected was that unlike the Parameter Space method where the user has flexibility within the bounds of the weighting functions to select an appropriate controller, the ARE method provides a single optimal solution for the given weights which may not directly meet the user's time response requirements.

In this work, the design of weighting functions was started with an appropriate shape based on the guidelines in [SP96, CS98] before an iterative process of controller design, closed loop simulation and tuning of the specifications was carried out. Accordingly, a first order weighting was selected with a high frequency breakpoint at 19 Hz (120 rad/s) to prevent excitation of high frequency dynamics. To ensure the weighting was proper, a low frequency breakpoint was included at 1.6×10^{-5} rad/s (10^{-4} rad/s) which does not affect the DC tracking behaviour. The inverse primary sensitivity weighting function was

$$W_S = \frac{50s + 8000}{120s + 0.01} \tag{8.18}$$

Figure.8.16 shows a Bode magnitude plot of $1/W_s$ and illustrates how the primary sensitivity function $||S||$ will be bounded according to the inequality $||S|| \leq 1/W_s$.

Complementary Sensitivity Weighting Function

The complementary sensitivity function was shaped using the multiplicative uncertainty model ($\Delta_m(\omega)$) as a guideline to provide additional robustness at frequencies where model uncertainty is greatest. Since the order of the controller is directly affected by the order of the weighting functions, and because the weighting function must be a proper rational function, an approximation is used which is judged sufficiently close to the desired shape.

The multiplicative uncertainty shown in Fig.8.17 was used to aid the design of the comple-

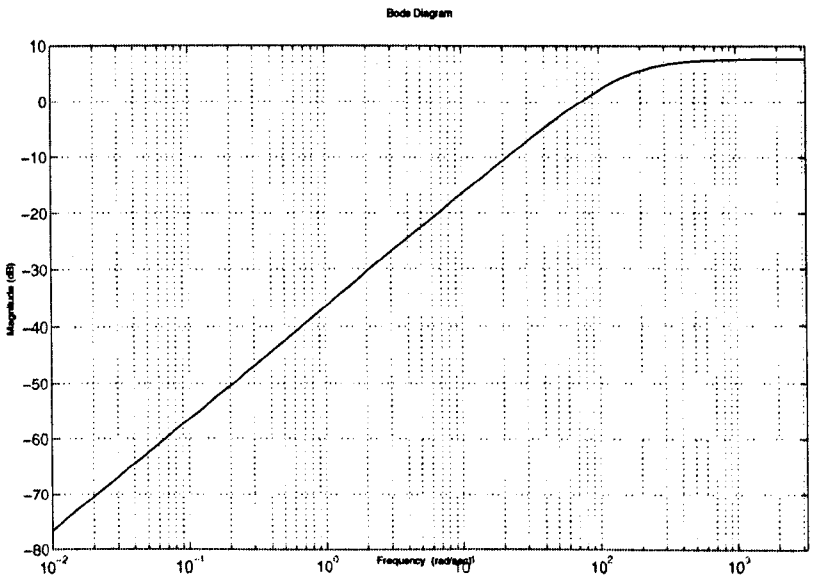

Figure 8.16: Inverse primary sensitivity weighting function $1/W_s$

mentary weighting function (8.19).

$$W_T = \frac{s}{1 \times 10^{-6} s + 500} \tag{8.19}$$

An attenuation of 20db/decade is only necessary at high frequencies and therefore a first order weighting was selected. The function is made proper by the inclusion of a high frequency pole above the operating frequencies.

Figure.8.18 shows a comparison between the selected weighting function, and the experimentally derived multiplicative uncertainty model. The figure illustrates how the approximate weighting function provides a close match at higher frequencies where robustness is most important, but that it is highly conservative at lower frequencies.

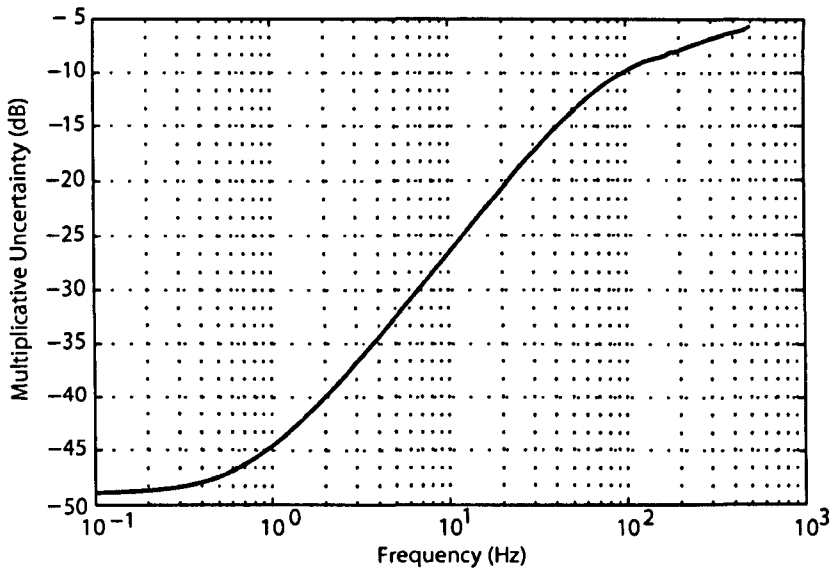

Figure 8.17: Multiplicative Uncertainty used to shape the complementary Sensitivity function

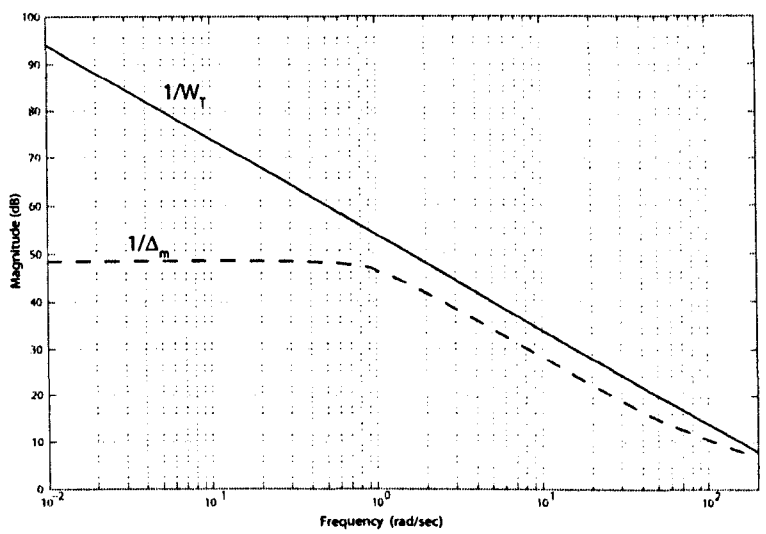

Figure 8.18: The complementary sensitivity function (T) is bounded by the complementary weighting function such that $|T(s)| \leq \frac{1}{W_T(s)}$

8.6.2 Controller and Simulated Closed Loop Response

A feedback controller was then synthesised using the DGKF algorithm as implemented in the Matlab Robust Control Toolbox. The discrete controller synthesised in this way is of 12th order.

The simulated results (Fig.8.19) show that the closed loop time response is predicted to have a response time of 26ms and a settling time of 30ms. There is no overshoot. The response is well damped and does not show evidence of any persistent oscillation, the initial response peaks at around 20ms before rising more gradually to its steady state response, a characteristic which can be attributed to the high order of the controller. The theoretical response of the controller is therefore shown to exceed the US EPA requirements, therefore making it a good candidate for implementation and experimental validation.

The expected robustness of the controller was investigated by checking the gain and phase margins of the loop function for the augmented system,

$$L(s) = G(s)[I + K(s)F_1(s)]^{-1}K(s)F_2(s) \tag{8.20}$$

For the chassis dynamometer controller the corresponding gain and phase margins were thus determined as as 31.6 dB and ∞° respectively.

8.6.3 Time Response

The ARE $\mathcal{H}_\infty$ controller was implemented in the chassis dynamometer control hardware and the closed loop performance of the system was tested using a series of step response tests. The tests in this case only cover the light-duty range of $\pm$500 Nm, which is somewhat lower than for the previously tested Parameter Space $\mathcal{H}_\infty$ controller. This was due to the fact that the full testing schedule was stopped by an auxiliary hardware failure, and could not be completed due to time and resource limitations. Fig.8.20 shows filtered and unfiltered closed loop response to a 500Nm step torque demand. It can be seen that the filtered closed loop system response achieves 90% of the settled response within 20 milliseconds, and displays overshoot of 5% above the settled response. The system settles to 2% within 45 milliseconds. In all cases, the presented controller design therefore exceeds the EPA performance benchmarks significantly.

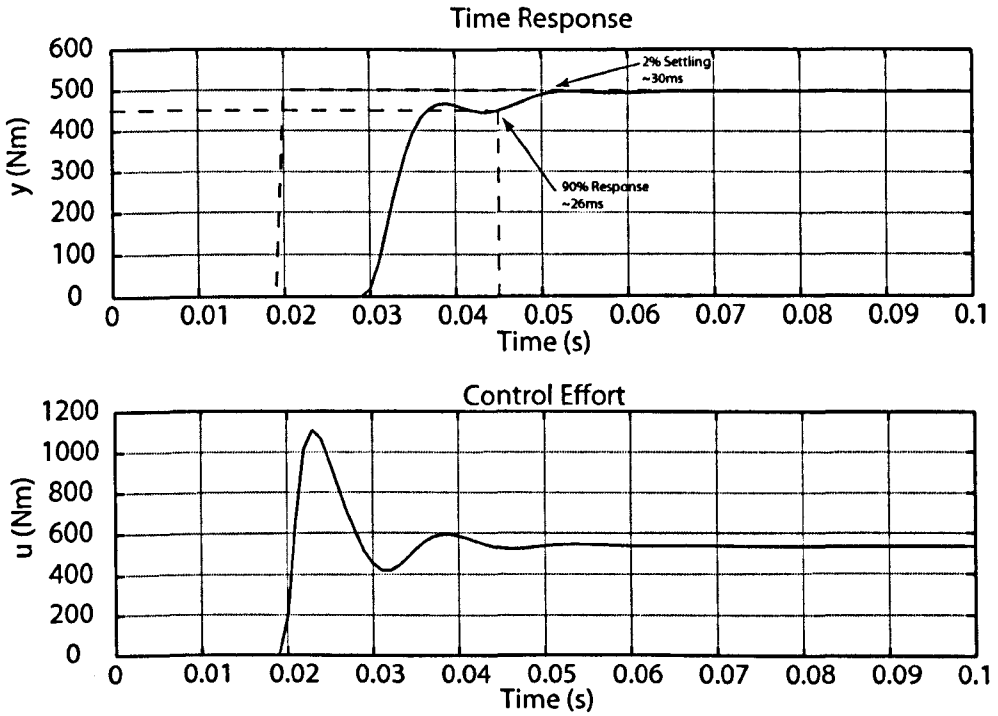

Figure 8.19: Simulated Time response of the candidate ARE controller

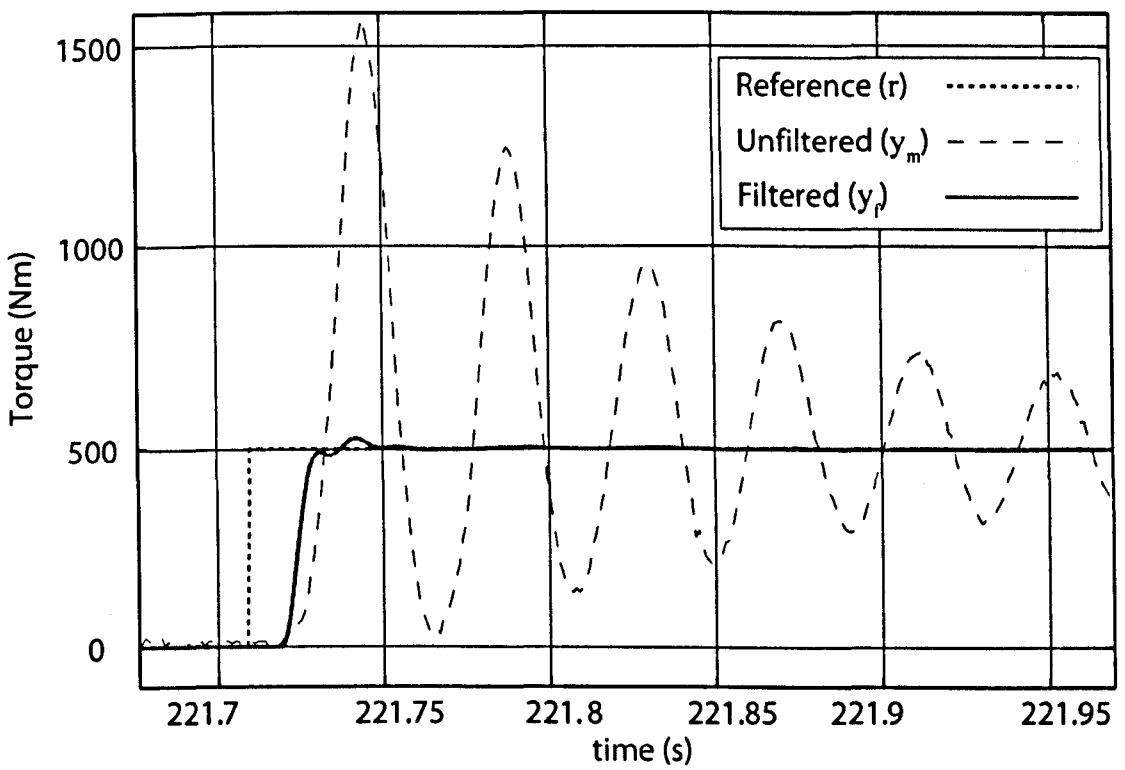

Figure 8.20: Closed loop response to a 500Nm torque demand step

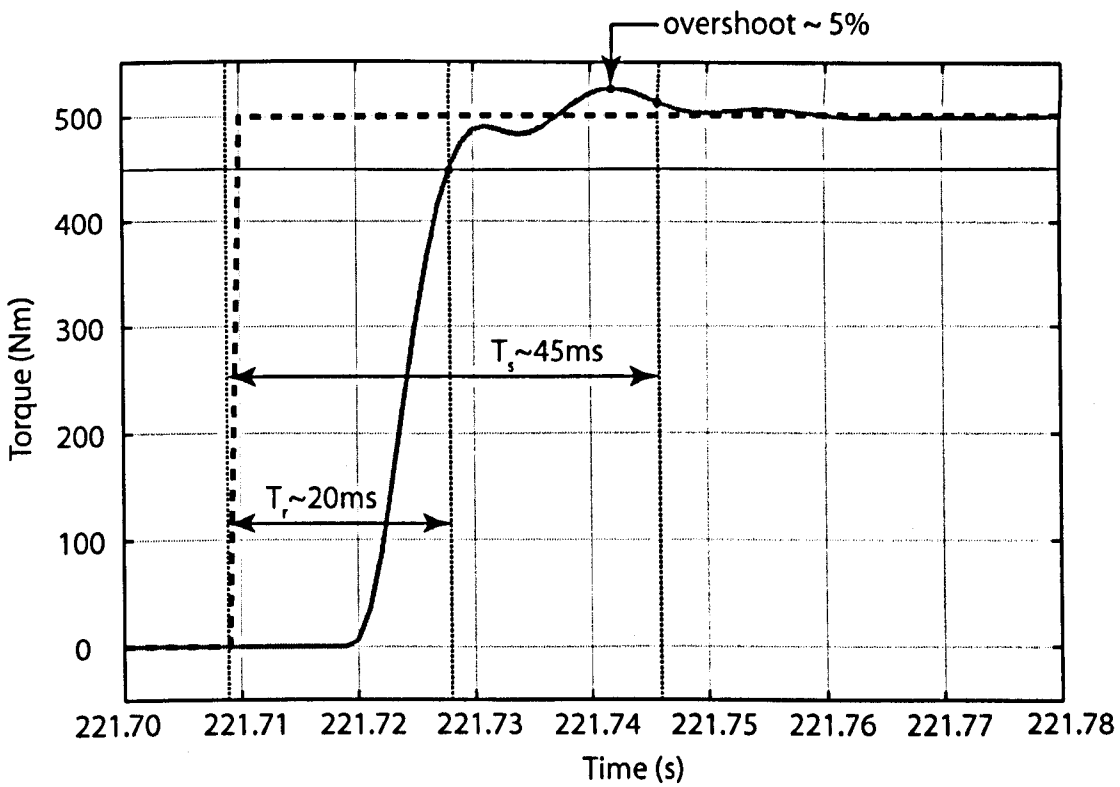

Figure 8.21: Detail of Closed loop step response

8.7 Conclusions

This section has described the design of robust feedback controllers for the chassis dynamometer torque control problem, The following summarised the main conclusions arising from this work:

1. The Parameter Space $\mathcal{H}_\infty$ Controller exceeded the US EPA performance criteria with a response time (90%) of 50ms and a settling time (2%) of 100ms. The maximum overshoot was 5%. The performance of this controller is impressive given its its low order (4th order) which is comparable with the commonly used PID structure which is commonly used in dynamometer control hardware.

2. The parameter space design method benefits from its transparent design procedure, where bounds which are defined by frequency domain specifications are expressed graphically. The design process provides flexibility for the user to tune the controller response within the specifications and does not force the user to rely entirely upon the weighting functions for a successful design.

3. The Algebraic $\mathcal{H}_\infty$ Controller surpassed the US EPA performance criteria significantly with a response time (90%) of 20ms and a settling time (2%) of 45ms. The maximum overshoot was 5%. The performance of this controller must be balanced against its high order (41st order) which would increase the cost of implementation significantly.

4. The Algebraic $\mathcal{H}_\infty$ control design method can provide high levels of performance but suffers from a lack of transparency in the design procedure which is almost entirely governed by the choice of weightings. It is known that weighting functions have a specific interpretation in the frequency domain, but do not transfer directly to the time domain. This means that the user must modify weighting functions in order to tune the time response of the controller which may not be a transparent process. The order of controllers designed by this method will tend to be of a high order which may be impractical for implementation.

5. For both candidate controllers a Kalman filter based on the identified plant models was designed and implemented as part of an augmented feedback control structure to attenuate

the sensor noise from the torque feedback signal in the closed loop system. This filtering strategy should be generally applicable to chassis dynamometer control.

Criterion	EPA-requirement	$\mathcal{H}_\infty$ PS	$\mathcal{H}_\infty$ ARE
response time to 90%	100ms	50ms	20ms
maximum overshoot-%	25%	5%	5%
settling time to 2%	150ms	100ms	45ms

Table 8.2: Benchmark time response results for Candidate Controllers

Part III

Engine Dynamometer Identification & Control

Chapter 9

Engine Dynamometer System Identification

The engine dynamometer system identification was performed using the equipment described in section 6.3. The configuration used during all of the tests described in this section relate to the engine operating at idle, with no throttle input applied. The engine's own PCM is at liberty to control the idle speed and to perform other closed loop control such as AFR regulation.

9.1 Quasi-Static System Characterisation: Engine Dynamometer

A quasi-static system characterisation was performed using a low frequency sine sweep input to the dynamometer drive while shaft torque, dynamometer speed and engine speed were measured. Figure 9.1 shows the shaft torque and engine speed responses. It is immediately apparent that the shaft torque displays significant variation when the dynamometer applies a positive (braking) load. It is also clear that the engine speed response is highly non-linear with dynamometer input and shaft torque. The most likely explanation for this behaviour is that as the dynamometer applies load to the engine, and its speed reduces, the idle speed control system of the test engine will respond and attempt to restore the engine speed to its nominal idle speed. This introduces an unmodelled torque disturbance to the system.

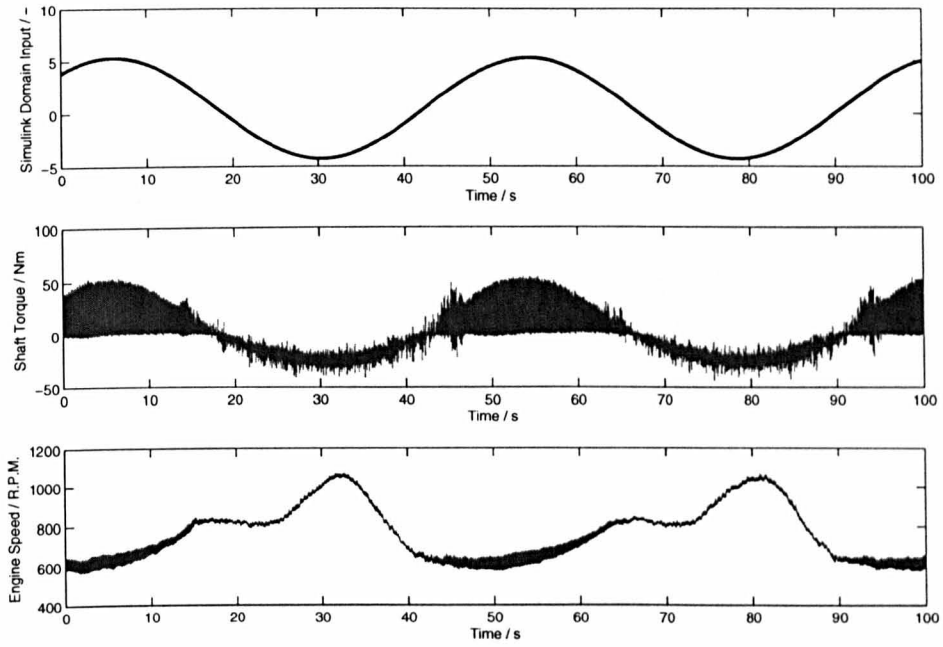

Figure 9.1: Sine Sweep Characterization

Figure 9.2 shows the relationship between the input to the dynamometer drive, and the measured shaft-torque. It shows that the DC behaviour is fundamentally linear but that the system is subject to significant disturbance. The unfiltered shaft torque measurement shows how the magnitude of the fluctuations increase significantly as the engine is loaded and its speed reduces, while the fluctuation in shaft torque is less significant when it is unloaded.

If the relationship between the shaft torque and engine speed or drive input and engine speed are considered (Fig. 9.3 & Fig.9.4), then the non-linearity (probably caused by the interaction of the idle speed control) is quite clear, what is also clear is how the magnitude of the torque fluctuations are highly dependent upon the operating speed of the engine.

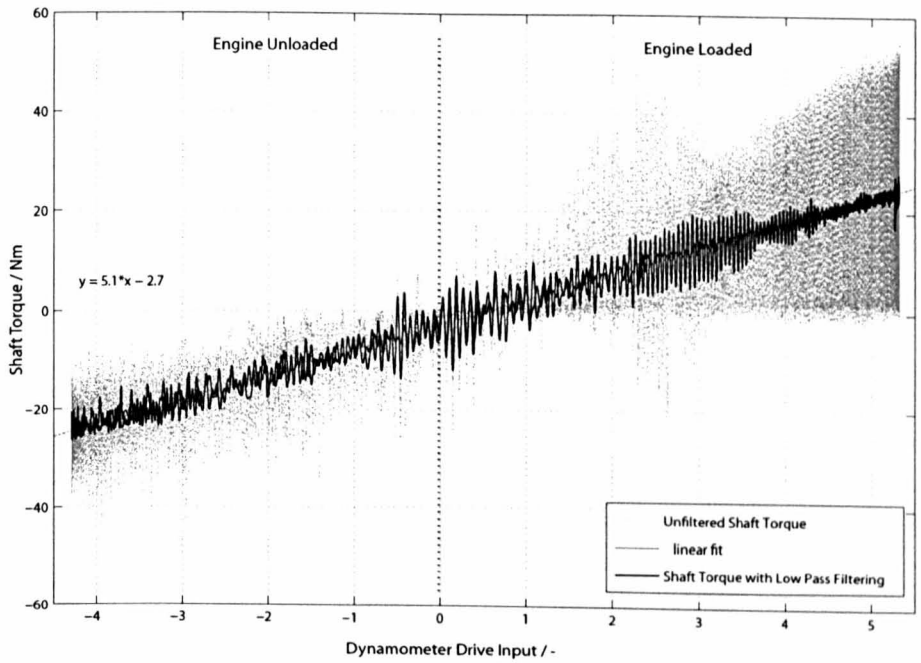

Figure 9.2: Relationship between Drive input, and Shaft Torque

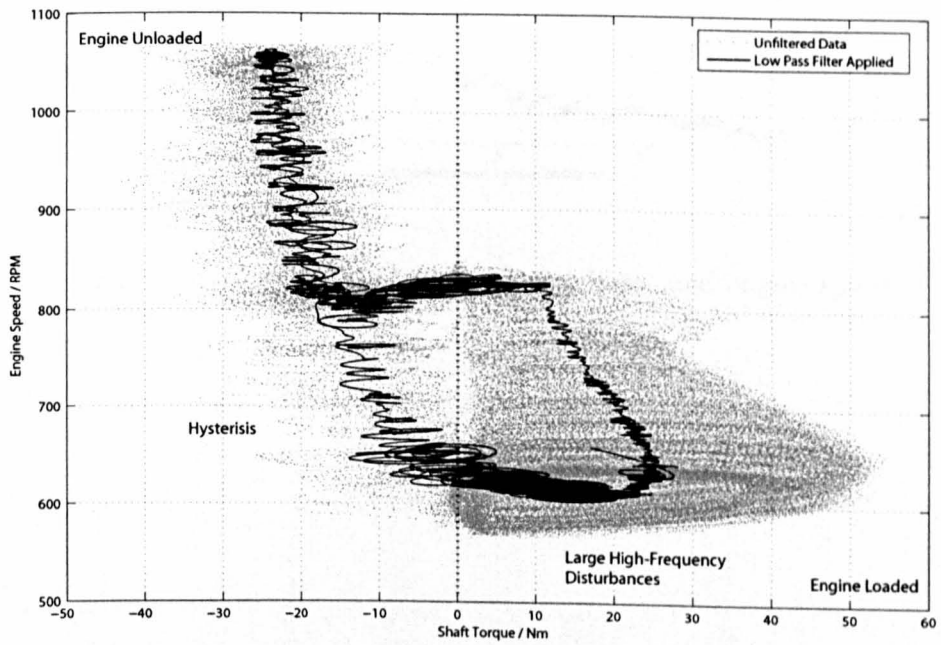

Figure 9.3: relationship between shaft torque and engine speed

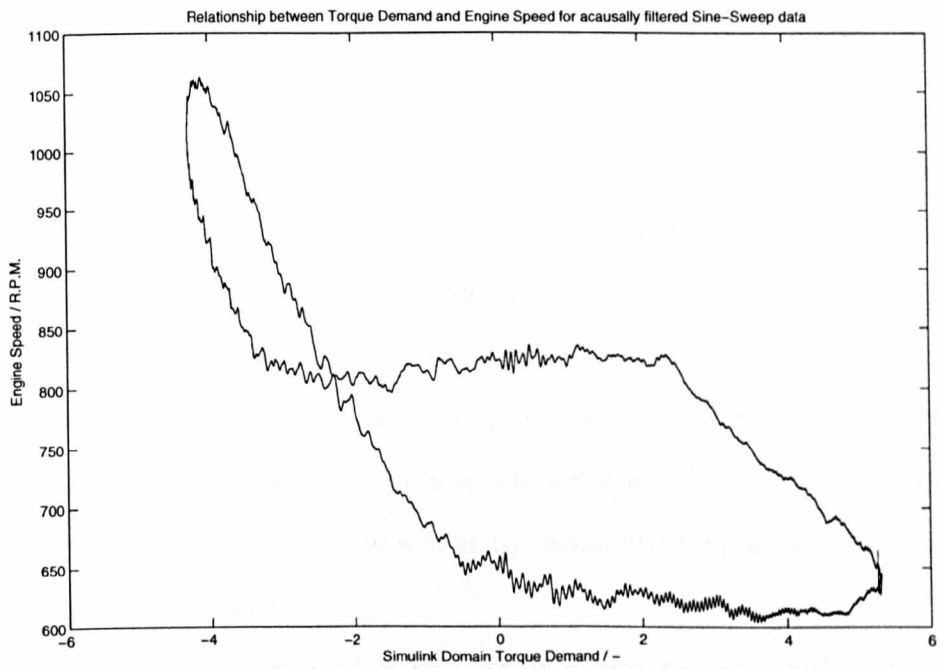

Figure 9.4: Relationship between Drive Input and engine speed

9.2 System Identification: Engine Dynamometer

9.2.1 Input Perturbation and Response Data Acquisition

The zero torque control problem is associated with a narrow operating range around the desired operating point where shaft torque is zero. For this reason, the input perturbation for system identification was designed to explore an envelope of shaft torque which corresponds to the likely range inside which the controller may have to operate. The excitation input (u) is to the dynamometer drive and the measured responses are the shaft torque (y_1), along with engine speed (y_2) and dynamometer speed (y_3).

A PRBS type perturbation input was selected for the identification process. It was decided that in order to explore the operating envelope, a range of input/output tests should be performed at different set-points covering the required envelope of operating conditions. Set-points were defined by a different biased mean value for each PRBS perturbation used. The input signals to the drive were designed to define an approximate target mean shaft torque. Based upon *a priori* knowledge of the dynamometer system, these targets were mapped to a Simulink domain input to the dynamometer drive. A range of ±10Nm was decided upon, with set-points at 5Nm intervals. The perturbation amplitude selected was ±5Nm. Table. 9.1 shows the set-points in terms of target shaft torque as well as the mean drive input and perturbation used in the system identification process.

The collected data was used to identify a set of system models which define the range of dynamics expected within the defined operating envelope. The nominal system model was identified at set-point 5 which is the nominal zero-torque condition. The remaining models were used to define the system uncertainty, and to establish the robustness of the controller.

Setpoint	Target Shaft Torque / N.m	Mean Input / -	Input Perturbation / -
1	-10	3.36	±0.96
2	-5	2.40	±0.96
3	0	1.44	±0.96
4	5	0.478	±0.96
5	10	-0.483	±0.96

Table 9.1: Mean amplitude of PRBS perturbation

Figure. 9.5 shows PRBS data for system identification set-point 3. The measured shaft

torque is shown in figure. 9.6.

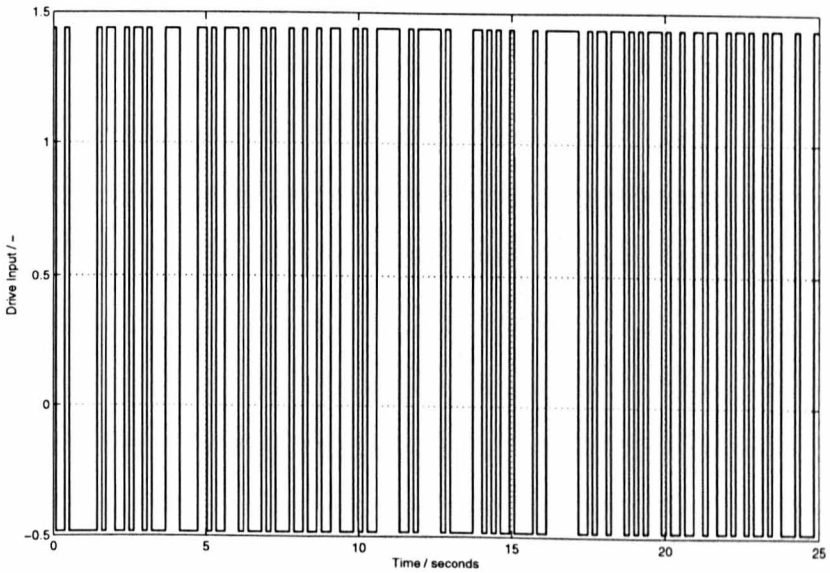

Figure 9.5: Example of PRBS input for setpoint 3

A spectral analysis was performed using the response data collected during the system identification tests. The Power Spectral Density of the data is plotted in figure.9.7. Two peaks are visible in the frequency response, indicating dynamic behaviour at distinct frequencies of 8Hz and 23.5Hz. The first peak coincides with the natural frequency of the dynamometer transmission shaft, the second peak is due to torque fluctuations known as 'crank pulsing' which occur because the torque is not generated continuously, but by separate combustion events. One power stroke occurs every 180 degrees of crank angle and so the crank pulsing frequency can be calculated using (9.1), were N is the engine speed in revolutions per minute. For the test data analysed in figure. 9.7, the mean engine speed (N) is 707 RPM, resulting in a calculated crank pulsing frequency of 23.6 Hz.

$$f_{cp} = \frac{2N}{60} = \frac{2 \times 707}{60} = 23.6Hz \tag{9.1}$$

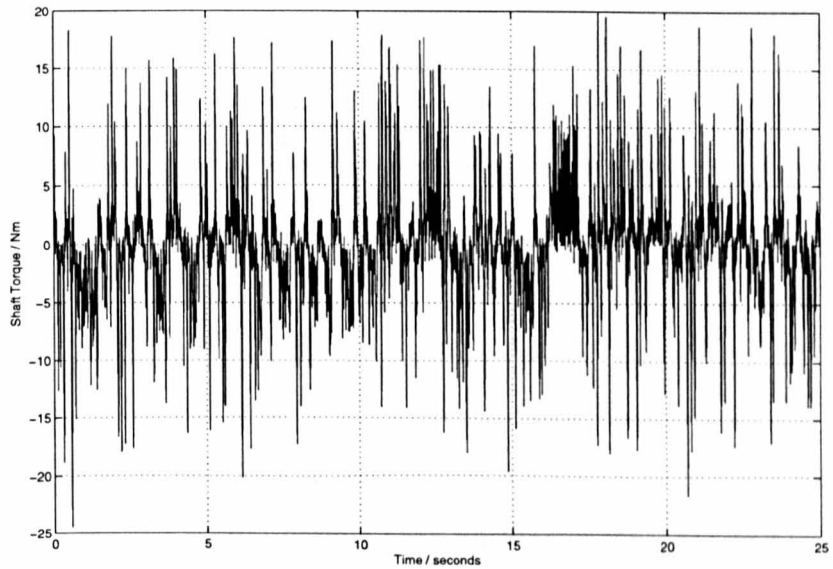

Figure 9.6: Measured shaft torque

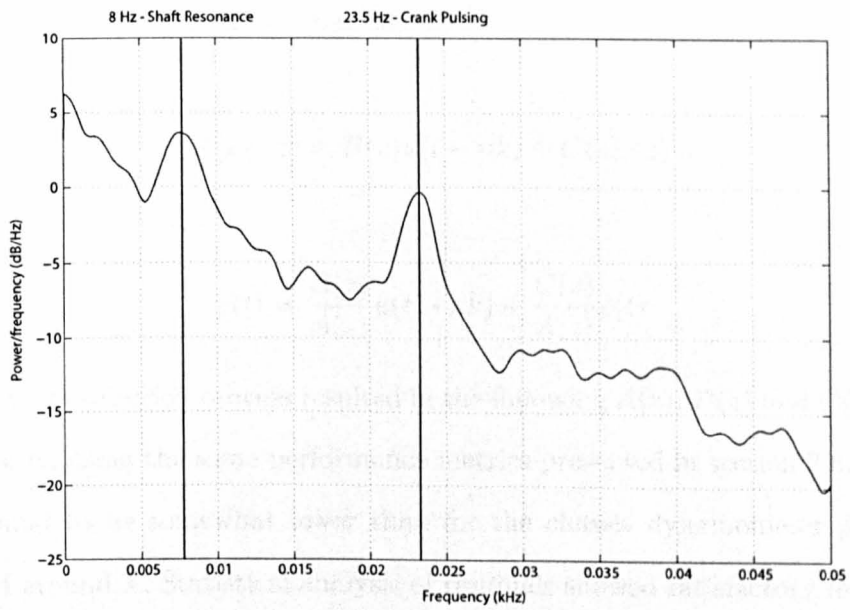

Figure 9.7: Spectral analysis of response data for system identification test

9.2.2 Data Pre-Processing

The mean values of both input and output components of the system identification data were removed to provide identification data sets with a zero mean. It was found that in order to keep the model order efficient, it was beneficial to re-sample the identification data to a sample time of 12 ms. Anti-aliasing filtering is applied to the data during re-sampling. With data re-sampled to 12ms, the time delay is one sample.

9.2.3 Model Structure Selection

Unlike the chassis dynamometer system, where the coloured measurement disturbances are due to superimposed sensor dynamics, the periodic disturbances seen in the shaft torque are not only real, but part of the control challenge since the objective of the ZTC problem is to reduce he fluctuations seen in the shaft torque when operating in the zero torque condition. The excitation caused by crank pulsing and the resulting harmonic disturbance must be captured in the model. For this reason an ARMAX model structure which allows for a more complex disturbance model was considered appropriate for this application.

The ARMAX model structure is described by equation. 9.2, which can be rearranged to give the transfer function form shown in equation. 9.3.

$$A(z)y(t) = B(z)u(t - nk) + C(z)e(t) \tag{9.2}$$

$$y(t) = \frac{B(z)}{A(z)}u(t - nk) + \frac{C(z)}{A(z)}e(t) \tag{9.3}$$

The model order selection process resulted in the following $A(z)$, $B(z)$ and $C(z)$ polynomials. Order was selected using the same performance metrics presented in section 3.6. Achievable R^2 values were found to be somewhat lower than for the chassis dynamometer problem, with a typical value of around X. Statistical analysis of residuals showed satisfactory results within the 95% confidence interval, indicating that full use was being made of the information availiable in the identification data.

$$A(z) = 1+a_1z^{-1}+a_2z^{-2}+a_3z^{-3}+a_4z^{-4}+a_5z^{-5}+a_6z^{-6}+a_7z^{-7}+a_8z^{-8}+a_9z^{-9}+a_{10}z^{-10} \quad (9.4)$$

$$B(z) = b_1z^{-1} + b_2z^{-2} + b_3z^{-3} \quad (9.5)$$

$$C(z) = 1 + c_1z^{-1} + c_2z^{-2} + c_3z^{-3} + c_4z^{-4} + c_5z^{-5} + c_6z^{-6} + c_7z^{-7} + c_8z^{-8} \quad (9.6)$$

9.2.4 Model Validation

Aspects of the model validation procedure are involved throughout the system identification procedure, but a proper validation is an important final step which must be performed before a candidate model can be accepted.

The model is tested using unseen validation data, with the input sequence used along with the identified transfer function model to generate a simulated output. The time response of the model output and the validation data (Fig.9.8) are first compared and examined for a reasonable degree of correlation. Likewise the residuals of the model response are compared with the validation data (Fig.9.9) and inspected for signs of correlation with the inputs (especially low frequency dynamics) which implies information which has not been identified. If the degree of visual correlation appears to be reasonable then statistical tests are performed to establish the quality of fit as well as the auto-correlation and cross-correlation properties of the residuals.

Figure 9.8 shows a comparison between the simulation output and validation data. It shows that the model output matches the validation data at low frequencies, but also that there is a significant amount of higher frequency content which is not captured by the model. The residuals (Fig.9.9) appear to be predominated by higher frequency components with a consistent distribution and does not show obvious signs of unmodelled dynamics. The visual inspection therefore provides enough confidence in the model for a statistical analysis to be worthwhile.

Cross-Correlation tests (Fig.9.10) provide an analysis of the degree of correlation between the input and the residuals and thus a measure of the unmodelled dynamic behaviour which

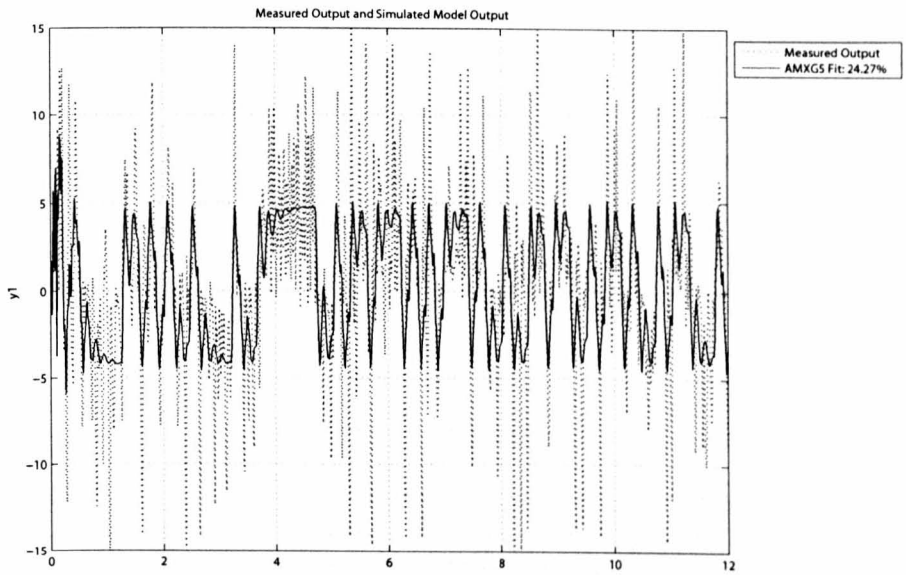

Figure 9.8: Comparison between validation data and model output

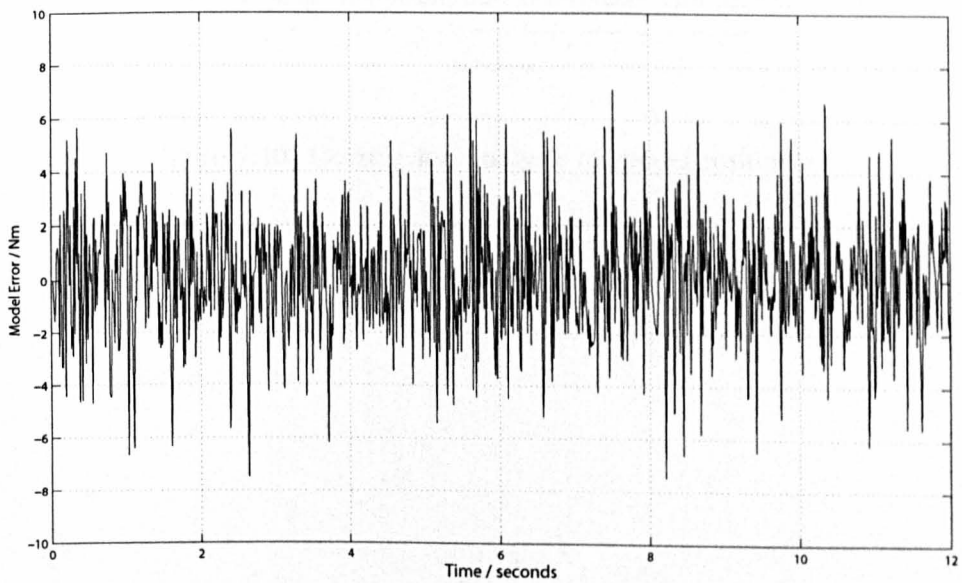

Figure 9.9: Model residuals

is present in the residuals. The results show that for all lags, the cross-correlation lies within the 95% confidence interval. This indicates that the model has made good use of the availiable information. The autocorrelation tests check for harmonic content and so provide a measure of the whiteness of the residuals. The results of this test (Fig.9.10) show that the residuals contain harmonic content but that this exists at a low enough level for the model to be accepted based upon the prescribed confidence interval. The validation tests therefore showed that the model satisfied the acceptance criteria, and that based on these measures the model could be adopted for use in the controller designs.

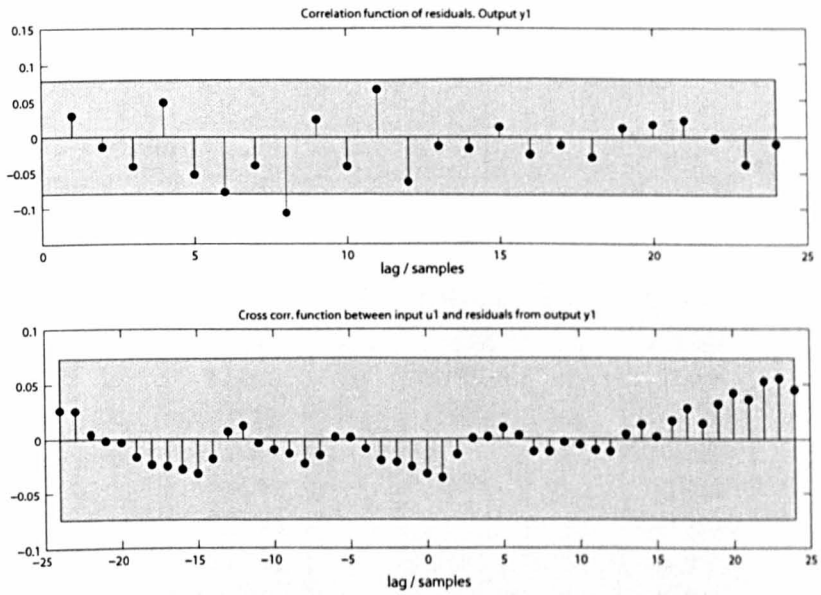

Figure 9.10: Correlation analysis of model residuals

9.2.5 Identified models

The structure of the system model was selected according to the selection procedure outlined in Chapter 3. The system and noise models are shown in 9.7 and 9.8. The model parameters were identified using the Matlab System Identification Toolbox, and are shown for the case of the nominal system in Table.9.2.

$$G(z) = \frac{B(z)}{A(z)} = \frac{b_1 z^9 + b_2 z^8 + b_3 z^7}{z^{10} + a_1 z^9 + a_2 z^8 + a_3 z^7 + a_4 z^6 + a_5 z^5 + a_6 z^4 + a_7 z^3 + a_8 z^2 + a_9 z + a_{10}} \tag{9.7}$$

$$H(z) = \frac{C(z)}{A(z)} = \frac{z^{10} + c_1 z^9 + c_2 z^8 + c_3 z^7 + c_4 z^6 + c_5 z^5 + c_6 z^4 + c_7 z^3 + c_8 z^2}{z^{10} + a_1 z^9 + a_2 z^8 + a_3 z^7 + a_4 z^6 + a_5 z^5 + a_6 z^4 + a_7 z^3 + a_8 z^2 + a_9 z + a_{10}} \tag{9.8}$$

$A(z)$	Value	$B(z)$	Value	$C(z)$	Value
a_1	-1.086	b_1	1.628	c_1	-0.1697
a_2	-0.1611	b_2	-0.8429	c_2	-1.306
a_3	0.06041	b_3	-0.4735	c_3	-0.1585
a_4	0.3667			c_4	0.4959
a_5	0.3486			c_5	0.5597
a_6	-0.2582			c_6	0.05224
a_7	-0.3219			c_7	-0.2671
a_8	-0.07029			c_8	-0.159
a_9	0.3641				
a_{10}	-0.1758				

Table 9.2: Nominal Transfer Function Parameters

The Nyquist plot of the set of identified plant models is shown in Fig.9.11 illustrating the uncertainty in the system over the operating range explored in the system identification experiments. Detail of the higher frequencies is shown in Fig.9.12.

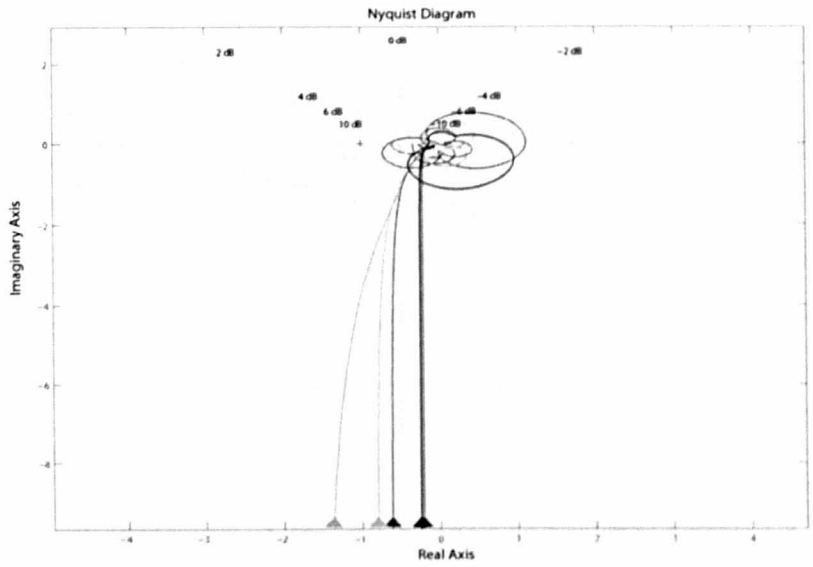

Figure 9.11: Nyquist Plot for the set of identified plant models

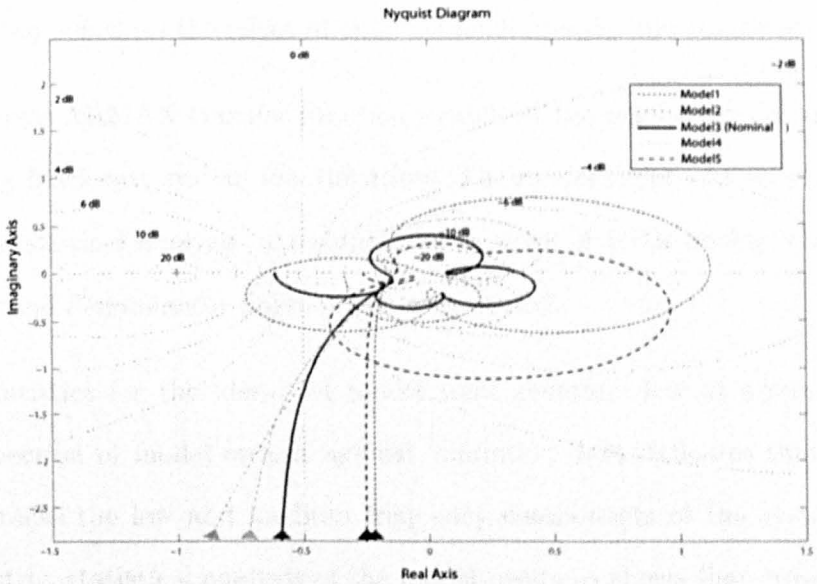

Figure 9.12: Detailed view of the Nyquist plot for all five identified system models

9.3 Conclusions

This section has described the linear system identification process as applied to the engine dynamometer system. The following summarised the main conclusions arising from this work:

1. Spectral analysis highlighted a torque disturbance associated with 'crank pulsing', it was established that this occurs at a frequency which is consistent with individual combustion events,and that it is therefore time varying due to its speed dependency. In addition, quasi-static characterisation of the system shows that the magnitude of the 'crank pulsing' is also speed dependent, showing significant increase as the engine speed drops below the engine' idle operating point.

2. Significant non-linearity was observed when the engine speed dropped below the engine idle set-point. This is though to be associated with the interaction of the engine idle speed regulator, along with the stochastic behaviour associated with combustion processes at low engine speeds.

3. Strong interactions between the dynamometer and test engine were apparent. This is due to the action of the engine's own control strategies, predominantly the idle speed control, which are responsive to the effect of external loading upon the engine at zero throttle.

4. A set of linear ARMAX transfer function models of the engine dynamometer plant were found using black-box system identification. The model order was selected using quality of fit and statistical analysis of residuals for a series of trials during which the order of numerator and denominator polynomials were varied.

5. The R^2 statistics for the identified model were generally low at around 0.25 although visual inspection of model output against validation data indicates that the model successfully tracks the low and medium frequency components of the system. Despite the low R^2 metric, statistical analysis of the model residuals shows that cross-correlation and autocorrelation are within the established limits for a satisfactory model. These results indicate that the models are successful in extracting a significant portion of the coherent dynamic information from the identification data. The noise model successfully captures

the two dominant frequencies of the noise content but fails to capture higher frequency content. It is thought that significantly increased noise model order would be required to identify these higher frequency components.

Chapter 10

Engine Dynamometer: Zero Shaft-Torque Control

This section describes the candidate zero shaft-torque controllers which were designed, implemented and subsequently tested on an engine dynamometer in an idle speed testing application. The dynamometer had been successfully modelled using a black-box system identification approach (Section.9). The controller designs which are presented in this section used the identified frequency domain models as the basis for three different systematic controller design approaches.

Section 10.1 presents a set of PI and PID controllers which were designed using the Parameter Space $\mathcal{H}_\infty$ method. These controller designs result in the same controller structure and order as the existing PI structure of the EDC and therefore acted as a benchmark for improvement potential through a systematic controller design methodology. The controllers were provided to the partner organisation as a set of parameters along with a suitable Simulink blockset which could be implemented directly in the software controller of the engine dynamometer. The controllers were successfully implemented and tested.

Section 10.2 presents controllers designed using an Algebraic Riccati $\mathcal{H}_2$ design algorithm. This approach was chosen in order to study whether a controller with minimum variance properties provides practical improvements over tracking control. The designs were again provided to the test engineers in an electronic format and implemented on the engine dynamometer system.

Finally, section 10.3 introduces a novel dynamometer approach using a SIMO multi-variable

controller structure. This approach applies a combination of tracking control and minimum variance control to the problem, using engine speed fluctuations as an additional feedback channel.

The work presented in this chapter was carried out in partnership with SRH systems using their Kyoto engine testing facility. The system identification work which is presented in Chapter.9 provided frequency domain models which are used in this section as the basis for the controller designs. The control design process itself was carried out as part of a collaborative investigation with Paul Dickinson who provided expertise in the application of $\mathcal{H}_2$ optimised Minimum Variance (MV) control methods.

It should be noted that throughout this section, the controller designs are referred to as candidate controllers since in each case, a range of designs were performed and provided for implementation on the engine dynamometer. The controllers are described in terms of robustness (high and low) and were implemented in order starting with the most robust. The reason for this approach was two-fold. Firstly it was important that the dynamometer system should not be unneccesarily subjected to oscillatory or unstable designs since this would be both potentially dangerous and costly in the event of damage to the dynamometer. For this reason it was thought prudent to implement the most robust controllers first and to reduce the robustness margins progressively giving the operator the opportunity to suspend testing when oscillation or instability became a problem. Secondly, it was though that a description in terms of robustness rather than potential levels of performance would be more appropriate since a controller with high theoretical performance could easily have low performance in practice if it was found to be oscillatory and thus detrimental to performance in terms of the zero torque control objectives.

10.1 SISO $\mathcal{H}_\infty$ Controller

As a basic benchmark for the ZTC problem, the Parameter Space $\mathcal{H}_\infty$ method was used to design a set of candidate PI and PID controllers with varying degrees of robustness. The PI and PID structures are directly comparable to the existing EDC which is a tuned PID.

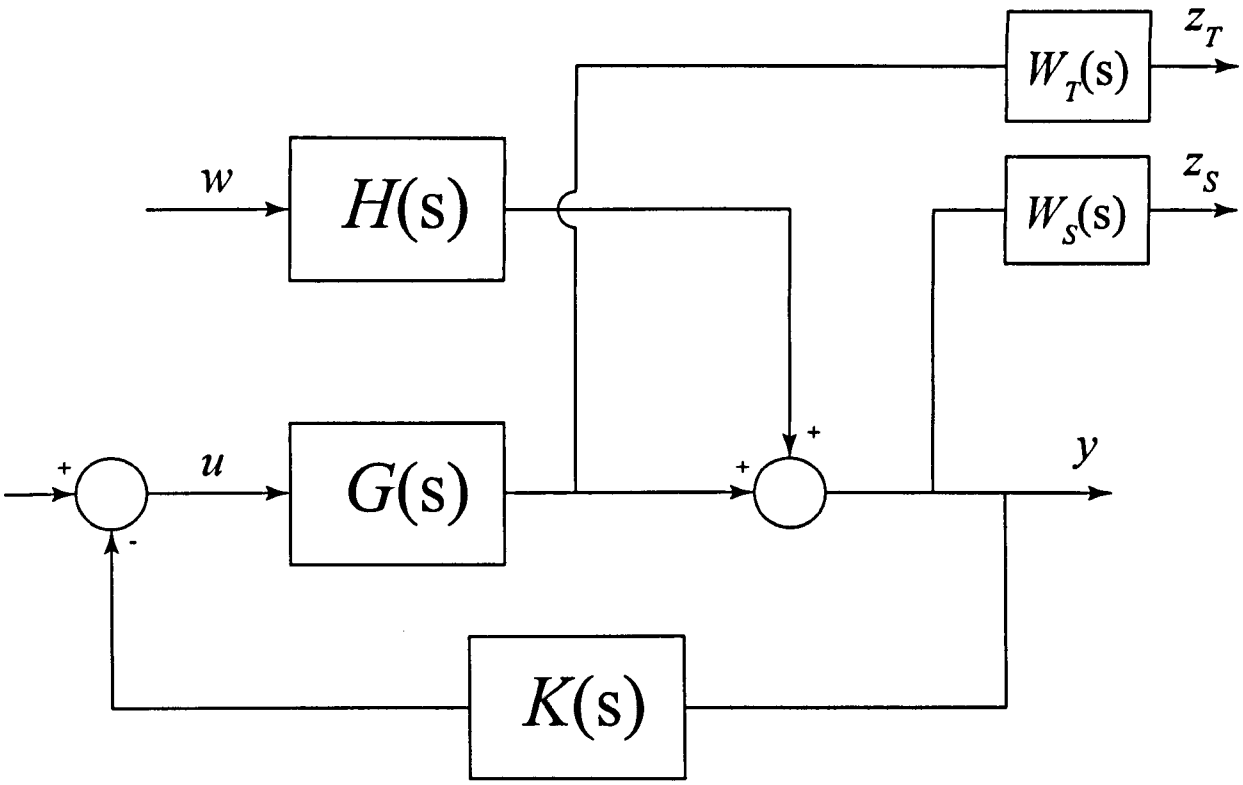

Figure 10.1: SISO Closed-Loop Dynamometer Controller Structure

The parameter space $\mathcal{H}_\infty$ controllers were designed using the same method as was outlined in Section 8.3. The designs used the nominal identified system model which was converted into its continuous (s-domain) form.

10.1.1 Weighting Functions

Primary and complementary Sensitivity weighting functions were selected using guidelines from [SP96], with the primary sensitivity weighting function chosen to provide tracking performance and therefore rapid rejection of disturbances to the measured shaft torque. The complementary sensitivity weighting function was shaped with regard for the plant uncertainty characterised during the system identification process. In order to explore the limits of performance, three

weighting functions were selected, representing High, Medium and Low levels of robustness to the predicted plant variation.

10.1.2 Candidate Controllers

A fixed second order controller structure was adopted for the parameter space designs in order to make a direct comparison, in terms of controller complexity, with the existing PID engine dynamometer controller (EDC).

$$K(s) = \frac{b_2 s^2 + b_1 s + b_0}{a_2 s^2 + a_1 s + a_0} \tag{10.1}$$

For each weighting function (Low, Medium and High robustness shapings), a PI controller (designed in only the $b_0 b_1$ plane and with the b_2 parameter set to zero) and a PID controller (Designed in both the $b_0 b_1$ and $b_1 b_2$ planes) were designed. Table.10.1 shows the parameters which were selected in each case.

The performance of each controller was tested in simulation before they were sent to the partner organisation for implementation and testing on the engine dynamometer.

Candidate	a_2	a_1	a_0	b_2	b_1	b_0
High Robustness PI	0.002	1	0	0	-0.0003029	0.9291
Medium Robustness PI	0.002	1	0	0	-0.01778	3.305
Low Robustness PI	0.002	1	0	0	-0.02573	3.831
High Robustness PID	0.002	1	0	8.148×10^{-5}	-0.04061	0.9199
Medium Robustness PID	0.002	1	0	1.042×10^{-4}	-0.04329	3.305
Low Robustness PID	0.002	1	0	-5.476×10^{-5}	-0.02594	3.831

Table 10.1: PI and PID Controllers

10.1.3 Controller Performance

Time response analysis of the zero shaft torque performance provided only limited objective information regarding the effectiveness of each design compared with the existing EDC. For this reason the statistical variance of the shaft torque about the zero torque set-point was adopted as the key performance metric. In each case, the performance of the candidate controller was tested at the zero shaft-torque set point over a period of 10 seconds.

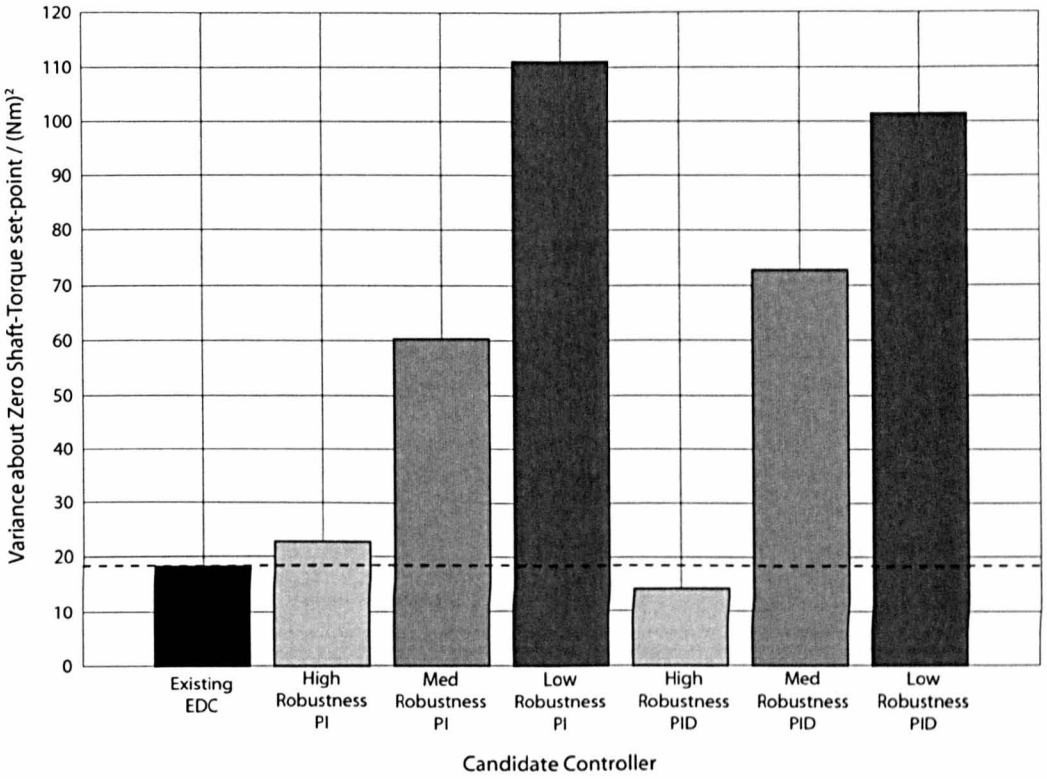

Figure 10.2: Performance of $\mathcal{H}_\infty$ PI and PID controllers

Figure.10.2 shows the variance of the measured shaft torque for each of the six candidate controllers along with the existing EDC for comparison.

10.2 SISO $\mathcal{H}_2$ Controller

The main objective of the zero shaft torque control problem was the reduction of deviation about a set-point, and therefore an algebraic Riccati approach was used to design a SISO $\mathcal{H}_2$ optimised minimum variance (MV) controller. It was expected that because the $\mathcal{H}_2$ norm characterises the signal energy, reducing this norm within the $\mathcal{H}_2$ optimised control framework would reduce the variance of the system response about the set-point.

The standard $\mathcal{H}_2$ and $\mathcal{H}_\infty$ formulation for a SISO feedback system is shown in Fig.10.3 which is the same as Fig.10.1 but repeated here for clarity.

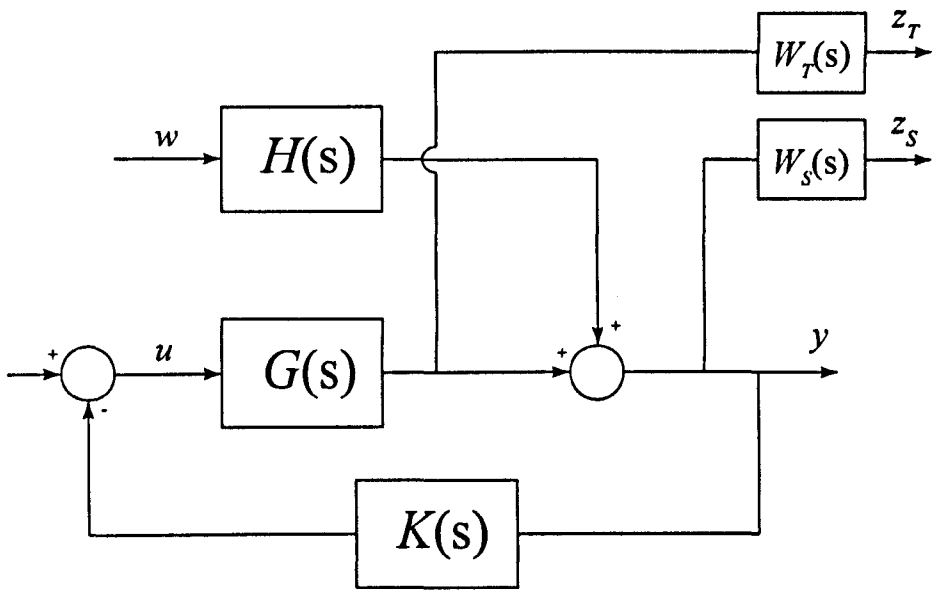

Figure 10.3: Closed Loop System with weighting Functions W_S and W_T

$Z_S(s)$ and $Z_T(s)$ are the weighted outputs given by z,

$$z = \begin{bmatrix} z_S \\ z_T \end{bmatrix} = \begin{bmatrix} HW_S & -GW_S \\ 0 & GW_T \end{bmatrix} \begin{bmatrix} w \\ u \end{bmatrix} \tag{10.2}$$

The system output is y, given by

$$y = Hw - Gu \tag{10.3}$$

The augmented system shown in Figure.10.4 is therefore given by

$$\begin{bmatrix} z \\ y \end{bmatrix} = P(s) \begin{bmatrix} w \\ u \end{bmatrix} = \begin{bmatrix} P_{11} & P_{12} \\ P_{21} & P_{22} \end{bmatrix} \begin{bmatrix} w \\ u \end{bmatrix} \tag{10.4}$$

$$\begin{bmatrix} z \\ y \end{bmatrix} = \begin{bmatrix} HW_S & -GW_S \\ 0 & GW_T \\ H & -G \end{bmatrix} \begin{bmatrix} w \\ u \end{bmatrix} \tag{10.5}$$

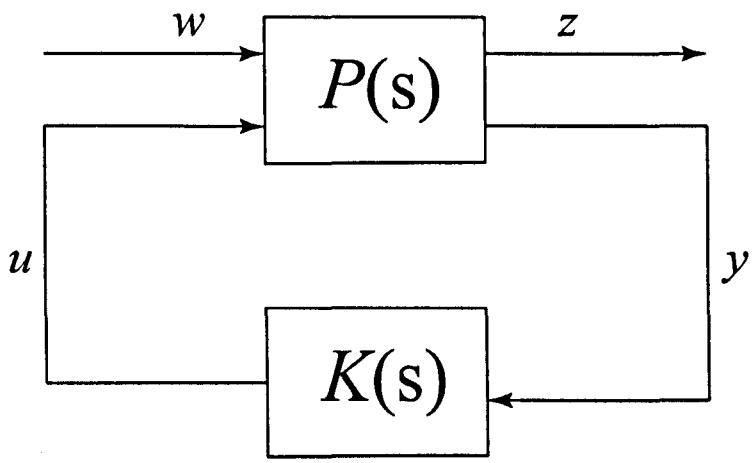

Figure 10.4: Block formulation of the closed loop system with augmented plant $P(s)$

10.2.1 Weighting Functions

The augmented plant formulation $P(s)$ was defined for the engine dynamometer system using the nominal transfer function model $G(s)$ and the noise model $H(s)$. Appropriate frequency domain specifications W_S and W_T were designed using guidelines presented in [SP96] along with an iterative process of tuning using simulation based on trial controller designs.

The primary sensitivity weighting functions was shaped to promote sufficient tracking performance by bounding the sensitivity of the closed loop system at low frequencies. Figure.10.5 shows the shape of the Primary sensitivity weighting functions which were selected for the controllers with the highest and lowest robustness.

The complementary sensitivity weighting functions were selected with the aim of providing different levels of robustness. Figure.10.6 shows the maximum and minimum weighting functions which were used. Both weighting functions provide a roll-off of -20dB/decade which reduces the

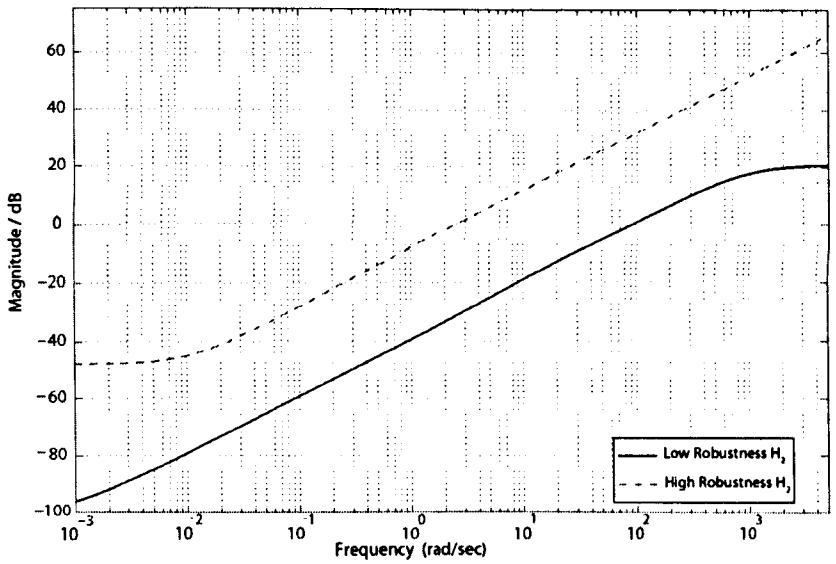

Figure 10.5: Primary sensitivity weighting functions for Highest and Lowest robustness controller designs

sensitivity of the closed loop system to noise and uncertainty as the frequency increases.

10.2.2 Controller Performance

The results achieved using the SISO $\mathcal{H}_2$ optimised MV controllers are shown in Figure.10.7. The results show that the candidate controllers displayed comparable or slightly lower performance than the existing EDC. It is therefore apparent that the SISO $\mathcal{H}_2$ optimised MV control approach alone is not suited to solving the zero shaft torque control problem. This may be due to the fact that the fluctuations are not just a product of the dynamometer torque output and shaft dynamics but also the interactions caused by idle speed control strategy correcting the engine torque when the speed deviates from the engine speed set-point. The result of this is that speed fluctuations have an effect upon the torque which cannot be corrected fast enough within the SISO control framework.

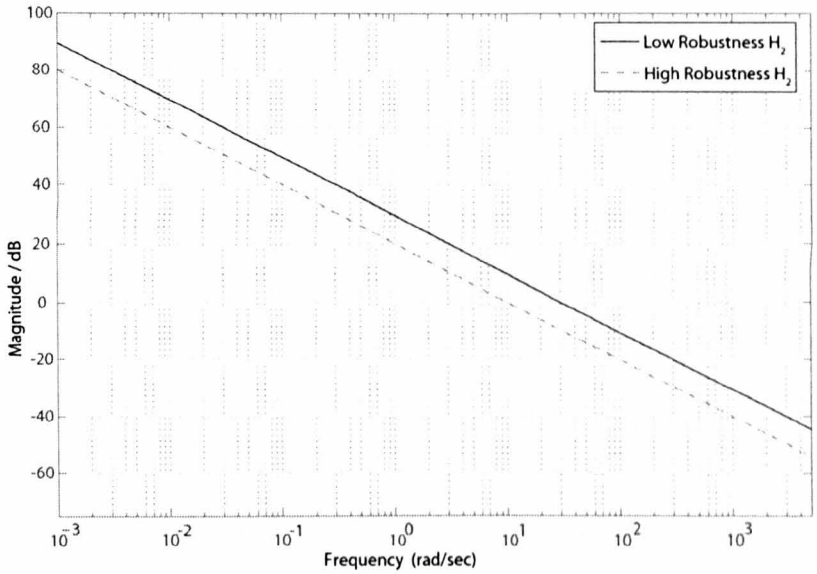

Figure 10.6: Primary sensitivity weighting functions for Highest and Lowest robustness controller designs

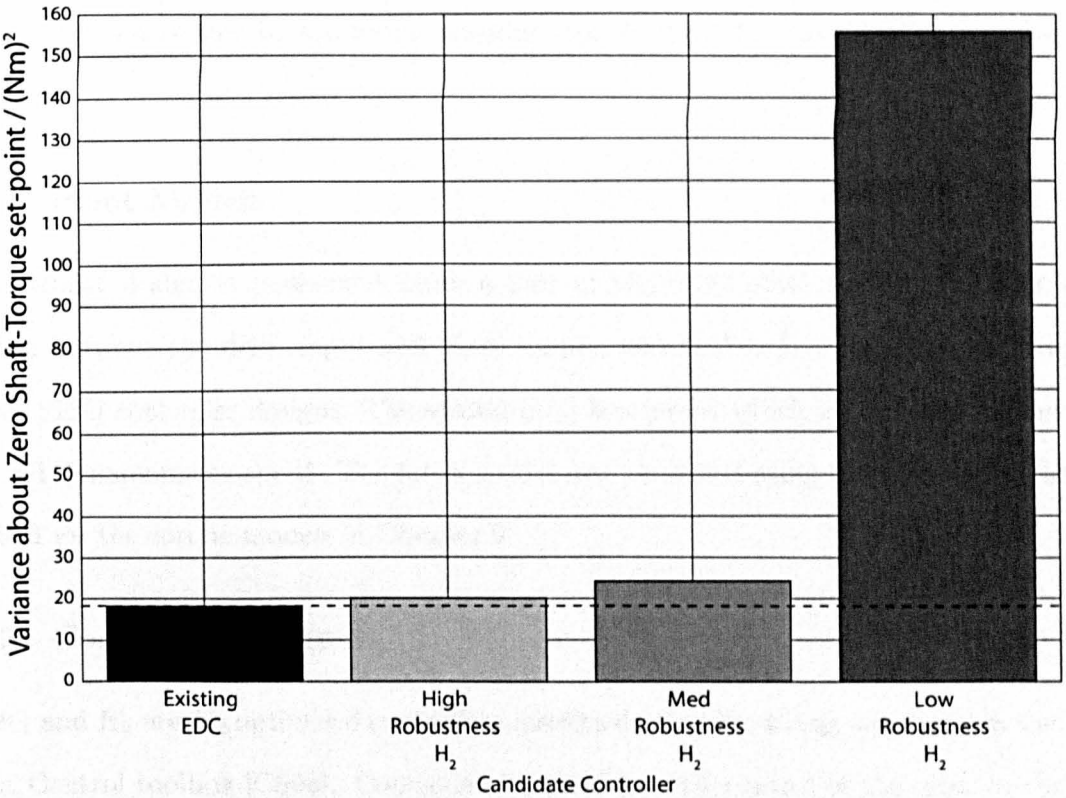

Figure 10.7: Performance of $\mathcal{H}_2$ controllers

10.3 SIMO $\mathcal{H}_2$ Controller

It is apparent that fluctuations in the engine speed have a significant part to play in the zero shaft torque control problem. The engine's idle speed control loop, which acts independently of the dynamometer controller, responds to speed deviations caused by load applied by the dynamometer and provides corrective action through its torque actuation channels, usually air and fuelling. This engine response, causes load disturbances in the transmission shaft, making the measured shaft torque fluctuations more severe and the control problem more difficult. In an attempt to address this problem, a novel SIMO $\mathcal{H}_2$ optimised controller structure is proposed.

In the SIMO control structure presented here, two controllers and two feedback loops are implemented. The first control loop tracks the torque demand set-point, while a second control loop provides variance control about the engine's idle speed set-point. The concept of this structure is that the inclusion of a second controller element, which seeks to reduce the variance of the engine speed about its idle set-point, will reduced the shaft torque fluctuations by limiting interaction between the two control systems and provide better scope for zero shaft torque control which is managed by the torque tracking control loop. The proposed structure is shown in Fig.10.8.

10.3.1 Plant Models

The controller design is performed using a pair of identified plant models, the first (G_1) is identified between the drive input and shaft torque, and is therefore the same as used in the previous SISO controller designs. The second (G_2) is a model which is identified between drive input and dynamometer speed. The latter model was identified using the same methodology as described for the torque models in Chapter.9.

10.3.2 Controller Design

Both K_1 and K_2 are $\mathcal{H}_2$ optimised controllers, designed using the `h2lqg` command in the Matlab Robust Control toolbox [CS98]. Controller K_1 provides MV control of the error in the engine speed about the idle speed set-point, while Controller K_2 is designed to add tracking control to the system about the shaft torque set-point.

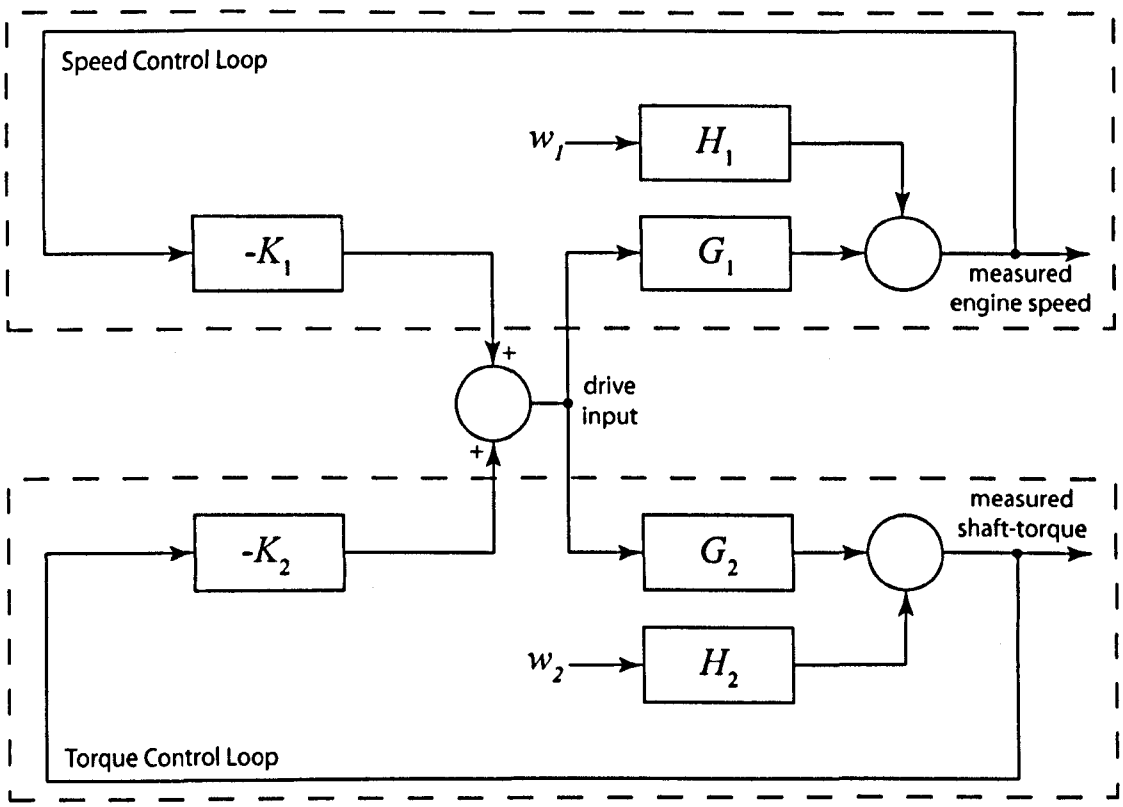

Figure 10.8: SIMO Controller Structure

The first step in the process is to design a H_2 optimised MV controller for the speed control loop. The formulation of the controller for the SISO speed control loop is the same as for the SISO $\mathcal{H}_2$ torque controller , and uses an augmented plant (P) including the plant model (G_1), colouring filter (H_1) and weighting functions W_{S1} and W_{T1} which specify the performance and robustness of the closed loop system. The augmented plant is used in the $\mathcal{H}_2$ design algorithm, as implemented in the Matlab Robust Control toolbox, to generate the controller K_1. This controller will provide MV performance but no tracking control. The purpose of this loop is to limit the speed fluctuations which lead to interactions with the engine idle speed control, and cause shaft torque disturbances.

The second stage in the process is to implement an additional control loop which will track the zero shaft torque set-point. In this case a $\mathcal{H}_\infty$ optimised controller is used since it has been found to provide better tracking performance characteristics than that which may be achieved with the $\mathcal{H}_2$ alternative.

The procedure for generating an augmented plant model is the same as previously but now the system includes the closed loop speed control system, with MV controller K_1. The plant (G) is therefore given by

$$G = \frac{H_1}{1 + G_1 K_1} \tag{10.6}$$

Which can be substituted into the expression for the augmented system [10.5] and used in the $\mathcal{H}_\infty$ ARE design algorithm.

The weighting functions W_{S2} and W_{T2} are designed to provide a trade-off between tracking performance and robustness. The augmented plant model is now used in the $\mathcal{H}_\infty$ algorithm, as implemented in the Robust Control Toolbox, to design controller K_2 which closes the second loop.

The final SIMO feedback system has two control loops, one which provides MV control for the speed loop, and a second which provides tracking control in the shaft torque loop. The overall performance achieved by the system will depend upon a trade-off between the performance and robustness achieved in each loop. In order to explore this trade-off, an number of designs were

carried out, beginning with conservative designs with large stability margins in both loops before incrementally reducing the robustness in both loops with the aim of improving performance in the torque control loop.

Weighting Functions

The performance and robustness of each of the two feedback loops are specified using frequency domain specifications in the form of weighting functions. The following section discusses the choice of weighting functions for each of the two feedback loops and the way in which they were modified in order to achieve a range of candidate controllers with varying degrees of trade-off between expected performance and robustness.

For the speed control loop, the weighting functions were selected to provide minimum variance control but no tracking performance. The primary sensitivity weighting function (Fig.10.9) is designed with 0dB gain at low frequencies and rolls off at higher frequencies to attenuate noise. The 0dB gain at low frequencies means that the controller will not provide tracking control. The complementary sensitivity weighting function is designed to provide robustness which is typically of increasing importance at higher frequencies where the system dynamics become less certain. The selected weighting functions have low gain characteristics at the important low frequencies (close to DC) but provide robustness at frequencies above the 0dB crossover frequency. Figure.10.10 shows W_{T1} and illustrates how this weight changes between the most robust design and the least robust design. It can be seen that for the most robust design, the 0dB crossover frequency is 10 rad/s and that above this frequency the gain increases before levelling out. This weighting should provide significant robustness margins but is likely to be conservative. In contrast, the complementary sensitivity weighting function for the less robust design does not cross over 0dB and as such provides no additional robustness beyond the nominal stability which is inherent in the design.

The weighting functions selected for the Torque control loop were chosen to perform a different role than those in the speed control loop. Firstly, the primary sensitivity weighting function (Fig.10.11) was shaped to provide sufficient tracking performance. The weight W_{S2} is designed to provide higher gains at low frequencies. A judgement regarding what level of gain is appro-

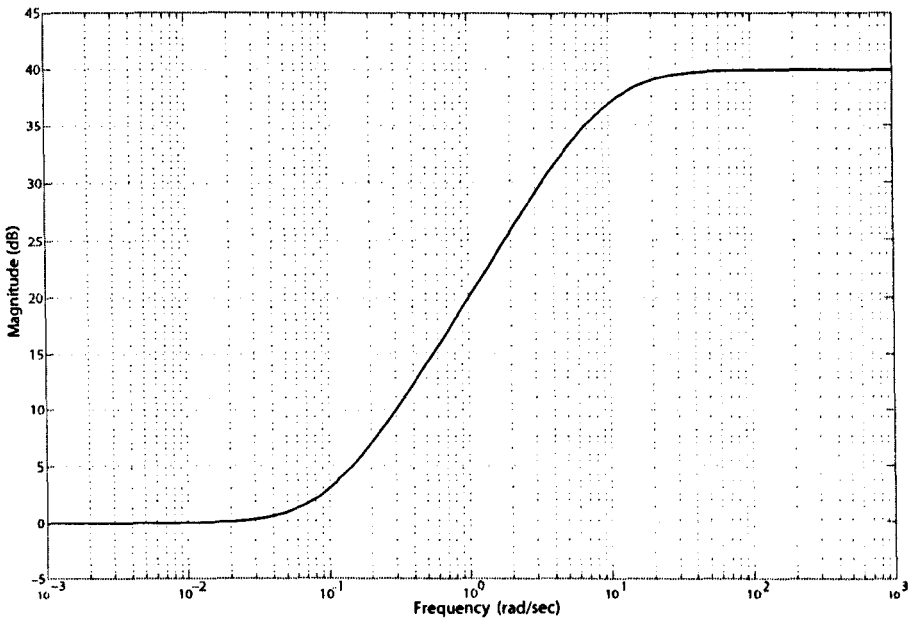

Figure 10.9: Weighting function W_{S1} for the Speed Control Loop

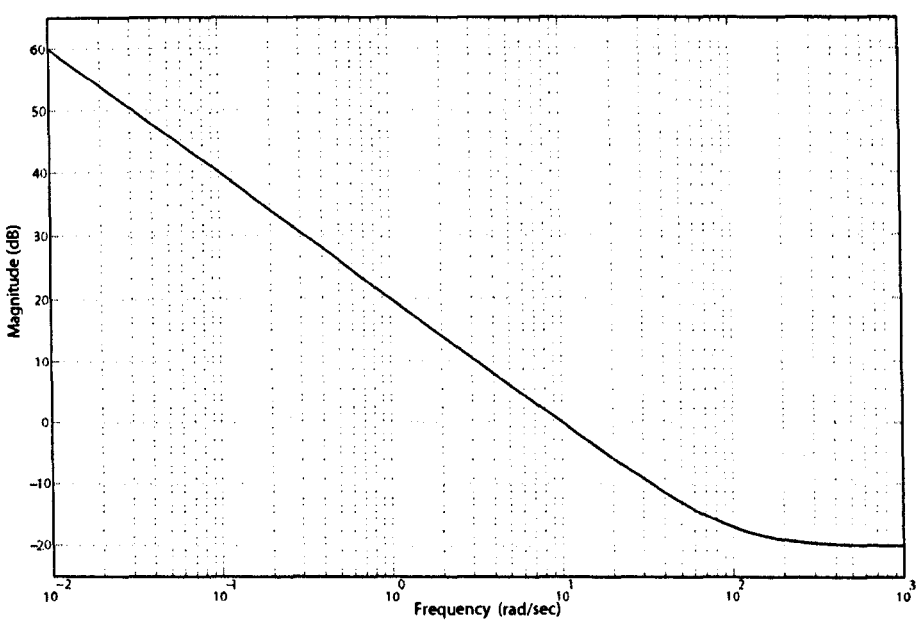

Figure 10.10: Weighting function W_{T1} for the Speed Control Loop

priate to provide sufficient tracking cannot be made transparently since the frequency domain specification does not translate directly into a specific level of time domain performance. For this reason, several designs were performed using different amounts of gain at the important lower frequencies in order to establish through experimentation what was appropriate. The complementary sensitivity weighting function (Fig.10.12) is shaped to provide a measure of robust stability in the face of plant uncertainty, especially at higher frequencies. Accordingly, the low frequency gain of W_{T2} is kept low but is ramped up at higher frequencies..

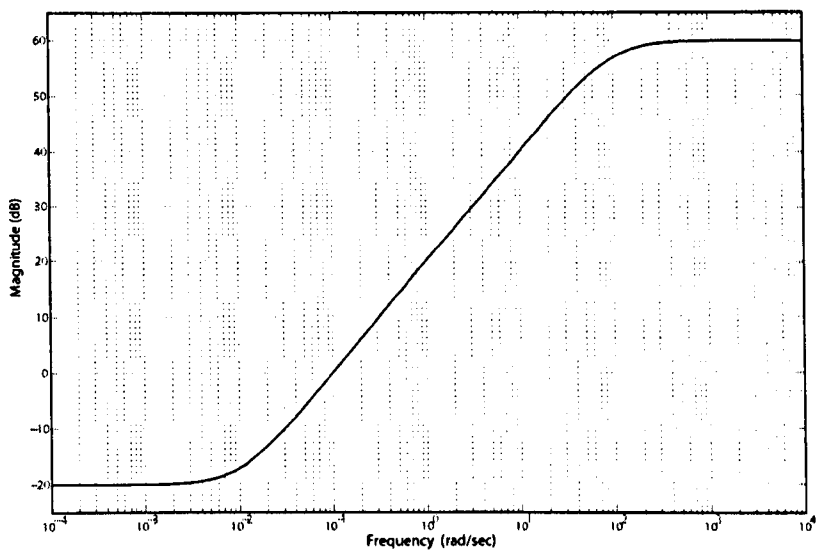

Figure 10.11: Weighting function W_{S2} for the Shaft Torque Control Loop

10.3.3 Controller Performance

The candidate SIMO controllers were implemented in the software controller of the dynamometer system with the addition of an engine speed feedback channel. The 8 candidate controllers were each tested at the zero shaft torque set-point and with a reference engine idle speed of 800 RPM.

The results in Fig.10.13 show the variance of the measured shaft torque for each of the candidate controllers, along with the existing EDC. It is apparent that in general the performance of the SIMO MV controllers increases as the robustness is decreased (in contrast to the SISO $\mathcal{H}_\infty$ controllers). It was found that the highest performing controller was MV8, which displays a level of variance which is less than half of that for the existing EDC.

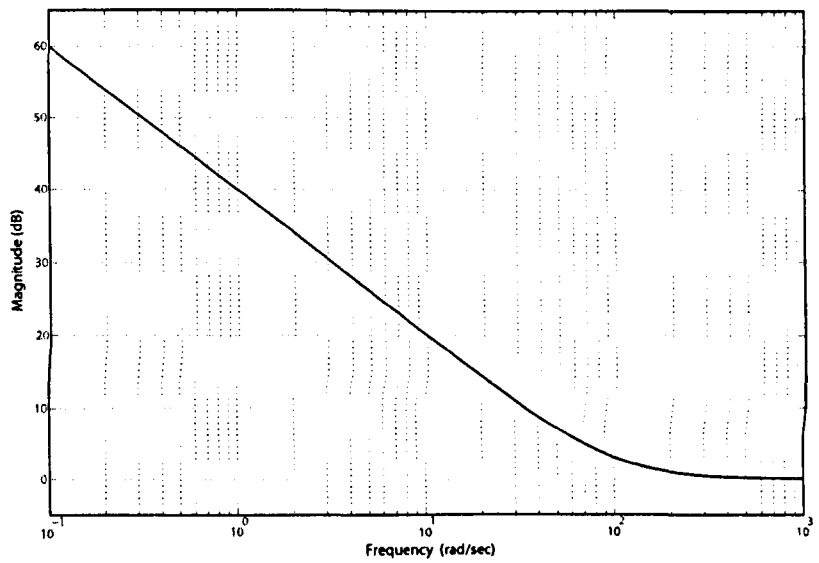

Figure 10.12: Weighting Function W_{T2} for the Shaft Torque Control Loop

Apart from MV7, all of the candidate controllers reduced the variance of the measured shaft torque compared to the existing EDC. Three candidates (MV5, MV6 and MV8) displayed variance levels of less than half that seen in the results for the existing EDC. The poor results observed for controller MV7 is likely to be due to the lower robustness in the speed feedback path causing near instability and thus an oscillatory response.

Figure.10.14 shows a comparison between the measured shaft torque during zero-torque control for the existing EDC (top) and the best zero-torque control candidate MV8 (bottom). The reduction in absolute level of deviation can be observed visually.

These results show that a SIMO controller structure may deliver significant improvement over both of the SISO controller methods which were presented previously.

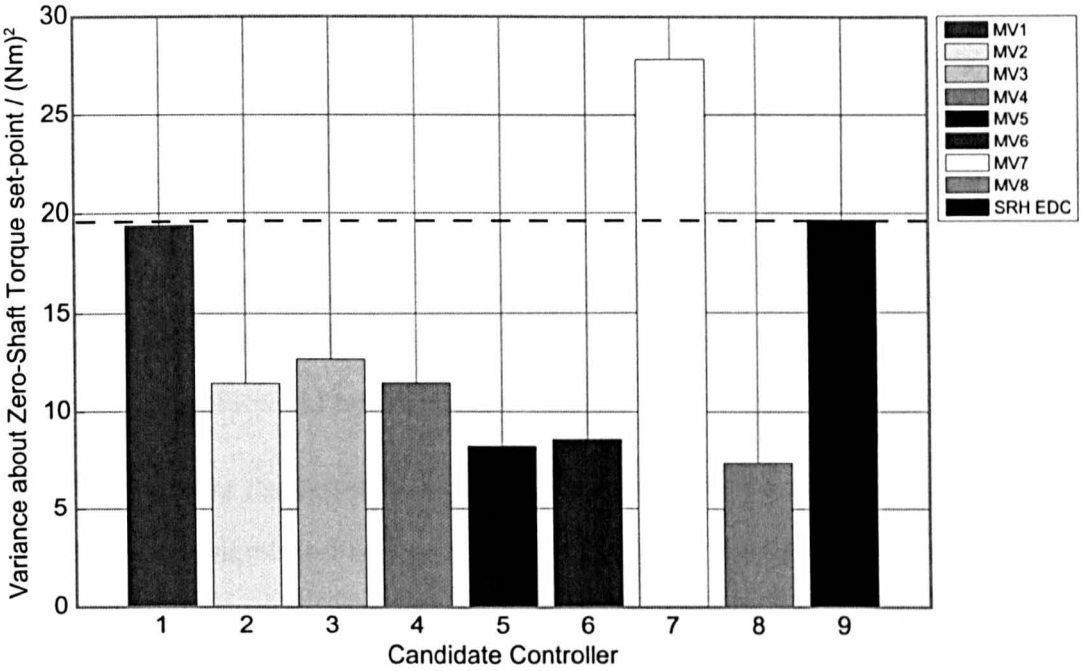

Figure 10.13: Variance Analysis of Candidate controllers compared with existing EDC

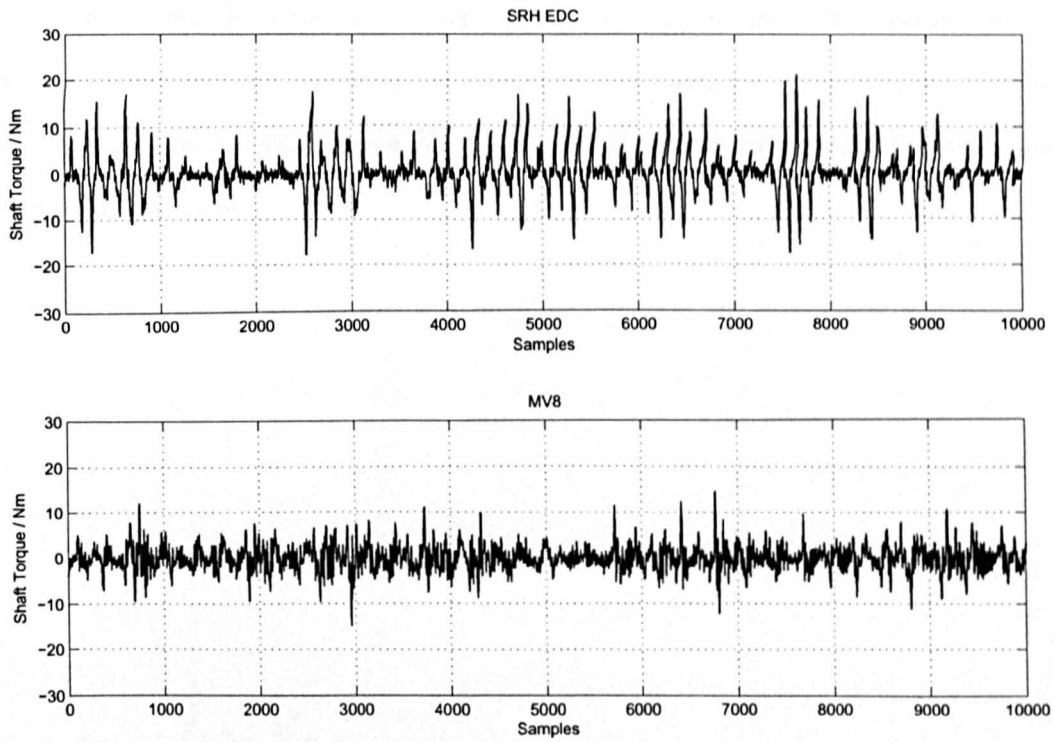

Figure 10.14: Comparison of ZTC performance for best candidate (MV8) and the existing EDC

10.4 Conclusions

This section has described the design of robust feedback controllers for the engine dynamometer zero shaft-torque control problem. The following summarises the main conclusions arising from this work:

1. The parameter space $\mathcal{H}_\infty$ PI and PID candidate controllers displayed similar performance to the existing, heuristically tuned PI EDC structure. This suggested that only small performance gains could be expected with a low order SISO controller.

2. The $\mathcal{H}_2$ controller displayed disappointing performance, providing little improvement compared with the significant increase in order which was required, and the cost of implementation that this would represent. It was therefore concluded that a SISO $\mathcal{H}_2$ controller was not a good solution to the zero shaft-torque control problem.

3. The SIMO control structure shows encouraging results. The variance of the measured shaft torque at the zero shaft-torque operating point is significantly reduced compared with any of the SISO controllers tested. It is apparent that the addition of a second control loop, which acts to minimise engine speed disturbances caused by dynamometer loading, helps to reduce the interaction between the dynamometer control strategy, and the engine's own idle speed controller.

Part IV

Conclusions

Chapter 11

Conclusions

The research carried out in this thesis is a study into how robust feedback control can be applied to automotive dynamometers. A methodology has been presented which successfully applies system identification, signal processing and modern robust control to satisfy the increasingly stringent torque control requirements in automotive powertrain testing. Two practical examples have been used to illustrate the proposed methodology. These examples have shown how the systematic approach can be successfully applied to real dynamometer control problems, yielding impressive results. The methodology combines the application of both new and well established techniques in a novel application.

11.1 Chassis Dynamometer Torque Control

The prescribed methodology was applied to the system identification and control of a transient chassis dynamometer with the objective of improving the transient torque control performance beyond that required by US EPA requirements. In the course of this work the following findings were of particular interest.

11.1.1 Filtering and Sensor Noise

An experimental investigation confirmed the presence of a harmonic disturbance which is superimposed upon the output from the dynamometer torque sensor. This disturbance was found to be caused by the structural dynamics of the torque measurement arrangement which is com-

monly used in gimble mounted dynamometer systems. The presence of this sensor noise has a significant and detrimental effect upon the quality of the feedback available from the torque sensor. Accordingly, two techniques were developed in order to reduce the effect of this noise. Firstly the harmonic disturbance was attenuated in the system identification output data by application of a non-causal bandstop filter. This was found to significantly improve the quality of the model which could be identified. Secondly, for online implementation in the control system, the application of a model based Kalman filter was shown to be a practical and effective method for attenuating the sensor dynamics in the feedback path. This method for attenuating oscillatory torque sensor dynamics should have general applicability for chassis dynamometer systems which utilise the torque arm method of torque measurement. These techniques were found to be essential in achieving the required transient torque control performance.

11.1.2 Direct Inverse Compensation

In order to solve the problem of how system nonlinearity in a dynamometer system such as the chassis dynamometer could be reduced, direct inverse compensation was applied and found to be a simple and effective solution. In this approach, a static inverse model of the DC system gain was identified and implemented directly in the forward path of the dynamometer control system. This method was shown to effectively linearise the system and significantly improved both the performance and robustness of the closed loop control which could be achieved compared with an uncompensated system.

11.1.3 Linear System Identification

It was found that black-box linear system identification could be successfully applied to the linearised dynamometer system and that by modelling the system over its operating envelope, a quantified model of the system uncertainty could be derived. The black-box approach meant that the structure and order of the identified model were selected based upon the quality and efficiency of the model which could be achieved, rather than simplified preconceptions about the physics of the system.

11.1.4 Closed-Loop Controller Design

The system identification procedure resulted in an experimentally validated frequency domain system model, along with an identified multiplicative uncertainty model. These models were ideally suited to use with a robust controller design method. Two methods were selected and applied to the torque control problem.

The Parameter Space $\mathcal{H}_\infty$ controller design approach was applied to the design of a robust controller for the linearised chassis dynamometer system. This approach was shown to provide excellent performance and robustness while delivering a third order fixed structure controller which is comparable with a PID. The performance of the controller was found to exceed the US EPA requirements by a significant margin. The response time (to achieve 90% of settled response) was 50ms, settling time (2%) was 100ms while overshoot was only 5%.

The optimal $\mathcal{H}_\infty$ ARE controller design approach was applied to the same problem and found to further improve both performance and robustness of the closed loop system. The response time was only 20ms with settling achieved at 45ms and overshoot of 5%. The increase in performance compared with the Parameter Space method was found to be achieved at the cost of controller efficiency as the order was increased from 3rd order to 41st order.

11.2 Engine Dynamometer Zero Shaft-Torque Control

The example of zero shaft-torque control of an engine dynamometer is a novel and practically challenging problem. It has been shown to display characteristics such as significant local non-linearity and disturbances caused by combustion instability at low speeds. In addition to the practical engineering difficulties associated with the problem itself, the work carried out in this thesis was performed remotely from the engine dynamometer test facility which was based in Kyoto, Japan. This work has therefore illustrated how the presented approach can be applied to the design of better dynamometer controllers even where the modelling and control is performed at a significant distance from the test facility itself.

11.2.1 Linear System Identification

The presented work shows how the engine-dynamometer system displays significant speed dependent behaviour which make the identification of a linear model particularly challenging. System nonlinearity which is due to interactions between the engine and dynamometer control strategies, along with particularly nonlinear engine behaviour below idle speed, mean that a linear system model can only be identified and validated for a narrow speed range. The shaft torque disturbances associated with periodic engine torque, also known as crank pulsing, were shown to be a significant, time varying, component of the total shaft torque disturbance which must be controlled to a minimum during idle speed testing.

11.2.2 SISO Closed-Loop Control

The limitations of the existing SISO PID controller structure were explored by designing a set of candidate controllers with the same PID structure. The Parameter Space $\mathcal{H}_\infty$ design approach was selected for this purpose due to the fact that a robust controller can be designed for a fixed controller structure such as a PID. The results showed that only small improvements in the level of shaft-torque fluctuations could be expected using this type of controller and that an alternative solution was neccesary.

The $\mathcal{H}_2$ control method was used to design a set of optimised SISO minimum variance candidate controllers. These candidate controllers were implemented and tested, but showed poor results. None of the candidate controllers provided an improvement over the existing controller. These results indicated that SISO minimum variance control, applied to the torque loop, was not sufficient to improve the zero shaft-torque control performance.

The result from both sets of SISO controllers indicated that SISO control was not well suited to the zero shaft-torque control problem. This was thought to be a result of the engine torque disturbances caused by speed fluctuation about the idle set-point.

11.2.3 SIMO Closed-Loop Control

A novel SIMO control structure was chosen with the aim of combining the performance of a $\mathcal{H}_\infty$ torque tracking controller with a $\mathcal{H}_2$ optimised Minimum Variance controller which responded

to correct for engine speed fluctuations about idle speed. The results achieved using the SIMO control structure showed significant improvements over those which were achieved with either $\mathcal{H}_\infty$ or $\mathcal{H}_2$ SISO control alone. The variance of shaft torque *disturbances were reduced by more* than half compared with the existing dynamometer controller. These results showed that by minimising the disturbances caused to engine speed by dynamometer loading, the interaction between the engine and dynamometer controllers could be reduced. This was thought to be the most significant factor in the improvements which were gained by using the SIMO controllers.

Appendix A

Total Road Load

A.1 Introduction

The primary function of a transient chassis dynamometer is to provide means by which realistic transient tests can be performed with a vehicle in controlled laboratory conditions. For this to be achieved, a good quality road load model [DG81] is essential for this will form the reference signal for the control system.

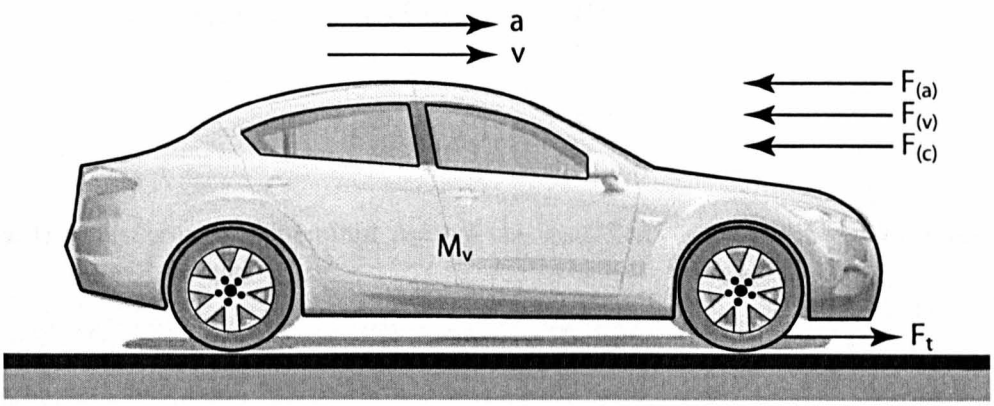

Figure A.1: Road Load Forces

Consider figure A.1, it shows a car in motion with an instantaneous velocity v and acceleration a. The vehicle's motion is maintained by a force F_T acting on the road surface through the driven tyres. This motion is resisted by a variety of forces which can be categorised into three

groups. *F(a)* denotes those forces which are dependent upon the acceleration of the vehicle, for example Inertial loads. *F(v)* denotes forces which are dependent upon the velocity of the vehicle, for example aerodynamic drag. *F(c)* denotes those other forces which can be reasonably considered to be constant, the conditions which must be observed for this to be the case are

1. No Gradient - It is assumed that the vehicle is operating on a flat straight road without any significant gradient.

2. No wind - It is assumed that the vehicle is not subjected to external wind loading other than that due to its own motion.

The total road-load is given by

$$F_t = F(c) + F(v) + F(a) \tag{A.1}$$

In the above, $F(c)$ describes those forces which are be considered constant and can be represented by the constant A_1.

The speed dependant component $F(v)$ describes those forces, primarily aerodynamic drag, which vary as a function of the vehicle velocity. It has been shown that these forces can be well described with a quadratic polynomial of the form [DG81],

$$F(v) = A_2 + Bv + Cv^2 \tag{A.2}$$

Finally, the acceleration dependant part of the road load can be expressed simply by

$$F(a) = M_v \frac{dv}{dt}$$

So, the total load can be expressed by

$$F_t = A_1 + A_2 + Bv + Cv^2 + M_v \frac{dv}{dt}$$

By letting $A = A_1 + A_2$

$$F_{\mathrm{t}} = A + Bv + Cv^2 + M_{\mathrm{v}}\frac{dv}{dt} \tag{A.3}$$

then let

$$F_{rl} = A + Bv + Cv^2 \tag{A.4}$$

which gives the simplified expression

$$F_T = F_{\mathrm{rl}} + M_{\mathrm{v}}\frac{dv}{dt} = F_{\mathrm{rl}} + F_{\mathrm{j}} \tag{A.5}$$

Equation A.5gives the total road-load which must be applied against the driven wheels at any point during operation. However, when operating the dynamometer, it is convenient to work in terms of the angular velocity of the roller instead of vehicle speed and to consider resistance Torque which must be applied by the PAU rather than the force which is to be applied at the tyre. The analysis below outlines how the translational system outlined thusfar can be represented in terms better suited to the chassis dynamometer's configuration and operation. The forces F_{rl} and F_{j} are now referred to the axis of the dynamometer, and the vehicle mass M_{v} is replaced by its equivalent inertia.

Consider figure A.2. It shows a schematic of the chassis dynamometer with a vehicle whose wheels are driving the rollers and PAU. Assume for now that the PAU is not active and that no Load is being applied against the vehicle. It is clear that, assuming no slip, the tangential velocity of the tyre at its periphery will be identical to that of the roller.

$$v = v_{\mathrm{t}} = v_{\mathrm{r}} \tag{A.6}$$

Where,

$$v_{\mathrm{t}} = \omega_{\mathrm{t}} r_{\mathrm{t}} \tag{A.7}$$

$$v_{\mathrm{r}} = \omega_{\mathrm{r}} r_{\mathrm{r}} \tag{A.8}$$

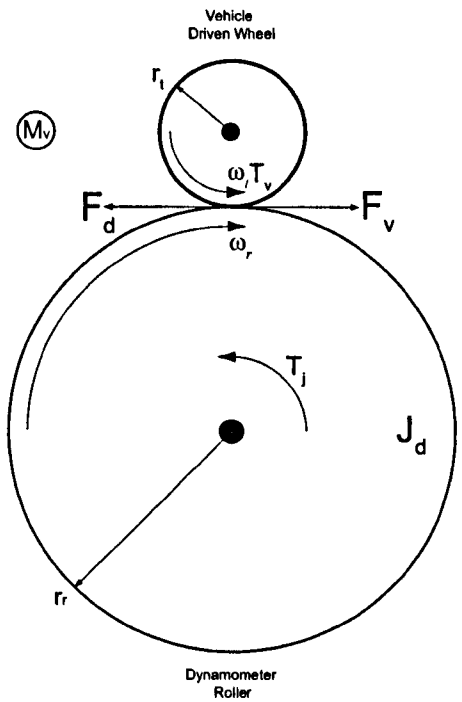

Figure A.2: Chassis Dyno

A.2 Road-Load Torque

The road load torque T_{rl} can be expressed as

$$T_{rl} = F_{rl} r_r = (A + B v_r + C v_r^2) r_r \tag{A.9}$$

Now substitute $v_r = \omega_r . r_r$

$$T_{rl} = F_{rl} r_r = (A + B \omega_r . r_r + C \omega_r . r_r^2) r_r \tag{A.10}$$

Simplification gives

$$T_{rl} = F_{rl} r_r = (A r_r + B \omega_r . r_r^2 + C \omega_r^2 . r_r^3) \tag{A.11}$$

$$T_{rl} = A_1 + B_1\omega_r + C_1\omega_r^2 \tag{A.12}$$

A.3 Inertia Load Torque

The resistance force F_j due to the vehicle inertia is given by

$$F_j = M_v\frac{dv}{dt} \tag{A.13}$$

Inertia load torque is given by

$$T_j = F_j r_r = (M_v\frac{dv}{dt})r_r \tag{A.14}$$

Substituting $v_r = \omega_r.r_r$ gives

$$T_j = (M_v r_r\frac{d\omega_r}{dt})r_r = M_v r_r^2\dot{\omega}_r \tag{A.15}$$

If the vehicle inertia, referred to the axis of the dynamometer, is

$$J_v = M_v r_r^2 \tag{A.16}$$

then this becomes

$$T_j = J_v\dot{\omega}_r \tag{A.17}$$

A.4 Total Road-Load Torque

The total road load torque which must act at the axis of the dynamometer is given by

$$T_t = A_1 + B_1\omega_r + C_1\omega_r^2 + J_v\dot{\omega}_r \tag{A.18}$$

This expression is equivalent to A.3 but is cast in terms which are more useful when considering the dynamometer application. ω_r is directly measurable and $\dot{\omega}_r$ can be calculated from

this so if the values of A_1, B_1 and C_1 along with J_v are known, then the total resistance torque can be calculated.

The road-load torque T_{rl} is applied by the PAU and will always oppose the motion of the roller, the application of T_j is less straight forward.

For direct application of the inertia torque T_j the dynamometer must behave as if it has a quiescent inertia of J_v. In some chassis dynamometers [TOO80] flywheel masses can be added to provide means of modifying the inertia until it matches the required value. This arrangement has the advantage that the inertial load is applied entirely by the acceleration acting on the inertia of the dynamometer, in this case only the road-load torque needs to be applied electrically. The disadvantage is cost and complexity. In the Liverpool chassis dynamometer, the physical inertia of the dynamometer is fixed and so some component of the inertia load must be applied by the PAU, the control of this load must be very fast to avoid the applied load from being significantly out of phase with the instantaneous acceleration [PM01]. The inertia which must be simulated electrically (J_e) is given by

$$J_e = J_v - J_d \tag{A.19}$$

Where J_d is the combined physical inertia of the dynamometer including the PAU (J_p) and the rollers (J_r).

$$J_d = J_p + J_r \tag{A.20}$$

J_v is defined as $J_v = M_v r_r^2$, so

$$J_e = M_v r_r^2 - J_p + J_r \tag{A.21}$$

The torque which must be applied to simulate this inertia for any given acceleration is calculated from the expression

$$T_e = J_e \dot{\omega}_r \tag{A.22}$$

A new expression can be defined which describes the total road-load torque which must be applied by the PAU

$$T_p = T_{rl} + T_e = A_1 + B_1\omega_r + C_1\omega_r^2 + J_e\dot{\omega}_r \tag{A.23}$$

$$T_p = T_{rl} + (M_v r_r^2 - J_d)\dot{\omega}_r \tag{A.24}$$

$$T_p = T_{rl} + J_e\dot{\omega}_r \tag{A.25}$$

The expected roll acceleration can be described by the expression:

$$\dot{\omega}_r = \frac{T_t - T_{rl}}{J} \tag{A.26}$$

References

[AB+00] J.C. Aguirre, M. Brezenski, et al. Dynamometer performance evaluation and quality asurance procedures for 48-inch, single roll, light duty chassis dynamometers. Technical report, Autoalliance, 2000.

[Age91] U.S. Environmental Protection Agency. Specifications for electric chassis dynamometers. Attachment A, RFP C100081T1, 1991.

[BB95] T. Basar and P. Bernhard. $\mathcal{H}_\infty$ - *Optimal Control and Related Minimax Design Problems* . Birkhüser, Boston, 1995.

[BBM97] G.R. Babbitt, R.L.R. Bonomo, and J.J. Moskwa. Design of an integrated control and data aquisition system for a high-bandwidth, hydrostatic, transient engine dynamometer. *Proceedings of the American Control Conference, Albuquerque, New Mexico*, pages 1157–1161, 1997.

[Bel95] J.T. La Belle. Dynamometer and method for simulating vehicle road load and/or inertial forces while providing compensation for the parasitic losses of the dynamometer. US Patent 5385042, 1995.

[BFT97] B.J. Bunker, M.A. Franchek, and B.E. Thomas. Robust multivariable control of an engine-dynamometer system. *IEEE Transactions on Control Systems Technology*, 5(2):189–199, 1997.

[Bla34] H.S. Black. Stabilised feedback amplifiers. *Bell Systems Technical Journal*, 13:1–18, 1934.

[BM99] G.R. Babbitt and J.J. Moskwa. Implementation details and test results for a transient engine dynamometer and hardware in the loop vehicle model. *Proceedings of the 1999 IEEE International Symposium on Computer Aided Control System Design*, pages 569–574, 1999.

[Bod40] H.W. Bode. Relations between attenuation and phase in feedback amplifier design. *Bell Systems Technical Journal*, 19:421–454, 1940.

[BS97] V. Besson and A.T. Shenton. Interactive control system design by a mixed $\mathcal{H}_\infty$-parameter space method. *IEEE Transactions on Automatic Control*, 42(7):946–955, 1997.

[BS99] V. Besson and A.T. Shenton. An interactive parameter space method for robust performance in mixed sensitivity problems. *IEEE Transactions on Automatic Control*, 44(6):1272–1276, 1999.

[BT83] D.G. Brown and S. Thompson. A novel approach to engine torque speed control. *SAE Technical Paper Series*, 831302, 1983.

[Can86] J.V. Candy. *Signal Processing: The Model-Based Approach.* McGraw-Hill, 1986.

[Car01] D. Carley. Method of controlling a chassis dynamometer. International Patent WO 01/65226 A1, September 2001.

[CMP96] A.J. Beaumont C.Y. Mo and N.N. Powell. Active Control of Driveability. *SAE*, 960046, 1996.

[CS98] R.Y. Chiang and M.G. Safonov. *Robust Control Toolbox - Users Guide.* The Mathworks Inc, 1998.

[D+00] R.E. Dorey et al. Vehicle calibration on the testbed (vcot). *SAE Technical Paper Series*, 2000-01-1144, 2000.

[DBM96] S. D'Angelo, C. Brownell, and W.G. Mears. Evaluating the performance of chassis dynamometers with electric inertia simulation. *SAE Technical Paper Series*, 960716, 1996.

[DFT91] J.C. Doyle, B. Francis, and A. Tannenbaum. *Feedback Control Theory.* Macmillan Publishing Co, 1991.

[DG81] S. D'Angelo and R.D. Gafford. Feed-forward dynamometer controller for high speed inertia simulation. *SAE*, 810749, 1981.

[DG+89] J.C. Doyle, K. Glover, et al. State-space solutions to standard $\mathcal{H}_\epsilon$ and $\mathcal{H}_\infty$ control problems. *IEEE Transactions on Automatic Control*, 34(8):831–846, August 1989.

[DH99] R.E. Dorey and C.B. Holmes. Vehicle Driveability - Its Characterisation and Measurment. *SAE Technical Paper Series*, 1999-01-0949, 1999.

[DM00] R.E. Dorey and E.J. Martin. Vehicle driveability - the development of an objective methodology. *SAE Technical Paper Series, 2000-01-1326, 2000.*

[DW89] R.E. Dorey and D. Wang. A hydrostatic dynamometer for engine testing. *2nd Bath International Fluid Power Workshop*, September 1989.

[Eva50] W.R. Evans. Control system synthesis by root locus method. *Transactions of the American Institute of Electrical Engineers* , 69:66–69, 1950.

[FD79] C.E. Feragus and S. D'Angelo. US patent 4161116: Inertia and road-load simulation for vehicle testing, 1979.

[Gau63] K.G. Gauss. *Theory of Motion of the Heavenly Bodies.* New York: Dover, 1963.

[GdRK+06] E. Gruenbacher, L. del Re, H. Kokal, M. Schmidt, and M. Paulweber. Online trajectory shaping strategy for dynamical engine test benches. In *Proceedings of the 2006 IEEE International Conference on Control Applications*, pages 3104–3109, October 2006.

[GO04] L. Guzzella and C.H. Onder. *Introduction to modelling and control of internal combustion engine systems.* Spinger, Berlin, 2004.

[JZJ+05] L. Jing, M.A. Zhimin, Z. Jiacai, S. Dafeng, and Z. Jian. A hardware-in-the-loop simulator based on dynamometers for traction control. In *IEEE International Conference on Vehicular Electronics and Safety, 2005*, pages 15–19, October 2005.

[KB60] R.E. Kalman and R.S. Bucy. A new approach to linear filtering and prediction problems. *Transactions of the ASME Journal of Basic Engineering*, 82D:35–45, 1960.

[KB61] R.E. Kalman and R.S. Bucy. New results in linear filtering and prediction theory. *Transactions of the ASME Journal of Basic Engineering*, 83D:95–108, 1961.

[KBJ+] P.J. King, K.J. Burnham, D.J. James, A.J. Martyr, and S.R. Sharpe. Modelling, simulation and control of a dynamometer torque loop in an engine test cell. In *J.R.Smith (Ed), Mathematics in the Automotive Industry.*

[KBJ+91a] P.J. King, K.J. Burnham, D.J. James, A.J. Martyr, and S.R. Sharpe. Implementation of a self-tuning controller to the dynamometer torque loop of an engine test cell. In *Proceedings of the International Conference on Control '91*, pages 110–114, March 1991.

[KBJ+91b] P.J. King, K.J. Burnham, D.J. James, A.J. Martyr, and S.R. Sharpe. Modelling and simulation of a combined engine and dynamometer system. *Journal of Systems Science*, 17:93–104, 1991.

[Kin92] P.J. King. *Adaptive Control Applied to an Engine Test Cell.* PhD thesis, Coventry Polytechnic, 1992.

[Kwa91] H. Kwakernaak. Robust control and $\mathcal{H}_\infty$-optimization - tutorial paper. *Automatica*, 1:110–114, 1991.

[Leo01] W. Leonhard. *Control of Electrical Drives (3rd Edition).* Springer-Verlag, 2001.

[Lju99] L. Ljung. *System Identification - Theory for the User.* Prentice-Hall, 1999.

[Lju05] L. Ljung. *System Identification Toolbox - Users Guide.* The Mathworks Inc, 2005.

[LS98] H.O. List and P. Schoeggl. Objective Evaluation of Vehicle Driveability. *SAE Technical Paper Series*, 980204, 1998.

[MDS06] C. Matthews, P. Dickinson, and A.T. Shenton. Chassis dynamometer torque control by direct inverse compensation. *6th Biennial UKAAC Control Conference, Glasgow*, 2006.

[MF37] J.R. MacGregor and L.T. Folsom. Automatic speed-load dynamometer control. *SAE*, 370044, 1937.

[MF50] J.R. MacGregor and L.T. Folsom. An engine dynamometer control for fuel evaluation by simulated road tests. *SAE*, 500155, 1950.

[NSHT00] M. Nomura, M. Suzuki, M. Hori, and M. Terashima. Decoupling torque control system for automotive engine tester. *IEEE Transactions on Industry Applications*, 36(2):467–474, 2000.

[Nyq32] H. Nyquist. Regeneration theory. *Bell Systems Technical Journal*, 11:126–147, 1932.

[Pet00] A.P. Petridis. PhD thesis, The University of Liverpool, 2000.

[PI95] K. Pfeiffer and R. Isermann. Automatic control of vehicle startup for emission tests on engine dynamometers. In *Proceedings of the American Control Conference*, pages 2596–2600, 1995.

[PM99] M.A. Plint and A.J. Martyr. *Engine Testing - Theory and Practice.* Butterworth-Heinemann, 1999.

[PM01] M.A. Plint and A.J. Martyr. Some limitations of the chassis dynamometer in vehicle simulation. *Proceedings of the Institution of Mechanical Engineers, Part D: Journal of Automobile Engineering*, 215(3):431 – 437, 2001.

[PS02] A.P. Petridis and A.T. Shenton. Inverse-NARMA: a robust control method applied to si engine idle-speed regulation. *Control Engineering Practice*, 11:279–290, june 2002.

[PS03] A.P. Petridis and A.T. Shenton. Linear robust control of identified nonlinear inverse compensated si engine. *Journal of Dynamic Systems, Measurment and Control*, 125:69–73, 2003.

[Sch02] K.K. Schwartz. Faraday and Babbage. *Notes and Records of the Royal Society*, 56(3):367 – 381, 2002.

[SM02] M. Suzuki and T. Maruki. US patent 6345542: Running resistance control apparatus of chassis dynamometer, 2002.

[SNP96] H. Singh, D.S. Naidu, and J.N. Peterson. Eigenvalue assignment of unified systems with slow and fast modes. *Proceedings of the 1996 IEEE International Conference on Control Applications, Dearborn, MI, USA*, 1996.

[Sor70] H.W. Sorenson. Least-squares estimation:from Gauss to Kalman. *IEEE Spectrum*, 7:63–68, 1970.

[SP96] S. Skogestad and I. Postlethwaite. *Multivariable Feedback Control - Analysis and Design.* Wiley, New Jersey, 1996.

[SS89] T. Söderström and Petre Stoica. *System Identification.* Prentice-Hall, 1989.

[ST+94] Y. Suzuki, K. Torikai, et al. High accuracy high response 48-inch roll chassis dynamometer. *SAE 940487*, 940487, 1994.

[Swe58] P. Swerling. A proposed stagewise differential correction procedure for satellite tracking and prediction. *Rept. P-1292, RAND Corp, Santa Monica, California*, 1958.

[Tho02] J.K. Thompson. An integrated process for moving testing from the track to the laboratory. *SAE Technical Paper Series*, 2002-01-1483, 2002.

[Thr04] M.J. Throop. High accuracy dynamometer torque calibrations: a systems approach. *SAE Technical Paper Series*, 2004-01-1782, 2004.

[TMR02] J.K. Thompson, A.J. Marks, and D. Rhode. Inertia simulation in brake dynamometer testing. *SAE Technical Paper Series*, 2002-01-1483, 2002.

[TOO80] A. Takamura, M. Ono, and S. Ohigashi. Chassis dynamometer provided with control device simulating road load. *SAE*, 800324, 1980.

[TRFV90] T. Tuken, R. Rees-Fullmer, and J. VanGerpen. Modeling, identification, and torque control of a diesel engine for transient test cycles. *SAE Technical Paper Series*, 900235, 1990.

[Tsc05] M. Tschersich. Chassisdyno companion version 1.0 - standard. Technical report, ASAM, 2005.

[TVRF92] T. Tuken, J. VanGerpen, and R. Rees-Fullmer. Adaptive torque control of a diesel engine for transient test cycles. *SAE Technical Paper Series*, 920238, 1992.

[Voi91] K.U. Voigt. A control scheme for a dynamical combustion engine test stand. In *Proceedings of the International Conference on CONTROL '91*, pages 938–943, March 1991.

[Wei49] N. Weiner. *The extrapolation, Interpolation and Smoothing of Stationary Time Series.* Wiley, New York, 1949.

[Wil02] M.V. Wilkes. Charles Babbage and his world. *Notes and Records of the Royal Society*, 56(3):353 – 365, 2002.

[WJ72] R.J. Wahrenbrock and J.B.Duckworth. Driveability testing on a chassis dynamometer. *SAE*, 720933, 1972.

[Yan98] D. Yanakiev. Adaptive Control of Diesel Engine-Dynamometer Systems. *Proceedings of the 37th IEEE Conference on Decision and Control, Tampa, Florida, USA*, 1998.

[Zam81] G. Zames. Feedback and optimal sensitivity: Model reference transformation multiplicative seminorms, and approximation inverses. *IEEE Transactions on Automatic Control*, 26(2):301–320, 1981.